V. Gerasimov
A. Monakhov

NUCLEAR ENGINEERING MATERIALS

Construction of Nuclear Power Plants

Ed. by Professor V. Dubrovsky, D. Sc. (Eng.)

This is the first engineering text in the USSR to describe the techniques used to translate basic principles of reactor physics, materials engineering, structural analysis and design, and engineering economics into practice in the design and construction of nuclear power plants. Each of the six chapters:

— outlines present-day reactors, systems, and components of nuclear power plants;

— discusses the siting and general layout of nuclear power plants;

— examines the planning and layout of nuclear power plant buildings and structures;

— describes the analysis and design of buildings and structures as applied to nuclear power plants;

— covers the analysis and design of radiation shielding;

— discusses the problems and features of nuclear power plant construction.

The book will be of primary value to college students and faculty members, and also to researchers and engineers concerned with the design and construction of nuclear power plants.

NUCLEAR ENGINEERING MATERIALS

This is a college textbook. The book discusses the requirements imposed on reactor materials. It characterizes coolants and discusses irradiation-produced changes taking place therein. The book examines the properties of structural and nuclear fuel materials and the manner in which they are influenced by service factors. The book also considers on an up-to-date level strength, compatibility, radiation and corrosion resistance of the structural and fuel materials.

The book will be of primary value to students of power engineering and to engineers working in the fields involving nuclear power.

V. Gerasimov
A. Monakhov

NUCLEAR ENGINEERING MATERIALS

В. В. Герасимов
А. С. Монахов

ТЕРИАЛЫ ЯДЕРНОЙ
НИКИ

V. Gerasimov
A. Monakhov

NUCLEAR
ENGINEERING
MATERIALS

Translated from
the Russian by
Peter Zabolotny

Contents

Preface

The environment of a nuclear reactor core is characterized by very high pressure, large thermal gradients, and intense nuclear radiation, all of which place very stringent demands on the materials of core components. The behavior of materials subjected to large mechanical and thermal stresses is not a new area of investigation (except possibly to the extremes encountered in modern reactor design), and a great deal is known about the manufacture of high-strength alloys and ceramics which can withstand these stresses. However, the nuclear reactor core subjects materials to an additional demand, that is, one posed by the intensive bombardment by nuclear radiation to which materials in the core are exposed. Over a period of time such radiation can dramatically alter the properties of the materials. For example, metals become brittle and swell, and corrosion enhances. The reactor engineer must be very careful to anticipate such radiation damage in his design, as well as to adopt a sufficient conservative design to compensate for the lack of experience available with behavior of the materials under very high irradiation fluences.

The effects of radiation on reactor materials have become particularly important in today's maturing nuclear reactor industry. In order to achieve the lowest possible power cost, nuclear fuel elements must be used in a reactor as long as possible. Actually the principal limitation on the amount of burnup is not the loss of ^{235}U or ^{239}Pu nuclei through fission but rather the attendant radiation damage to the fuel and the cladding material, which could lead to fuel element failure if the fuel were left in the core too long.

We have attempted to write a reactor materials analysis text more tailored to the needs of the engineering students not specializing in the modern fields of materials technology.

List of Symbols

T_{melt}	Melting point
T_{boil}	Boiling point
ρ	Density
c_p	Specific heat capacity
λ	Thermal conductivity
α	Coefficient of linear expansion
a	Thermal diffusivity
σ_u	Ultimate strength
σ_y	Yield point
δ	Elongation
ε	Deformation
$\dot{\varepsilon}$	Deformation rate
a_i	Impact strength
Φ	Neutron fluence
φ	Neutron flux density
τ	Time
C	Concentration
b	Burger's vector
N	Avogadro's constant

1 | Structural Scheme of Nuclear Power Plant

The heart of any nuclear plant (Fig. 1.1) is reactor *1* incorporating reactor core *15*. Here heat is generated in the nuclear fuel due to the fission process. Coolant *13* transfers heat to steam generator *3* from which heat is transferred to secondary circuit II. Steam produced in the steam generator then goes to steam turbine *4*. Such a nuclear power plant is known as *two-circuit*. Radiation is available in circuit I, whereas in circuit II is not.

In the direct cycle, steam is generated in the reactor core (Fig. 1.2) and goes directly to the turbine. The direct-cycle assembly needs no steam generator. This arrangement is known as *single-circuit*. In the single-circuit system equipment operates under irradiation.

With liquid metals (sodium, for example) utilized as coolants, heat from the coolant (liquid metal) is transferred to the secondary (outside) circuit through an intermediate link. In that case, radiation is available only in circuit I. The intermediate link separates the radioactive primary circuit of liquid metal from the working medium circuit (the steam-water circuit), thus preventing their interaction. Such systems are called *three-circuit* systems (Fig. 1.3).

The heat energy of steam expanding in a steam turbine converts into mechanical energy driving the turbine that in turn drives electric generator *5* to produce electrical power. The steam having left the turbine condensates in condenser *6* because heat is carried away by cooling water. The condensate goes to the steam generator (two- and three-circuit arrangements) or to the reactor (single-circuit arrangement) through a system of low- and high-pressure reheaters *8* and deaerator *9*. Nuclear power plants utilizing gas and organic coolants in the primary circuit operate by the two-circuit scheme.

Depending on the energy of neutrons used to produce the fission chain reaction, the reactors are subdivided into *thermal-* (slow-), *intermediate-* and *fast-neutron reactors* (Table 1.1).

TABLE 1.1 Classification of Neutrons

Neutrons	Slow (thermal)	Intermediate	Fast
Energy, 10^{-19} J	< 1.6	1.6-1600	> 1600
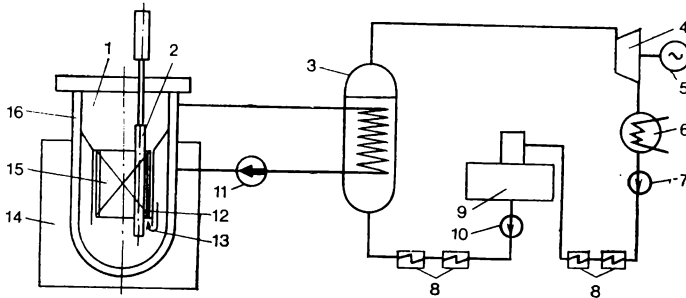
Fig. 1.1 Diagram of two-circuit nuclear power plant with water-cooled and moderated (VVER) reactor

1—reactor; *2*—control and safety rods; *3*—steam generator; *4*—turbine; *5*—electrical generator; *6*—condenser; *7*—condensate pump; *8*—reheaters; *9*—deaerator; *10*—feed pump; *11*—recirculation pump; *12*—neutron reflector; *13*—coolant; *14*—biological shield; *15*—core; *16*—reactor vessel
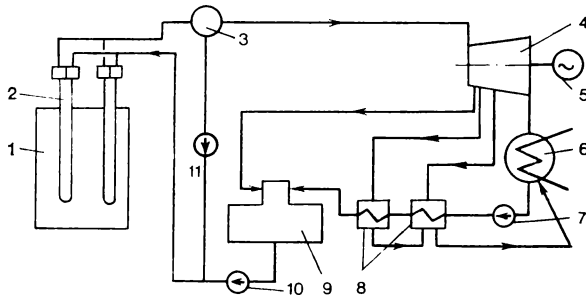
Fig. 1.2 Diagram of single-circuit nuclear power plant with uranium-graphite reactor

1—uranium-graphite reactor; *2*—fuel channel; *3*—drum-separator; *4*—turbine; *5*—electrical generator; *6*—condenser; *7*—condensate pump; *8*—reheaters; *9*—deaerator; *10*—feed pump; *11*—recirculation pump
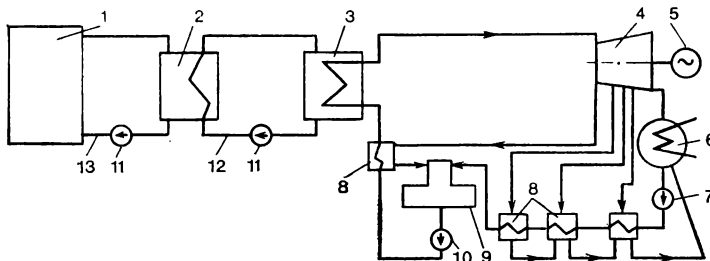
Fig. 1.3 Diagram of three-circuit nuclear power plant

1—reactor; *2*—intermediate heat exchanger; *3*—steam generator; *4*—turbine; *5*—electrical generator; *6*—condenser; *7*—condensate pump; *8*—reheaters; *9*—deaerator; *10*—feed pump; *11*—electromagnetic recirculation pump; *12*—intermediate circuit with nonradioactive coolant; *13*—primary circuit with radioactive coolant

At present, nuclear power engineering in all countries uses thermal-neutron reactors, though the future nuclear power plants will utilize fast-neutron reactors, as they solve the fuel problem. By the fuel distribution in the reactor core, reactors are classified as *homogeneous* and *heterogeneous*. Homogeneous reactors are those in which the fuel is in the form of a homogeneous mass (solution, mixture, suspension, or chemical combination with the moderator or coolant). In heterogeneous reactors, solid fuel in the form of pellets is arranged in fuel elements where fuel is separated from the moderator and coolant by the fuel element clad. All atomic power stations and transportation power units utilize only heterogeneous reactors.

As to the coolant in use, reactors are subdivided into *pressurized water reactors* (PWR), *boiling, heavy-water, gas reactors,* and *reactors with liquid-metal* and *organic coolants.* By the construction configuration, reactors are classified as *vessel-* and *channel*-type reactors. In the vessel-type reactors the core is inside a vessel in which the coolant also performs the function of moderator. In the channel-type reactors the coolant and the moderator are separated. The coolant flows around the fuel elements in many individual fuel element channels (Fig. 1.4).

Mainly used in the USSR are vessel-type PWR (Novovoronezhsk, Kolsk, Armenian atomic power stations, and others) and channel-type graphite-moderated high energy boiling-water reactors (BWR) (Leningrad, Kursk, Chernobylsk atomic power stations and others).

Reactors may also be classified by their application: electrical power generation, heat generation, fuel breeding, etc. The classification is somewhat conventional. Hence, the reactor shown in Fig. 1.1 may be classified as a vessel-type pressurized-water heterogeneous thermal-neutron reactor.

Nuclear fuel in the form of assembled fuel elements (Fig. 1.5) is loaded into the reactor core. In the thermal-neutron reactors, moderators slow down fast neutrons to the level of thermal neutrons to sustain chain reaction. Fast-neutron reactors have no moderators.

A number of fast-neutron pilot reactors, the БОР series, and an industrial nuclear power plant, the БН-350 series (sodium-cooled reactor), are now in operation in this country. A more powerful plant utilizing fast neutrons, the БН-600 series, has been built.

Only three radionuclides, ^{235}U, ^{233}U, ^{239}Pu, can be utilized as nuclear fuel. Naturally occurring uranium contains 0.71% of ^{235}U, or 7.1 kg per one ton; balance being essentially ^{238}U. Fissible nuclides ^{233}U and ^{239}Pu are obtained from ^{232}Th and ^{238}U, respectively. ^{233}U and ^{239}Pu are known as secondary nuclear fuels.

To reduce the reactor core volume and thus its external dimensions, the amount of fissile nuclides (^{235}U, ^{233}U, ^{239}Pu) in the fuel mixture is increased, i.e. use is made of an enriched fuel. Enrichment of fuel highly increases its cost.
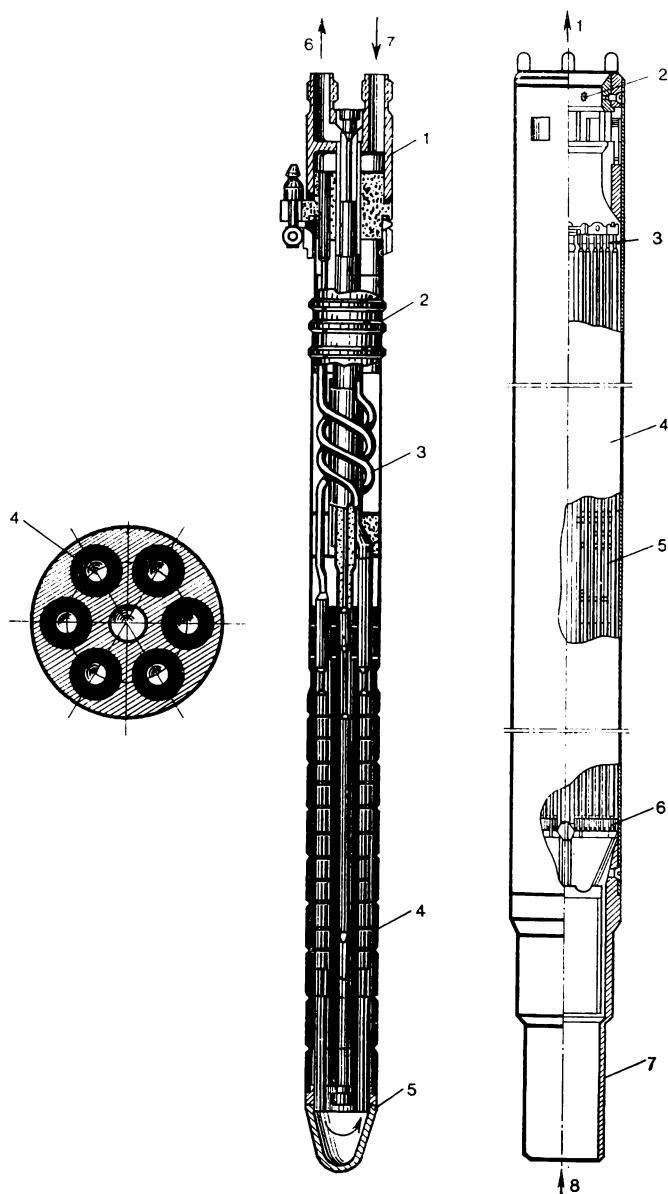
Fig. 1.4 Fuel channel of uranium-graphite reactor, Beloyarsk Atomic Power Station

1—top end cap; *2*—sealing rings; *3*—expansion compensator; *4*—fuel element; *5*—bottom end cap; *6*—coolant outlet; *7*—coolant inlet

Fig. 1.5 Fuel assembly for water-cooled and moderated reactors

1—coolant outlet; *2*—assembly top cap; *3*—hold-down grid; *4*—assembly container; *5*—fuel element; *6*—lower grid; *7*—lower end cap; *8*—coolant inlet

Fuel elements 6-14 mm in diameter are combined into fuel assemblies. Figure 1.5 shows a fuel element assembly for a PWR. Fuel elements are devices containing solid nuclear fuel and providing, when placed in the reactor core, a chain fission reaction, heat energy generation, and breeding of isotopes ^{233}U and ^{239}Pu when the elements include breeders. Generally a fuel element comprises a tube containing pellets of nuclear fuel, end caps, and expansion springs.

Depending on the type of nuclear fuel the fuel elements are classified as based on metallic fuel, with ceramic fuel and dispersion-type.

As to the shape, the fuel elements are cylindrical, tubular, plate, ball-like, and also more intricate in configuration: available in the form of blocks with holes for coolant flow, twisted tapes and the like.

The purpose of the fuel element cladding is to isolate the nuclear fuel from the coolant to prevent its contamination with particles of nuclear fuel and fission products. The end caps seal the fuel in the cladding tube and, together with the expansion springs, serve to secure the fuel elements in operation in the required position.

To slow down neutrons in the thermal neutron reactors use is made of low-atomic-weight materials. Typical moderators include light water, heavy water, graphite, beryllium, beryllium oxide, and certain organic liquids.

To prevent leakage of neutrons outside the core, the latter is surrounded by a reflector of leaking neutrons. Reflectors are made of the same materials as the moderators.

The fission heat is carried away by the following coolants: light water (with and without boiling in the reactor), heavy water, gases (carbon dioxide, nitrogen, hellium, hydrogen and their mixtures), liquid metals (sodium, potassium, bismuth, lead, mercury) and organic liquids (an example is a diphenyl mixture).

The reactor power is regulated by varying the amount of neutron absorbing material inserted into the reactor core. Such materials are usually inserted into the reactor core in the form of rods having different profile, or may be introduced as the absorbing additives to the fuel and to the structural materials of the reactor core. Use is also made of "mild" regulation. If that is the case the neutron absorbing material circulates as a solution either with the coolant or in an individual loop. The material may be boric acid, cadmium salts, etc. The "mild" regulation is obligatory for water-cooled and water-moderated power reactors. This causes radiolysis, corrossion attack on structural materials and control of absorber concentration.

The scram control of a reactor is accomplished by means of scram control rods. The construction and requirements imposed on the material of such rods are the same as those for the control rods. Used as the materials for control rods and scram control system are

materials including B, Cd, Hf, In, Ag, Eu, Gd, and Sm well absorb-
ing neutrons.

The pressure vessel of powerful reactors has impressive size (up
to 4 m in diameter and up to 12 m in height). The vessel operating
at high coolant pressure and temperature cannot be fabricated of
the stainless austenitic steels because of their low strength.

Reactor pressure vessels are made of steels 48TC, 1X18H10T*
(for vessels of small diameters). When a reactor vessel is fabricated
of perlitic steel, then in order to decrease corrosion products giving
off to the coolant and also to reduce the hydrogen absorption by
the vessel, which affects its ductility, its inner surfaces are built up
with austenitic stainless steel. In place of metallic building up the
vessel, material resistance to corrosion can be increased by forming
a protective oxide film on its surface (an example is treating the
surface with complexones or by other techniques).

The reactor vessel operates under high pressure and temperature
of the coolant, intense nuclear radiation (no visual inspection of the
vessel material in service), and high speed of the coolant which,
though very pure, is a corrosive medium. To reduce the radiation
effect on the reactor vessel, the reactor core is surrounded by a cylind-
rical shroud made of corrosion-resistant steel.

The steam generator vessel and other vessels used by nuclear power
plants are fabricated of steels 22K, 15XM, 16ГHM, and steel 20.

The amount of coolant circulating in the reactor core is large, as
the water in the reactor is heated, but not to a high temperature
(293-308 K). Therefore it is circulated in the primary circuit through
several (from 2 to 8) loops. Even with such a number of loops, the re-
sultant diameter of the circulation tubes is large (up to 850 mm).
With a view to reducing the ingress of corrosion products in the
coolant, the circulation tubes are made either of austenitic stainless
steels or of perlitic steels with internal building-up of corrosion-re-
sistant steel. The heating surface of steam generators is also formed
by many stainless steel tubes from 10 to 24 mm in diameter. Sub-
stituting carbon steels for austenitic in the reactor circuits repre-
sents one of the problems facing the nuclear power technology.

The heat exchange in the steam generator (as the case is in the
reactor) is mainly convective and is accomplished at small tempe-
rature gradients (from 288 to 293 K). Therefore the heating surface
is formed by a great number of small diameter tubes. To arrange
them in a more compact manner, the tubes are arranged at a close
spacing. The steam generators of modern powerful nuclear power
plants (atomic power stations) represent unique large units (Fig. 1.6)
with a vessel of considerable size (up to 4 m in diameter and up to

* For the composition of the Soviet-made steels and alloys refer to Chs 8
and 9.

15 m long). The steam generator connects the primary and secondary circuits. Therefore very stringent leakage requirements are imposed on it.

The elements of the secondary circuit equipment are almost the same as in the case of fossil-fuelled power plants. Perlitic steels are used for the steam tubing from the steam generator to the turbine and condensate-feed tubing from the condenser to the steam generator. The heating surfaces of the condenser and low-pressure reheaters installed on the condensate route are fabricated of corrosion-resistant materials such as brass, stainless steels, nickel silver, nickel alloys, since they operate in a very corrosive environment. The heating surfaces of high-pressure reheaters (found on the feed route) are made of carbon steels.

In single-circuit atomic power plants, the heating surfaces of reheaters may not be made of alloys containing copper, as cuprous sediments are not tolerable in a reactor.

A specific feature to the nuclear power plants is in that their materials are exposed to intensive bombardment by nuclear radiation. Protection against the neutron radiation is by the use of materials well moderating and absorbing neutrons. Protection against γ-radiation is by materials containing heavy elements. Therefore the protection against radiation is

Fig. 1.6 Steam generator of vertical type

1 — steam outlet; 2 — separating devices; 3 — feedwater inlet; 4 — vessel; 5 — upper tube plate; 6 — tubes of heat exchanging surface; 7 — lower tube plate; 8 — coolant inlet; 9 — coolant outlet

achieved by the use of light water, concretes with various additives (heavy concrete, colemanite, Portland cement, barium cement and the like) and also metals (Pb, Fe and others).

All nuclear power units now in service utilize the fission energy of nuclear fuel. However, energy released by nuclear fusion may be
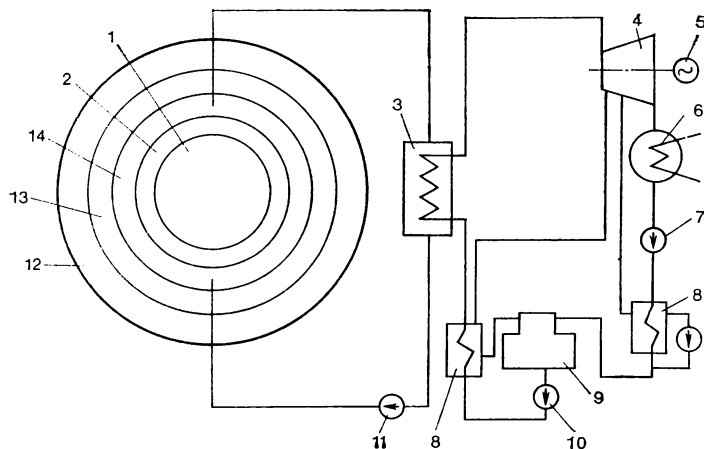
Fig. 1.7 Diagram of thermonuclear power plant of the Tokmak type
1 — vacuum chamber; *2* — vacuum wall; *3* — steam generator; *4* — turbine; *5* — electrical generator; *6* — condenser; *7* — condensate pump; *8* — reheaters; *9* — deaerator; *10* — feed pump; *11* — recirculation pump; *12* — radiation

utilized as well. The units employing this method are known as *thermonuclear*. The following nuclear fusion reaction may take place in the reactors of these units:

$$_1^2D + _1^3T \rightarrow _2^4He + _0^1n + 17.6 \text{ MeV}, \qquad (1.1)$$

where $_1^2D$ = deuterium and $_1^3T$ = tritium.

Released in that are neutrons with energy of 14 MeV and free energy of 17.6 MeV.

The thermonuclear power plant using reaction (1.1) is very difficult to be created. The high-energy neutrons in the products of this reaction predetermine in the first stage of developing thermonuclear reactors a symbiosis: fusion plus fission, i.e. the thermonuclear neutrons will produce ^{239}Pu from ^{238}U which is a fertilized fissible isotope for ordinary nuclear reactors.

The most studied at present are hybrid thermonuclear plants, type Tokmak. They underlie the development of a series of projects of hybrid thermonuclear power plants with a steam-generator cycle of converting the nuclei fusion and fission energy into electrical power. A version of a hybrid thermonuclear power plant with a standard turbine in use is shown in Fig. 1.7. Heating of plasma and nuclear fusion (1.1) take place in vacuum chamber *1*. The plasma formation and confinement are performed by a superconducting electromagnetic system with the aid of an eddy electric field. The blanket surrounding the vacuum chamber is comprised of vacuum wall *2*, zone of neutron

energy conversion and plutonium production *14*, zone of tritium re-
production *13*, and radiation shield *12*.

The thermal capacity of the hybrid reactor is 6650 MW. The sta-
tion consumes about 40 kg of tritium and produces as much as 4200 kg
of plutonium per year. The fuel elements of the plutonium production
zone are ball-like in shape. A uranium-molybdenum alloy with molyb-
denum cladding is used as a fuel.

TABLE 1.2 Structural Materials Used in Nuclear Engineering and Fields
of Their Application

Material	Application	Highest operating temperature, K
Austenitic stainless steels	Fuel element clads, fuel element channels, primary circuit tubing, steam generator surface, pumps	973
Perlitic low-alloy steels	Superheated steam tubing of single-circuit reactor plants, steam generators and reactor pressure-vessels	773
Carbon steels	Saturated steam tubing of single- and two-circuit reactor plants, tubing of condensate-feed system	623
Boron stainless steels	Rods of the control and safety system	873
Zirconium alloys	Fuel element clads, fuel element assemblies and fuel element channels of water- and liquid metal-cooled reactors	673
Aluminum alloys	Fuel element clads and fuel element channels of water-cooled reactors	523
Magnetic alloys	Fuel element clads cooled by carbon dioxide	673
Titanium alloys	Steam generator heating surface of water-cooled reactors	673
Nickel alloys	Intermediate heat exchangers with liquid-metal coolants, heating surface of steam generators and reheaters	1073
Low-melting metals and their alloys	Fuel element clads and other components of the primary circuit	1273-1773
Copper alloys	Heating surfaces of reheaters, condensers and auxiliary heat exchangers	473

In thermonuclear reactors, the material of the first wall is operating under the most severe conditions. It is subjected to the effect of high-energy fluences, helium, hydrogen and tritium nuclear fluences, and also of protons and electrons. The service life of the first wall must be sufficiently long, since its replacement is very difficult and calls for engineering automatic control mechanisms (robots). To this end use must be made of radio engineering, electrical engineering and electrical insulation materials resistant to ionizing radiation. Certain requirements are imposed on materials operating at cryogenic temperatures with concurrent action of ionizing radiation fluences.

Given in Table 1.2 are structural materials employed in nuclear engineering and their applications.

2

Requirements Imposed on Reactor Materials

2.1 General

The capital investment required for the construction of nuclear power plants is usually greater than that required for conventional fossil-fuelled power plants of the same power output. This is accounted for by higher costs of the materials utilized in the construction of the first nuclear power plants. A modern nuclear power plant represents a complicated engineering installation. The materials utilized in nuclear power plants are exposed to very severe environmental conditions. Nuclear power plants can be widely implemented into the national economy, provided they can compete with conventional fossil-fuelled power plants. Like conventional power engineering nuclear power engineering is known for the growth of unit power of blocks and power of the main and auxiliary equipment. Designing new nuclear power plants that meet modern demands for power, economy and reliability continuously impose new stringent requirements on reactor materials.

Nuclear superheating of steam was first carried out in this country at the Beloyarsk Nuclear Power Plant after I. V. Kurchatov. This called for creating materials capable of operating under radiation conditions at 783 K. In high-temperature gas-cooled reactors, as well as in liquid-metal cooled fast neutron reactors the materials are also exposed to high temperatures. Nuclear engines and thermonuclear power plants will call for materials capable of operating at temperatures up to 3273 K.

The materials in use must ensure the structural strength of the nuclear power plant components, i.e. must be *strong*, *ductile* and capable in certain cases of operating under *high dynamic stresses*. The materials must lend themselves to *machining*; be easily forged, cut, rolled, and welded. Mechanical properties of the materials must not change during prolonged service at high temperatures, or when the mechanical stresses acting on the material vary in value and direction. Certain materials are subject to vibration. Therefore, they must not suffer from fatigue, small-cycle fatigue including, and must possess high cyclic strength.

The structural components of nuclear power plants, especially fuel elements, fuel element channels, control system rods and safety rods, must hold their shape. The core materials are subject to severe

radiation which may affect their properties: the materials become brittle and lose shape. Therefore, the reactor materials must have *high radiation stability*.

In operation the reactor materials contact coolants which may contain corrosive impurities. Moreover, coolants themselves, though very pure, are corrosive. This causes corrosion, erosion, and cavitation of materials. Hydrogen liberated in corrosion may dissolve in the material and cause its embrittlement. Hence, another requirement imposed on materials is their *corrosion resistance*.

The material of nuclear fuel element can is subject to still more severe conditions. When in service it contacts nuclear fuel for a prolonged period of time at high temperatures. Their interaction may ruin the clads of fuel elements. This generates one more requirement, *compatibility*.

Nuclear power engineering imposes special requirements on the physical properties of materials. Nuclear fuel must ensure *high heat liberation* and *high burnup*, and must be very *radiation-stable*.

In the thermal-neutron reactors, structural materials must have a *small thermal neutron absorption cross section*, otherwise the neutron balance in the core becomes disturbed and the nuclear reaction may terminate. To carry out and sustain a chain reaction, a more enriched fuel should be used, the result being a higher fuel cost. This places stringent *purity demands* on the reactor core materials. The content of impurities with a large neutron absorption cross section in these materials must be kept to a minimum.

In addition, the moderator and reflector materials must *effectively slow down the fast neutrons*. The control and safety reactor systems employ materials with a large neutron absorption cross section. It is advisable that the reactor materials be only weakly activated in a neutron flux. This especially concerns the core materials. Radionuclides of corrosion products accumulate in the reactor circuit and hinder its servicing. Radionuclides of a large half-life, cobalt in particular, are especially objectionable. Nickel used to alloy the steel contains minute quantities of cobalt.

Particular requirements are imposed on the thermophysical characteristics of the materials. The *coefficient of thermal expansion* must be the lowest. Compensation of heat stresses generated by thermal expansion of materials causes certain difficulties in designing nuclear power plants.

Another important characteristic of reactor materials is *thermal conductivity*. Low thermal conductivity accounts for a large temperature gradient across the material. In ceramic nuclear fuel, this may result in melting of the fuel element centre and also causes thermal stresses dangerous to the structure integrity. A low heat conductivity of a material greatly increases the size of heat exchangers, which is objectionable in the transportation power plants.

In a number of cases the reactor materials must be *gas tight*. The gaseous fission fragments may penetrate through the fuel element cladding and increase the coolant activity. The gaseous fragments penetrating through the tubing wall and also coolant leaks increase radiation and thus hinder operation and maintenance of the nuclear power plant. Naturally, we mean gas migration through the parent metal rather than through defective welded joints.

The cost of materials of nuclear power plant equipment is also of great importance It tells on the cost of electrical power and economic advantages of nuclear power plants over conventional sources of electrical power. Thus, substituting perlitic steel for stainless austenitic steel in the reactor circuits and condensate-feed system of single-circuit atomic power stations of the RBMK series saves several dozen million roubles.

Given below are the requirements imposed on the reactor materials depending on what reactor components are made of them.

2.2 Requirements Imposed on Reactor Core Materials

Fuel Element Clads. The clads of fuel elements operate under the most severe conditions in the reactor core. To reduce neutron absorption, the fuel element clads are made of minimum thickness. During the service the clad material may be subjected to distortion by radiation damage to the nuclear fuel. Great temperature gradients generate thermal stresses in the clad. The clad material must withstand thermal cycles, resist corrosion in the coolant, and be compatible with the fuel at operating temperatures. Being in the core, the clad material is exposed to radiation. This may affect its physical and mechanical properties.

Situated in the reactor core are the parts fastening the fuel elements, and also the fuel element channels. These components may experience appreciable mechanical loads, hydraulic shocks, erosion and corrosion. Nevertheless, they operate under conditions not so severe as those of the fuel element clads. Any material suitable for fabrication of the fuel element clads fits for other structural components of the core.

Of various requirements imposed on the material of the fuel element cladding the most essential are:

(1) Minimum neutron absorption cross section.

(2) Mechanical dependability, permanent shape and size of clads and thus of fuel elements as a whole.

(3) High thermal conductivity providing heat transfer for a prolonged period of time without causing excessive thermal stresses in the clad.

(4) High resistance to erosion and corrosion in the coolant.

(5) Compatibility with the nuclear fuel.

When defining the requirements for the fuel element clads, take into account specific features of a given reactor. When natural uranium is used as a fuel, minimum neutron absorption becomes the most important requirement. In the case of enriched fuel, the fuel element clads may have a higher neutron absorption cross section, stainless steel is an example.

High thermal conductivity combined with dependable cooling of the fuel element clads with all types of coolants ensure trouble-free and safe operation of the reactor. High conductivity of the clad material and cladding layers contacting the nuclear fuel is necessary to reduce the temperature difference between the coolant, fuel element clad and fuel. A temperature gradient in the clad may cause thermal stresses reaching several megapascals.

With fuel element clads operating at 773 K and more, the strength characteristics of material become important. The clads must be made of high-temperature-strength materials.

In the boiling water reactor, impurities concentrate on the surface of the fuel element, and this enhances the corrosive action of water. The cladding material must resist corrosion, especially local attack, such as pitting or stress corrosion. The corrosion- and erosion-resistance of the cladding and its compatibility with nuclear fuel present the most complicated and important problem of operating nuclear reactors. Corrosion takes place at high temperatures, high speeds of coolant flow, large heat flows, and mechanical strains in a metal. Radiation changes the metal properties and coolant composition and this aggravates the situation.

To assess the mechanical reliability of the clad, the most important are the following characteristics of the material: strength and ductility in short-term tests, long-term strength and creep-resistance, fatigue limit at operating temperatures, and stability of the cladding size following cyclic temperature changes. Radiation variations of these characteristics must be known as well.

In order to obtain the necessary information on the material properties under service conditions, one has to carry out complicated, long-term expensive tests, including tests directly in the reactor.

Trouble-free operation of a channel-type reactor largely depends on the performance of the channels. Damage to a channel wall due to corrosion, erosion, or cavitation admits coolant to the graphite blockwork. This essentially changes the neutron balance in the reactor and disturbs its normal performance. Creep of the material distorts the shape of a channel and it gets stuck in the graphite blockwork. This hinders the replacement of the fuel element channels in recharging the reactor.

Creep itself leads to channel damage. The channel material must not undergo hydrogenation, for it causes brittle failure. The material to fabricate the fuel element channels and channels of control and

safety system must possess high strength and be highly creep-, corrosion- and erosion-resistant and free from embrittlement.

Neutron Moderator and Reflector. The moderating and reflecting material should contain the lowest possible amount of impurities, especially elements with a large neutron absorption cross section. In graphite moderated reactors, radiation swelling or contraction of graphite blocks and bushings hinders the channel replacement. This places high radiation- and oxidation-resistance demands on graphite. Fairly important for the reactor physics are the graphite density and purity.

Absorbing Materials of the Control and Safety System. The absorbing materials must have a large thermal neutron absorption cross section. Thermal neutron reactors utilize nearly black rods. Generally, a body is known as "black" for thermal neutrons, if the thermal neutron absorption cross section is far larger than the scattering cross section.

In certain cases epithermal neutrons are to be absorbed. For example, hafnium is referred to as "black" near the absorption resonances at 1, 1.2, 2.38 and 7.8 eV. Like hafnium, most of epithermal absorbers are of a resonance type. To improve the efficiency of a control rod it is made of a mixture of absorbers selected so that the resonance maxima of one absorber lie inbetween the resonance maxima of another. Examples are alloys of Cd, Ag, In and mixtures of rare earth elements. Neutron absorption results in energy release and the rods heat up. In the absorbers where the (n, α) reaction proceeds (among which is B) all the energy is practically released in the control rod. In the absorbers where the (n, γ) reaction occurs much of the energy together with γ-radiation is carried away from the rod. In both cases in water-cooled and moderated reactors having a high density of energy release, the amount of heat generated in the rods may be very high. This necessitates cooling of the rods. When the rods are provided with cladding, a good thermal contact must be ensured between the absorber material and cladding for heat to be transferred through the cladding.

The efficiency of the rods in an operating reactor changes with time. Gradually, as the nuclear reactions proceed, a considerable number of nuclei of the absorbing material decay. The efficiency of the rods varies only little in the case of the absorbing nuclide burnup. This takes place when the product of a nuclear reaction in a rod is a stable long-lived nuclide with a large absorption cross section. Classed with these materials are dysprosium and europium.

The control and safety system materials must possess a large neutron absorption cross section and in certain cases within a wide spectrum of neutron energies. The materials must be radiation-stable.

A change in the geometry of the absorbing material may render the control and safety system inoperative. From the standpoint of

economy it is good practice to use uncooled channels of the control and safety system. Therefore, the absorbing element and its cladding must possess high-temperature strength and resist corrosion at high temperatures.

Metalwork in Channel-type Reactors. In the channel-type graphite-moderated reactors, core equipment operates at high temperatures under intensive radiation. Therefore, it should be heat- and radiation-stable.

In water-cooled and moderated reactors, the coolant exercises corrosive and erosive influence. Therefore, the structural materials must be corrosion- and erosion-resistant with a small neutron absorption cross section.

Reactor Pressure Vessel. The reactor pressure vessel and top dome are subjected in operation to mechanical stresses from overpressure in the reactor, thermal stresses at stationary and in particular at nonstationary operating temperatures, vibration stresses and additionally shock stresses in transportation units. Being exposed to all types of radiation the vessel material must be highly strong and sufficiently ductile. The irradiation of the reactor vessel during the entire service life (up to 30 years) must cause no embrittlement of the material. In view of this a high radiation requirement is imposed on the vessel material. The vessel material must have high thermal conductivity and low coefficient of thermal expansion to prevent high temperature stresses. It must also be resistant to small-cycle fatigue.

The vessel material must be resistant to corrosion. Contamination of the coolant with radioactive products of corrosion impairs the radiation situation and hinders the equipment maintenance and repair. Local corrosion may generate stress concentrators in the metal and make its ruin more possible. Hydrogenation combined with irradiation may cause embrittlement of the vessel material. To reduce corrosion in the pressure vessel, its inner surface is built up to a thickness of 8-12 mm with corrosion-resistant material. This also decreases the pressure vessel hydrogenation.

The vessel material must be well workable and weldable in large thicknesses. High local stresses in welded joints call for subsequent thermal treatment. Thermal treatment of large pressure vessels is a serious problem.

It is worth mentioning here that high strength of the pressure vessel material allows the vessel mass and size to be reduced, which is of utmost importance in many cases.

2.3 Requirements Imposed on Materials of Components Outside the Core

The essential components operating outside the core of water-cooled and water-moderated reactor are the main circulation tube lines, steam generators, pumps and auxiliary reactor systems. In the case of single-circuit BWR also included in the assembly are a turbine and a condensate-feed system.

Materials of *tube lines* and *steam lines* must be strong and must resist brittle fracture. The tubing and piping materials (their surface is generally large) must resist corrosion. Corrosion products absorbed by a coolant increase radiation. They can also deposit on the surface of fuel elements.

The speed of flow in the tube lines is high, up to 10 m/s, and in the circulation pumps it is still higher. The pump parts must be made of materials resistant not only to corrosion but also to erosion and cavitation. The same requirements are imposed on materials for fittings and accessories.

The *drum-separators* of large atomic power stations with a channel-type BWR are fairly large (up to 20 m long and 2.5 m in diameter). Many tube nozzles are welded to the drum shell. This places high strength requirements on the material at the sufficient levels of ductility, resistance to small cycle fatigue, workability, and resistance to corrosion.

2.4 Materials Utilized in Reactor Engineering

Structural materials used in reactor engineering are represented by metals and their alloys. This is because alloys of metals are known for high strength combined with sufficient ductility and strain hardening.

The metallurgy of metal and alloy production and treatment is well mastered. Machining of metals and alloys by cutting and pressing, forging, stamping, rolling is widely used in industry. Diverse methods of welding are adequately mastered.

Pure metals are not widely used in nuclear power engineering. They are applied when high ductility is required and no impurities are tolerable. Nickel and copper of high purity are used as materials for gaskets and washers. Clads of fuel elements in research reactors are made of highly pure aluminum. Pure beryllium is used as the moderator and reflector material. Aluminum of industrial purity (content of impurities not in excess of 0.5%) is used to fabricate research reactor tanks and a number of reactor core components.

Generally reactor engineering employs metal alloys. Thus, aluminum-based alloys are used for making fuel element clads and fuel channels of water-cooled reactors for producing plutonium, and for making channels of the control and safety systems of the channel-

type BWRs. The highest operating temperature at which aluminum alloys may be used together with water coolant is 523 K. At higher temperatures the existing alloys of aluminum do not withstand corrosion.

In carbon-dioxide-cooled reactors the fuel element clads are fabricated of magnesium alloys (alloys, type magnox). Their low high-temperature strength and resistance to corrosion limit the operating temperatures to 673 K. When operating at higher temperatures the fuel element clads must be made of stainless austenitic steel with the use of enriched nuclear fuel.

Zirconium alloys are used for making fuel element clads of water-cooled reactors and fuel channels of channel-type boiling reactors. The maximum permissible temperature of 623 K is limited by the corrosion resistance of zirconium alloys and their creep. The Al, Mg, Zr based materials are machinable and have a small absorption cross section and, consequently, are widely used in reactor cores. The iron based alloys have found wide application in reactor engineering. Note first the austenitic stainless steels. Their wide use should be attributed to their high resistance to corrosion in different coolants, high-temperature strength, and machinability. With enriched nuclear fuel, the austenitic stainless steels are used for manufacturing fuel element clads, channels and other core equipment, and also for plating (surface building up) of reactor pressure vessels, drum-separator shells, circulation pipework made of large-diameter tubes of low-alloy steels. Outside the core the austenitic steels serve to manufacture the pipework of the primary circuit (up to diameter of 550 mm), steam generators, heat exchangers, tube lines of condensate-feed and recirculating water systems, circulation pumps and fittings. The maximum operating temperature of 973 K is limited by high-temperature strength of austenitic stainless steels.

Perlitic low-alloy steels are used for fabricating steam generator shells of water-cooled and moderated reactors, superheated steam pipes, drum-separators, and heat exchangers. Along with carbon steels, they are utilized as materials for superheated steam pipes and pipe lines for condensate-feed system.

As has been demonstrated recently, low-alloyed and carbon steels are used to manufacture recirculation loop and condensate-feed system of boiling reactors. They are less resistant to corrosion. Their use, however, in water-cooled reactors has become possible because of the strict observance of the water cooling specifications and thorough changing of the coolant of corrosion products. Metal structures of the channel-type reactors are made of perlitic steels. The top temperature limit of using low-alloyed steels (773 K) and carbon steels (623 K) is dictated by their high-temperature strength. These steels are machinable and fairly cheap.

Nickel- and titanium-base alloys are used for making steam gene-

rators and heat exchangers when a need arises for materials resistant to corrosion and stress corrosion. Nickel alloys are used to manufacture heat exchangers of reactors cooled by liquid sodium. The maximum operating temperatures are 673 K for titanium alloys and 1073 K for nickel alloys. Their corrosion-resistance is high. A large neutron absorption cross section makes their use in the core of thermal neutron reactors objectionable. Use of titanium alloys in certain cases is dictated by their low specific gravity.

In space nuclear engines, thermoelectric and thermoemissive converters, materials operate at a temperature up to 3273 K. Used under such conditions are high melting metals (W, Mo, Nb) and their alloys. They are used for fuel element clads and core components. They exhibit great high-temperature strength and are compatible with nuclear fuel. Tungsten and molybdenum, however, are insufficiently machinable and embrittle at temperatures relatively low as compared with their melting point.

Copper alloys having good thermal conductivity are used for making pipe stills of condensers and heat exchangers. A drawback of these alloys is their low corrosion-resistance at high speed of medium, especially sea water. Besides, corrosion products of copper alloys promote coolant activation and deposit on fuel elements.

Graphite, a nonmetallic structural material should be considered separately. Graphite is used to make brickwork in channel-type reactors. To prevent graphite burnup the graphite brickwork is blown through with nitrogen or helium deprived of oxygen. The content of impurities with a large neutron absorption cross section in graphite should be minimized. An essential drawback of graphite is that it changes size and shape subjected to radiation and high temperature.

In space nuclear engines and high-temperature gas-cooled reactors, graphite is used as a structural material for fuel element matrices. Graphite also is well suited for high-temperature operations (up to 2273 K and above).

Nonmetallic compounds of uranium are mostly utilized as nuclear fuel. Pure uranium serve, for example, to make fuel element rods of plutonium production reactors.

In fast neutron reactors, along with uranium dioxide, use is made of uranium alloys. A drawback of uranium and a number of its alloys is their low radiation stability. When the fuel element clad leaks, low corrosion-resistance of uranium in water at high temperatures leads to swelling of the block, impairing the heat yield, and finally to emergency situation.

Nuclear fuel is generally used in the form of uranium compounds: intermetallic compounds, oxides, carbides, nitrides, etc. They can operate at high temperatures and are, as a rule, radiation stable. Low thermal conductivity should be mentioned among the drawbacks of some of these compounds, uranium dioxide, for example.

3

Strength, Compatibility, and Radiation Stability of Reactor Materials

When in service the reactor materials, in particular the core materials, are subjected to high mechanical loads and radiation at temperatures up to 800 K and higher. Trouble-free operation of nuclear power plants may be provided only by reactor structural materials featuring high strength, high-temperature strength. and sufficient radiation stability. Materials of fuel element clads must be compatible with the nuclear fuel.

To properly choose the materials one should know how their properties vary during the service life of nuclear power plants. Solution of this problem and improvement of the above-mentioned characteristics of the materials are one of the main tasks of the reactor material engineering.

The properties of metals and alloys are essentially dependent on the defects of crystal lattice. The ability of metals to withstand mechanical loads, radiation stability, and compatibility are determined by point and linear defects of crystal lattice. Soviet scientists Ya. I. Frenkel, A. A. Bochvar, S. T. Konobeevskiy, A. S. Zaimovskiy, and others have shown that properties of metals and alloys depend on crystal lattice defects.

The progress of Soviet material engineering makes it possible in certain cases to evaluate quantitatively the effect of service factors on material properties and predict material characteristics on the basis of data on material composition and structure. This can be achieved only when one gains a deep insight into the nature and properties of the metal lattice defects.

3.1 Defects of Crystal Lattice

The structure and properties of the crystal lattice determine to a great degree the properties of metals and alloys. The crystal lattice of metals and alloys is a regular periodically repeated three-dimensional array of metal atoms. Departures from regularity are known as defects and they can be classified in two types: *point* defects and *line* defects.

Point Defects. Those are vacancies and interstitials. *Vacancies* are vacant lattice sites and *interstitials* are atoms that

are not in a normal lattice position. The formation of a point defect leads to lattice distortion, affects the periodicity of the array of atoms in the lattice, and finally changes the metal structure and properties.

Now we think it necessary to consider how vacancies arise. After receiving additional energy an atom located in a crystal lattice site breaks its links with the neighboring atoms and moves into an interstitial site to form an interstitial atom. The energy of binding to neighboring atoms is characterized by the crystal lattice energy E_{cr} equal in value and opposite in sign to the energy released in forming a crystal lattice of individual atoms not bonded to one another. This energy is expressed either in kilojoules per mole, or in electron volts per atom. In metals of technical importance, the energy of crystal lattice is close to 420 kJ/mole. According to Eyring's rule, the activation energy of a process, i.e. the value of the energy barrier the atom has to overcome during a process, is 1/4 of the energy of the bond to be broken to realize the process. The activation energy producing a vacancy $Q_v = 0.25E_{cr} \approx 1$ eV ≈ 100 kJ/mole.

In crystal lattice the atom energy is on the average close to kT or RT. There is, however, a finite probability that the atom will have at a certain moment an energy equal to Q. This energy will be imparted to the atom owing to energy fluctuation known as the thermal fluctuation. According to the Boltzmann distribution the probability that an atom receives energy Q in thermal fluctuation is as follows: $W = \exp(-Q/RT)$. The probability of a vacancy formation at room temperature is:

$$W_v = \exp(Q_v/RT) = \exp(-E_b/4RT)$$
$$\approx 10^{(-420/4 \cdot 2.3 \cdot 8.27 \cdot 0.298)} \approx 3 \cdot 10^{-19}.$$

One cubic centimeter of iron contains vacancies:

$$n = (d/A)NW = (7.8/56) \cdot 6.03 \cdot 10^{23} \cdot 3 \cdot 10^{-19} \approx 2.5 \cdot 10^4,$$

where d is the density; A is the atomic weight; N is the Avogadro number.

Vacancies may form in another way. An atom of the surface layer of a metal in evaporation may not break away from the crystal but rather move to its surface, thus beginning the formation of a new surface layer. His site may be occupied by one of the neighboring atoms of the same layer or an atom from an internal layer. Thus, a vacancy is formed without making an atom take up an interstitial site (Fig. 3.1). Vacancies can migrate into the bulk of metal. Accidental collisions of individual vacancies may unite them into pairs (divacancies). Their total surface decreases and the gain in the surface energy ensures the stability of a divacancy. However, most vacancies in pure metals in the state of thermal equilibrium are mono-
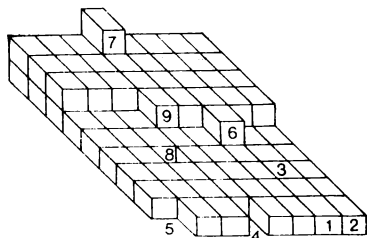
Fig. 3.1 Positions of atom on crystal surface

1 — complete edge; *2* — complete corner; *3* — complete surface; *4* — incomplete edge; *5* — incomplete corner; *6* — step; *7* — adsorbed atom; *8* — vacant site; *9* — semicrystalline atom

vacancies. A vacancy aggregate may lead to the formation of submicroscopic pores.

Interstitials occupy octahedral and tetrahedral interstitial sites (Fig. 3.2).

In the body-centred cubic lattice (BCC), the radii of the largest balls that can be arranged in octahedral and tetrahedral sites without distorting the lattice are $r_6 = 0.115R$ and $r_4 = 0.291R$, respectively (R is the metal radius). With the face-centred cubic (FCC) and hexagonal close-packed (HCP) lattices, the corresponding radii are $r_6 = 0.414R$ and $r_4 = 0.225R$.

In HCP lattices the volume of the octahedral interstitial sites is greater than that in BCC lattices. However, the total volume of voids in BBC lattice is greater than that in FCC and HCP lattices, because these types of crystal lattices differ in the number of interstitial sites proper. The BCC lattice has three octahedral and six tetrahedral interstitials per each atom, while the HCP lattice has one octahedral and two tetrahedral interstitials per atom.

In the octahedral interstitial site, six atoms surround an atom, while in the tetrahedral interstitial site it has only four neighbors. The atomic radius depends on the coordination number:

Coordination number	12	8	6	4	3	1
Relative atomic radius	1	0.97	0.96	0.88	0.82	0.72

The covalent radii r (coordination number 1) for a series of interstitial atoms are as follows:

	H	C	N	O
r, nm	0.028	0.077	0.070	0.066

Experimentally the radius of interstitial atoms is determined by the size of the lattice unit cell of one or another metal by dissolving in this metal a certain quantity of an element forming interstitial atoms. Introduction of interstitials in interstitial sites distorts the crystal lattice and its energy increases. This affects the rate of many processes, such as diffusion, dissolution, etc.

Interstitial atoms may form configurations more complicated than lattice atoms do. In particular, two interstitial atoms may form
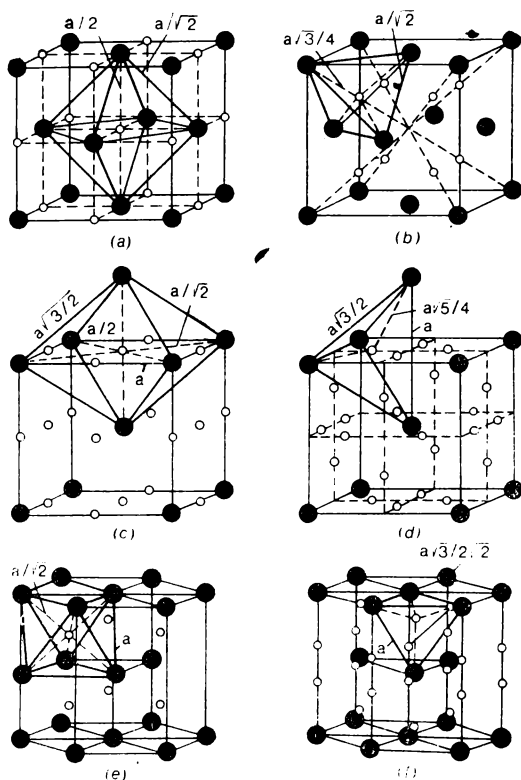
Fig. 3.2 Location of octahedral (a, c, e) and tetrahedral (b, d, f) voids in FCC (a, b), BCC (c, d), and HCP (e, f) lattices

a stable configuration, a dumbell. An atom in the centre of two adjacent FCC cells may be replaced with two interstitial atoms in the direction [100]. The atom at the centre of the face looks as if it were splitted into two interstitial atoms and has formed a dumbell.

An "extra" atom in the crystal lattice may form a denser chain of atoms, a crowdion (Fig. 3.3). In the crowdion a chain of $n + 1$ atoms occupies a length of ab (six instead of five atoms under normal conditions). A crowdion easily moves along its axis (a billiard-ball displacement of atoms).

Line Defects of Crystal Lattice. Dislocations. Line defects are extended departures from regularity in crystals and they are often called dislocations. An atom located in the dislocation core is displaced from its equilibrium position by no more than a half of the interatomic distance. The displacement of an atom dislocated from the equilibrium position is characterized by the Burgers vector,

Fig. 3.3 Crowdion in FCC lattice [110]

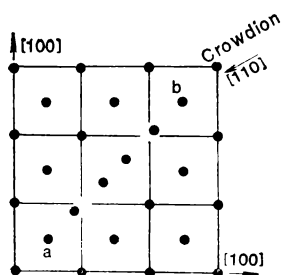$b \approx 10^{-8}$ cm. The dislocation core diameter constitutes 2-10 interatomic distances.

As the theory of elasticity states with a number of assumptions, to displace a dislocation per an interatomic distance the following energy should be applied:

$$Q_d = \alpha G b^2 a = \alpha \quad 9.8 \cdot 10^{-20} \text{ J/at}$$

$$\approx \alpha \quad 60 \quad \text{kJ/mole},$$

where G is the shear modulus equal for iron to 80 GPa; a is the interatomic distance equal to $2.5 \cdot 10^{-8}$ cm; $\alpha = 0.5$ to 1.

On the average, $Q_d \approx 41.8$ kJ/mole.

The quantity of dislocations is determined by their number per 1 cm^2, ρ. Acting stress σ and ρ are interrelated as follows:

$$\rho^{0.5} = 2\pi\sigma/G\mathbf{b}. \tag{3.1}$$

The density of dislocations in annealed metal generally makes up 10^6 to 10^8 cm^{-2}; in monocrystals, 10^3 to 10^4 cm^{-2}; in strain hardened metals 10^{10} to 10^{11} cm^{-2}; and in heavily plastically deformed metals 10^{12} to 10^{13} cm^{-2}.

In the region of dislocation core the lattice is significantly distorted. The radius of interstitial particles increases. The interstitial atoms being in a distorted interstitial site deform the crystal lattice to a lesser degree. The energy of the crystal lattice also increases to a lesser extent. Therefore, it is energetically advantageous for the interstitial atoms to be near the dislocation kernel. The energy of the dislocation-to-interstitial atom binding Q_b is the difference between the energy of the lattice distorted when an atom is introduced in the interstitial position near the dislocation kernel and in that of a perfect crystal lattice. The difference is equal to 0.5 eV ≈ 50 kJ/mole. Clusters of interstitial atoms around a dislocation are known as *Cottrell atmospheres*.

The concentration of impurity and interstitial atoms in the Cottrell atmosphere is maximum at the dislocation kernel and decreases with distance from it. The concentrations of impurity atoms near the dislocation kernel C_d and in the bulk of a metal C are interrelated as follows:

$$C_d = C \exp (Q_b/RT). \tag{3.2}$$

Near the dislocation line about half of the unit cells are extended and half are compressed. A stable atmosphere of interstitial impurity atoms is sustained at a distance about three interatomic distances from the dislocation line. In this connection we may assume that when all interstitial positions along the dislocation line are occupied

(a)   (b)
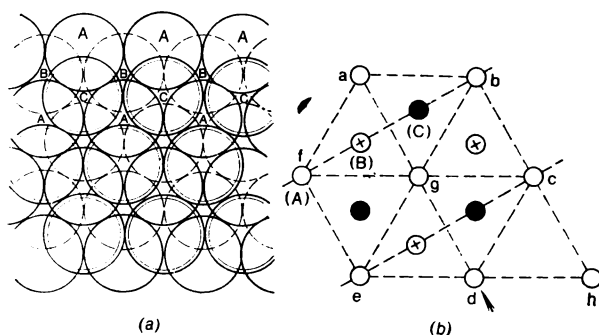
Fig. 3.4 Plane of packing (111) in FCC lattice
a — A, B, C are bottom, next, and top layers of atoms, respectively; *b —* positions of atoms
at the apices of equilateral triangles in three adjacent layers *A, B* and *C*

by interstitial atoms, i.e. the Cottrell atmosphere is saturated or
condensed, the concentration of impurity atoms in it is close to
50 per cent. The solubility of nitrogen in α-Fe at room temperature
approximates 2 per cent of the atomic content. According to the
above-mentioned relationship, the Cottrell atmosphere will be sa-
turated with nitrogen.

The atmospheres of interstitial atoms decelerate the motion of
dislocations in plastic deformation. Under the effect of applied stress-
es, dislocations either "detach" from the impurity atoms surrounding
it, or drag them behind. In the former case, the applied stresses
should perform the work equal to the total bonding energy of all
the atoms of the Cottrell atmosphere on the dislocation section hav-
ing a length of the order of the Burgers vector. In the latter case,
the dislocation decelerates and in practice moves at a rate of diffu-
sion of interstitial atoms.

The dislocation movement in plastic deformation is hindered by
various obstacles such as intermetallic compounds, nonmetallic
impurities, other dislocations, etc.

Cross slip and stacking faults. When encountering obstacles, screw
dislocations pass by *cross slip* from one slip plane to another. In
order to take part in a cross slip, an extended screw dislocation must
rejoin. Screw dislocations cleave to form *stacking faults.*

A stacking fault in an FCC lattice forms as follows (Fig. 3.4).
In the (111) plane all atoms touch one another, i.e. are close-packed.
The atom centres are in positions *A*. Each atom is surrounded by
six atoms. In order to preserve the close-packed structure in placing
another layer over the first layer, the centres of atoms in the second
layer must fit the hollows formed by the neighboring atoms in the
first layer. For example, the centres of atoms in the second layer are
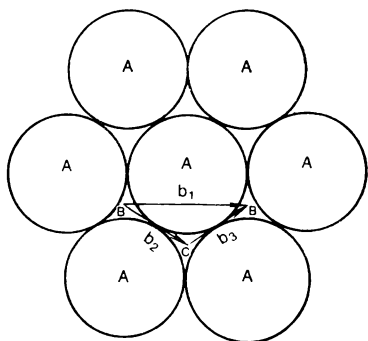positioned over the hollows *B*. If the centres of atoms in the third

Fig. 3.5 Layer of densest packing of atoms A and Burgers vectors of unit (b_1) and partial (b_2, b_3) dislocations

layer fit the hollows of the second layer located above hollows C of the first layer, the result will be a close-packed FCC lattice. If in the third layer the atomic centres are arranged over the hollows of the second layer positioned above the atomic centres A of the first layer, this will form a hexagonal close-packed lattice. The arrangement of the sphere centres in the close-packed planes can be represented as $ABABAB...$ With FCC structure, the alternation assumes the form of $ABCABCABC...$ If in the FCC lattice the layer with the atomic centres in position C is shifted so that the atomic centres fit positions A, layers will alter as $ABCABCABCABC$. A layer of atoms packed in the same manner as in the HCP lattice will appear in the FCC lattice. This layer of atoms is known as the stacking fault.

At an interface between the FCC structure and HCP structure the crystal lattice deforms and atoms gain additional energy, i.e. become dislocated. However, the energy obtained by the atoms is considerably less than 41.8 kJ/mole characteristic of perfect dislocation. The less the extra energy, the more probably the system will remain in this state. The system comprising two atomic planes (boundaries of FCC and HCP lattices) separated by a stacking fault is known as the *extended dislocation* consisting of two partial (imperfect) dislocations. Displacement of perfect dislocation ensures identical translation. Thus, in the HCP lattice, atoms with centres in position B will be displaced also to position B (Fig. 3.5). So, an identical translation of the crystal lattice takes place.

Sometimes dislocations can move so that the crystal lattice in the displacement zone is not translated identically, though a new position of atoms is mechanically stable. The atomic centre will change from position B to position C (see Fig. 3.5). These dislocations are known as *partial*. The Burgers vector and hence the energy of the dislocations are less than those of a unit dislocation in a given lattice. So, it is energetically more advantageous for a unit dislocation to extend into two imperfect dislocations.

However, in order to allow a screw dislocation to participate in cross slip, the partial dislocations must rejoin into a perfect dislocation. This process calls for certain energy and is thermally activated. The distance between the imperfect dislocations makes up the width of a stacking fault d (cm). This is inversely proportional to the

energy of a stacking fault γ (J/cm²): $\gamma = KG\mathbf{b}_2\mathbf{b}_3/d$, where K is the constant and $\mathbf{b}_2$ and $\mathbf{b}_3$ are the Burgers vectors of the imperfect dislocation (see Fig. 3.5).

The stacking fault energies of various metals are tabulated below:

Metal	Mg	Al	Ti	Ag	α-Fe	Ni	Cu	Zr	Steel 08X18H10T
γ, 10^7 J/cm²	310	250	10	25	130	350	40	220	20
d/b	—	1.5	—	12	—	4	10	—	45

Imperfect dislocations rejoin not along their entire length, but through the formation of individual ties. The activation energy of tie formation is $Q_t \approx Gb^2d/30$.

The activation energy of cross slip is below 1 eV for metals having a FCC structure and high energy of stacking faults, such as aluminum, but it abruptly rises with a decrease in the energy of faults. In BCC metals cross slip proceeds easily.

Alloying may substantially change the energy of stacking faults. Thus, in austenitic steel containing 18% of chromium and 8% of nickel, an increase in the nickel content increases the energy of stacking faults. It is worth recalling here that stacking faults in the FCC lattice have a HCP structure. The solubility of elements in the lattices should generally vary. At a sufficiently high temperature, the atoms of the alloying element redistribute by diffusion between the stacking fault and the FCC lattice, in the same way as elements redistribute between two phases. Impurity atoms, or atoms of the alloying element, either diffuse into the stacking fault, or leave it. Their average concentration in the main volume with the FCC lattice practically remains unchanged. The region of changed concentration of impurity atoms, or atoms of the alloying element, in the stacking fault of an extended dislocation is known as the *Suzuki atmosphere*. Suzuki considered that the extended dislocation chemically interacts with the dissolved atoms.

The dislocation moves under the action of the applied force as follows. In the starting position at moment τ_0 the dislocation consists of N_0 atoms. The probability that a dislocated atom will jump is $W = (1/6) \exp(-Q/RT)$. The cofactor 1/6 indicates that the atom moves in a certain direction, namely, in the direction of the force action. The motion of the atom locally distorts the crystal lattice. This reduces the activation energy of moving an atom neighboring the atom displaced first. Therefore, the displacement of the first atom will be followed by the displacement of its neighbor. The quantity of dislocated atoms displaced per unit time will be

$$-dN/d\tau = (1/6) \nu N \exp(-Q_1/RT) = KN,$$

where v is the frequency of temperature vibrations equal to 10^{13} s^{-1}. Solving this differential equation, we obtain $N = N_0 \exp(-K\tau)$, assuming that the entire dislocation will move through a distance equal to the Burgers vector, when the quantity of atoms displaced to the new position is $N = 0.9\,N_0$.

With allowance made for the above-mentioned, we may determine time τ within which the dislocation will move: $N/N_0 = \exp(-K\tau)$. Hence

$$\tau = -2.3 \cdot 6 \cdot \log(0.9) \exp(Q_1/RT)/v \approx 6 \cdot 10^{-14} \exp(Q_1/RT).$$

The dislocation displacement rate is

$$\dot{\varepsilon} = b/\tau = (10^{-8}/6 \cdot 10^{-14}) \exp(-Q_1/RT)$$

$$= 1.66 \cdot 10^5 \exp(-Q_1/RT) = \dot{\varepsilon}_0 \exp(-Q_1/RT). \qquad (3.3)$$

The value of $\dot{\varepsilon}_0 = 10^5$ cm/s is equal in order to the sound velocity in metals. The force moves the atom from its equilibrium state and the energy of the atom increases by Δq proportional to the applied force σ and displacement l: $\Delta q = \sigma \Delta l$. Note that $dl = a\,d\varepsilon$, where ε is the deformation of the crystal lattice when the atom moves for Δl, and a is the interatomic distance equal to $2.5 \cdot 10^{-10}$ m.

Metal grains the planes of which form an angle of 45° with the direction of the forces applied deform plastically. The forces can be resolved into a normal component making one atomic plane tear off another, i.e. producing *brittle failure*, and a tangential component τ causing displacement of the atom along the atomic plane, i.e. *plastic deformation*.

From the geometrical point of view and taking into account the relation between the acting force, deformation, and shear modulus ($G = 80$ GPa)

$$\tau = 0.7\sigma = \varepsilon G; \quad \sigma = \varepsilon G/0.7.$$

Hence

$$dq = (\varepsilon G a/0.7)\,d\varepsilon; \quad q = 0.7\,aG\varepsilon^2. \qquad (3.4)$$

One square centimeter of iron alloy surface contains n moles:

$$n = (dN/A)^{2/3}N^{-1} = [(7.8/56) \cdot 6 \cdot 10^{23}]^{2/3}\,(6 \cdot 10^{23})^{-1}$$

$$= 3.18 \cdot 10^{-9}, \qquad (3.5)$$

where $d = 7.8$ g/cm^3 stands for gravity; $A = 56$ is the atomic weight; N is the Avogadro number.

The energy of dislocated atoms is $Q_d = 42$ kJ/mole. Dislocation of an atom produces the following unit cell deformation in the crystal lattice

$$Q_d = 4.2 \cdot 10^4 = 0.7aG\varepsilon_d^2/10^4 \cdot 3.18 \cdot 10^{-9}. \qquad (3.6)$$

From the given relationship $\varepsilon_d = 0.30$, hence

$$\mathbf{b} = \varepsilon_d a = 0.31 \cdot 2.5 \cdot 10^{-8} = 0.78 \cdot 10^{-8} \approx 10^{-8} \text{ cm.} \tag{3.7}$$

Evaluate the deformation of the lattice when one atomic plane is torn off another. Then $Q = E_{cr}$, where $E_{cr} = 405$ kJ/mole and is the energy of the iron crystal lattice; $E = 205$ GPa and stands for the modulus of elasticity:

$$E_{cr} = 4.05 \cdot 10^5 = 0.7 \cdot a E \varepsilon^2 / 10^4 \cdot 3.18 \cdot 10^{-9}. \tag{3.8}$$

Hence $\varepsilon \approx 0.60$ and generally

$$\varepsilon^2 = KQ \text{ or } Q = \varepsilon^2/K \text{ (kJ/mole).} \tag{3.9}$$

The latter relationship can be used to evaluate the atomic displacement l from the equilibrium state in temperature vibrations. Assuming $Q = RT$, we obtain:

$$l = 0.248 \, (KRT)^{0.5} = 0.248 \, (0.77 \cdot 10^{-3} \cdot 827 \cdot 0.291)^{0.5} = 0.011 \text{ nm,}$$

where 0.248 nm is the minimum interatomic distance. Experimentally determined l for iron at 291 K equals 0.0107 nm.

Given below are experimental values of K obtained for various metals:

Metal	Al	Ti	Fe	Ni	Cu	Zr
$K \cdot 10^3$	1.50	1.09	0.77	0.85	1.18	0.77

With K and E_{cr} taken into account, the average value of ε_{cr} for 21 metals is equal to 0.604.

Now we shall evaluate the energy gained by an iron atom when it is displaced through a distance corresponding to ε_d under a stress equal to the yield limit $\sigma_y = 210$ MPa:

$$Q = 0.7 a \varepsilon \sigma_y / 10^4 \cdot 3.2 \cdot 10^{-9} = v \sigma_y = 0.41 \text{ kJ/mole,} \tag{3.10}$$

where $v = 0.7 a \cdot \varepsilon 10^{-3} \cdot 10^6 / 10^4 \cdot 3.2 \cdot 10^{-9}$ is the activation volume.

If the energy is in kJ/mole and σ is in MPa, then

$$v = 1.64 \cdot 10^{-3}. \tag{3.11}$$

The energy is very small and does not even exceed the energy of temperature vibrations RT. This makes us suppose that in loading the crystal lattice, the stress acting on a given atom increases by γ which is introduced by the academician S. N. Zhurkov and known as the *coefficient of overstress*.

So far no exhaustive methods have been devised to calculate the coefficient. However, approximate models allow us to approach the
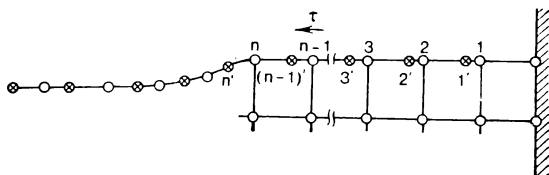
Fig 3.6 Displacement of atoms in ¦crystal lattice under mechanical stresses

evaluation of γ. Let us consider one of these models. Tangential component τ acting in the atomic plane parallel to the extra plane displaces the atoms from positions 1, 2, 3, $\ldots n-1$, n to positions $1'$, $2'$, $3'$, $\ldots (n-1)'$ and n' (Fig. 3.6). As a first approximation, we may assume that the position of the atoms in the extra plane remains unchanged.

Atom 1 moves from its equilibrium position by a distance of $l_1 = \varepsilon a$, where by Hooke's law, $\varepsilon = \tau/E$. The displacement of atom 2 is $l_2 = 2\varepsilon a$, and atom n displaces through $l_n = n\varepsilon a$. Upon reaching the yield point $\varepsilon \approx 10^{-3}$, and atom n displaces by the distance equal to the Burgers vector: $l_n = b = n\varepsilon a$. Then $b/a = \varepsilon_d = n\varepsilon = n \cdot 10^{-3}$. It follows from this relationship, taking into account $\varepsilon_d = 0.31$, that $n = 310 = \gamma_0$.

Atom n displaced through distance b from its equilibrium position became a dislocated atom, though under the action of forces not in excess of the yield point. If the force ceases to act upon the plane, then all atoms of this plane, except atom n, will return to their starting position. Atom n will remain in the position of a dislocated atom.

It should be noted, however, that due to some reasons certain atoms of the plane in question may be displaced from their equilibrium position before the force τ is applied. Under the action of interstitial atoms located in interstitial sites the atoms of the crystal lattice are displaced from their equilibrium position 1 to position $1'$ through distance l (Fig. 3.7). The lattice is deformed by $\varepsilon' = b/a$.

Under the action of force τ the atoms move to position 1 corresponding to their equilibrium position not distorted by the interstitial atoms in the crystal lattice. The lattice though deformed by ε' has formally the same interatomic distance. Hence, the above-ob-
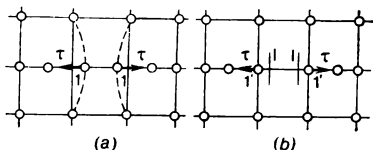

Fig. 3.7 Distortion of interstitial solid solution lattice
a — prior to deformation under applied stresses; b — after deformation

tained $n = 310$ is characteristic only of an ideal nondistorted lattice, and it will be more correct to designate it n^0.

A real crystal lattice is always distorted to some degree. An interstitial atom, say carbon, located in a tetrahedral void distorts the crystal lattice by

$$\Delta r = r_C - r_4 = 0.041 \ \text{nm}, \tag{3.12}$$

where r_C is the radius of the interstitial carbon atom equal to 0.077 nm; r_4 is the radius of the tetrahedral void in the BCC lattice of iron equal to 0.036 nm. Hence, the lattice is deformed by $\varepsilon = \Delta r/a = 0.041/0.248 = 0.165$ nm, where $a = 0.248$ nm is the minimum interatomic distance in the BCC lattice of iron.

Distortion of the crystal lattice increases its energy. If the energy caused by the deformation becomes $Q_m = 4\,RT$, then it is energetically advantageous for the crystal lattice to change to a new modification. Under normal conditions, in the case with iron $\varepsilon_m^2 = K \cdot 4RT = 0.77 \cdot 10^{-3} \cdot 4 \cdot 8.27 \cdot 298 \cdot 10^{-3} \approx 7.6 \cdot 10^{-3}$; $\varepsilon_m \approx \approx 8.7 \cdot 10^{-2}$.

Deformation is a linear characteristic. Iron containing 0.035% C has in any crystallographic direction

$$n_1 = (100 \cdot 12/56 \cdot \%C)^{1/3} \approx 8.5 \tag{3.13}$$

atoms of iron per an atom of carbon and hence 8.5 interatomic distances.

Comparing ε and ε_m shows that in order to preserve the starting crystal lattice, deformation ε caused by the introduction of a carbon atom must cover n_2 interatomic distances:

$$n_2 = \varepsilon/\varepsilon_m = 0.165/0.087 \approx 1.9. \tag{3.14}$$

Then the fraction of deformed interatomic distances

$$S = n_2/n_1 = 1.9/8.5 = 0.22, \ \text{and} \tag{3.15}$$

the fraction of nondeformed interatomic distances

$$1 - S = 1 - 0.22 = 0.78. \tag{3.16}$$

Therefore, in the scheme considered above, only

$$\gamma_0 \, (1 - S) = 310 \cdot 0.78 = 242 = \gamma \tag{3.17}$$

unit cells can deform by $\varepsilon = 10^{-3}$ rather than $n_0 = \gamma_0 = 310$ (γ is the coefficient of overstress).

With increased deformation, the number of dislocated atoms increases and the crystal lattice distorts. When all n_0 crystal cells are distorted to a maximum (see Fig. 3.6) and the interatomic distance does not change under the action of forces τ applied to each atom, all forces $\tau_1, \tau_2 \ldots, \tau_{n-1}, \tau_n$ add together and atom 1 experiences

the total force $\Sigma\tau = n_0\tau$, i.e. the acting stress increases $n_0 = \gamma_0$ times.

The bond between atoms 1 and 0 will break after the deformation according to (3.8) reaches 0.6. From Hooke's law

$$\sigma_u = \varepsilon_b E/0.7\gamma_0 = 0.6\cdot205/0.7\cdot310 = 0.567 \text{ GPa.} \qquad (3.18)$$

This is close to the *ultimate strength* of steel, grade 20.

The plastic deformation must begin at a stress equal to the yield point:

$$\sigma_y = \varepsilon_d G/0.7\gamma = 0.30\cdot80/0.7\cdot242 \approx 0.14 \text{ GPa,} \qquad (3.19)$$

which is close to the yield point of iron containing 0.035% C.

Similar dependencies may serve for determining γ of nuclear reactor materials:

Material   Steel 20   22K   08X18H10T   Zirconium produced by iodide method
    γ 173   160   156

Using the relationships similar to equations (3.12) through (3.19), we shall evaluate σ_y for a number of steels and alloys. The calculated values and experimental results agree satisfactorily. This allows a fairly conventional model to be used for approximate quantitative evaluations of the mechanical characteristics of steels and alloys (Table 3.1).

TABLE 3.1 σ_y for Steels and Alloys, MPa

Material	Fe, 0.035% C by mass	Steel 20	08X18H10T	Cu alloyed to 10% of atomic content		
				Al	Ni	Zn
Calculated	140	180	200	74	55	62
Experiment-al	147	220	200	80	75	60

In metals containing impurities in an amount of 0.01 to 0.001%, the number of unit cells distorted by interstitial atoms is small. In this case, we may assume $\gamma \approx 300$. This taken into account gives σ_y for a number of pure metals as tabulated below.

TABLE 3.2 σ_y for Pure Metals, MPa

Metal	Al	Ni	Cu	Zn	Ge	Ag
Calculated	39.9	115	68	54.8	58.8	43.2
Experimental	29-35	78	55-69	78	51	53

Now let us evaluate *elongation* δ. As a first approximation, δ = $100\varepsilon_1$, where ε_1 is the deformation in the direction parallel with the forces applied. Slip takes place in a plane making 45° with the direction of applied forces. Hence, $\varepsilon_1 = \varepsilon \cos 45°$, where ε is the deformation in the slip plane. At a stress taken from the relationship similar to (3.19), $\varepsilon = 0.7\gamma\sigma/G$. In the case under consideration $\sigma = \sigma_u$; σ_u is found from (3.18). Taking into account the above-mentioned gives us (%):

$$\delta = 10^2 \cos 45° \cdot 0.7 \cdot 0.6 \cdot E\gamma/0.7G\gamma_0.$$

$G = E/2\,(1 + \nu)$, where ν is Poisson's ratio for iron alloys approximating 0.28. Then

$$\delta = 10^2 \cdot 0.42E\, 2(1 + 0.28)\, \gamma/E\gamma_0 \approx 107\gamma/\gamma_0. \tag{3.20}$$

At $\gamma/\gamma_0 \approx 0.5$, the iron alloys have δ = 53%.

The elongation of austenitic steels is close to 50%. Hypothetically plastic deformation may cause slip in all (111) planes in γ-Fe and in all (110) planes in α-Fe that are oriented in a similar way with regard to the forces applied. The elongation then will be proportional to the number of such planes, while the latter is inversely proportional to the centre-to-centre distance of atoms lying in the neighbouring slip planes *a*.

In α-Fe, at $a = 0.268$ nm $d_\alpha = \sqrt{2} \cdot a/2 = 0.202$ nm. In γ-Fe, at $r_{Fe} = 0.126$ nm $d_\gamma = 2r \cos 60° = 2 \cdot 0.126 \cdot 0.5 = 0.126$ nm. Hence, $\delta_\alpha = \delta_\gamma d_\gamma/d_\alpha = 51 \cdot 0.126/0.202 = 31.8$. And indeed, the elongation of the α-lattice steels is close to 30%.

Therefore, the approximate model not being universal and exhaustive, gives as a first approximation a number of important characteristics of metals, including γ at stresses close to the yield point.

As follows from Fig. 3.6, an extra plane and dislocations in the metal produce γ which is determined by the number of atoms found in a crystallographic direction per a dislocated atom. In the equilibrium state the probability of forming a dislocated atom is

$$W = 10^{-Q/RT}, \tag{3.21}$$

where $Q = 41.8$ kJ/mole is the energy of a dislocated atom. At 293 K

$$\gamma_0 = (10^{41.8/19.1 \cdot 293 \cdot 10^{-3}})^{1/3} = 308, \tag{3.22}$$

which is close to 310 obtained before.

Therefore, we may suppose that the atom is subjected to force $\sigma_1 = \sigma\gamma$, when it experiences the mechanical stress σ. With account of (3.4) through (3.6) the energy of the atom in plastic deformation

increases by

$$q_1 = 0.7a\sigma\gamma\varepsilon_d/10^4 \cdot 3.18 \cdot 10^{-9}$$
$$= 0.7 \cdot 2.5 \cdot 10^{-10} \cdot 0.31\gamma\sigma/10^4 \cdot 3.18$$
$$\times 10^{-9} \cdot 10^{-3} = U\gamma\sigma, \tag{3.23}$$

where $v = 1.64 \cdot 10^{-3}$ is the activation volume.

An interstitial carbon atom deforms n_1 interatomic distances in steel 20 by $\bar\varepsilon = \varepsilon/n_1 = 0.165/4.75 = 3.47 \cdot 10^{-2}$.

Deformation produces additional energy in each atom:

$$q_2 = \bar\varepsilon^2/K = (3.47 \cdot 10^{-2})^2/0.77 \cdot 10^{-3} = 1.56 \text{ kJ/mole}. \tag{3.24}$$

The activation energy of dislocation displacement decreases by the sum $q_1 + q_2$:

$$Q_1 = Q - q_1 - q_2. \tag{3.25}$$

The *dislocation displacement rate* is determined as

$$\dot\varepsilon = \dot\varepsilon_0 \exp(-Q/RT) = \dot\varepsilon_0 \exp[-(Q - v\gamma\sigma + q_2)/RT], \tag{3.26}$$

where Q (kJ/mole) is the activation energy of dislocation displacement in an undeformed metal equal to the activation energy of self-diffusion (Table 3.3).

TABLE 3.3 Activation Energy of Self-diffusion and Dislocation Displacement

Metal	Si*	Ni-Cr Alloy**	Ge*	Ni**
Dislocation displacement	192-213	290	268	268
Self-diffusion	230-240	286	290	276

* Stress, 5 MPa.
** The starting grain size, 100 μm.

TABLE 3.4 Activation Energies of Self-diffusion and Activation Volumes

Characteristic	α-Fe	γ-Fe	Ni	Al	α-Ti	Cu	α-Zr
Activation energy of self-diffusion, kJ/mole	235-273	270	280	142	121	205	92
Activation volume v, 10^3 kJ/(mole MPa)	1.64	1.64	1.52	2.3	2.44	1.6	3.2
Number of moles per 1 cm², 10^{-9}	3.2	3.2	3.3	2.5	2.4	3.2	2

As a first approximation, the activation energy of self-diffusion and the energy of crystal lattice (E_{cr}) are related as $Q = 0.56E_{cr}$.

Table 3.4 gives the activation energies of self-diffusion and the activation volumes for a number of commercial metals.

3.2 High-temperature Strength and Deformation of Metals

In service of nuclear power plants their components undergo mechanical stresses. The tendency of reducing the volume of structural materials utilized in the core zone to decrease neutron absorption and the weight of, say, transportation facilities, leads to increased stresses in structural metal. One of the problems facing the designer is to minimize the weight of metallic components without affecting the performance of the plant.

The components of nuclear power plants are designed so that in all operating modes the metal operates within the elasticity region. Sometimes, however, materials are allowed to operate within the elasto-plastic region. Plastic deformation changes the shape, say, of fuel elements. Excessive stresses in structural components especially combined with environmental effects lead to failure of material.

Deformation and Failure. Mechanical stresses arising in service produce strain in a metal increasing with stress. At the initial stages, when stress in the metal is small, strain is reversible and depends practically linearly on the stress applied. As the stress is removed, the strain disappears. This is known as *elastic deformation*. Dimensional changes in elastic deformation are due to a reversible distortion of a crystal lattice. Elastic deformation takes place only under stresses that do not exceed a certain value known as *yield point* (elastic limit).

Stress above σ_y produces permanent deformation called *plastic*. On a graph of stress versus strain a yield point of a perfect material is shown by an almost straight horizontal section at which strain increases at a constant stress. However, in practice, this portion on the curve cannot always be revealed. Then a stress producing plastic deformation of 0.1 or 0.2% is taken as the *conditional yield point* designated as $\sigma_{0.1}$ or $\sigma_{0.2}$.

Prior to failure, materials subjected to a growing stress acquire plastic or residual deformation. Metal in this case fails plastically. In brittle failure, the material first undergoes elastic deformation and then reaching a certain stress fails without plastic deformation. The interatomic distances in elastic deformation become so large that the interatomic forces attenuate and one atomic plane separates from the other. The limiting stress (in terms of force per original

unit area of cross section) at which a material completely breaks down, is known as the *ultimate strength* (σ_u). In brittle materials, the ultimate strength equals the yield point, whereas in plastic materials, the ultimate strength naturally exceeds the yield point. The stresses above the yield point produce in plastic materials both elastic and plastic deformation.

A stress not exceeding the yield point distorts the crystal lattice owing to displacement of atoms from equilibrium positions. Tensile loads increase interatomic distances along the axis of the displacement, while compressive loads reduce them. Forces of metallic bonding tend to return the displaced atoms to the original position. A system of forces in equilibrium acting on all displaced atoms per unit area of cross section is known as *stress*. It equals the load per the same area. Until the yield point has been reached, removal of the external load returns each atom to the equilibrium state. The elastic deformation and stress become equal to zero. The elastic displacement of an atom is always small even in atomic scale. The work done in elastic deformation of a metal is preserved as the strain energy of the distorted lattice.

Plastic deformation of crystals occurs either by *slip* or by *twinning*. In slip, thin layers of a crystal move like cards in a deck. Slip occurs along a certain crystallographic plane (slip plane) and in a certain crystallographic direction (slip direction). In the FCC and HCP lattices, slip planes are generally planes of the densest packing of atoms. In the FCC lattice, this is the plane (111) and in the HCP lattice, the basal plane (0001). As the temperature rises other planes start to participate in slip. They, however, must also have a relatively high density of atoms.

Slip is most easily revealed by slip lines which form when slip planes intersect a crystal surface. The distance between slip planes differs with metal and is, on the average, 10^{-4} cm, i.e. about 10^3 atomic diameters. The neighboring slip planes may be displaced by up to 10^2 atomic diameters. In most metals under considerable tension, the distance between slip planes does not change with deformation, i.e. deformation occurs over the slip planes that have already been formed.

The stress initiating slip in a given atomic plane is known as the *critical shear stress*. It lies within 1 to 2 MPa for a number of metals, though the theory gives 3.5 GPa. To explain why slip taking place in practice occurs under relatively small stresses the theory of dislocations has been developed.

Changes in the dislocation structure in deformation. Figure 3.8 gives a schematic stress-strain curve for FCC monocrystals. The curve clearly shows three stages. Stage *I* represents the so-called easy slip, when dislocation mainly occurs in one (primary) slip system. In monocrystals, dislocations move over long distances (of the order

of the specimen diameter). Strain hard-
ening is low, and slip traces are long.

Fig. 3.8 Stress-strain curve
for FCC monocrystals

With growth of deformation stage
II sets in. Slip continues in the se-
condary systems. Elastic interaction
of dislocations increases. This results
in the formation of the Lomer-Cottrell
sessile dislocations. In FCC metals, for
example, they form when two extend-
ed dislocations with the Burgers vec-
tors forming an angle of 120° meet
at the intersection of their slip planes.
The slip lines shorten and the average
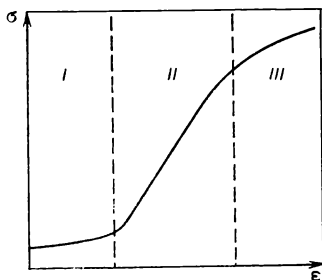distance covered by the dislocations
decreases.

At still heavier deformations the slope of the stress-strain curve
decreases. Stage *III* sets in. It represents the thermally activated
cross slip of screw dislocations under the growing stress. The cross
slip produces partial stress relaxation. The dislocations group into
volume nets (cell structure of dislocations) with less distorted lattice
regions (blocks) located inside them. The higher the stacking fault
energy, i.e. the narrower the extended dislocations and the easier
their cross slip, the easier the cell structure is formed. The cross
slip annihilates individual dislocations of opposite signs, which
also decreases elastic stresses.

The motion of dislocations can be stopped by an obstacle which
they cannot overcome by *cross slip*. The dislocation movement can
also be decelerated, for instance, by phase particles dispersed in the
matrix. Different specific volume of phases generates a field of elast-
ic stresses. Interacting with dislocations, the field decelerates their
movement and blocks them. Dislocations are decelerated to a maxim-
um when the dispersed particles are spaced at 50-250 interatomic
distances.

The grain or block boundaries hinder the dislocation migration,
as neither the slip plane nor the Burgers vector remains unchanged
in passing the boundary. The boundary energy depends on the
angle at which the grains are tilted with regard to each other.

Dislocations moving in the intersecting slip planes, can also
block each other and form a sessile dislocation of Lomer-Cottrell.

If cross slip is hindered, then a flat dislocation pile-up forms in
front of the obstacle. The number of dislocations in a pile-up can
be determined as:

$$n = 2\pi L\sigma/G\mathbf{b},\qquad\qquad(3.27)$$

where L is the length of the section on which dislocations pile up, cm.

According to the above-mentioned, we may assume

$$L = \gamma_0 a = 310 \cdot 2.5 \cdot 10^{-8} = 7.75 \cdot 10^{-6} \text{ cm.} \qquad (3.28)$$

For steels $G = 80$ GPa; $\mathbf{b} = 10^{-8}$ cm; $\sigma = \sigma_u = 550$ MPa. Then $n = 2 \cdot 3.14 \cdot 7.75 \cdot 10^{-6} \cdot \sigma / 8 \cdot 10^4 \cdot 10^{-8} \approx 0.06\sigma \approx 33$, if σ is expressed in megapascals.

In steel 20, there are $\gamma = 186$ undistorted unit cells per each atom of carbon in any crystallographic direction. If we take that the average diameter of a dislocation core equals six interatomic distances, then the section should contain $186/6 = 31$ dislocations.

A flat dislocation pile-up represents *crack embryo*. In a sessile dislocation of Lomer-Cottrell meet two flat dislocation pile-ups forming a crack embryo of the length $C = 2L$.

Brittle fracture occurs in a material, i.e. one atomic plane breaks off from another, when dislocation motion has been blocked and stresses continue to increase. In brittle fracture, *cracks grow* in a catastrophic way. The stress at which cracks start to grow *catastrophically* is determined from Griffith's relationship:

$$\sigma_{cr} = \sqrt{E\rho/C} = 1.4 \text{ GPa,} \qquad (3.29)$$

where, for steel 22K, $E = 200$ GPa is the modulus of elasticity; $\rho = 1.5 \cdot 10^{-4}$ J/cm^2 is the surface energy; $C = 7.75 \cdot 10^{-6}$ cm stands for a critical crack length.

For steel 22K, $\sigma_u = 560$ MPa and reduction of cross-sectional area $\psi = 0.48$. Hence, the steel fractures at:

$$\sigma_{true} = 5.6 \cdot 10^2 / 0.48 \approx 1.17 \cdot 10^3 \text{ MPa} = 1.17 \text{ GPa}$$

which agrees well with (3.29).

Cracking. When the acting stress is below its critical value, cracks do not grow catastrophically. Nevertheless, they grow with time and thus the so-called delayed failure occurs. As a crack propagates, atoms in the two-dimensional dislocation pile-up rupture brittly.

Cracking consists in breaking the bond between two dislocated neighbors. The bond may cleave when the atoms in temperature vibration move in opposite directions. The probability of atomic movement in any direction is 1/6. The probability of concurrent movement of two atoms in opposite directions $W_1 = 1/6 \cdot 1/6 \approx \approx 2.8 \cdot 10^{-2}$.

The atomic bond splits when the bond energy is Q^{surf}. The surface has half as many neighboring atoms as the interior of the crystal. Hence, the lattice energy of the surface atoms is $E_{cr}^{surf} = 0.5 E_{cr}$. According to Eyring's rule the activation energy is

$$Q^{surf} = 0.25 E_{cr}^{surf} = 0.25 \cdot 0.5 E_{cr} = 0.125 E_{cr}.$$

It is materially greater than RT, the energy of temperature vibrations. Hence, the oscillation amplitude of the atoms will considera-

bly exceed the amplitude of temperature vibrations. An atom will be displaced only when temperature vibrations move its neighboring atoms away from it. The probability of this is $W_2 = 1/6 \times 1.6 \approx \approx 2.8 \cdot 10^{-2}$.

When bonds between two displaced atoms break, the crack will extend through a distance equal to the Burgers vector, i.e. through 10^{-8} cm. The bonds break on the section where a pile-up of n dislocations has been blocked. The head of the pile-up is under the action of a total force $\Sigma\sigma = n\sigma = 6.08 \cdot 10^{-3} \sigma$.

In this case, when the bonds break, the maximum deformation will make up 0.6 rather than 0.31 as with dislocating an atom. Therefore, the activation volume $v_1 = 2v$.

Taking into account the above-mentioned, we obtain the following rate of steel cracking (cm/s):

$$v = v_0 \exp\left(-Q/RT\right) = bvW_1W_2 \cdot 10^{\dfrac{-(0.125E_{cr} - v_1 n\sigma)}{RT}}$$

$$= 10^{-8} \cdot 10^{13} \cdot 2.8 \cdot 10^{-2} \cdot 2.8 \cdot 10^{-2} \cdot 10^{\dfrac{-(0.125 \cdot 405 - 2 \cdot 1.64 \cdot 10^{-3} \cdot 6 \cdot 10^{-2}\sigma^2)}{19 \cdot 0.293}}$$

$$\approx 78 \cdot 10^{\dfrac{-(50.63 - 2 \cdot 10^{-4}\sigma^2)}{19 \cdot 0.293}}, \qquad (3.30)$$

where $v = 10^{13}$ s^{-1} is the frequency of temperature vibrations; σ is in MPa, and $T = 293$ K.

The atoms whose bonds break as the crack propagates may be bonded to adsorbed oxygen or water, or to oxygen of the oxide film. Therefore, the activation energy in (3.30) is increased by $\Delta Q = = 0.125 E_b$, where E_b is the energy of the atom-to-oxygen bonding.

High-Temperature Strength. In nuclear power engineering and in boiler service, steels operate at high temperatures and therefore must resist their effect. *High-temperature strength* is the ability of a material to withstand mechanical stresses at high temperatures. The stress causing metal failure at an elevated temperature materially depends on the time of load application: the critical stress may be high when the load is applied for a short period of time and low when it is applied for a long period of time.

The higher the temperature of a metal, the lower the breaking stress at a given duration of the stress action. Generally the metal strength is determined by the temperature and the time of load application.

Figure 3.9 gives a general dependence of strength on duration of load application at various temperatures. At temperature T_1 (room temperature for steels) the strength of metal is practically independent of the loading time. Under a stress somewhat below the yield point designated in the figure by $\times$, a metal fails in 10^8 s, i.e. in several years. At a higher temperature, the dependence of strength on the time of load application becomes more pronounced. At a sufficiently
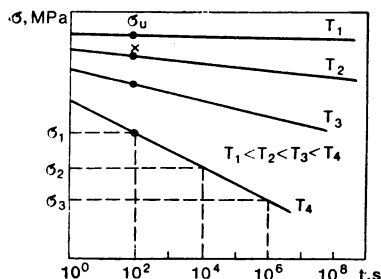
Fig. 3.9 Strength versus temperature and testing time

high temperature the strength markedly decreases with testing time. Therefore, the breaking stress cannot unambiguously characterize the strength of a material; the time of load application should also be indicated. Thus, at temperature T_4 the stress σ_2 causes failure in 10^6 s, while the stress σ_1 produces failure in 10^2 s, i.e. 10^4 times as fast. Therefore, at low temperatures the time factor may be neglected, while at high temperatures its effect becomes decisive.

To evaluate the strength of metal with account of the time factor the notion of *long-term strength* should be introduced. The long-term strength is an ultimate strength at a given duration of testing, or the stress causing failure at a given duration of load application. The long-term strength is designated by σ with a subscript indicating the testing time in hours. For example, σ_{100} stands for a stress producing failure in 100 hours. Given below is the high-temperature strength of steel 08X18H10T at various temperatures:

T, K	823	873	973	1023
σ_{100}, MPa	350	250	140	100

High-temperature strength of materials is characterized by the *creep limit*, a stress producing at a given temperature deformation at a specified rate. Thus, $\sigma_{0.1/1000}$ stands for a stress causing a net 0.1% deformation in 1000 hours. Given below is the creep limit $\sigma_{1/1000}$ for steel 08X18H10T at various temperatures:

T, K	823	873	923	973
$\sigma_{1/1000}$, MPa	120	80	55	30

At a high temperature the ability of a material to resist fracture is characterized by the long-term strength which is the stress producing failure of the material after a certain exposure. The breaking stress σ

(MPa) depends on time τ (h) as follows:

$$\sigma = a - b \log \tau. \tag{3.31}$$

Table 3.5 gives a and b for steels, grades 08X18H10T and 20 at various temperatures.

TABLE 3.5 Values of a and b at Various Temperatures

Grade	T, K	a	b	Grade	T, K	a	b
08X18H10T	823	460	50-70	08X18H10T	973	250-310	65
08X18H10T	873	390-450	70-80	20	723	310	46
08X18H10T	923	330-380	50-80	20	773	240	30

Creep. At high temperatures metals undergo the slow plastic deformation under sustained relatively small stresses. This phenomenon is known as *creep*.

Creep changes the dimensions and shape of components and may end in their failure. At temperatures below the recrystallization temperature and under small stresses, the creep rate continuously decreases until the deformation ceases completely. The plastic deformation at low-temperature creep does not exceed several per cent. The rate of low-temperature creep reduces with time because as dislocations meet the impurity atoms, particles of second phase, and the like their motion decelerates and the metal hardens.

High temperatures facilitate cross slip and dislocations climb owing to the intensification of diffusion. As a result the metal loses strength. With temperature rise, the dislocation mobility increases and so does creep. Deformation may reach tens and hundreds per cent.

The curve of high-temperature creep (Fig. 3.10a) shows three stages: unstable creep (stage *I*), stable creep (stage *II*), and accelerated creep (stage *III*) preceding failure. In long-term service, the creep is evaluated by its rate in stage *II*. Creep usually occurs at temperatures above (0.3 to 0.4) T_m, i.e. within the temperature range when alloys may change their structure owing to the redistribution of alloying elements between the phases because of coagulation and the like.

In logarithmic coordinates, the deformation in creep versus time is expressed by straight lines *11'*, *22'*, *33'*, and *1'1''* and *2'2''* (Fig. 3.10b) forming convergent bundles. Lines *11'*, *22'* and *33'* corresponding to stage *I* and partially to stage *II* of creep intersect at point *B* at log ε = 1.4. This gives a deformation of 25%. The latter value approximates the elongation (25%) of the ЭП-44 steel at 823 K, the results of creep testing are shown in Fig. 3.10.
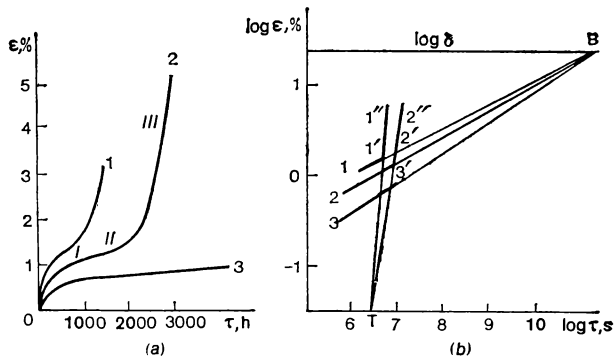
Fig. 3.10 Creep curves of ЭП-44 steel (C 0.2-0.3; Ni < 0.45, Cr 1-1.5, Mo 0.8-1.1, V 0.7-1.0; Nb 0.1-0.25, B 0.005) in Cartesian (*a*) and logarithmic (*b*) coordinates at 350 (*1*), 300 (*2*), and 250 (*3*) MPa. Testing temperature is 823 K

Another series of straight lines *1′1″* and *2′2″* corresponding. to stage *III* of creep intersect at point *T* at log ε = − 1.5. This gives a deformation of $3 \cdot 10^{-2}\%$. This value may be identified with the limit of elasticity for a given steel.

The analysis of creep curves (in logarithmic coordinates) of other materials gives the same results.

The metal surface may adsorb the coolant atoms or molecules thus decreasing the surface energy of the metal. This facilitates cracking, dislocation migration to the surface, etc. Liquid metals whose atoms penetrate microcracks, may reduce the resistance of materials to plastic deformation and intensify failure.

Fatigue Failure or Failure due to Stress Reversals. Each stress reversal adds to the accumulation of defects in a metal. When the total number of defects reaches a certain value, the metal fails. Under stresses below the yield point, failure occurs after 10^6 to 10^7 cycles. As has been experimentally found, pulsations in the paths of water-cooled and moderated power reactors occur at a frequency of 10 to 20 Hz. Pulsation sources may be flow disturbances inside the reactor and in the main circulation pump. Maximum stresses from oscillations reach 0.1 MPa.

In starting up and shutting down the nuclear power plants the metal deformation due to thermal stresses may reach 0.5% and more. This is known as *small-cycle fatigue*. Failure at about 600 K may occur after 3000 to 5000 cycles. The water coolant accelerates failure. In particular, the surface of drum-separators made of high-strength steel cracks from low-cycle fatigue. Surfacing with austenitic stainless steel markedly increases the resistance of atomic power station equipment to small-cycle fatigue.

If temperature varies in the range such that the maximum temperature of the thermal peak exceeds the temperature of the material recrystallization the latter appreciably deforms. When the cycle temperature varies within 300-800 K, specimens of aluminum change their length by 4% after 30 cycles. The higher the cooling rate, the greater the material elongation. Brittle materials subjected to temperatures varying quickly and greatly in magnitude (thermal shock) quickly fail under internal stresses.

3.3 Compatibility of Reactor Materials

Compatibility characterizes the interaction between the nuclear fuel and the fuel element cladding. A nuclear fuel and its cladding material are recognized as compatible under the specified conditions, if contacting each other for a long period of time they do not interact, or interact at a negligibly small rate, and this does not affect the shape or sealing of fuel elements.

The compatibility of materials in a number of cases determines the service life of fuel elements and their maximum operating temperature, and is one of the most important criterions in choosing the cladding material. The interaction of fuel and cladding gives products of different density: smaller or greater than that of the original materials. In the former case, the dimensions of the fuel elements may change, while in the latter, the contact between the fuel and the cladding may be disturbed. Thinning of the cladding along with stresses arising in the fuel elements may cause failure of the cladding and washout of the nuclear fuel into the coolant.

The interaction between the materials of fuel and cladding mainly proceeds by *diffusion*. The durability of fuel elements can be evaluated in terms of diffusion rate.

In a solid body with an ideal lattice, atoms may vibrate only about an equilibrium point. To move an atom from one lattice node to another or to an interstitial site, the regularity of the lattice structure must be disturbed at least for a short period of time. It may be suggested that atoms displace by changing places with neighboring atoms. In this mutual displacement the lattice must appreciably distort. In order to pass the interchanging atoms their neighbors must be forced apart by at least two atomic diameters.

Another mechanism of diffusion has been proposed by the Soviet scientists A.F. Ioffe and Ya.I. Frenkel. They have shown that in real crystal lattices an atom may leave a lattice node for an interstitial site. The atom occupies the same position as the alloying element atom in a solid interstitial solution. When the lattice deforms in the vicinity of an atom occupying an interstitial site, the potential barrier the atom has to overcome to move to a new interstitial site is less than the potential barrier an atom has to overcome to leave

a lattice node for an interstitial site, i.e. an atom occupying an interstitial site becomes more mobile. Moving to an interstitial site the atom leaves the lattice node, forming a vacancy. Consuming little energy a neighboring atom may occupy a vacant lattice position leaving a vacancy behind. This is known as migration of vacancies.

A vacancy and an interstitial may naturally recombine and the lattice restores regularity. According to Frenkel, a certain equilibrium concentration of point defects (interstitials and vacancies) corresponds to each temperature. Their number rises with temperature.

The mass of substance crossing unit area in unit time, M [mole/(cm^2 s)], is proportional to the concentration gradient dC/dX (mole/cm^3):

$$M = D\, dC/dX. \tag{3.32}$$

The constant of proportionality D (cm^2/s) is called the diffusion coefficient.

This is the first Fick's law. It can be obtained by the following reasoning. Consider two planes at distance a from each other. The volume concentrations of the diffusing substance in these planes are $C_1 < C_2$, and the concentration gradient is dC/dX. Then, $C_2 = = C_1 + adC/dX$. The thickness of the planes is a. The number of particles per unit area in the planes is aC_1 and aC_2.

Suppose that particles may jump from one plane to another at a frequency v, the probability of jumping in both directions being the same. The total number of particles having left any plane per unit time will equal the product of the particle jumping frequency by the concentration of particles in this plane. However, since the probability of jumping in both directions is the same, the actual number of particles which have gone from one plane to another in unit time is equal to

$$M_1 = 0.5vaC_1; \quad M_2 = 0.5vaC_2 = 0.5va\,(C_1 + adC/dX).$$

The difference between the numbers of particles gone in opposite directions is equal to the flow of particles:

$$M = M_2 - M_1 = 0.5vaC_1 + 0.5a^2\,(dC/dX)$$
$$-0.5vaC_1 = -0.5va^2\,(dC/dX).$$

Hitherto it was supposed that each atom can participate in diffusion; it must break bonds with the neighboring atoms. The activation energy of the process, as shown above, is $Q_1 = 0.25\,E_b$.

The probability that an atom will have an energy equal to the activation energy is equal to:

$$W_1 = \exp\,(-Q_1/RT) = \exp\,(-0.25\,E_b/RT). \tag{3.33}$$

Breaking the bonds. the atom moves to a vacancy, but the probability of the vacancy formation equals

$$W_v = \exp\,(-Q_v/RT) = \exp\,(-0.25\,E_b/RT). \tag{3.34}$$

Both events are independent and the probability of their concurrent occurrence is as follows

$$W = W_1 W_v = \exp\,[-(Q_1 + Q_v)/RT]$$
$$= \exp\,(-0.5\,E_b/RT). \tag{3.35}$$

Hence $M = 0.5va^2 \exp\,(-Q/RT)dX/dC$.

Comparing this expression with Fick's law, we obtain

$$D = 0.5va^2 \exp\,(-Q/RT) = D_0 \exp\,(-Q/RT), \tag{3.36}$$

where

$$D_0 = 0.5va^2. \tag{3.37}$$

On the average, we may assume $v = 10^{13}$ 1/s; $a = 3\cdot10^{-8}$ cm. Then $D_0 = 0.5\cdot10^{13}\,(3\cdot10^{-8})^2 = 4.5\cdot10^{-3}$ cm²/s, which is close to the values obtained from experiments.

In a deformed metal. the lattice is distorted. In the dislocation core, the ionized atoms are displaced from their equilibrium positions and possess increased energy. Therefore the activation energy of diffusion along the dislocation lines is less than that in the perfect lattice. The rate of diffusion along the dislocation lines is naturally greater. Thus the deformation of the metallic nuclear fuel and the fuel element cladding promotes their interaction and impairs compatibility.

Evaluate the activation energy Q_d of the diffusion along the dislocation line. The atoms in the dislocation core have an extra energy of 41.8 kJ/mole. Hence

$$Q_d = 2\,(0.25E_{cr} - 41.8) = 0.5E_{cr} - 83.6$$
$$= Q - 83.6. \tag{3.38}$$

This is confirmed by experiment. The crystal lattice at the grain boundaries is distorted in the same way as in the dislocation core. Therefore the diffusion along the grain boundaries also differs considerably from that in the perfect lattice.

Surface Diffusion. Diffusion can also occur in the surface layer of a metal. In that case breaking of the bond with the lattice should not coincide in time with the vacancy formation. Breaking the bond with the lattice an atom may occupy any neighboring position, since it moves over a plane. Therefore the activation energy of the surface diffusion must be half that of the volume diffusion. This is also proved by experiments (Table 3.6).

TABLE 3.6 Activation Energy of Volume and Surface Diffusion, kJ/mole

Metal	W	Ta	Mo	Nb	Fe	Ni	Cu	Pb	Ge	Si
Q_s	306	231	277	200	121	90	53	34	129	189
Q	504	462	407	400	240-273	280	205	116	287	462
Q_s/Q	0.61	0.46	0.68	0.5	0.5-0.45	0.32	0.26	0.29	0.45	0.41

Only for Ni, Cu and Pb the activation energy of surface diffusion approximates $0.25/Q$.

The energy of surface atoms differs from that of the atoms in the bulk of the crystal by the surface energy. For most metals the surface energy $\gamma = 1.5 \cdot 10^{-4}$ J/cm². One square centimeter usually contains 10^{15} atoms. Then the energy of a surface atom $E_s = 1.5 \cdot 10^{-4}/10^{15} = 1.5 \cdot 10^{-19}$ J/atom.

The frequency of the surface atom vibrations can be evaluated as $E_s = h\nu$, where $\nu_s = E_s/h = 1.5 \cdot 10^{-19}/6.6 \cdot 10^{-34} = 2.27 \cdot 10^{14}$ 1/s. Thus for the surface diffusion

$$D_{0surf} = 0.5\nu_s a^2 = 0.5 \cdot 2.27 \cdot 10^{14} (3 \cdot 10^{-8})^2$$
$$= 0.1 \text{ cm}^2/\text{s}. \tag{3.39}$$

In the case of surface diffusion the preexponential member is greater and the activation energy is lower than in volume diffusion. Therefore, the surface diffusion proceeds more intensively.

To evaluate roughly the distance covered by the front of the diffusing substance, δ (cm), use the following relationship:

$$\delta^2 = 4D\tau \approx D\tau, \tag{3.40}$$

where τ is the time in which the diffusion front moves through distance δ, s.

In solid solutions, the lattice is distorted. Therefore the energy of atoms increases and the activation energy of diffusion decreases. *Diffusion in solid solutions* proceeds more intensively than self-diffusion. Diffusion is especially effective in the subtractional solid solutions and in nonstoichiometric compounds wherein the concentration of vacancies is high.

When assessing the compatibility of the nuclear fuel with the fuel element cladding, one has to know the diffusion coefficient of uranium in various metals. The activation energy of uranium diffusion into a metal is determined by the activation energy of self-diffusion in the metal in question. For some metals the following relationship between the activation energy of the uranium diffusion into a metal Q

and the activation energy of self-diffusion Q_{self} is valid:

$$Q = 0.7 \ Q_{self}.$$

The activation energy of aluminum self-diffusion is 142 kJ/mole. Therefore the activation energy of uranium diffusion into aluminum should be 100 kJ/mole. At 523K the coefficient of uranium diffusion into aluminum is $D = Q_0 \cdot 10^{-100/19 \cdot 523 \cdot 10^{-3}} \approx 1.5 \cdot 10^{-10}$ cm^2/s, where $D_0 = 1.7$ for the aluminum self-diffusion.

The depth of uranium penetration into aluminum, δ, in 2000 hours is $\delta = (4 \cdot 1.5 \cdot 10^{-10} \cdot 2 \cdot 10^3 \cdot 3.6 \cdot 10^3)^{0.5} \approx 6.6 \cdot 10^{-2}$ cm.

The experimentally defined value is close to 10^{-2} cm. The greater the lattices of the elements diffusing into uranium and uranium differ, the lower the activation energy of the elements' diffusion into uranium. The difference between the activation energies of self-diffusion of the diffusing element Q_{self} and uranium Q_U may be taken as the measure of this difference. As a first approximation, diffusion of a number of elements in γ-uranium, Q, is expressed as:

$$Q = 158 - 0.62 \ (Q_{self} - Q_U).$$

Uranium and its alloys contacting with the material of the fuel element cladding may form the *intermetallic compounds*. The greater the elements of the material differ in their metallic and chemical properties, such as the atomic radii of the metals, electronegativity of the elements, valency and ionization potentials of atoms, the greater the probability of the intermetallic compounds formation. Intermetallic compounds form, in particular, when uranium contacts the aluminum cladding.

Table 3.7 shows that with temperature intermetallic compounds form faster.

TABLE 3.7 Interaction Between Uranium and Aluminum: Temperature Effect

T, K	Time to appearance of intermetallic compounds	Phases formed (in decreasing order)
373	No reaction observed	—
473	No reaction observed	—
523	240 h	UAl_2
573	24 h	UAl_2, UAl_4, UAl_3 (traces)
623	6 h	UAl_2, UAl_4, UAl_3
673	1 h	Same
773	Immediately	Same

Compatibility of Uranium. UAl_2 and UAl_3 form metallic films bonded to U and, seemingly, have no essential effect on heat transfer and contact of U with Al. The UAl_4 intermetallic compound does

not form a phase well bonded to Al or UAl$_3$. The UAl$_4$ disintegrates into powder. This disturbs the contact of U with Al.

To improve the compatibility between the fuel element cladding and fuel, a diffusion barrier is made by placing, for instance, nickel between uranium and aluminum. Intermetallic compounds form far slower in the U–Ni system than in the U–Al system. A layer of Al$_2$O$_3$ 20 μm thick covering the surface of Al prevents its interaction with U up to 823 K. The compatibility of uranium with a number of metals is illustrated in Table 3.8.

TABLE 3.8 Compatibility of Uranium with Some Metals

Metal	T, K	Results of 200-h testing	Metal	T, K	Results of 200-h testing
Al	573	Noncompatible	Nb	873	Compatible
Be	873	Noncompatible	Stainless	773	Insignificant in-
Cr	873	Compatible	steel		teraction
Cu	873	Compatible		923	Same
Fe	773	Compatible		973	Intensive interac-
	873	Noncompatible			tion
Mo	873	Compatible	Ta	1173	Compatible
Ni	773	Compatible	Tc	973	Compatible
Ni	873	Noncompatible		1173	Noncompatible
				973	Compatible
			Zr	1073	Noncompatible

The cladding material interacts with the fuel to produce the *low-melting compounds*. Thus, Fe, Mn, Ni react with U to form the intermetallic compounds and eutectic with a melting point 988–1013 K.

At a temperature somewhat below the eutectic temperature the system interacts slowly. At a temperature above the eutectic temperature (1033–1073 K) the interaction is so fast that Fe, Ni, and stainless steel become fully fused with uranium in 21 hours. Tungsten does not solve in solid uranium and solves, but very slowly, in liquid uranium. Tantalum slowly dissolves in uranium at 1573 K. The compatibility of refractory metals with uranium decreases in the following order: W, Ta, Nb, Zr, Ti, and Mo.

3.4 Radiation Stability of Structural Materials

The structural materials of a nuclear reactor core are subject to the action of neutrons, electrons, γ-rays, and so on.

Recent years have aroused a considerable interest in the occurrence and nature of radiation damage and its effect on the properties of the reactor materials. The Soviet scientists A.A. Bochvar, S. T. Ko-

nobeevskiy, A. S. Zaimovskiy and others contributed greatly to this field of science.

Neutrons, especially fast, produce much damage.

The interaction with neutrons changes the structure and mechanical properties of materials. Neutron irradiation increases the disordering of the structure and facilitates the decay of a solid solution.

When neutrons having an energy of 2 MeV collide against a metal lattice the time to reduce the neutron energy to 100 eV is less than 10^{-13} s, i.e. the deceleration energy is transmitted to the lattice atoms in primary collisions practically instantaneously. Having received considerable energy, a lattice atom can be knocked out of the lattice node and occupy an interstitial site. This produces a vacancy. The interstitial vacancy pair is stable only when the atom is displaced from the vacancy at a distance exceeding the lattice constant. A displaced atom possessing increased energy can in turn cause displacement of other atoms. This increases the number of defects. The number of displaced atoms per one primarily knocked out atom in the irradiation of a reactor metal with 1 MeV neutrons is 390 for iron, 140 for beryllium, and 900 for graphite.

Displaced atoms may produce a number of stable configurations; in the FCC lattice an atom may occupy an interstitial site. A displaced atom together with one of the neighbouring atoms of the lattice may form a paired combination (dumb-bell), with the centre in the lattice node. The dumb-bell atoms may form a chain with the atoms occupying normal positions in the lattice. The latter type of defects is known as *crowdion* (see Fig. 3.3).

Damage to the crystal lattice by fast particles may be considered as a result of particle collisions or an effect created by a fast thermal process. The path of a fast particle in substance may be divided into two stages. The first stage of high energy leaves only single defects such as vacancies, displacement atoms. In the second stage, when the fast particle has lost most of its energy, its run between sequential atomic collisions reduces greatly, i.e. it more often collides with lattice atoms. In the latter case random motion prevails causing complete disorder in the system. This disorder should not be interpreted as the appearance of single defects in the lattice, since the lattice itself ceases to exist.

The region surrounding the place where the fast particle has stopped has increased temperature and pressure. The substance in this region is in the form of a liquid or solid gas known as "atomic plasma". After cooling the lattice restores, but the atoms occupy new positions, e.g. they become relocated. Hence, the name: the *displacement spike*. The lattice surrounding the spike region has an effect on the orientation of the crystallizing region in which the initial crystal structure almost fully restores. Screw dislocations preserve and dislocation loops 10-50 nm in diameter are formed. The region of the displacement spike

in which melting with subsequent crystallization occurs is the cylindrical region at the end of the displacement atom path. This region is 2-4 interatomic distances in diameter. It contains along the path from 4 to 12 lattice atoms per each interatomic distance.

If the energy transferred by a particle in the metal irradiation is insufficient to cause local melting of metal and make atoms interchange positions, then local heating may produce as though a local thermal treatment. This region is known as the *thermal spike*.

In polymeric materials irradiation causes ionization, *cross-linking*. Irradiation of semiconductors changes the concentration of carriers.

Defects (vacancies, interstitials) generated under irradiation may move over considerable distances, as the bonding between them weakens. At a high temperature (high mobility) such defects move at random within the crystal lattice. A wandering defect may encounter a defect of an opposite sign and recombine with it, go to the grain boundary of a polycrystal where it can be adsorbed, if this decreases the total boundary surface energy. With an increase in temperature the defect may again migrate into the grain body. Dislocations may adsorb defects. The former are always present in annealed and cold-worked metals.

The interaction of the crystal lattice with fast neutrons produces most defects formed in irradiation of materials. Electrons and γ-quanta, however, can also form defects. Subjected to the electron irradiation, atoms give off energy in small portions not sufficient to allow a primarily knocked out atom to cause subsequent displacement. Therefore, electrons can produce only single defects. Atoms displace mainly from the elastic collisions with electrons. The energy transferred to an atom by a fast electron (E) is estimated by the relationship $E = 2E_i \; (E_i + 2m_0C^2)/MC^2$ where E_i is the initial kinetic energy of an electron; m_0 is the electron mass; M is the atomic mass; C is the light velocity. If the energy of a γ-quantum is 1 MeV and more, it is transferred to an electron by the Compton scattering mechanism. The Compton scattering plays the principal role in the energy range of 0.5 to 1.0 MeV for the elements with the atomic numbers below 60 and in the range of 1 to 5 MeV it is the main source of fast electrons for all elements of the Periodic Table. When radiation is scattered at an angle greater than 90 degrees, the energy transferred to an electron from the γ-quantum is of the order of the energy of the γ-quantum. Compton electrons capable of transferring energy above 25 eV to the atoms of the medium produce interstitials.

The lattice defects adsorbing at dislocations block the latter. The defects create the Cottrell atmospheres at the dislocations and reduce their mobility.

Energy Absorbed by the Crystal Lattice in Irradiation. A heat pulse can propagate in a solid body at the velocity of sound or slower. Therefore, in the time of the deceleration of a high-energy particle,

the heat pulse may move through several interatomic distances from the place of deceleration. Hence, we may consider that an almost point-type 1-3 MeV source of heat appears in the deceleration region. It produces a radial flow of heat increasing the temperature of the region surrounding the place of deceleration. Thus, when a fragment having an energy of 2 MeV decelerates in uranium, a region $2.44 \times$ $\times 10^{-17}$ cm³ in volume and $1.8 \cdot 10^{-6}$ cm in radius, heated to 2273 K exists for $0.9 \cdot 10^{-11}$ s. The displacement spike in iron lattice 0.247 nm in radius consumes an energy of 20 keV.

Rapid cooling produces nonuniform distribution of density in the lattice region in question.

The maximum energy E (eV) consumed in the displacement spike depends on the atomic weight A as follows: $E = -17\,900 + 563A$.

Estimate the average energy received by the metal atoms when irradiated with fast neutrons ($E > 10^6$ eV) at a flux density $\varphi =$ $= 10^{13}$ cm⁻² s⁻¹. The nuclear cross-section S_0 is about 10^{-24} cm. In order to make the probability of hitting a nucleus with a neutron equal to 1, the irradiation must take τ s at $\varphi = 10^{13}$ cm⁻² s⁻¹; $\tau = 1/10^{13} \cdot 10^{-24} = 10^{11}$ s.

Therefore, an atom, on the average, receives the energy:

$$E = 10^6/10^{11} = 10^{-5} \text{ eV/(at s).} \tag{3.41}$$

At a fast neutron fluence $\Phi = 10^m$ cm⁻² the number of neutron collisions with atoms in 1 cm³ of metal is

$$P = 10^m \cdot S_0 \cdot 10^{23} = 10^m \cdot 10^{-24} \cdot 10^{23} = 10^{m-1}, \tag{3.42}$$

where 10^{23} is the number of atoms in 1 cm³.

Strength Characteristics and Irradiation. Changes in the structure of metals under irradiation affect the strength of materials. The yield point begins to increase already at a fluence of 10^{17} cm⁻². For a number of metals the yield point is proportional to the cube root of the fluence. The ultimate strength varies with irradiation in a more complicated manner. With copper and nickel, for instance, the ultimate strength is independent of irradiation till a fluence of 10^{19} cm⁻². At higher fluences the ultimate strength behaves like the yield point.

The dependencies of the yield point and ultimate strength on irradiation differ in that relatively low doses of irradiation produce metal hardening, while at high doses the yield point approaches the ultimate strength and the ductility margin decreases. The maximum elongation to rupture also decreases. The metal becomes more brittle. Thus, the irradiation with fast neutron fluence of 10^{20} cm⁻² increases the yield point of carbon steels 2 to 3 times (from 450 to 1100 MPa) and reduces the elongation from 22 to 4%.

In a number of cases, when the experimental data are not available, we have to estimate a change in the mechanical properties of

steels, say the yield point, under irradiation. To this end, we may use a simplified model discussed below.

In iron-base alloys each collision with a fast neutron produces 390 interstitial atoms. At a fluence of 10^m cm^{-2}, the number of such atoms is n (cm^{-3}):

$$n = 390 \cdot 10^{m-1}. \tag{3.43}$$

In any crystallographic direction per each interstitial there are n_{ir} atoms located in sites of the perfect lattice:

$$n_{ir} = [(d/A)(N/n)]^{1/3}$$
$$= [(7.8/56)(6 \cdot 10^{23}/390 \cdot 10^{m-1})]^{1/3} \approx 1.29 \cdot 10^7/10^{m/3}. \tag{3.44}$$

According to the approximate model in question a displaced atom of iron 0.126 nm in radius occupies a tetrahedral void 0.036 nm in radius.

The crystal distorts by $\Delta r_{ir} = 0.126 - 0.036 = 0.09$ nm and this produces the following deformation in a unit cell of α-iron:

$$\varepsilon_{ir} = \Delta r_{ir}/a = 0.09/0.286 = 0.315. \tag{3.45}$$

As is already known, the maximum deformation of a unit cell is:

$$\varepsilon_m = 0.087. \tag{3.46}$$

Hence, we may assume that in the chosen crystallographic direction the number of unit cells that have undergone the maximum deformation owing to the formation of an interstitial atom is

$$P_{ir} = \varepsilon_{ir}/\varepsilon_m = 0.315/0.087 \approx 3.6. \tag{3.47}$$

The fraction of interatomic distances deformed to a maximum owing to the formation of interstitials is

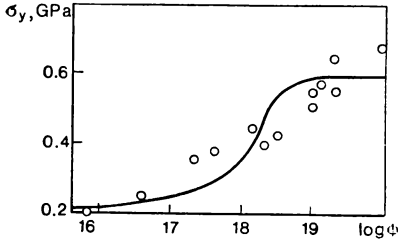$$S_{ir} = P_{ir}/n_{ir} = 3.6 \cdot 10^{m/3}/1.29 \cdot 10^7 = 2.79 \cdot 10^{-7} \cdot 10^{m/3}. \tag{3.48}$$

Analogous to (3.17)

$$\gamma_{ir} = \gamma_0 (1 - S - S_{ir}), \tag{3.49}$$

where γ_{ir} is the coefficient of overstress for the irradiated material.

Combining (3.48) and (3.49) we obtain:

$$\gamma_{ir} = \gamma - \gamma_0 S_{ir}$$
$$= \gamma - 310 \cdot 2.79 \cdot 10^{-7} \cdot 10^{m/3}$$
$$= \gamma - 8.65 \cdot 10^{-5} \cdot 10^{m/3}. \tag{3.50}$$

Fig 3.11 σ_y versus fast-neutron fluence
solid line – calculation by (3.52) with account of (3.58); light circles – experiment

Taking into account the above-considered relationships

$$\sigma_{y_{ir}} - \sigma_y = \Delta\sigma = (0.3G/0.7)\,[(1/\gamma_{ir}) - (1/\gamma)]$$

$$= (0.3G/0.7)\,[(\gamma - \gamma_{ir})/\gamma_{ir}\gamma]$$

$$\approx 0.3 \cdot 8.47 \cdot 10^4\,(\gamma - \gamma + 8.65 \cdot 10^{-5} \cdot 10^{m/3})/0.7\gamma^2$$

$$= 0.3 \cdot 8.47 \cdot 10^4 \cdot 8.65 \cdot 10^{-5} \cdot 10^{m/3}/0.7 \cdot 2.25 \cdot 10^4$$

$$= 13.9 \cdot 10^{-5} \cdot 10^{m/3} \qquad (3.51)$$

at $\gamma \approx 150$. Hence, $(\Delta\sigma/10^{m/3}) \cdot 10^5 = 13.9$. The experimentally determined value is close to 10.

Taking into account (3.19) the yield point of steel 20 after irradiation with a 10^m cm^{-2} neutron fluence is

$$\sigma_{y_{ir}} = 0.3G/0.7\gamma_{ir} = 190/(1 - 4.58 \cdot 10^{-7} \cdot 10^{m/3})\ \text{MPa}. \qquad (3.52)$$

Calculated by (3.52) and experimentally defined values of the yield point of steel 20 are given in Fig. 3.11.

Note that at the defined fluence of 10^m all unit cells in any crystallographic direction will undergo maximum deformation. Taking into account (3.43), (3.47), we obtain:

$$n^{1/3} = (390 \cdot 10^{m-1})^{1/3} = 1/a \cdot P_{ir} = 1/2.5 \cdot 10^{-8} \cdot 3.6,$$

where a is the interatomic distance, i.e. $m = 19.55$. Therefore, at a neutron fluence in excess of $3.5 \cdot 10^{19}$ cm^{-2} the yield point should not increase materially, which is observed experimentally.

Figure 3.11 shows that the experimental and calculated data agree satisfactorily. The difference between 25 calculated and experimental values of the yield point at a given fluence and before the irradiation has been defined in eight grades of hardened perlitic steels. Statistical processing with account of the Student t distribution has shown that no significant differences exist between the results of calculation and experiment.

Now, let us estimate changes in the ultimate strength at irradiation. According to the Griffith relationship:

$$\sigma_u = \sqrt{E\rho/2L}, \tag{3.53}$$

where $\rho = 1.5 \cdot 10^{-4}$ J/cm^2 = 0.5 eV/at.

The interaction with neutrons increases the energy of atoms in a metal. At a fluence of 10^m cm^{-2}, the energy of each atom, surface atoms including, increases by ρ_1:

$$\rho_1 = qn \cdot 10^{m-1}/[(d/A)\,N] = 25 \cdot 390 \cdot 10^{m-1}/[(7.8/56) \cdot 6 \cdot 10^{23}]$$
$$= 1.16 \cdot 10^{-20} \cdot 10^m \text{ eV/at,} \tag{3.54}$$

where $q = 25$ eV is the energy of an interstitial; $n = 390$ is the number of interstitials formed in interaction with a fast neutron; $d = 7.8$ g/cm^3 is the iron density; $A = 56$ is the atomic weight of iron; N is Avogadro's constant.

The surface energy is

$$\rho_{ir} = \rho + \rho_1 = 0.51 + 1.17 \cdot 10^{20} \cdot 10^m \text{ eV/at.} \tag{3.55}$$

The ratio

$$\rho_{ir}/\rho = 1 + 2.28 \cdot 10^{20} \cdot 10^m. \tag{3.56}$$

From (3.53) and (3.56) follows:

$$\sigma_{u\ ir} = (E\rho_{ir}/2L)^{0.5} = (E\rho/2L)^{0.5}\,(\rho_{ir}/\rho)^{0.5}$$
$$= \sigma_u\,(1 + 2.28 \cdot 10^{20} \cdot 10^m)^{0.5}. \tag{3.57}$$

Table 3.9 gives calculated by (3.57) and experimentally defined values of the ultimate strength for steel 20. When no irradiation takes place, $\sigma_u = 500$ MPa.

The difference between 12 calculated and experimental values of the ultimate strength at a given fluence has been defined in four grades of hardened perlitic steels. Statistical processing with account of the Student t distribution has shown that no significant difference exists between the calculated and experimental data. At a fluence of 10^{19} cm^{-2}

$$\sigma_y \approx 0.9\ \sigma_u. \tag{3.58}$$

It should be noted here that

TABLE 3.9 Values of σ_u for Steel 20

Fluence $(E >$ > 1 MeV), 10^{18} cm^{-2}	σ_u, GPa	
	Calculated	Experimental
1	0.5	0.5
3.16	0.52	0.55
10	0.55	0.61
10^2	0.9	0.85

this, like any other model, illustrates the phenomenon only in principle and estimates the effect of irradiation at low temperatures on σ_u and σ_y only to a first approximation. In practice use should be made of the appropriate experimental data.

For the effect of the neutron fluence on the mechanical characteristics of the austenitic chrome-nickel stainless steel see Table 3.10.

TABLE 3.10 Austenitic Stainless Chrome-nickel Steel (17-19% Cr, 9-12% Ni) at Room Temperature after Irradiation with Fast Neutrons at Different Fluences

Fluence, cm^{-2}	σ_u, MPa	σ_y, MPa	Elongation, %	Fluence, cm^{-2}	σ_u, MPa	σ_y, MPa	Elongation, %
$T=373$ K				$T=573$ K			
—	675	340	53	—	550		40
10^{17}	730	380	48	$3 \cdot 10^{19}$	650		27
$5 \cdot 10^{17}$	720	530	45.5	$6 \cdot 10^{19}$	680		21
$4.3 \cdot 10^{18}$	875	710	37	10^{20}	720		18
$9 \cdot 10^{18}$	780	680	34.5	$3 \cdot 10^{20}$	750		14
10^{20}	880	780	23	$5 \cdot 10^{20}$	770		18
				$7 \cdot 10^{20}$	790		12

The elongation of steels decreases with fluence. Estimate the effect of irradiation on the elongation of the austenitic stainless steel. From (3.20) we obtain:

$$\delta_{ir}/100 = \varepsilon \approx \gamma_{ir}/\gamma_0 = \gamma_0 \, (1 - S - S_{ir})/\gamma_0$$
$$= 1 - S - S_{ir}; \tag{3.59}$$
$$\delta_{ir} = 100 \, (1 - S) - 100 S_{ir} = \delta - 100$$
$$\times \, 1.68 \cdot 10^{-7} \cdot 10^{m/3}$$
$$= \delta - 1.68 \cdot 10^{-5} \cdot 10^{m/3}; \tag{3.60}$$
$$\delta - \delta_{ir} = \Delta\delta = 1.68 \cdot 10^{-5} \cdot 10^{m/3} \tag{3.61}$$

Hence,

$$(\Delta\delta \cdot 1.68 \cdot 10^{-5}/10^{m/3}) \cdot 10^5 = 1.68. \tag{3.62}$$

The values defined experimentally lie within 0.4 -1.

The irradiation at $T = 373$ K has a far less influence on the ductility of the austenitic steels. Even at a fluence of 10^{22} cm^{-2}, the elongation of the austenitic stainless steel makes up 30%.

At an irradiation temperature above 623 K the radiation defects partially anneal. Thus, at a fluence of $1.6 \cdot 10^{21}$ cm^{-2} the elongation of the austenitic chrome-nickel stainless steels, grade 08X18H10T, varies with the irradiation temperature as follows:

T, K   563   723-773

δ, %   1   58

The radiation defects anneal and, therefore, the mechanical properties recover at 693-923 K. The temperature of complete annealing is 0.5-0.55 of the absolute melting temperature of steel.

Let us consider in more detail the *annealing of radiation defects* and, in particular, the temperature at which it takes place. As a first approximation, we may assume that, if a displaced atom moves through a distance equal to the radius of a dislocation loop formed in the interaction of a fast neutron with the lattice ($r = 2.5 \cdot 10^{-7}$ cm), it will take its place in the undistorted lattice and the radiation defect will cease its existence. In most commercial metals $\gamma \approx 160$. Hence, the volume fraction of the distorted unit cells n equals $(\gamma/\gamma_0)^3 \approx 0.1$. Therefore, the number of the distorted unit cells in 1 cm³ is close to $10^{23} \cdot 0.1 = 10^{22}$. Suppose that a fast neutron displaces 400 atoms from their equilibrium positions. The density of a neutron flux having an energy above 0.5 MeV is $3 \cdot 10^{13}$ (cm² s)$^{-1}$. Taking into account (3.42), $M_1 = 3 \cdot 10^{12} \cdot 400$ displaced atoms are formed per second. Simultaneously, according to the Fick's law

$$M_2 = D \cdot 10^{22}/r \approx (10^{-Q/19.1 \cdot T \cdot 10^{-3}}) \, 10^{22}/r$$

atoms displaced from the equilibrium position per second move to the undistorted lattice region. Note that for most commercial metals $D_0 \approx 1$ cm²/s.

In equilibrium $M_1 = M_2$. Hence, $3 \cdot 10^{12} \cdot 400 = 10^{-Q/19.1 \cdot T \cdot 10^{-3}} \times 10^{22}/r$. Herefrom $T = Q \cdot 10^3/296.5$, where Q is the activation energy of self-diffusion, kJ/mole. The radiation defect annealing temperatures calculated by the latter relationship satisfactorily agree with the experimental data (Table 3.11).

The radiation defects distort the crystal lattice, thus increasing the energy of the atoms. The activation energy of diffusion decreases

TABLE 3.11 Calculated and Experimental Radiation Defect Annealing Temperatures

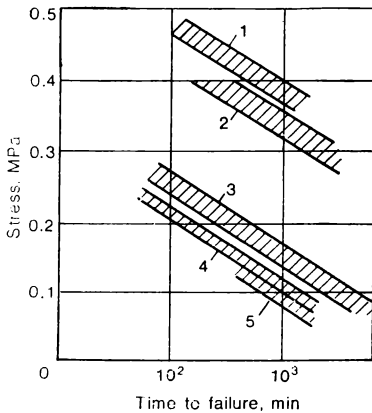| Material		0X18H10T	Steel 20	Be	Al	Graphite (carbon)	Zircalloy-2	Cu	Mg
Q, kJ/mole		270	240	156	142	680	92.1	205	134
T, K	Calculated	910	810	530	480	2300	604*	690	450
	Experimental	800-900	750-830	623-700	423	2200-2300	550-770	600	470

* Taking into account $D_0 = 3 \cdot 10^{-8}$ cm²/s

Fig. 3.12 Long-term strength of 08X18H9T steel at various temperatures (fluence 10^{20} cm^{-2})
1—600°C, nonirradiated; *2*—600°C, irradiated at 450°C; *3*—700°C, nonirradiated; *4*—700°C, irradiated at 450°C; *5*—700°C, irradiated at 550°C

and hence the diffusion coefficient increases. According to (3.9), (3.44), and (3.45) the lattice energy increases by

$$\Delta Q = \varepsilon^2/K = \left(\frac{r - 0.414r}{2rn_{ir}}\right)^2 \Big/ K$$

$$= \left(\frac{0.586 \cdot 10^{m/3}}{2 \cdot 1.29 \cdot 10^7}\right)^2 \Big/ 0.85 \cdot 10^{-3}$$

$$= 6.07 \cdot 10^{-13} \cdot 10^{2m/3},$$

where $0.414\ r$ is the radius of the octahedral void in a close-packed lattice; $K = 0.85 \cdot 10^{-3}$ for Ni. Using (3.36) we obtain for 573 K:

$$d \log D/d\ (10^{2m/3}) = \Delta Q/RT = 6.07 \cdot 10^{-13}/19.1 \cdot 0.573$$

$$= 5.6 \cdot 10^{-14}.$$

When beryllium diffuses in nickel, the experimentally defined value is equal to $7.6 \cdot 10^{-14}$.

The irradiation of the austenitic steel at a temperature above 873 K produces *radiation embrittlement*. The phenomenon is characterized by decreasing the long-term strength and elongation in short-term tensile tests of specimens at temperatures above 873 K. In some materials this effect is irreversible and in some only partially reversible. Thus, annealing at a temperature of 1373-1423 K completely restores the properties of irradiated materials.

The embrittlement is also observed in high-temperature testing of specimens of the austenitic stainless steel pre-irradiated at a low temperature. This is illustrated in Fig. 3.12 which shows the data on the

long-term strength of steel 08X18H9T irradiated at 873 to 973 K. Ageing steels demonstrate the greatest high-temperature embrittlement. Thus, the irradiation with a $(1\text{-}3) \cdot 10^{20}$ cm^{-2} fluence at a testing temperature of 973 K during 1000 h decreased the long-term strength of an ageing steel, containing 18% Cr and 28% Ni and additionally alloyed with tungsten, by 40 per cent and that of steel 08X18H9T, only by 15 per cent.

Neutron irradiation may affect the properties of the absorbing materials. Thus, the absorbing materials containing boron accumulate helium. At a high temperature the pressure of helium in micropores rises and this leads to the item deformation because of gas swelling.

The metal of the fuel element cladding of fast reactors is subjected to the action of high temperature and considerable fluxes of neutrons. The irradiation with a fluence above $(4\text{-}8) \cdot 10^{22}$ cm^{-2} at temperatures of 700-760 K produces the *radiation swelling* of the austenitic stainless steel by 10%, and the irradiation with a fluence of $3.5 \cdot 10^{22}$ cm^{-2} at 800 K, by 20%.

At a fluence of $(2\text{-}3) \cdot 10^{23}$ cm^{-2} swelling may reach 50 to 70%. This generates vacancy accumulations. The interstitials resulting from the interaction of neutrons having an energy above 0.1 MeV with the crystal lattice become fixed on the dislocation loops. Changes of a steel volume at 760-780 K depend on the fluence as follows:

$$\log (\Delta V/V, \ \%) = -45 + 2 \log \Phi.$$

Radiation swelling also depends on temperature. Thus, at a fluence of $7 \cdot 10^{22}$ cm^{-2}

T, K	634	673	698	723	748	773
$\Delta V/V$, %	2.7	3.0	4.3	6	5	3

At 733-833 K cold deformation up to 20% reduces swelling two- to threefold. At a temperature of 853 K the positive effect of cold deformation sharply drops. With increasing the content of Ni from 10 to 40% at a fluence of 10^{23} cm^{-2} and 898 K, the ratio $\Delta V/V$ drops from 50 to 1.2%. A further increase in the Ni content produces only an insignificant effect. This gives grounds to suggest that the interstitials fix themselves at the stacking faults. The width of the latter decreases as the nickel content increases from 10 to 40%.

In the thermonuclear fusion plants, the thermonuclear plasma radiation changes the surface and volume properties of the structural materials. Their interaction with neutrons and ions possessing high energy produces micropores in metals, the phenomenon is known as the *blister effect.*

When irradiating the austenitic stainless steel by argon ions of an energy of 70 keV and at a fluence of $2 \cdot 10^{17}$ cm^{-2}, each atom in the lattice undergoes 50 displacements. Part of the displaced atoms are

bonded by dislocations. The vacancy accumulations generate pores having an average diameter of 22 nm. One cubic centimeter contains up to $3 \cdot 10^{16}$ pores. The relative volume of pores is 20-40%. Increasing the Ni content in a steel to 45%, the pore size decreases to 10 nm and porosity drops to 0.5%. A decrease in the blister effect is also achieved by preliminary ionic alloying when creating the protective coating.

The irradiation of the austenitic stainless steel, grade 01X18H40M5, with helium ions at 723-873 K produces pores and cracks in the metal.

With increased helium content in the austenitic stainless steel the steel elongation reduces:

Content of He in steel, %	$\dfrac{\text{Elongation, no He}}{\text{Elongation in presence of He}}$
$5 \cdot 10^{-4}$	17
$2 \cdot 10^{-3}$	11

The thermonuclear plasma radiation erodes the first wall. The intensity of the process depends on the material. Thus, when the material contains Be, B, Ti, V, Mo, TiC, the wall thins per year by $(3-6) \cdot 10^{-2}$ cm, and when it has W and SiC, by $2.7 \cdot 10^{-3}$ cm.

In ferritic steels (carbon steels, low-alloy steels), irradiation not only raises the yield point and reduces elongation, but also increases the *critical point of brittleness* (cold-brittleness temperature) and reduces the impact strength. For carbon steel 20, the impact strength at $T > 300$ K is 29 J/cm^2. Decreasing the temperature to 240 K abruptly reduces the impact strength to 2.9 J/cm^2. The temperature at which the impact strength abruptly drops, i.e. steel embrittlement occurs, is known as the *temperature (threshold) of cold-brittleness*. In ferritic and perlitic steels, the cold brittleness temperature rises with the fluence.

The dependence of the temperature of cold-brittleness of steel 20 on the neutron fluence can be illustrated by the following data:

Φ, cm^{-2}	0	$2.7 \cdot 10^{18}$	10^{19}	10^{20}
T, K	240	298	343	363

The irradiation with a fluence of 10^{20} cm^{-2} makes these steels cold-brittle already at a temperature exceeding the room temperature. This must be taken into account when estimating the service life of a reactor vessel made of a steel of the perlitic class.

Let us assess the effect of irradiation on the temperature of cold-brittleness. We suppose that cold-brittleness occurs, when all inter-atomic distances are distorted, i.e. when

$$S_{ir} \approx 1. \tag{3.63}$$

Taking into account (3.44), (3.45), and (3.48) we have:

$$S_{ir} = 0.314 \cdot 10^{-7} \cdot 10^{m/3} / \varepsilon_{cr} \cdot 1.29; \tag{3.64}$$

$$\varepsilon_{cr} = (K \cdot 4R)^{0.5} (T \cdot 10^{-3})^{0.5} = 0.16 (T \cdot 10^{-3})^{0.5}. \tag{3.65}$$

Hence

$$S_{ir} = 0.312 \cdot 10^{-7} \cdot 10^{m/3} / 0.16 \cdot 1.29 (T \cdot 10^{-3})^{0.5}$$
$$= 1.51 \cdot 10^{-7} \cdot 10^{m/3} / (T \cdot 10^{-3})^{0.5}. \tag{3.66}$$

As a first approximation, steel embrittles when $S \approx 1$. Hence

$$(T \cdot 10^{-3})^{0.5} = 1.51 \cdot 10^{-7} \cdot 10^{m/3}; \tag{3.67}$$

$$T = 22.8 \cdot 10^{-12} \cdot 10^{2m/3}; \tag{3.68}$$

$$\Delta T / \Delta (10^{-12} \cdot 10^{2m/3}) = 22.8. \tag{3.69}$$

The experimental value of the ratio (3.69) is equal to 14.3.

The dependence of the temperature of cold-brittleness on the fluence may be also represented as follows. Expand into a series the last multiplier in the right-hand side of (3.68):

$$T = 22.8 \cdot 10^{(2m - 2.18)/3} \approx 22.8 \cdot (2 \cdot 10^{(m - 18/3)} - 2) \approx 45.6 \cdot 10^{-6} \cdot 10^{m/3}$$
$$- 45.6. \tag{3.70}$$

Then

$$\Delta T / \Delta (10^{-6} \cdot 10^{m/3}) = 45.6. \tag{3.71}$$

TABLE 3.12 Calculated and Experimental Values of ΔT

Fluence, cm^{-2}	ΔT	
	Calculated	Experimental
10^{17}	5	4
10^{18}	23	25-30
10^{19}	106	70-100

The experimental value of (3.71) is equal to 30-50. When the fluence rises above 10^{20} cm^{-2} ($E > 1.0$ MeV), the temperature of cold-brittleness practically does not rise. All unit cells of the lattice in any crystallographic direction are already deformed and the formation of new interstitials does not change the situation. The values of ΔT calculated by (3.69) are in satisfactory agreement with the experimental data (Table 3.12).

4   Coolants in Nuclear Reactors

The heat generated in a reactor is removed by a primary coolant flowing through the reactor. Most common coolants used in power reactors today are ordinary water (boiling water reactors and pressurized water reactors), heavy water, gases (nitrogen, helium, carbon dioxide, hydrogen, and their mixtures), liquid metals (sodium lithium, potassium, bismuth, lead, and their alloys), and organic coolants (a diphenyl mixture, for instance).

The practical considerations that govern the choice of a coolant are:

(1) Small corrosive and erosive effect on the reactor materials.

(2) High heat capacity and high heat transfer capability, and low viscosity.

(3) High boiling point and low melting point.

(4) High heat resistance and radiation stability.

(5) Low thermal neutron absorption cross section.

(6) Minimum explosion hazard, combustibility, and toxicity.

(7) Availability and low costs.

(8) Weak activation.

Small corrosive and erosive effect of a coolant ensures a trouble-free operation of equipment and radiation safety of the attending personnel. Heavy specific heat flows in a reactor make heat engineering characteristics one of the decisive factors governing the choice of a coolant.

High heat resistance and radiation stability of coolants exclude the penetration of any kind of impurities into the coolant which might affect the coolant properties and cause other objectionable after-effects.

4.1 Liquid-metal Coolants

Liquid metals find their application in fast and thermal reactors. The use of liquid metals as coolants in nuclear reactors in place of water has a number of advantages. Water as a coolant in fast reactors moderates neutrons, therefore its use is unexpedient. In liquid metals the temperature is independent of pressure, which is the case with ordinary water. This allows us to build high-temperature coolant circuits with low pressures in them. Irradiation of liquid metals, as

a rule, produces no such phenomena as the radiolytic decompo-
sition of water. Low pressure of saturated vapours, and high heat
resistance and radiation stability of liquid-metal coolants make
them the coolants of choice.

The most essential drawback of the majority of the liquid-metal
coolants is their low heat capacity per unit volume as compared
with water. This limits heat accumulation in a liquid-metal coolant.
Certain liquid metals (sodium is an example) react vigorously with
water, and this complicates the design of the thermal circuit of
a nuclear power plant. However, a higher thermal conductivity of
liquid-metal coolants ensures a more intensive heat removal from the
fuel elements, which is of special importance in fast reactors. (Ta-
ble 4.1 gives some physical properties of liquid metals.) In sodium-

TABLE 4.1 Physical Properties of Liquid Metals

Property	Bi	Pb	Li	Hg	K	Na	Na-44%K (by weight)
Melting point, K	544	600	453.5	234.2	336.7	370.8	292
Boiling point, K	1750	2010	1609	630	1033	1156	1098
Specific heat at 673 K, kJ/(kg deg)	0.1481	0.1473	4.3263	0.13766	0.7640	1.2782	1.0510
Density at melting point, kg/cm³	10	10.7	0.61	13.7	0.82	0.93	0.89
Thermal conductivity at 673 K, kJ/(m h deg)	56.0656	54.3920	169.4520	45.3964	142.2560	246.2560	96.6504
Thermal neutron absorption cross section, 10^{-28} m²	0.034	0.17	71	374	1.97	0.52	0.96

cooled fast reactors the heat flow density on the fuel elements
reaches $2.5 \cdot 10^6$ W/(m² s).

The drawback of the liquid-metal coolants (except mercury) is
that they solidify at room temperature. This calls for a heating sys-
tem to melt the metals and complicates the construction.

The smallest neutron absorption cross section is featured by Bi,
Pb, Na, Ga. Therefore, they are most suitable for the use as coolants
in thermal reactors. The most perspective coolants for fast reactors are
Hg, Li, and Na. Neutrons may form radionuclides in the liquid-
metal coolants, impairing the radiation situation in the circuit. In
terms of induced radioactivity most objectionable properties are
inherent in Na and K. The former forms radioactive nuclide ^{24}Na,
a $3.31 \cdot 10^{-13}$-J γ-emitter, the latter, ^{38}K, a $3.46 \cdot 10^{-13}$-J γ-emitter,
the emitting energy being given on the average. In an $80 \cdot 10^{-13}$ J

power reactor the radioactivity level of ^{24}Na lies within 10^4-10^7 Ci. The radioactivity level quickly drops after the reactor is shutdown since the half-life of ^{24}Na is small.

Corrosion in Liquid-metal Coolants. The contact of structural materials with liquid-metal coolants produces the following types of corrosion: (1) dissolution of a metal in the coolant melt, including selective dissolving of some components of the alloy; (2) mass transfer; (3) intercrystalline corrosion.

The *dissolution* of a solid metal in a liquid metal proceeds in two stages. The first stage involves cleavage of the bonds between atoms in the solid metal lattice and the formation of new bonds with atoms of the liquid metal or its impurities. This takes place in the liquid-metal layer adjacent to the solid metal, the so-called boundary layer. At the second stage, the dissolved atoms diffuse through the boundary layer into the liquid metal. Any of the stages may be decelerated, and thus control the net dissolution rate. In most cases it is the second stage. The metal dissolution involves a reverse reaction: the separation of dissolved atoms from the liquid metal.

When the rates of both reactions become equal, the liquid metal becomes saturated with dissolved atoms. In the general form the kinetic equation of dissolution is as follows:

$$n = n_\infty \left[1 - \exp \left(- \alpha \, \frac{S}{V_m} t \right) \right], \tag{4.1}$$

where n is the concentration of dissolved atoms at time t; n_∞ is the saturation concentration; α is the dissolution rate constant; S is the surface of solid metal in contact with liquid metal; V_m is the volume of liquid metal; t is the time.

The saturation concentration depends on temperature as follows:

$$\log (n_\infty \cdot 10^4) = 1.8266 - 558.5/T. \tag{4.2}$$

The solubility of an element in liquid metals is a function of the atomic number of the metal being dissolved. In liquid-metal solutions (as in hard solutions) the solubility increases with a decrease in the difference between the atomic radii of the components. Under isothermic conditions the rate of a solid metal dissolution decreases with time following the exponential law. Therefore, the melt agitation intensifies the dissolution. **The deformation** changing the energy state of atoms increases the dissolution rate.

In alloys, components may dissolve selectively. **The predominant** transition of a more soluble component into a liquid metal depletes the surface layer of this component. This may lead to phase transformations. Thus, the selective dissolution of nickel transforms austenite into ferrite in the surface layer when the austenitic chrome-nickel steels corrode in liquid Pb, Bi, Li.

Mass transfer takes place in systems where individual sections are subjected to different temperatures. In the zone with a lower temperature, the solution owing to a decreased solubility becomes oversaturated, and crystals of the dissolved element separate. Part of the crystals remain in the cold zone, while the other part move with the liquid-metal flow to the hot zone. Here the metal dissolution intensifies, since the solution concentration in the cold zone decreases. The mass transfer does not decelerate unlike the isothermal dissolution. Mass is transferred from the hot zone to the cold zone to a greater extent when the cold zone surface is far larger than that of the hot zone and may lead to lock formation. The austenitic stainless steel 1X18H10T corrodes in lithium owing to mass transfer at a rate of about $0.1 \ g/(m^2 \ h)$ with the hot zone temperature 853 K, temperature gradient 410 K, and flow rate 0.15 m/s. For low-alloy steels this magnitude may be an order greater.

Mass may be also transferred isothermically. In the alloy dissolution, the alloying elements pass into the liquid metal and are carried by the melt to another metal. Alloying elements may form with the other metal solid solutions or intermetallic compounds.

Most widespread is the transfer of carbon from steels containing less strong carbide formers to those with more strong, and also the transfer of oxygen and nitrogen from metal to metal and from the gas phase through the liquid metal to the solid metal. An example of the isothermic transfer is the joining of two solid metals which in an intimately tight contact are immersed in a liquid metal (the so-called *self-welding*).

The *intercrystalline corrosion* proceeds because the atoms at the grain boundary possess a higher potential energy as compared to the atoms inside the grain. Therefore, the activation energy of the grain boundary atoms is lower, and the probability of their transition to the melt and. hence, the dissolution rate are higher. The corrosion front deepens along the grain boundaries, i.e. the intercrystalline corrosion takes place. Even on complete saturation, the intercrystalline corrosion does not cease owing to the intensive local mass transfer.

Sometimes the concentration of certain elements increases at the grain boundaries. If these elements readily dissolve in the melt, the intercrystalline corrosion intensifies. A more intensive diffusion of easily dissolved atoms along the grain boundaries also promotes the intercrystalline corrosion. In particular, the intercrystalline corrosion of chromium steels in bismuth is attributed to the prevailing boundary diffusion of chromium. Ions of oxygen or sodium oxide chemically interact with the alloy components, in particular, with the impurity atoms found at the grain boundaries. Thus, the oxygen of the melt enhances the intercrystalline corrosion.

The rate of intercrystalline corrosion increases with elastic stress-

es in a metal. Thus, the depth of intercrystalline corrosion of steel 15X5M in eutectic Pb-Bi at 823 K increased from 25 to 50 μm in 1000 h when the stress increased from 1.47 to 9.8 MPa.

Alkali metals interact with oxygen dissolved in a solid metal. For example, Nb, Ta, Ti, Zr free of oxygen poorly dissolve in alkali metals. Under certain conditions, when the free energy of formation of a solid metal oxide is greater than that of an alkali metal oxide, the alkali metals deprive the solid metals of the oxygen dissolved in them. The alkali metal, lithium for example, penetrates niobium along the grain boundaries where niobium oxides may concentrate. The higher the oxygen content in niobium, the greater the depth of lithium penetration.

Wetting of a solid metal by a liquid-metal affects the mechanical characteristics of the solid metal even in the absence of corrosion. A highly ductile starting material capable of elongating by hundreds per cent grows brittle under the effect of a liquid-metal layer. Long-term strength and fatigue resistance change. This is associated with the adsorptive influence of the medium. The liquid metal penetrates the solid metal along the dislocation lines formed at the earlier stages of deformation. The adsorbed liquid metals reduce the energy barrier preventing dislocations from gliding out to the surface, and the metal loses strength. The metal may crack, when dislocation pile-ups pass out from the metal bulk to the surface. The medium penetration into the cracks widens them and makes the metal more brittle. The adsorptive effect of liquid metals on solid metals is now under intensive study which is still far from completion. Materially contributed to the solution of this problem the Soviet scientists: academicians P.A. Rebinder and S.T. Kishkin, and also E.D. Schukin, V.I. Likhtman, A.V. Ryabchenkov and others.

Corrosion Control. A number of methods have been suggested to reduce the corrosion rate of structural materials in liquid metals. The isothermic dissolution of a pure metal may be essentially reduced by *pre-saturating the melt with this metal*. This technique, however, is objectionable as it increases intercrystalline corrosion and mass transfer. Thus, adding to eutectic Pb-Bi a better soluble component of the alloy, Ni in this case, in an amount of 0.6%, reduces the corrosion rate of steel 1X18H10T at 873 K in 1000 testing hours from 1.4 to 0.3 mm/year. When several solid metals are dissolved in the melt, their maximum solubility in a number of cases is below that determined for each metal separately. The addition of Cu, Fe, or Zr to liquid mercury reduces the critical solubility of titanium by one half. The preliminary dissolution in a liquid metal of components essentially reducing the saturation concentration of a solid metal reduces the corrosion rate of the latter under isothermic conditions.

When a liquid metal does not reduce the oxides of a solid metal, the creation of an oxide film on the surface of the latter decelerates

the metal dissolution. In the presence of an oxide film, atoms of the metal being dissolved can reach the melt only after passing through the film. Diffusion in the solid phase proceeds at a far lower rate than in the liquid phase. Alloying iron with chromium facilitates the formation of an oxide film on the iron surface. Adding 4.8% Cr reduces sevenfold the rate of iron dissolution in bismuth at 823 K. The rate of corrosion of the high-chromium steels in bismuth reduces at 873-1223 K in the presence of oxygen in the argon protective atmosphere.

It should be noted that the saturation concentration remains unchanged even when the metal surface is covered with an oxide film. Oxide films also reduce mass transfer. Thus, an oxide film 100 nm thick on the metal surface increases the time taken to lock a circuit of steel 1X18H10T in liquid lead at the temperatures of the hot and cold zones of 1083 and 773 K, respectively, from 100-140 to 500 h. The corrosion centres appear in places where the oxide film was destructed. However, the protection by oxide coatings is only a provisional measure. The films break from mechanical damage, different coefficients of linear expansion of oxides and metals in thermal cycles, and erosion. With alkali metals reducing oxides of most structural materials, this method of protection is unsuitable.

Plating of a metal poorly soluble in the melt also reduces the rate of corrosion of the metal under protection. The molybdenum plating applied by the thermal diffusion technique protects high-nickel steels against corrosion in lithium. A surface protective coating is obtained by introducing certain elements into the surface layer of a metal. For example, nitriding the surface layer of titanium and its alloys reduces the rate of their corrosion in mercury at 811 K.

The contamination of alkali metals with oxygen intensifies corrosion. A melt is cleaned of oxygen in "cold" traps. The solubility of oxygen (oxides) in liquid metal decreases with decreasing temperature. Part of a metal circulating in the system is by-passed through a device where the temperature is close to the melting point of the liquid metal. The oxides deposit on steel chips filling the cold trap. The proper use of the technique reduces the oxygen concentration to 0.005%. For a more complete deoxidation of a liquid metal (e.g., when the melt contacts the refractory metals) use is made of "hot" traps with getters: Ti, Zr, Y, Mg. Hot traps are usually mounted on a by-pass and have a temperature inside them such that the oxygen dissolved in the liquid metal reacts with the getter when the liquid metal passes the trap.

Elements vigorously reacting with oxygen may also be introduced into the liquid metal. Thus, sodium or magnesium introduced into mercury materially reduce the corrosion of steel. The elements added to a melt to protect the structural materials against corrosion are known as *inhibitors*. Inhibitors bind the oxygen or form protec-

tive films. An inhibitor must possess a small neutron absorption cross section, be well soluble in the liquid metal and not become essentially activated in the irradiation zone. Since the inhibitor has to bind oxygen, the free energy of formation of the inhibitor oxide must be more negative than that of the liquid metal oxide. Barium meets the above listed requirements. Adding it in an amount of 1% to the liquid sodium at 823 K reduces mass transfer in a circuit of stainless steel 10- to 100-fold. An inhibitor should be introduced into a melt, if the latter contains more than 0.01% of oxygen. The introduction of small amounts of zirconium or titanium (0.005%) into liquid Bi, Pb, Hg essentially reduces the corrosion of steels. Films of zirconium and titanium nitrides and carbides form on the surface of steels. The films create an additional barrier to the movement of atoms from the solid metal to the melt and hinder the crystallization of the dissolved solid metal in the cold zone. Thus, inhibitors in the given systems reduce the mass transfer as well. Helium and argon containing 0.002-0.005% of oxygen and 0.003% of carbon create a protective atmosphere.

Sodium. It has certain advantages over other liquid-metal coolants: a relatively low melting points, satisfactory heat-transferring properties, and moderate pumping power consumption. Less attractive are its nuclear and chemical properties. The commercial sodium contains not more than 0.3-0.4% (by mass) of impurities:

K	Ca	Fe	Mg	Si	O_2	H_2	C
0.01-0.05	0.01-0.02	0.001	0.001-0.2	0.001-0.2	0.003	0.005	0.006

Potassium forms alloys with sodium and mixes with it in any proportion; Pb, Cd, Cs, and Ag also produce alloys with sodium, their total content in sodium does not exceed 0.001%. The net content of Fe, Cr, Mo, Ni, and Ta is not above 0.01%. The presence of oxygen in the form of sodium oxide, Na_2O, makes the metal aggressive. The density of liquid sodium is somewhat below that of water under normal conditions.

The metallic sodium has a silvery white colour clearly seen on a fresh cut, since sodium is usually coated with an oxide film. Sodium is exclusively reactive. Dry oxygen combines with sodium at room temperature. The reaction, however, rapidly ceases owing to the formation of an oxide film on the metal surface. Even traces of moisture in the air intensify the oxidation. At a temperature close to the melting point, sodium slowly reacts with hydrogen to form hydrides. Sodium does not react with nitrogen to 673 K and with carbon dioxide, to 873 K. In the latter case carbon dioxide reduces to carbon

monoxide and even to carbon. Sodium reduces the oxides of most metals forming either pure metals or alloys with them. At the core temperature, sodium and graphite do not interact. Sodium vigorously reacts with water. In reactors sodium may contact water when a seal fails in a heat exchanger, or when a circuit not dried sufficiently is filled with sodium. The reaction of sodium with water yields much heat and gaseous hydrogen. The amount of hydrogen in sodium indicates the degree of seal failure in heat exchangers. When a sodium-to-water contact area is large an explosion may take place. Sodium also reacts with structural materials causing their corrosion.

For a Fe-Na system within 498-773 K the rate constant of dissolution is

$$\alpha = -0.007 - 2388/T. \tag{4.3}$$

Pure iron resists the attack by sodium when the latter contains a small amount of oxygen to 863 K. At 773 K and with an oxygen content of 0.014% the corrosion rate of carbon steel is $1.4 \cdot 10^{-3}$ g/(m^2 h). Low-alloyed steel containing 5% of chromium corrodes under these conditions at a lower rate. Increasing the chromium content to 13% does not add to the steel resistance.

TABLE 4.2 Resistance of Structural Materials to Corrosion in Na, K, and Na-K Alloys

Structural Materials	Temperature, K								
	373	473	573	673	773	873	973	1073	1173
Carbon steel	P	P	P	P	P	L	L	L	N
Low-chromium steel	P	P	P	P	P	L	L	L	N
Austenitic chrome-nickel steel	P	P	P	P	P	P	P	L	L
Ni, Ni-Cr alloy, Hastelloy	P	P	P	P	P	P	P	P	P
Cu (electrolytic)	P	P	P	L	N	N	N	N	N
Brass	P	P	—	—	—	N	N	N	N
Mo, Ta, Nb, W	P	P	P	P	P	P	P	P	P
Ti	P	P	P	P	P	P	L	L	L
Zr	P	P	P	P	P	P	—	—	—
Cr	P	P	P	P	P	P	P	P	P
Al	P	P	—	L	L	N	—	—	—
Be	P	P	P	P	P	P	L	L	L
Mg	L	L	—	N	N	N	—	—	—
Quartz, glass, Pyrex glass	P	P	P	L	L	—	—	—	—

Note. P — permissible resistance covering resistance groups I-IV (Table 4.3); L — low resistance, group V; N — no resistance, group VI

The corrosion rates of the austenitic stainless steels at 773-988 K are lower than those of chromium steels. The austenitic stainless steels and their welded joints sustain the action of sodium containing 0.005% of oxygen up to 973 K. Sodium only slightly reacts with uranium. When the fuel element cladding is damaged uranium poorly reacts with liquid sodium at operating temperatures. Graphite corrodes intensively in liquid sodium under static conditions only when carbon dissolved in sodium either deposits on more cold sections of the circuit, or carburizes the austenitic stainless steels. The resistance of steel welded joints in sodium ranges with that of the parent metal. Silver resists the sodium attack up to 523 K. Sb, Bi, Cd, Au, Pb, and cast iron do not resist the action of sodium. At 473 K, asbestos reacts with sodium. Polytetrafluorethylene (teflon) is not resistant in sodium.

Sodium and eutectic Na-K are less corrosive than Li, Hg, Pb, and Bi. Table 4.2 gives data on the resistance of certain structural materials in sodium, potassium and their eutectic.

As has been mentioned above, the contamination of liquid metals with oxygen augments corrosion (Table 4.3). In particular, in the presence of oxygen in sodium, brown scale forms on the steel surface and readily peels off. The product of the reaction between iron and sodium oxide is $(Na_2O)_2FeO$. The oxygen contamination of sodium increases the nickel solubility. Pure zirconium, niobium, tantalum reacting with oxygen-containing sodium absorb oxygen from the melt and form on their surface a layer of solid oxygen solution, which in turn may react under certain conditions with alkali metals.

The corrosion rate of Armco iron at 813 K increases, with increasing the oxygen content from 0.005 to 0.16%, from 0.28 to $83.3 \cdot 10^{-2}$ g/(m²h), respectively. At 773 K the increase of the oxygen content in sodium from 0.01 to 0.1% increases the corrosion rate of low-alloy steel containing 5% Cr from 1.4 to $38.8 \cdot 10^{-2}$ g/(m² h) and to 10.83×10^{-3} g/(m² h) of steel 1X18H10T. As to the steel corrosion, the maximum permissible content of oxygen is 0.01%.

Zirconium is more sensitive to the oxygen contamination of sodium than the austenitic stainless steels. The rate of zirconium corrosion grows even when the oxygen content in sodium is 0.003%. With zirconium in use, the maximum permissible content of oxygen in sodium is 0.001%.

As the oxygen content in sodium increases from 0.002 to 0.04%, the rate of iron mass transfer at 813 K rises from 0.14 to $14 \cdot 10^{-2}$ g/(m² h).

The intensification of mass transfer with an increase in the oxygen content in the melt is associated with a possible formation of an oxide of the type $(Na_2O)_2FeO$ in the hot zone and its dissociation in the cold zone, or with the direct reaction between the oxygen ions

TABLE 4.3 Corrosion of Certain Metals and Alloys

Corrosion-resistance group	Corrosion depth index, 10^{-3} m/year	Negative mass corrosion index, 10^{-4} g/(m² h)						Corrosion resistance, 10-severity scale
		Iron and its alloys	Nickel and its alloys	Copper and its alloys	Lead and its alloys	Aluminum and its alloys	Magnesium and its alloys	
I. Perfectly resistant	≤0.001	≤0.0009	≤0.001	≤0.001	≤0.0013	≤0.0003	≤0.0002	1
II. Fairly resistant	0.001-0.005 0.005-0.01	0.0009-0.0045 0.0045-0.009	0.001-0.005 0.005-0.01	0.001-0.005 0.005-0.01	0.0013-0.0065 0.0065-0.013	0.0003-0.0015 0.0015-0.003	0.0002-0.001 0.001-0.002	2 3
III. Resistant	0.01-0.05 0.05-0.1	0.009-0.045 0.045-0.09	0.01-0.05 0.05-0.10	0.01-0.05 0.05-0.10	0.013-0.065 0.065-0.13	0.003-0.015 0.015-0.03	0.002-0.01 0.01-0.02	4 5
IV. Moderately resistant	0.1-0.5 0.5-1	0.09-0.45 0.45-0.9	0.1-0.5 0.5-1	0.01-0.5 0.5-1	0.13-0.65 0.65-1.3	0.03-0.15 0.15-0.3	0.02-0.1 0.1-0.2	6 7
V. Low-resistant	1-5 5-10	0.9-4.5 4.5-9	1-5 5-10	1-5 5-10	1.3-6.5 6.5-13	0.3-1.5 1.5-3	0.2-1 1-2	8 9
VI. Nonresistant	>10	>9	>10	>10	>13	>3	>2	10

and the iron atoms:

$$Fe + O^{2-} \rightarrow FeO + 2e; \qquad (4.4)$$

$$2Na^+ + 2e \rightarrow 2Na. \qquad (4.5)$$

Getting into a sodium flow, iron monoxide reduces. The reduced iron is transferred to the cold zone where it precipitates because of the solution supersaturation.

Carbon present in sodium carburizes the surface layer of stainless steels similar to carburizing in the isothermic carbon transfer. Oxygen of the melt promotes carbon transfer. The Soviet investigators V. S. Lyashenko and B. A. Nevzorova have shown that the sodium melt contains partially dissociated sodium oxide, i.e. oxygen ions O^{2-} are present in the melt. At a temperature above 773 K the cementite in carbon steels partly dissociates to form positively charged carbon ions C^{2+}.

At the first stage, the ions interact ($C^{2+} + O^{2-} \rightarrow CO$) and liquid sodium transfers carbon monoxide to the other parts of the circuit. At the second stage, the bond between carbon and oxygen in the carbon monoxide adsorbed on the metal surface becomes catalytically weakened, and sodium reacting with oxygen detaches it from the molecule. If the steel surface layer contains active carbide formers, they react with carbon and carburize steel. This produces a graphite layer on the surface of pure iron. The content of oxygen in sodium does not reduce, and carbon may be transferred at a low content of oxygen in the melt. After steel 1X18H10T had been allowed to contact a carbon steel containing 0.73% C for 4000 h the carbon content in its surface layer 0.2 mm thick increased from 0.08% to 2.34, 2.59, and 3.0% at the oxygen content in sodium 0.005, 0.05, and 0.1%, respectively.

Carbon transfer in lithium probably occurs by the following reactions:

$$Fe_3C + 2Li \rightarrow Li_2C + 3Fe; \qquad (4.6)$$

$$mLi_2C + nCr \rightarrow Cr_nC_m + 2mLi. \qquad (4.7)$$

Potassium. The essential advantage of potassium used as a coolant in nuclear power engineering over sodium is in its lower melting point. The other properties of potassium are less attractive. The physical and thermal properties of potassium and sodium are nearly the same. As to the chemical properties, potassium is more reactive than sodium. Potassium vigorously reacts in the air with oxygen and water, and at high temperatures with hydrogen and carbon dioxide. Nitrogen does not react with potassium and may be used for creating a protective atmosphere. Graphite and potassium form solid solutions. At a temperature above 473 K graphite absorbs potassium in considerable amounts. Corrosion attack of potassium on structural materials is similar to that of sodium (see Table 4.3). Sodium-potas-

sium alloys containing 40 to 90% of potassium are in the liquid state
at room temperature. This eliminates the necessity of constructing
the heating systems to melt a liquid-metal coolant prior to starting
the reactor. A eutectic alloy containing 77.2% K has a minimum
melting point (261.5 K). Sodium-potassium alloys can be obtained
by direct alloying in an inert atmosphere. The physical properties
of the eutectic approximate those of sodium and potassium.

Lithium. Lithium excels sodium in heat transfer and heat capa-
city per unit volume at 773 K. Natural lithium, however, contains
7.4% of stable nuclide ^6Li which has a large thermal-neutron absorp-
tion cross section. Reducing the content of this isotope is an expensive
process. Metallic lithium is silvery white in colour, rapidly becomes
dull in the air and is coated with dark-brown products of corrosion.
Lithium is the lightest metal on the Earth. As to the chemical pro-
perties, lithium approximates the alkali-earth metals. At room tem-
perature it slowly reacts in the air with oxygen and nitrogen. In a
damp atmosphere it rapidly oxidizes forming lithium hydroxide.
Pure lithium ignites in the air at 913 K. Impurities, if any, reduce the
fire point to 473 K. Lithium, like other alkali metals, is stored in
dried kerosene or mineral oil. Solid lithium reacts with water less
vigorously than sodium. In the liquid state, however, it interacts
with water more vigorously. Lithium combines with oxygen, nitro-
gen, hydrogen, and carbon dioxide. Inert gases utilized to protect
lithium against oxidation must be cleaned not only from oxygen and
water vapours but also from nitrogen.

Commercial lithium is far more corrosive with regard to structural
materials than sodium and potassium. Stainless steel having a low
content of carbon satisfactorily resists corrosion in lithium at 973 K.
At 1173 K, Mo, W, Nb, Ta and Armco iron are corrosion-resistant in
lithium. Table 4.4 gives corrosion resistance of a number of metals
in lithium.

The presence of nitrogen in lithium increases the solubility and
corrosion of Fe, Cr, Ni, Nb, Ti, and stainless steels. Nitrogen ren-
ders lithium more corrosive than does oxygen. Nitrogen in lithium
augments selective corrosion and mass transfer of the austenitic
chrome-nickel stainless steels. The aggressiveness of liquid lithium
at a temperature below 723 K increases when it contains lithium
hydroxide. At a higher temperature the hydroxide dissociates.

In operation the necessity may arise to clean the circuit of alkali
metals used as coolants. Prior to cleaning the metal is drained from
the circuit. When the circuit cools down to 333-343 K, which is below
the boiling point of alcohol, it is blown through with inert gas. Then
ethanol or methanol is injected in small amounts into the circuit
through the bottom drain. Provision should be made to discharge
oxygen given off during the reaction between the alcohol and alkali
metals. The amount of alcohol required for cleaning must be twice the

TABLE 4.4 Corrosion Resistance of Structural Materials in Lithium

Structural material	Temperature, K							
	473	573	673	773	873	973	1073	1173
Armco iron	P	P	P	P	P	P	P	P
Low-carbon steel	P	P	P	L	L	N	N	N
Ferrite stainless steels (27% Cr)	P	P	P	P	P	P	P	L
Austenitic chrome-nickel stainless steel	P	P	P	P	P	L	L	N
Ni, Ni-Cr alloy, Hastelloy	L	L	L	L	N	N	N	N
Mo, Ta, Nb, W	P	P	P	P	P	P	P	P
Ti, Zr, Cr, Be	—	—	—	—	—	—	L	L
Quartz	L	L	N	N	N	N	N	N
Glass	N	N	N	N	N	N	N	N
Graphite of high density	N	N	N	N	N	N	N	N

Note. Designations as in Table 4.2.

weight of the supposed alkali metal residue. When the amount of metal residue is unknown, the volume of alcohol should be 6-8% of the system volume. Prior to use, the alcohol should be checked for water content. The alcohol may be used only if no flash, sparking, or intensive gas emission is observed when a little piece of alkali metal is dissolved in it.

During washing of the circuit it is good practice to agitate the alcohol. Upon completion of the first washing, the alcohol may be drained and diluted by 20% with water. This solution is utilized in the second washing. Finally the circuit is washed with pure water. Recently steam washing has been introduced into practice. This process calls for thoroughly developed sequence of operations and control. In particular, the system is filled with inert gas for decelerating the reactions, superheated steam and then wet steam are fed in small portions. When the alkali metals are used as coolants the design should provide the equipment to clean them before charging into the circuit and a room for their decomposition after use.

Bismuth. Commercial bismuth contains 0.1 to 0.2% of impurities. Bismuth resists oxidation in dry and wet air and even in the oxygen atmosphere at room temperature. At a high temperature, the metal ignites in the air and forms an oxide. At 873 K hydrogen and nitrogen do not react with bismuth. At 873 to 1073 K, steam in contact with bismuth decomposes and carbon dioxide reduces to pure carbon.

Hydrogen, nitrogen, helium, and argon protect bismuth against oxidation at a temperature up to 873 K, and helium and argon, at higher temperatures. At 1658 K, bismuth dissolves 0.012% of carbon. Iron and carbon steel resist corrosion in bismuth up to 973 K (Table 4.5).

TABLE 4.5 Corrosion Resistance of Structural Materials in Bismuth

Structural material	Temperature, K						
	573	673	773	873	973	1073	1173
Fe	P	P	P	P	P	L	L
Carbon steel	P	P	P	P	P	—	—
Stainless ferritic (12-27 % Cr) and chrome-nickel steels	P	P	P	L	L	L	N
W and Ta	P	P	P	P	P	P	—
Mo	P	P	P	P	P	P	P
Nb	P	P	P	P	P	L	L
Al	P	—	—	N	N	—	—
Be	P	P	P	P	P	P	P
Cr	P	P	P	P	P	L	L
Cu	L	L	N	N	N	N	N
Graphite	P	P	P	P	P	P	P
Pyrex glass	P	P	P	N	N	N	—
Fused quartz	P	P	P	P	P	P	P

Note. Designations as in Table 4.2.

Chromium stainless steels are somewhat less resistant. Adding magnesium, zirconium, titanium to bismuth in an amount of 0.005 to 0.05% improves the resistance of steels and reduces mass transfer. Zirconium, nickel, alloys and steels containing nickel participate actively in the reaction with bismuth. Bismuth reacts with metallic uranium dissolving it in considerable amounts. A bismuth-uranium alloy may be used in liquid-metal fuel systems.

Lead. The thermophysical properties of lead are not good enough. Its heat capacity is nearly 1/10th that of sodium, thermal conductivity is low, and specific gravity is relatively high. At room temperature lead resists oxidation in the air. Up to 973 K lead melt is protected against oxidation by a dense oxide film. The oxide film melts at 973 to 1173 K, and the oxidation rate abruptly rises. Hydrogen and nitrogen do not react with lead up to 873 K. These gases and also argon and helium are used to protect melted lead against oxidation. Melted lead practically does not react with graphite. Resistant in melted lead are carbon steel, a number of stainless steels, tantalum, titanum, niobium, and beryllium.

The contamination of lead with oxygen, antimony, arsenic, tin, and zinc increases its corrosive influence.

Used as a liquid-metal coolant more often is the Pb-Bi eutectic (44.5% Pb and 55.5% Bi) rather than lead and bismuth separately. The melting point of the alloy is 398 K. The thermophysical properties of the alloy, except its thermal conductivity, are close to the average values of those of bismuth and lead. Its chemical properties approximate those of its constituents.

The austenitic stainless steels are not sufficiently corrosion-resistant in eutectic Pb-Bi at 873 K. The reaction with the eutectic involves selective dissolution of nickel from the austenitic steel. This accounts for the austenite-to-ferrite transformation; ferrite is detected on the steel surface by X-ray analysis. Presaturation of the eutectic with nickel in an amount of 0.6% increases the resistance of the austenitic stainless steel to corrosion. The formation of oxide films on the steel surface owing to the oxidation of steel constituents or the addition of potassium and barium to the eutectic as inhibitors reduces the rate of steel 1X18H10T corrosion. In that case the steel may be used up to 773 K.

Though iron and low-alloyed steels are more corrosion-resistant in eutectic Pb-Bi than steel 1X18H10T, their high-temperature strength is low. This limits their use under given conditions. The chromium stainless steels are resistant in eutectic Pb-Bi.

Gallium. It is a rather rare and therefore expensive metal. It has attracted attention as a coolant mainly because of its low melting point (302.8 K). The chemical properties of gallium are close to those of aluminum. It slightly reacts with water and steam. Gallium produces a rather corrosive effect: when immersed in it, tantalum and tungsten resist corrosion only up to 873 and 1073 K, respectively. Carbon and stainless steels lose their corrosion resistance already at 373 to 573 K.

4.2 Organic Coolants

Organic coolants have some advantages over water. A small vapour pressure of organic liquids makes the construction and operation of the circuit easier. Organic coolants produce a small corrosive influence and, therefore, the reactor may employ cheap carbon steels. Low induced radioactivity of organic coolants requires a minimum biological shielding. The most serious drawback of organic coolants is their poor ability to withstand temperature and irradiation. The decomposition (pyrolysis) of organic compounds at high temperatures dramatically affects their properties. The pyrolysis products may deposit on fuel elements and badly impair the heat exchange, which results in damage to the fuel elements. This does not allow organic coolants to be used in the power industry. The organic coolants are diphenyl, monoisopropyldiphenyl, and a diphenyl mixture. These substances are stable at temperatures up to 593 to 673 K. At high

temperatures, they intensively decompose to form high-molecular substances, having high melting points, and gases such as hydrogen, methane, etc.

Irradiation destructs organic coolants to produce polyphenyl and hydrogen radicals. The former interact with each other and form high-molecular polymers having high boiling points. Hydrogen radicals give hydrogen. The reaction between phenyl and hydrogen radicals produces methane and other light hydrocarbons. The gas phase formed in the radiolytic decomposition of hydrocarbons includes 85-95% of hydrogen and 2-10% of methane. The most resistant to irradiation is n-terphenyl, while diphenyl is the least resistant. At a temperature below certain critical value (about 673 K for diphenyl), the radiolytic decomposition of organic coolants is independent of temperature. At temperatures above the critical value, the decomposition of organic coolants in the irradiation zone grows and the yield of products having high boiling points increases. The radiolytic decomposition of polyphenyls may be reduced by adding a stabilizer, say benzene, to them.

Commercial diphenyl is a yellow solid crystalline substance. The main impurities it contains are ash (up to 0.1%) and water (up to 0.5%). Diphenyl is the cheapest and most easily available organic coolant. Its melting point is 342.5 K and boiling point, 529 K. The heat exchange coefficient of diphenyl is less than that of water. When in the reactor circuit, diphenyl always contains the decomposition products, substances having a high boiling point. Their content in an amount of 30 to 40% is tolerable. Carbon steel, stainless steel, and uranium are resistant in diphenyl at 673 K, while magnesium and zirconium alloys are nonresistant. The latter decompose owing to hydrogenation. Polyphenyl mixtures, monoisopropyldiphenyl, and diphenyl mixtures resist the effect of temperature and radiation better than diphenyl. A mixture of 21.5% of diphenyl $(C_6H_5)_2$ and 73.5% of diphenyl ether $(C_6H_5)_2O$ has a lower melting point than diphenyl. Its radiation stability, however, is not high.

4.3 Gas Coolants

Gas coolants have found fairly wide application in nuclear power plants. Their use in a single-circuit cycle simplifies the design of the plant. The thermal neutron absorption cross section of gas coolants is small. Therefore they are utilized in the natural-uranium reactors. Objectionable properties of gas coolants are low density, heat capacity per unit volume and thermal conductivity. This requires that considerable amounts of gas be passed through the reactor, increasing the plant costs and making the plant more complicated, and calls for more power to circulate the coolant. To improve the heat transfer capabilities and reduce the power consumption in coolant circulation,

the gas system is operated under a pressure of several MPa's. This also complicates the design and operation of the circuit.

Corrosion in Gas Coolants. Oxygen in the form of impurities accounts for gas corrosion. The reaction between metal and gas starts with the gas adsorption. One square centimeter of clean metallic surface contains on the average about 10^{15} atoms which can adsorb gas. In adsorption, the free energy of gas decreases and the process continues spontaneously. Adsorption may be of two kinds: physical adsorption and chemisorption. In *physical adsorption* gases are held on the surface by the van der Waals forces. The activation energy of the process is insignificant and physical adsorption proceeds almost instantaneously as soon as gas molecules touch the surface. In *chemisorption* the reaction is slower because it needs the activation energy. Chemisorption is known as the activated adsorption. It depends on the crystallographic orientation of defects on the metal surface. It is supposed that chemisorption predominates on "activated" sites or areas of the surface. It is thought that chemisorption proceeds only until a monomolecular layer of adsorbate has been formed on the surface. Physical adsorption takes place on all surfaces and may produce multimolecular layers. In adsorption oxygen molecules dissociate.

Variation of energy in adsorption is shown in Fig. 4.1. Point M_1 corresponds to a stable equilibrium of an adsorbed atom having energy q_1 fixed at a distance d_1 from the surface after the molecule dissociation. Point M_2 corresponds to a stable equilibrium of a nondissociated molecule having energy q_2 at a distance d_2 from the surface. The transition from the state of molecular adsorption to a more stable state of atomic adsorption, the difference in their energies $E = q_1 - q_2$, requires energy to overcome the barrier whose height $E_d - E_a$ is the activation energy of chemisorption. The adsorbed atoms may sometimes rearrange in the surface layer of the metal and become ionized.

The adsorption of the oxygen atoms or ions produces *surface oxygen structures*, i.e. ordered arrangement of ions or atoms of oxygen representing the symmetry of the metallic matrix and depending on its crystallographic orientation. In close-packed lattices, for example in plane (111) of FCC metal, the most stable centres of adsorption, i.e. places where adsorbed atoms or ions are arranged, lie above the centre of gravity of a group of three contacting atoms (positions A, B, C in Fig. 3.1) rather than above the atoms proper. Therefore, the adsorbed atoms or ions form a plane lattice on the metal surface. Each type of crystal plane has a most probable configuration of the adsorbed layer. This configuration corresponds to the geometry requirements and the number of bonds between the metal and oxygen. In plane (100) of a BCC iron, the adsorbed oxygen atoms arrange so that a two-dimensional compound having a formula corresponding to FeO is produced. Note that such an arrangement of oxygen and iron ac-
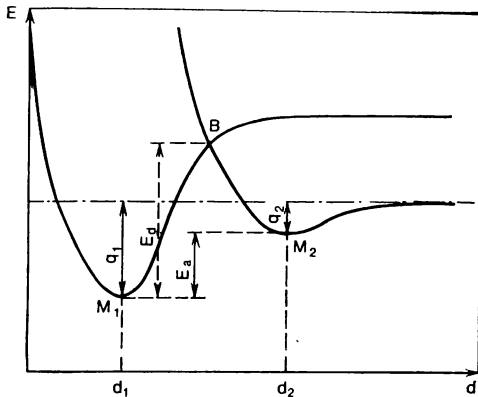
Fig. 4.1 Variation of the system's energy in adsorption

counts for the structure correspondence of α-Fe and FeO formed in oxidation on this plane.

Oxygen and the surface atoms are bonded ionically. The adsorbed substance (oxygen) has a greater electron affinity than a metal. Therefore, electrons owing to the tunnel effect move from metal to oxygen, fill the free levels of chemisorbed oxygen, and ionize them. The bond between the adsorbed oxygen and matrix is stronger than the bond between oxygen and metal in the oxide of the same stoichiometric composition. This is associated with that in chemisorption the bond is partially covalent.

The further growth of the oxide film progresses through *embryo formation*. We suppose that dislocations, surface defects, and impurities serve as places of embryo generation. Here a two-dimensional structure of adsorbed oxygen changes into a three-dimensional structure with a regular alternation of metal and oxygen atoms. Such a rearrangement supposes a short-distance migration of surface atoms of oxygen and metal. After the formation of randomly distributed oxide embryos, the oxidation occurs through the growth of individual crystallites until the surface is fully covered with the oxide film. In addition to the oxide covering the metal, the hair-like crystals, "whiskers" about 10^3 nm in length and 10 to 15 nm in diameter, are observed on the metal surface. Whiskers or plates, however, contain only a small fraction of the oxide.

In the oxide growth, ions of metal and oxygen migrate through the oxide. The migration essentially depends on *defects of the oxide structure*. Point defects may be either neutral, or charged. Anionic vacancies and interstitial cations are positive and cationic vacancies and interstitial anions are negative with regard to the surrounding lattice.

The nucleation of point defects of one sign is followed by the gene-

ration of defects of the opposite sign in order to preserve the electro-neutrality of the crystal.

The oxidation of metals with a dense oxide film formed by the reaction products is well described by the *Wagner theory*. According to this theory, the volume diffusion of ions or corresponding point defects, or transfer of electrons through the growing scale determines the net rate of the reaction. Therefore, we consider that the reaction at the phase boundaries proceeds rapidly and the thermodynamic equilibrium between the oxide and gaseous oxygen establishes at the oxide-to-oxygen interface and between the metal and oxide at the phase boundary between them.

The motive force of the reaction is the change of the free energy owing to the formation of metal oxide. Concentration gradients arise in the oxide. At the MeO/O_2 boundary the partial pressure of oxygen is equal to the oxygen pressure in the gas phase, while at the Me/MeO boundary it is equal to the equilibrium pressure of oxide dissociation (dissociation pressure) in contact with metal. The concentration of cations at the Me/MeO is maximum. At MeO/O_2 cations react with oxygen. The concentration of oxygen, or its ions, at the boundary is far above the concentration of cations, since the latter diffuse to the boundary. The diffusion, therefore, limits the reaction and the oxide formation proceeds rapidly. The lack of cations in the formation of an oxide lattice generates the cationic vacancies. The concentration of the O^{2-} anions at the Me/MeO boundary is low. This creates the anionic vacancies.

Thus, the concentration of O^{2-} and cationic vacancies is the highest at the MeO/O_2 boundary and the lowest at Me/MeO, while the concentration of cations and anionic vacancies is the highest at the MeO/O_2 boundary. The concentration gradient makes cations and anionic vacancies diffuse from Me/MeO to the MeO/O_2 boundary, and anions (O^{2-}) and cationic vacancies, from MeO/O_2 to the Me/MeO boundary. Electrons, owing to the tunnel effect, migrate from Me/MeO to MeO/O_2. The rate of film growth is determined by the gradients and rates of the constituents diffusion. This leads to oxidation by a parabolic law.

The mobilities and diffusion coefficients of cations, anions, their vacancies, and electrons are different. This leads to the charge separation in the growing oxide film. The resultant space charge sets up an electric field in the oxide film. The motion of ions, electrons, and vacancies through the oxide film, should be described with account of the diffusion caused by the chemical potential and migration generated by the electrical potential, i.e. the ionic and electron conduction of the oxide. The cation transfer numbers in oxides are small. Oxygen migrates 10^3-10^6 times faster than a cation. Oxides may be electron conductors (e.g. magnetite), insulators, or electronic or hole semiconductors.

The *oxidation kinetics* may be considered on the basis of the Wagner theory. The oxidation is controlled by the rate of diffusion of the reacting substances. Then, the oxidation proceeds by a parabolic law:

$$X^2 = K\tau, \qquad\qquad (4.8)$$

where X is the amount of the oxidized metal, g/m^2; τ is the time; K is the rate constant of oxidation.

The oxidation rate constant K depends on temperature as follows:

$$K = a \exp(-W/RT), \qquad\qquad (4.9)$$

where a is the constant; W is the activation energy.

This is known as the Arrhenius equation. A graph of $\log K$ versus $1/T$ has the form of a straight line and can be used to determine the activation energy.

The oxidation can be described not only by a second-order parabola, but also by a third-order parabola; n may sometimes be a fractional number. When an oxide film possesses good protective properties, the oxidation follows a logarithmic law:

$$X = K \log \tau + A. \qquad\qquad (4.10)$$

If an oxide film features no protective properties, the oxidation is not decelerated in time and proceeds at a constant rate following a linear law:

$$X = K\tau. \qquad\qquad (4.11)$$

To evaluate the resistance of a metal to oxidation we should start from determining whether an oxide of a given metal can form under given conditions, i.e. at the specified temperature and oxygen pressure p_{O_2}. This information can be obtained by measuring the Gibbs thermodynamic potential or the free energy of the oxide formation:

$$2Me + O_2 \rightleftarrows 2MeO. \qquad\qquad (4.12)$$

The change in the thermodynamic potential of the reaction

$$\Delta Z^\circ = -RT \ln (1/p_{O_2}) = RT \ln p_{O_2} \qquad\qquad (4.13)$$

characterizes the metal affinity for oxygen.

Thermodynamically the possibility of a metal oxidation is evaluated in terms of the *oxide dissociation pressure*. This is determined by the oxygen pressure of the gas phase in equilibrium with the oxide at a given temperature. The reaction of metal oxidation is in chemical equilibrium when the oxygen vapour pressure p_{O_2} equals the oxide dissociation pressure p_{MeO}. At $p_{O_2} > p_{MeO}$, the reaction proceeds towards the oxide formation. At $p_{O_2} < p_{MeO}$, the oxide dissociates into metal and oxygen. The oxide dissociation pressure rises with temperature. However, the rate of oxidation also increases with tem-

perature. Therefore, thermodynamically the probability of metal oxidation decreases with temperature, while the true rate of oxidation (certainly provided this process is thermodynamically possible) increases with temperature.

From the thermodynamic point of view, most metals of interest to reactor engineers are liable to oxidation. To predict the resistance of metals to gas corrosion, one has to evaluate the protective properties of the oxide film.

The *Pilling-Bedforth ratio* evaluates as a first approximation the protective properties of an oxide. The continuity condition consists in that the oxide volume (V_{ox}) must be greater than the volume of metal consumed in oxidation (V_{Me}). At $V_{ox}/V_{Me} < 1$ the film cannot be continuous, and at $V_{ox}/V_{Me} > 1$ the film can be continuous.

If the Pilling-Bedforth ratio is below unity the film cannot be continuous and, therefore, cannot protect metal from corrosion. If the ratio exceeds unity, the film forms a continuous coating. This, however, is not enough to conclude that the film protects metal, since it may be porous or may badly adhere to the metal, etc. Though it covers the entire surface of the metal, it provides poor protection. Therefore, the $V_{ox}/V_{Me} > 1$ condition is necessary but not sufficient to treat the film of oxide as protective.

The protective properties of an oxide film essentially depend on its adhesion to a metal. In this connection we have to consider the mutual orientation of the oxide and metal lattices. A reaction product has a regular structure when, first, the monocrystal plane serves as a substrate and, second, the reaction proceeds at a rate such that the resultant product orients according to the substrate. An oxide may have a preferable orientation even when the metal grains are oriented. If the lattice structure of the oxide is identical to that of the substrate (epitaxy) the oxide lattice as if continues the lattice of the metal. To realize the epitaxy, both lattices must have one or several plane cells nearly similar in shape and size. The condition is satisfied when three-dimensional cells of two crystals coincide. Unit cells of these lattices should be equal in size within 15%. In epitaxy, the lattice parameters of the substrate and oxide may approximate each other in the boundary plane, i.e. adapt themselves to each other. An example of epitaxy of α-Fe and its oxide is shown in Fig. 4.2. The epitaxy improves the adhesion of the oxide film to the metal and thus the protective properties of the oxide.

Differences in the specific volumes of metal and oxide and changes in the lattice parameters of metal and oxide in epitaxy generate *stresses in the oxide film*. In a polycrystalline material, heavy stresses may arise at grain boundaries because of the difference in the oxidation rates of neighboring grains having different surface crystallographic orientations and also because of the prevailing oxidation at grain boundaries. Stresses in an oxide film increase with its growth.
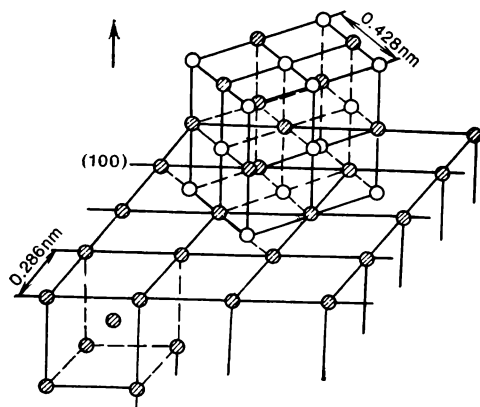
Fig. 4.2 Epitaxy of crystal lattices of α-Fe and its oxide

When stresses exceed the ultimate strength, the film destructs and its continuity disturbs. The destruction usually originates at edges, hole edges, etc. The destruction of a film naturally affects its protective properties. The law of film growth changes. When the strength of a film is high and its adhesion to the metal poor, the compressive stresses result in blistering and peeling of the oxide film.

Oxide films up to 40 nm thick cause the appearance of temper colors on the metal. This is associated with the optical interference in the oxide. The film color depends on the film thickness. As a rule, good protective properties are featured by the oxides having a spinel lattice, magnetite being an example. Spinel has a cubic lattice with a great number of atoms.

An oxide film may comprise several layers. Thus, an oxide film on iron (scale) consists of several oxides of iron. Directly contacting the metal surface is the layer of FeO, an oxide with a least content of oxygen, then follows Fe_3O_4, and the outer layer contains Fe_2O_3. Iron monoxide (wüstite) FeO has a cubic lattice like that of sodium chloride. This oxide is resistant at temperatures above 843 to 848 K. It does not form at lower temperatures and decomposes when slowly cooled from a higher temperature:

$$4FeO \rightarrow Fe + Fe_3O_4. \tag{4.14}$$

The oxygen content of wüstite as a rule exceeds the stoichiometric content. The oxide Fe_3O_4 (magnetite) has a cubic lattice of the spinel type. In the crystal lattice of magnetite, there are two ions of ferric iron per each ion of ferrous iron. Unlike other iron oxides, except γ-Fe_2O_3, this oxide is ferromagnetic. When heated in an oxidizing medium, magnetite changes into iron oxide α-Fe_2O_3. Hematite α-

Fe_2O_3 has a rhombohedral structure. The film formed on alloys often consists of composite oxides $Cr_2O_3 \cdot NiO$, for instance.

If oxygen dissolves in the alloy during the oxidation, a less noble constituent may form an oxide inside the alloy. The oxide interlayers, often known as subscale, may be formed under the interface between the oxide and scale. For the internal oxidation to take place, the rate of oxygen diffusion in the alloy must exceed by far the rate of the alloying element diffusion.

So far, we have considered the formation of solid oxides. In a number of cases the oxidation produces liquid oxide phases. An example is the oxidation of an alloy containing as a constituent a metal producing a low-melting oxide. This often occurs when the oxidation of metals and alloys proceeds in the presence of MoO_3 and V_2O_5 having melting points of 1068 and 947 K, respectively. The liquid oxide phases may lead to very rapid failure of the alloy known as the *black way oxidation*.

One of the types of gas corrosion is *decarburization* of steel. Sufficiently movable atoms of carbon diffuse in the zone of metal oxidation and get oxidized. The surface layer of metal naturally becomes depleted of carbon and changes its mechanical properties. Reducing the amount of oxidizing agents in the gas phase (CO_2, O_2) decelerates decarburization. When the content of CO and CH_4 in the gas phase is sufficient, the surface may even carburize. It is good practice to choose, if possible, such a composition of the gas medium that metal oxidation be suppressed. Only noble gases are totally inert with regard to metals. Often used are protective atmospheres of nitrogen with additions of hydrogen, CO, and CH_4. With high contents of hydrogen, CO, and CH_4, the mixture becomes explosive. To create a protective atmosphere use is also made of a natural gas and waste gases of furnaces.

To protect against oxidation the parts operating under particularly severe conditions, their surface is plated with high-resistant alloys such as stellite and Nichrome. In certain cases the part is plated with aluminum by immersing it into molten aluminum. The thermodiffusion coating also gained wide recognition. The metal of plating is converted into the gas phase in the form of a volatile compound of this metal; its diffusion into the protected metal creates a protective coating on its surface.

To increase the high-temperature strength of iron it is alloyed with chromium, aluminum, silicon, i.e. the elements possessing an essential affinity for oxygen. The Pilling-Bedforth ratio must be satisfied. Atoms of the alloying constituent must be smaller in size than the atoms of the parent metal in order to allow the alloying element to diffuse towards the surface more readily to form an oxide of a high electrical resistance. To make the protective oxide film resistant to high temperature, the oxide of the alloying constituent must have

a low dissociation pressure and high points of melting and sublimation.

Carbon Dioxide. At present carbon dioxide is the most widespread among gas coolants. It is a colorless gas readily liquefying at cooling or compression. At rapid evaporation of liquid carbonic acid part of it freezes and converts into a snow-like mass. The thermal neutron absorption cross section of carbon dioxide is small. The decomposition of carbon dioxide in the irradiation field materially depends on the parameters of the gas. Thus, at a pressure close to the atmospheric pressure, carbon dioxide practically does not decompose under irradiation. With an increase in pressure, the resistance of carbon dioxide reduces, and at 1 MPa its decomposition becomes noticeable. The primary reactions of the carbon dioxide decomposition under irradiation are as follows:

$$CO_2 \rightarrow CO + O; \qquad\qquad (4.15a)$$
$$CO_2 \rightarrow C + O_2. \qquad\qquad (4.15b)$$

The decomposition by the first reaction prevails. Carbon later reacts with carbon monoxide and oxygen to form carbon dioxide. The impurities in carbon dioxide which react with carbon or oxygen facilitate the decomposition of carbon dioxide under irradiation. This is because binding of carbon or oxygen by the impurities reduces the rate of recombination:

$$C + 2O \rightarrow CO_2. \qquad\qquad (4.15c)$$
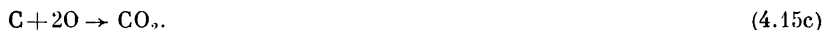
For the suggested composition of the carbon dioxide utilized in a nuclear plant, see Table 4.6. The induced radioactivity of carbon

TABLE 4.6 Impurities in Carbon Dioxide Used as Coolant in the Reactor of Electrical Power Station in Calder-Hall, mg/kg

Volume content, %		Moisture	Ar	H_2	O_2	N_2	C_2H_6	CH_4
CO_2	CO							
99.5	0.38	10	3	16	17	94	1	13

dioxide is accounted for by nuclides ^{16}N, ^{19}O, ^{41}Ar, and ^{14}C formed under irradiation. The former two are formed from oxygen, the latter, from argon and nitrogen. When heated to 1273 K, carbon dioxide starts to dissociate:

$$2CO_2 \rightarrow 2CO + O_2. \qquad\qquad (4.15d)$$

The reaction is accelerated in the presence of graphite. This results in the accumulation of carbon monoxide in the circuit in the amount of 0.37-0.65%.

In the graphite-carbon dioxide system carbon may be transferred from a high-temperature zone to that of lower temperature. The reaction of graphite with carbon dioxide at a high temperature

$$CO_2 + C \rightarrow 2CO \tag{4.16}$$

yields carbon monoxide. In the zone of reduced temperature a reverse reaction takes place

$$2CO \rightarrow CO_2 + C \tag{4.17}$$

giving graphite which deposits on the surface. As the gas reactor service experience states, these deposits are small. At elevated temperatures, carbon dioxide oxidizes a number of structural materials.

Now, let us consider the *resistance* of a number *of structural materials to gas corrosion* in carbon dioxide. Magnesium is sufficiently resistant in dry carbon dioxide. The contamination of carbon dioxide with water increases the rate of magnesium corrosion 4-5 times

TABLE 4.7 Composition of Magnesium Alloys Resistant in Carbon Dioxide

Alloy	Mass content of alloying additions, %				
	Al	Be	Ca	Zr	Mn
Magnox	1	0.05	0.1	—	—
	1	0.05	—	—	—
AM-503	—	—	—	—	1.5
ZA (France)	—	—	—	0.6	—
Mg-Be	—	0.01-2	—	—	—
Mg-Be-Zr (USSR)	—	0.1	—	0.6	—

its previous value. At a temperature above 873 K, magnesium burns in the carbon dioxide atmosphere. Table 4.7 gives magnesium alloys resisting the carbon dioxide attack.

Aluminum, zirconium, and their alloys are sufficiently resistant to corrosion in carbon dioxide at 573 to 773 K. Carbon steels are also effective under these conditions. Water in carbon dioxide, however, abruptly intensifies high-temperature attack on carbon steels. This was observed at nuclear power plants in Great Britain.

Helium. Helium is extremely promising as a coolant for fast-neutron reactors. This is a colorless gas having no odour. It is a noble gas extremely inert in chemical respect. Helium is the lightest of inert gases and next to hydrogen in weight of all known gases. As to its nuclear, physical and chemical properties helium is one of most attractive gas coolants. The maximum absorption cross section is shown by ^3He. Its content in natural helium is small and makes up 10^{-7} to $10^{-6}\%$. Pure helium practically has no induced activity.

Under the actual operating conditions, the activity of the coolant is accounted for by impurities, the fission products including. Most often helium is contaminated with nitrogen and argon. Though with impurities present, helium has no essential induced activity. Helium may be cleaned of the radioactive impurities by treating with activated charcoal.

In the helium-cooled reactor, the helium properties are close to those of an ideal gas. Heat capacity of helium is below that of carbon dioxide. To accumulate a notable amount of heat in helium, the inlet to and outlet from the core must differ considerably in temperature. This interferes with the use of helium as the coolant. Heat conductivity of helium is 10 times that of carbon dioxide. This facilitates heat transfer, reduces the dimensions of heat exchangers, makes helium promising as a filler in channel reactors. Helium is extremely fluid. Even at a modern level of technology, the designing of system tight to helium is quite a problem. When choosing helium as the coolant one should also take into account its high cost.

Helium itself causes no oxidation of the reactor materials. Corrosion of metals and alloys is the result of its contamination with oxygen, carbon dioxide, and steam. To prevent this, the total content of impurities should not exceed 0.01%. Oxygen in helium may lead to carbon transfer in the circuit due to the formation of carbon dioxide and its dissociation.

Air. The use of air as the coolant requires its thorough drying. At a relative air humidity above 9% all structural materials with the exception of the stainless austenitic chrome-nickel steel intensively corrode. When utilizing air as the coolant in an open loop scheme, argon present in the air may activate it.

Dissociating Gases. The use of dissociating gases N_2O_4, Al_2Cl_6, Al_2Br_6 and others, and also their mixtures as coolants improves the performance of nuclear power plants on account of reducing the weight and overall dimensions of the principal equipment, and first of all reducing the specific amount of metal per gas turbine, its unit power remaining high. Good thermophysical properties of dissociating coolants ensure high efficiency and convective heat transfer with the resultant reduction of the overall dimensions of heat exchangers. When fast-neutron reactors use dissociating gases, N_2O_4 in particular, as coolants, the performance of the core improves as compared with the use of sodium.

The dissociating gases used as coolants and actuating medium in fast-neutron reactors reduce the pressure required to achieve the effective heat transfer from 20-25 MPa (helium and steam) to 8-14 MPa (N_2O_4).

When a dissociating gas is utilized as an actuating medium in a closed gas turbine cycle, the gas in the initial state with a maximum molecular weight (and a minimum gas constant) is compressed in

a compressor and heated in a reheater and a reactor to a maximum temperature of the cycle. The gas dissociates consuming heat for the chemical reaction to take place. The mass reduces (the number of moles and gas constant increase to the maximum). When expanding in the turbine, the gas cools down in the reheater and cooler, recombines giving off heat in the chemical reaction and changes the number of moles and gas constant to their minimum values. Then, the gas goes to the compressor, and the cycle is repeated. A high gas constant of the actuating medium in the turbine compared with its value in the compressor reduces the power fraction consumed to compress the gas to 30-45%.

The heat consumed in dissociation

$$N_2O_4 = 2NO_2 \text{ and } 2NO_2 = 2NO + O_2 \tag{4.18}$$

is 57.3 and 112.9 J/mole, respectively. The melting and boiling points of N_2O_4 are -383 and $+294.3$ K, respectively. At 0.1 MPa dissociation proceeds within 299-1123 K, and at 10 MPa, within 298-1473 K.

In flow of N_2O_4 at 773 K and 5 MPa, the corrosion rate of steel 1X18H10T is $5 \cdot 10^{-3}$ g/(m² h). Changing the speed of flow from 10 to 25 m/h only slightly increases the rate of attack. The rate of corrosion of steel 1X18H10T decreases with time. Thus, with the exposure increased from 100 to 10 000 h, the corrosion rate drops nearly hundredfold. The corrosion rates increase with pressure increasing to 5 MPa. With further increase of the pressure, the corrosion resistance of the stainless steels remains practically unchanged. Welded seams demonstrate no predominant corrosion. Chromium stainless steels, hardened austenitic stainless steels, titanium alloys behave in a similar manner.

The corrosion resistance of the perlitic steels under the abovementioned conditions is by far lower. Their corrosion rate at 773 K and 5 MPa is 0.05 g/(m² h). At 473 K and 5 MPa, corrosion rates of highly strong aluminum alloys are $(1-5) \cdot 10^{-2}$ mm/year. Increasing the pressure from 2 to 5 MPa increases tenfold the rate of aluminum alloys corrosion.

4.4 Water Coolant

Specific Features of Water Coolant. Thermal neutron reactors often employ water as the coolant. Moreover, water may be used not only as the coolant but also as the moderator. The absorption cross section of water is $6 \cdot 10^{-29}$ m². Within the whole range of temperatures and pressures of interest for nuclear power engineering, the thermophysical properties of water are well studied. M. A. Styrikovich, M. P. Vukalovich and other Soviet scientists have made a considerable contribution to the problem.

The most serious drawback with water is its high saturated vapour pressure which rapidly increases with temperature. This requires high pressure systems, which naturally raises the plant costs and makes the plant operation more difficult.

The main requirement imposed on ordinary water in nuclear engineering is its purity. In certain cases, however, added to water are substances used, as a rule, to decrease its corrosivity, or to suppress its radiolytic decomposition. When designing nuclear power plants employing the water coolant, much attention is paid to the quality of water, i.e. *water regime of the reactor*. The water composition, and permissible impurities are determined by the Specifications, or rated values, for filling make-up and circuit water. Usually specified are the following indices: (1) salinity (electrical conductivity); (2) dry residue (in modern practice this index is not used); (3) pH value; (4) oxygen content; (5) hardness; (6) content of chlorides; (7) content of corrosion products.

The pH of water depends on structural materials in the system. When the circuit utilizes aluminum alloys the water pH must be 4 to 6. In the circuit employing perlitic steels pH equals 9 to 10. The feed water for nuclear power plants is prepared by deep chemical demineralization with the aid of ion-exchange filters. Oxygen is removed either in thermal deaerators, or by means of ion-exchange filters. Prior to filling with water the primary circuit must be blown through with inert gas. To combine oxygen, hydrazine (N_2H_4) is added to the circuit water. The water directly in the primary circuit is purified with the aid of ion-exchange filters or filters utilizing high-temperature inorganic sorbents processing the bypass stream. The condensate-feed and recirculation circuits of a channel-type reactor and a tank of a vessel-type BWR are filled with chemically demineralized water saturated with air. Nuclear power plants are also furnished with equipment for decontamination of blow-off, waste and other waters.

The conductivity of water grows with temperature as follows:

T, K	293	333	373	423	507	573
$\varkappa$, μS/cm	$5 \cdot 10^{-2}$	0.2	0.7	2.0	3.2	2.8

This intensifies, in particular, the contact corrosion.

Even most general considerations show that the purer the water, the less its electrical conductivity. In practice, the water purity, salinity, for example, may be estimated by the water electrical conductivity. The water containing no foreign ions should have electrical conductivity of $5 \cdot 10^{-2}$ μS/cm. In industry, thorough and multiple purification of water results in $\varkappa = 0.1$ μS/cm. The primary circuit uses water of $\varkappa$ below 1 μS/cm. The presence of oxygen, alkalis, chlorides, and other salts in water increases its electrical con-

ductivity and makes it corrosive to structural materials. In crevices and stagnant spaces water may evaporate and, hence, the local salt concentration increases. Therefore, the content of salts in the water must be minimized. The copper, magnesium, and calcium salts, and the products of iron corrosion form scale on the fuel elements. This results in their overheating and failure. So, the content of these substances in water must be strictly controlled and maintained at a minimum level.

The ion-product constant for water changes with temperature:

T, K	298	366	422	474	522	555	573
$K_w \cdot 10^{-14}$	1	43	208	500	645	628	575

Air-saturated chemically demineralized water has pH = 5.3. This should be attributed to the presence of CO_2 in the air.

Literature generally gives pH measured at room temperature. With temperature, however, the concentration of hydrogen and hydroxyl ions changes. Pressure has but a slight effect on the ionic product of water.

With an increase in temperature the *solubility of gases* in water, e.g. oxygen, first decreases reaching its minimum at 373 K and then increases with temperature.

The main sources of gases in water coolant are: (1) gases dissolved in the feed water; (2) radiolysis; (3) corrosion with hydrogen depolarization; (4) gas pressurizers; (5) fission fragments.

In a gas pressurizer, the primary circuit water dissolves the gas constituents it contains. The water in the gas pressurizer dissolves gas in the amounts corresponding to the Henry law. Gas is transferred from the pressurizer to the primary circuit by diffusion. At 363 K, the coefficient of oxygen diffusion is close to 10^{-5} cm^2/s. The diffusion coefficient of cations and anions approximates this value.

When the volume of water in the primary circuit decreases, it is replenished with the gas-saturated water from the pressurizer. With hydrogen contained in the primary circuit taken into consideration, the overall content of gases in the water may reach several hundreds of cubic centimeters per litre. This may hinder the operation of the circulation pumps. The situation is still more aggravated, when the gas pressurizer operates at a high temperature as dictated by the layout scheme. The solubility of gases in water is the lowest at 373 K and grows fairly high at 573 to 623 K. The solubility of gases in water of the primary circuit at the core outlet is high. The water enters the circulation pumps at a temperature lower than the water temperature at the reactor outlet. The gas solubility in water decreases with temperature. The evolved gas may upset the pumps.

The gas pressure in pressurizers reaches 15 MPa. Even at a small volume content of oxygen in the gas (of the order of 0.1%), the par-

tial pressure of oxygen in the gas makes up 0.015 MPa. This results
in a high concentration of oxygen in the primary circuit water and
hence affects the corrosion resistance of structural materials.

Hydrogen accumulates in the primary circuit of pressurized water
reactors (PWR) because of the radiolytic water decomposition and
corrosion. Radiolytic oxygen produced in the first period of the
reactor operation is spent in corrosion. As a result, the hydrogen
content of the primary circuit water lies within 5 to 50 cm^3/l, which
accounts for the suppression of the radiolytic decomposition. To
combine oxygen hydrazine is injected in the primary circuit at the
beginning of the reactor operation. In boiling water reactors (BWR)
the radiolytic hydrogen and oxygen are carried away with steam and
discharged from the system by an ejector. On leaving the condenser,
the water contains neither gases nor hydrogen.

When the water enters the core, it decomposes radiolytically
to produce oxygen and hydrogen. In the steam phase, where the
density of substance is essentially lower than in the condensed phase,
the recombination is sluggish. Thus, in BWRs where radiolytic hyd-
rogen cannot accumulate in the circuit, the radiolysis is not suppress-
ed and the coolant always contains a certain amount of oxygen:
the circulating water, 0.03-0.3 mg/l, the steam-and-water mixture,
4-6 mg/l, and saturated steam, 10-30 mg/l.

The radiolytic decomposition is suppressed, if the steam in the
boiling system is not throttled to the atmospheric pressure and no
hydrogen is removed from it. This is observed in closed boiling loops
where hydrogen accumulates and suppresses the radiolytic decom-
position. The mechanism of the radiolytic decomposition will be
considered later.

The properties of water, its corrosive properties, for example,
change essentially in those sections of the circuit where impurities
contained in the coolant concentrate. This may take place in crevices
of welded joints in the fuel element channels of BWRs. Water or
steam-and-water saturated mixture moves inside the channel at
600 K. On the outside, nitrogen heated to 653 K passes over the chan-
nel. The water in a crevice evaporates owing to the heat flow from
the outer wall to the inner wall of the channel. The vapour pressure
in crevice exceeds the pressure in the tube. The steam escapes the
crevice till the pressure in the crevice and the tube is equalized. The
vapour left in the crevice overheats. Since the channel is of an eva-
porating type, the pressure in it is not constant and fluctuates about
an average value, sometimes exceeding the pressure in the crevice.
New portions of water enter the crevice and water evaporates con-
tinuously.

In compliance with the distribution coefficient, the equilibrium
concentration of chlorides in water 10^4 times exceeds that in satu-
rated steam. A minute amount of chlorides is carried away with steam.

Practically all chloride ions remain in the crevice water. Chlorides concentrate in the crevice and, though their content in the steam-and-water mixture is low ($2.5 \cdot 10^{-6}$%), the solution becomes more and more concentrated. According to the Raoult law the boiling temperature of a solution increases with concentration. The maximum medium temperature in the crevice is 653 K. At 13 MPa, this is a boiling point of a solution containing 42% of chlorides.

The concentration of chlorides takes place in the evaporation zone of a direct flow steam generator rated for 4 to 5 MPa. The solubility of chlorides in steam is small. Practically all chlorides carried with water remain in the evaporation zone. Similar phenomenon is observed at the first stage of a direct flow turbine preheater in BWRs. The concentration of chlorides leads to corrosion cracking of the austenitic stainless steels.

In coolant concentration by boiling, the NaOH concentration increases to a dangerous value. This results in the development of caustic embrittlement and failure of metal. When water is alkalified by a volatile alkali, ammonium hydroxide, the phenomenon is not observed. In evaporation and concentration ammonium hydroxide decomposes into water and gaseous ammonia. Ammonium hydroxide is a weak alkali; its dissociation constant under normal conditions equals $1.79 \cdot 10^{-5}$ and decreases with temperature.

In two-circuit reactors, the coolant is water circulating at high pressure. In boiling water reactors, steam-and-water mixture leaves the reactor core. In most BWRs now in operation, the pressure at the core outlet is 7-8 MPa. The solubility of chlorides in steam under this pressure is small. Boiling concentrates chlorides in the water of recirculation circuit, and the chloride-ion content reaches 0.1 mg/kg. The concentration of corrosion products increases, along with chlorides, and this promotes the growth of deposits on the surface of fuel elements.

In BWRs wet steam is delivered to the turbine. In the low pressure cylinder the steam moisture may erode the blades.

Nuclear superheating of steam to 780 K at 13 MPa was accomplished for the first time in this country. The solubility of chlorides in steam at this pressure is high, and, therefore, they would not concentrate on the fuel element cladding in steam drying and superheating.

Heavy water, D_2O, as compared with ordinary water, possesses a somewhat lower ability of moderating fast neutrons. However, it practically does not absorb thermal neutrons. Therefore, heavy water is the best moderator for thermal-neutron reactors. Heavy water may also be used as the coolant (Table 4.8).

The heavy water content of natural water is 0.017%, which corresponds to one molecule of heavy water per 7000 molecules of light water. Separation processes suitable for large-scale production of

TABLE 4.8 Thermophysical Properties of Heavy Water

Property	H$_2$O	D$_2$O
Molecular weight, g/mole	18.016	20.029
Density at 293 K, g/cm^3	0.998	1.106
Temperature of maximum density, K	276.980	284.210
Melting point at normal pressure, K	273.000	276.820
Boiling point at normal pressure, K	373.000	374.430
Critical temperature, K	647.150	644.500
Critical pressure, MPa	22.565	22.280
Critical density, g/cm^3	0.308	0.340
Melting heat, kJ/kg	331.900	317.100
Heat of evaporation, kJ/kg	2253.000	2067.000
Heat capacity at 293 K, kJ/(kg deg)	4.180	4.196

heavy water include electrolysis, distillation and chemical exchange. Presence of ordinary water in heavy water affects its properties as a moderator, i.e. light-water impurities in heavy water are objectionable. High costs of pure heavy water make us utilize in nuclear reactors less costly heavy water containing about 10% of light water impurities. Salts are 10% less soluble in heavy water than in light water.

The *activity of a water coolant* in a nuclear power plant increases in service. The oxygen of water becomes radioactive. Fission products find their way to the coolant. Radioisotopes form in the structural materials of the core and pass as corrosion products to the coolant. The coolant also contains the corrosion products formed on the surface of structural materials outside the core. When passing through the core, they also become activated.

Oxygen Activity. Slow neutrons produce in the core ^{19}O by the reaction ^{18}O (n, γ) ^{19}O. This isotope gives hard γ-radiation. This radiation, or the so-called *oxygen activity*, determines the level of coolant radiation in the circuit pipelines of the operating reactor and dictates to a considerable extent the requirements for biological shielding. The half-life of ^{19}O is 26.9 s. The oxygen activity rapidly drops after the reactor is shut down, and the circuit activity is determined by the fission fragments and radioactive products of corrosion. Natural water has only 0.002% of ^{18}O. Fast neutrons also initiate the reactions: ^{16}O (n, p) ^{16}N and ^{17}O (n, p) ^{17}N. The ^{16}N isotope decays with a 7.11-s half-life and ^{17}N, with a 4.174-s half-life. These nuclides react with oxygen to form nitrates and nitrites and with hydrogen to give ammonia. In single-circuit BWRs these compounds may be carried over with steam to the turbine, affecting the radiation situation.

The coefficient of ion distribution between steam and water at 553 K approximates 10^{-4}. Taking into account the solubility of ions in the moisture contained in steam, the distribution coefficient rises to 10^{-3}. With molecular ^{16}O, the ratio between activities in steam and water is 0.05 to 0.1.

In heavy water, the (n, γ) reaction produces much deuterium.

When the fuel element cladding get damaged, the fission products and the fuel itself may find their way to the water causing the so-called *fission-fragment activity*. Some fission fragments accumulates under the fuel element cladding. Their amount depends on the coefficient of their diffusion in the fuel, their half-life and volatility. Fission and subsequent decay produces more than 250 radionuclides, of which 33 are inert or volatile gases. These are mainly Br, Kr, I, Xe. Certain imperfections, say, flaws in metal and defects in welded seams, may disturb the cladding. Gas leaks occur most often and generally precede a grave damage to the cladding. The fission-fragment gas activity in the water of the primary circuit is dangerous in the case of leakage and ingress of the gases into the operating rooms. When the cladding is damaged considerably and the fuel contacts the coolant, nuclides of Mo, Sr, Ba, La, Zr, Nb and U are found in the water of the primary circuit. The greatest contribution to the coolant activity in the case of damage to the cladding is made by ^{133}Xe decaying with a 5.245-day half-life.

Note also, that in filling the fuel elements some fuel gets to the outer surface of the cladding. In service, the fission fragments pass to the water of the primary circuit. Naturally, the filling-up of fuel elements and washing of the external surfaces of claddings should be carried out so as to minimize the contamination. ·

The water of the primary circuit may also be contaminated by *activated products of corrosion*. They are formed either when the products of corrosion of the core materials get into the water, or when the corrosion products formed outside the core get activated. Most of corrosion products are formed by the former way. The radioactivity of corrosion products is mainly accounted for by ^{51}Cr, ^{54}Mn, ^{56}Mn, ^{58}Co, ^{60}Co, ^{59}Fe and others.

Stainless steel contains Co as an impurity of Ni. Stellite surfacing may serve as a source of Co. Metallic scrap utilized in steel melting may contain Co in the form of a surfacing material. Perlitic steels, therefore, may contain much Co.

The coolant of BWRs contains ^{64}Cu and ^{65}Zn when feed-water heaters and condenser are made of copper alloys.

The corrosion products, the active products including, are carried by the water over the circuit, deposit on the metal surfaces and surfaces of the fuel elements and accumulate in zones of stagnation. This activates the primary circuit equipment and hinders its servicing and repair. Twenty four hours following the shutdown, the level

of γ-radiation at the external tube surface (the CM-1 reactor, USA) was $(1.55 \text{ to } 1.8) \cdot 10^{-5}$ Ci/(kg h). An activity of up to $6.45 \cdot 10^{-4}$ Ci /(kg h) was recorded in certain places which may be attributed to a local accumulation of corrosion products. After two years of operation (several months after the shutdown) about 80% of activity was accounted for by ^{60}Co and ^{58}Co. Immediately after the reactor shutdown, the nuclides of Fe and Mn account for a half of activity.

Deposition of Corrosion Products. The knowledge of the kinetics of the process is necessary in order to make the quantitative prediction of the growth of the equipment activity, and to estimate the performance of fuel elements and efficiency of heat exchangers. Iron oxide mainly deposits as magnetite particles, $d \approx 10^{-4}$ cm in diameter. In the Brownian motion, the particles jump over distances comparable in size with water molecules ($\delta \approx 10^{-8}$ cm). If a particle is at a distance δ from the surface, then it reaches the surface in one displacement. That part of particles, which possesses an energy necessary to overcome the energy of hydration binding particles with water molecules, participates in the elementary event of forming deposits. Only those particles can participate in depositing which are directly near the surface, within a layer having a thickness of $d \approx 10^{-4}$ cm. The surface concentration of particles per 1 cm^2 is

$$C_s = Cd10^{-3}, \tag{4.19}$$

where C is the iron concentration in a coolant, g/l.

According to the theory of absolute reaction rates, the rate of precipitation V [g/(cm^2 s)] is

$$V = \nu W \exp(-Q/RT) C_s = \nu d \cdot 10^{-3} W \exp(-Q/RT) C = KC, \tag{4.20}$$

where K is the precipitation rate constant; ν is the particle oscillation frequency, s^{-1}; W is the geometric factor; Q, kJ/mole, is the activation energy of breaking bonds with molecules of water.

From the theory of mass transfer, the fluence of particles through a layer of thickness δ is

$$\Phi = (\nu\delta/2) \, \Delta C. \tag{4.21}$$

Fick's law gives Φ

$$\Phi = D\Delta C/\delta. \tag{4.22}$$

In aqueous media, the diffusion coefficient is inversely proportional to the size r of diffusing particles. The diffusion coefficient of ions having $r_0 = 10^{-8}$ cm is close to $D_0 = 10^{-5}$ cm^2/s. Hence,

$$D = D_0 r_0/d = 10^{-5} \cdot 10^{-8}/10^{-4} = 10^{-9} \text{ cm}^2/\text{s} \tag{4.23}$$

Combining (4.3), (4.4) and (4.5) gives:

$$\nu = 2D/\delta^2 \approx 10^{-9}/10^{-16} = 10^7 \text{ s}^{-1}. \tag{4.24}$$

Each of surface ions Fe^{2+}, Fe^{3+}, and O^{2-} of magnetite particles is bonded to a water molecule by hydration forces. In the case of Fe^{3+}, the maximum bond energy E is 443 kJ/mole of H_2O. When a particle passes from one phase to another, to the surface in this case, the activation energy is

$$Q = 0.125E = 54.9 \text{ kJ/mole.} \qquad (4.25)$$

The Fe^{3+} ion separates from the hydrated molecule of water when in thermal vibrations the ion and the water molecule move in opposite directions. The probability of this event

$$W = (1/6) \ (1/6) = 2.78 \cdot 10^{-2}. \qquad (4.26)$$

Then

$$K = vWd \cdot 10^{-3} \exp\left(-Q/RT\right) = 2.78 \cdot 10^{-2} \cdot 10^{-54.9/RT}. \qquad (4.27)$$

For temperatures within 553-573 K, $K = (1.53-2.42) \cdot 10^{-7} \approx$ $\approx 2 \cdot 10^{-7}$. This agrees well with the experimental value of K equal to $4 \cdot 10^{-7}$.

The obtained relationships are useful for assessing the kinetics of depositing and the accumulation of activity on non-heat-transfer surfaces. The precipitation rate constants of radionuclides are given in Table 4.9.

TABLE 4.9 Precipitation Rate Constants

Nuclide	Duration of exposure, 10^3 h	K, 10^{-7} cm/s	Nuclide	Duration of exposure, 10^3 h	K, 10^{-7} cm/s
^{60}Co	1	1.60	^{59}Fe	1.0	0.58
	4	0.97		2.6	1.57

The precipitation of corrosion products proceeds concurrently with their washing off. The activation energy of bond cleavage in a magnetite film is 138 kJ/mole. The rate of transfer of corrosion products to the coolant, V [g/(cm² s)], is proportional to the quantity of corrosion products precipitated on 1 cm², G (g/cm²):

$$V_1 = vGW \exp\left(-Q_1/RT\right) = K_1 G; \qquad (4.28)$$

$$K_1 = vW \cdot 10^{-Q_1/RT} = 10^7 \cdot 2.78 \cdot 10^{-2} \cdot 10^{-138/RT}. \qquad (4.29)$$

At 553 K, $K_1 = 2.43 \cdot 10^{-8}$. The experimental data gives $K_1 = 10^{-8}$.

The rate of corrosion of structural materials decreases with time. In 10^4 h, the rate of releasing the products of corrosion of the austenitic stainless steel into water becomes less than the rate of washing off the corrosion products deposited on the equipment surfaces. The rates of deposition and washing off equalize with time, provided the

hydrodynamic regime remains unchanged:

$$CK = GK_1. \qquad (4.30)$$

Taking into account that an actual surface is three times the geometrical surface, a monolayer of magnetite particles 10^{-4} cm in size deposited over 1 cm^2 with a density of 3 g/cm^3 contains

$$G = 3 \cdot 3 \cdot 10^{-4} \approx 10^{-3} \text{ g/cm}^2. \qquad (4.31)$$

From (4.12) and (4.13), we have the equilibrium concentration of corrosion products in a water coolant:

$$C_0 = GK_1/K = 10^{-3} \cdot 10^{-8}/4 \cdot 10^{-7} = 2.5 \cdot 10^{-5} \text{ g/l}, \qquad (4.32)$$

which approximates the value observed at nuclear power plants employing the equipment made of the austenitic stainless steels.

In surface boiling at 7.0 to 12.5 MPa, the steam practically does not carry away the corrosion products, and their concentration at the heat transferring surface increases. The amount of corrosion products delivered by the water to the surface where boiling occurs, V_2 [g/(cm^2 s)], is

$$V_2 = (q/10^4 \cdot 3.6 \cdot 10^3 \cdot q_1) \, C_0, \qquad (4.33)$$

where $q = 4.2 \cdot 10^6$ kJ/(m^2 s) is the heat flux; $q_1 = 1254$ kJ/kg is the heat of vaporization at 553-573 K.

The rate of removal of corrosion products from the surface owing to diffusion is

$$V_3 = DC \cdot 10^{-3}/\delta; \quad \delta = 10^{-4} \text{ cm}. \qquad (4.34)$$

At steady-state rates

$$V_2 = V + V_3, \qquad (4.35)$$

where V is the precipitation rate.

The solution of (4.17) gives a steady-state concentration of corrosion products at the heat transferring surface where the surface boiling takes place under the above-considered conditions:

$$C_0' \approx 10^2 C_0. \qquad (4.36)$$

The thickness of a year deposit on the fuel element surface is

$$\delta = KC_0'\tau/3 = 2 \cdot 10^{-7} \cdot 10^2 \cdot 2.5 \cdot 10^{-5} \cdot 3 \cdot 10^7/3 = 5 \cdot 10^{-3} \text{ cm}.$$

The experimental data yields δ equal to $(4-9) \cdot 10^{-3}$ cm. Irradiation practically has no effect on the kinetics of deposition of corrosion products and their washing off.

One of the measures to control the activation of the primary circuit equipment due to corrosion product deposits is a correct choice of structural materials and water regime. Blowing through the primary circuit and the bypass purification of water are only slightly

effective since the corrosion products deposit on the circuit internal surfaces and, in particular, on the fuel elements at a considerable rate.

The chemically demineralized water of high purity utilized as the coolant in the majority of nuclear reactors in this country represents a diluted solution. It is of utmost importance to predict the outcome of one or another process occurring in the water coolant (e.g. the processes described above) and its effect on the behaviour of structural materials. The consideration of chemical equilibria in solutions will tackle the problem.

Chemical Equilibrium in Solutions. The thermodynamic equilibrium is characterized by that a system capable of energy exchange with the environment remains unchanged (thermodynamically) until the external conditions vary. If a process can be realized both in the forward and in the reverse direction and so that not only the system itself and but also the surrounding medium return to the starting state, then the process is called *reversible*. In order that a process be reversible, it is enough that in each smallest stage it be infinitely close to the equilibrium state. When a system contains components A, B, D, and E and

$$mA + nB \rightleftarrows pD + qE,$$
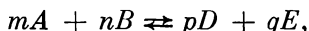
its equilibrium condition is expressed by the equation:

$$K_c = C_D^p C_E^q / C_A^m C_B^n,$$

where K_c is the equilibrium constant, and C denotes the concentration of components.

In the gas phase, expanding gas performs work (at $T = \text{const}$) $A = p\,\Delta V$; $dA = p\,dV$. Substituting $p = RT/V$, we obtain

$$A = \int_{V_1}^{V_2} (RT/V)\,dV = RT \ln (V_2/V_1).$$

For ideal gases, at $T = \text{const}$ molar volumes are inversely proportional to concentrations

$$A = RT \ln (C_1/C_2).$$

Suppose that a reaction

$$mA + nB \rightleftarrows pD + qE$$
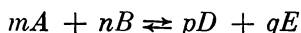
takes place in the gas phase. Inject m moles of A and n moles of B into the reaction space. The concentration of components to the moment of injection was c_A and c_B, respectively. After the injection the concentration of gases A and B changed reversibly to C_A and C_B. The isothermal work of changing the concentration of m moles of ideal gas A from c_A to C_A and n moles of ideal gas B from c_B to C_B

was done:

$$a_1 = RT \ln (c_A^m/C_A^m) + RT \ln (c_B^n/C_B^n).$$

Remove p moles of gas D and q moles of gas E from the reaction space. (Their concentration in the reaction space is C_D and C_E and c_D and c_E outside it.) The work of this isothermal process is

$$a_2 = -RT \ln (c_D^p/C_D^p) - RT \ln (c_E^q/C_E^q).$$

If the gases D and E are removed from the equilibrium space at a rate of their formation, the equilibrium will not be disturbed. The sum of all works equals the maximum reaction work A, because all stages of the process were carried out in a reversible manner:

$$A = a_1 + a_2 = RT \ [\ln (c_A^m/C_A^m) + \ln (c_B^n/C_B^n) - \ln (c_D^p/C_D^p)$$
$$- \ln (c_E^q/C_E^q)] = RT \ [\ln (C_D^p C_E^q/C_A^m C_B^n) - \ln (c_D^p c_E^q/c_A^m c_B^n)]$$
$$= RT \ (\ln K_c - \ln \Delta c).$$

The maximum work of a reversible process is independent of its pathway. Therefore, it may be represented as a difference between two values of a certain function G that characterize the initial and the final state:

$$A = -(G_2 - G_1) = -\Delta G. \tag{4.37}$$

The function G is known as the *thermodynamic potential* at a constant volume. It is often called the Gibbs *free energy*. A decrease in G is equal to the maximum work of a reversible isothermal process. Since the system performs work, the thermodynamic potential of the final state (G_2) is smaller than that of the initial state (G_1). The maximum work of the process is positive. Hence, a minus sign in (4.37). The change in the free energy in the course of a reversible process, the equilibrium constant, and the concentrations of the starting products are related as follows:

$$\Delta G = -A = -RT \ln K_c + RT \ln \Delta c.$$

This expression is often called the *Van't Hoff isotherm.*

The change in the thermodynamic potential under the isothermal conditions determines the direction of spontaneous processes in isolated systems. The spontaneous isothermal processes always occur in a constant volume towards the decrease in the thermodynamic potential. The same holds true if the reaction proceeds in diluted solutions rather than in gases. Then, strictly speaking, concentrations should be substituted by activities

$$\Delta G = -RT \ln K_a + RT \ln \Delta a.$$

The maximum useful work A of reaction serves as the measure of the chemical affinity of the reacting substances. It follows from the

isotherm equation that A may assume any value depending on the starting and final concentrations of the reacting substances. Therefore, the chemical affinity is the maximum useful work of a reaction, when the starting and final concentrations of all reactants are equal to unity. Then $A = RT \log K_c = -\Delta G$.

Thus, the greater the maximum work of the reaction, or the more negative the value of the free energy, the higher the chemical affinity of the reacting species. The participation of solids in the reaction affects A and $K_c^{\Delta G}$. Their concentration, however, does not enter the expressions for $\ln \Delta c$ and K_c as their transfer from the reservoir to the equilibrium space involves no work.

In dissociation of a substance, an equilibrium establishes in the solution between the concentrations of the substance and the products of its dissociation. If the concentration of a binary electrolyte is C_0 mole/l and the *degree of its dissociation* is α (a fraction of dissociated molecules), then the concentration of a nondissociated residue equals $C_0(1 - \alpha)$ and the concentration of both ions, $C_0\alpha$. Introducing these values into the equation for the equilibrium constant of dissociation, we obtain

$$K_c = C_0\alpha^2/(1 - \alpha)$$

or, in terms of activities,

$$K_a = C_a\alpha^2/(1 - \alpha).$$

The dissociation constant essentially depends on temperature. Thus, the addition of 5 to 10 mg/l of ammonia to water at room temperature produces pH 8-9, i.e. an alkaline medium. As the dissociation constant decreases with temperature, water with the same amount of ammonia at 573 K is practically a neutral medium. This should be taken into account when evaluating the water coolant attack on the reactor materials.

The pH may change in crevices and clearances owing to hydrolysis. When dissolved in water, sodium acetate, NaAc, salt derived from a strong base and a weak acid, dissociates into Na^+ and Ac^-. A small quantity of H^+ in water nearly completely combines with Ac^- into acetic acid, since it is a weak slightly dissociated acid. The loss of H^+ is made up for by further dissociation of water, this results in the formation of an equivalent amount of OH^-.

The OH^- ions do not combine with Na^+, since the NaOH is a strong fully dissociated base. The hydrolysis (i.e. the interaction of a substance with water to generate H^+ or OH^-) results in the accumulation of nondissociated acetic acid and hydroxyls, imparting an alkaline reaction to the solution. This may be represented as follows:

$$\left.\begin{array}{l} NaAc = Na^+ + Ac^- \\ H_2O = H^+ + OH^- \end{array}\right\} = Na^+ + OH^- + HAc.$$
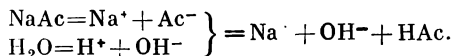
The degree of hydrolysis, β, gives the fraction of salt molecules that have undergone hydrolysis. If C_0 moles of NaAc are dissolved in 1 l of water, the salt dissociation produces C_0 ions of Ac^-. Following hydrolysis, $[Ac^-] = C_0 (1 - \beta)$ and $HAc = [OH^-] = C_0\beta$. The acid and OH^- form in equivalent quantities. For the reaction

$$Ac^- + H_2O = HAc + OH^-$$
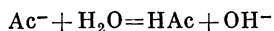
the constant of hydrolysis is

$$K_h = [HAc] [OH^-]/[Ac^-].$$

Substituting the above-obtained concentrations into this expression gives:

$$K_h = (C_0\beta)^2/C_0 (1 - \beta) = C_0\beta^2/(1 - \beta).$$

In most cases the degree of hydrolysis is small and $(1 - \beta)$ may be equated to unity.
Then,

$$K_h = C_0\beta = [OH^-]^2/C_0.$$

Hence,

$$[OH^-] = \sqrt{K_h C_0} \text{ and } \beta = \sqrt{K_h/C_0}.$$

Free alkalis in the boiler water cause caustic brittlement of metals.

Electrochemical Processes. An electrical current passing through a solution causes transfer of electrical charges and, therefore, performs work. The electrical work, A, is equal to the product of the potential difference between the electrodes by the transferred charge. The potential difference is called the *electromotive force* (emf) φ. If in a galvanic cell one mole of electrolyte ions converts into an equivalent number of moles of other ions and molecules, the charge transfer work equals $nF\varphi$, where n is the ion valency, and $F = 96.5$ kJ/eV. Then, $A = nF\varphi = -\Delta G$.

If a galvanic cell operates in thermodynamically reversible mode, A is the maximum useful work at a constant pressure, and, as shown above,

$$\Delta G = RT (-\ln K_a + \ln \Delta a),$$

where K_a is the equilibrium constant in terms of activity; and a is the starting activity of the reactants. Hence

$$\varphi = (RT/nF) (-\ln K_a + \ln \Delta a).$$

Passing to decimal logarithms we obtain under normal conditions and with $a = 1$ the *standard potential* of the electrochemical reaction:

$$\varphi^0 = -(0.059/n) \log K_a.$$

Hence

$$\varphi = \varphi^0 + (RT/nF)\ln a.$$

To make a galvanic cell reversible, the processes in it should proceed infinitely slowly and the current be very small, i.e. pass through an infinitely large resistance or be compensated for by equal in value and opposite in sign emf. The emf measurements are done by potentiometric method: by comparing the emf with that of a standard cell, which is generally the Weston cell wherein the following reaction takes place:

$$Cd + Hg_2SO_4 + (8/3)H_2O \rightleftarrows CdSO_4(8/3)H_2O + 2Hg.$$
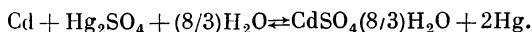
A positive electrode, mercury pool, is covered with Hg_2SO_4 paste and a negative electrode is the amalgam of mercury with 10-14% cadmium. The electrolyte is the saturated $CdSO_4$ solution. The Weston cell operates reversibly, if the currents drawn from it are very small. Its emf is defined as 1.018 V at 293 K.

When a metal is immersed into a solution, part of atoms go from the lattice nodes to the electrolyte. When a mole of metal goes into the solution, the work is done equal to the difference between the thermodynamic potentials of a mole in the metal lattice and a mole in the form of ions in the solution. The reaction occurring in a metal dissolution may be represented as follows:

$$Me \rightarrow Me^{2+} + 2e.$$

The potential of this reaction is expressed by the Nernst equation:

$$\varphi = \varphi^0 + (RT/nF)\ln a\, Me^{2+}.$$

For diluted solutions concentration may be substituted for activity; φ^0 represents a potential with regard to a certain, always the same, electrode whose potential is conventionally assumed as zero at activity 1 and is known as the *standard potential* of the given electrode. The value of the standard potential determines the tendency of a metal to send ions to a solution. For lithium violently reacting with water this value equals -3.01 V while for inert gold it is $+1.70$ V. The standard potentials of commercial metals lie within these values forming a known electromotive series.

In the metal-to-aqueous media interaction, the *electrochemical reactions* with the participation of the hydrogen ions play an essential role. The hydrogen electrode is an electrode system in which hydrogen is in contact with the solution of hydrogen ions. It consists of a half-cell in which platinum foil is immersed in an acidic solution saturated with hydrogen. The reaction

$$(1/2)H_2 \rightleftarrows H^+ + e$$
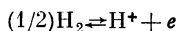
takes place on the electrode.

The potential of the hydrogen electrode at $n = 1$ is

$$\varphi_{H_2} = \varphi_{H_2}^0 + (RT/F) \ln a_{H^+}.$$

The potential of the hydrogen electrode at hydrogen pressure 0.1 MPa in a solution with activity 1 for H^+ is assumed as a *standard hydrogen electrode* equal to zero. The potential of the hydrogen electrode depends on the activity of H^+:

$$\varphi_{H_2} = (RT/F) \ln a_{H^+} = 0.059 \ \text{pH}$$

at a hydrogen pressure of 0.1 MPa. At any other hydrogen pressure, the hydrogen electrode potential is:

$$\varphi_{H_2} = (RT/F) \ln a_{H^+} - (RT/F) \ln \sqrt{P_{H_2}}.$$

An electrode immersed in a solution of its own ions and exchanging these ions with the solution is called the *electrode of the first kind*. For such an electrode

$$\varphi = \varphi^0 + (RT/nF) \ln a.$$

Copper immersed in a solution of copper vitriol and a hydrogen electrode may be the examples of such an electrode. Electrodes exchanging anions with a solution are known as the *electrodes of the second kind*. An example of such an electrode may be silver coated with a layer of a sparingly soluble salt and immersed in a solution of a readily soluble salt with the same anion, the so-called silver chlorine electrode on which reaction

$$Ag \rightarrow Ag^{\cdot} + e$$
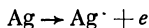
occurs. The potential of this electrode depends on the silver ion concentration by the Nernst equation:

$$\varphi + \varphi^0 + (RT/nF) \ln a_{Ag^+}.$$

In a solution of chlorides, silver forms a sparingly soluble compound AgCl. The concentration of the silver ions relates to the concentration of the chloride ion as follows:

$$a_{Ag^+} = L_{AgCl}/a_{Cl^-},$$

where L_{AgCl} is the *solubility product*.

The potential of the silver electrode in the chloride solution is

$$\varphi = \varphi^0 + (RT/nF) \ln L_{AgCl} - (RT/nF) \ln a_{Cl^-}$$

or at

$$\varphi^0 + (RT/nF) \ln L_{AgCl} = \varphi^{0\prime} \quad \varphi = \varphi^{0\prime} - (RT/nF) \ln a_{Cl^-},$$

i.e. the potential of the second kind electrode is conventionally reversible with regard to the anion. Also widely used as a reference ele-

ctrode is the calomel electrode on which proceeds the reaction:

$$2Hg + 2Cl^- \rightleftarrows Hg_2Cl_2 + 2e$$
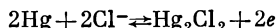
The potential of a saturated calomel half-cell, i.e. in the saturated Hg_2Cl_2 at 293 K, is equal to 0.245 V against the normal hydrogen electrode.

In the case of the oxidation-reduction electrode, the oxidation and reduction take place in the solution. The inert electrode does not participate in the reaction. It serves only as a source of electrons. For example, in a solution containing ions of ferrous and ferric iron, the following electrochemical reaction

$$Fe^{2+} \rightleftarrows Fe^{3+} + e$$
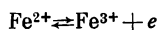
takes place on the inert electrode, e.g. platinum.

The ferric iron serves as an oxidizer and the ferrous iron, as a reducer, the reaction being the redox. The electrode potential relates to the reactant concentrations as follows:

$$\varphi = \varphi^0 + (RT/nF) \ln (a_{Fe^{3+}}/a_{Fe^{2+}}).$$

A cell consisting of two different electrodes and using a chemical reaction as a source of current is known as chemical. A cell in which two electrodes of the same metal are immersed in solutions of different concentrations of one salt of the same metal is called the *concentration cell*. The transfer of the electrolyte from one solution to another generates the electric current.

Corrosion Potential. In corrosion the metal surface is usually coated with oxide films and deposits of corrosion products. The metal surface may adsorb oxygen, water molecules and ions present in the medium. This disturbs the dependence of the potential of the metal being dissolved on the concentration of its ions expressed by the Nernst equation. When the metal contacts the electrolyte, a certain potential is set up called the corrosion potential. Let us now consider the difference between the corrosion potential and the metal potential satisfying the Nernst equation. (Material contribution to the investigation of corrosion potentials has been made by the Soviet corrosion scientist G. V. Akimov.)

Thus, the anodic reaction on the electrode of the first kind yields metal ions to the solution where they take part in the cathodic process. As a result the rates of cathodic and anodic processes equalize. If only atoms and ions of the same element participate in the anodic and cathodic processes, an equilibrium potential establishes. The dynamic equilibrium involves the exchange current, characterizing the rate of the electrode processes (Fig. 4.3a).

The potential of the electrode depends on the concentration of its ions in the medium by the Nernst equation. If the anodic process releases electrons owing to the formation of the metal ions and the
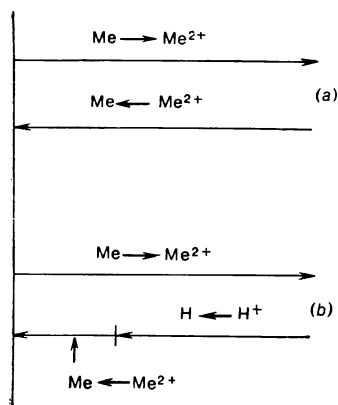
Fig. 4.3 Reactions at establishing equilibrium (a) and non-equilibrium corrosion (b) potentials

cathodic process combines them, say, with the hydrogen ions, i.e. ions of different elements participate in the anodic and cathodic processes a *non-equilibrium corrosion potential* (see Fig. 4.3*b*) establishes at the metal-to-medium boundary. Naturally, in this case, too, the rates of cathodic and anodic processes equalize and the potential assumes a certain more or less constant in time value known as the corrosion potential.

In practice, when the metal contacts the electrolyte, a corrosion potential is generated on the metal. Therefore, the standard potentials of metals serve only for the approximate assessment of their electrochemical activity. Thus, the normal potentials of aluminum and zinc are -1.663 and -0.763 V, respectively. However, under real conditions the formation of the protective oxide film makes the corrosion potential of aluminum somewhat more positive than that of zinc. Suppose that the metal-to-electrolyte contact generates a corrosion potential of the first kind. When the potential is shifted in the negative direction from the equilibrium value a cathodic reaction ta placekes on the electrode. Otherwise, an anodic reaction of metal dissolution occurs on the electrode.

The production of chemical changes in a compound or solution by causing its oppositely charged constituents or ions to move in opposite direction under a potential difference is called the *electrolysis*. In an electrolytic cell the electrode connected to the negative pole of the source is a cathode, and that connected to the positive pole, an anode. The reduction occurs on the cathode, for example, $Cu^{2+} + 2e \rightarrow Cu$, and the oxidation takes place on the anode, e.g. $Zn \rightarrow Zn^{2+} + 2e$. A change in the galvanic circuit, in particular in the electrode potential, in electrolysis is known as the *electrochemical polarization*. An electrode may polarize owing to a changed concentration near the electrodes (concentration polarization) and the deceleration of any stage of the electrode process (chemical polarization). Agitating the medium decreases the concentration gradient in the solution and hence lowers the concentration polarization.

The additional voltage required to cause electrolysis is called the *overvoltage*. Hydrogen releases at zero potential on a platinum-plated platinum immersed in a solution with 1 N hydrogen ion con-

centration and hydrogen pressure 0.1 MPa. On a smooth platinum electrode hydrogen releases at a potential of —0.2 V. The overvoltage is determined as the difference between the potential of the electrode when the reaction occurs at a certain rate and the equilibrium potential of the same reaction. The overvoltage of the hydrogen ion discharge depends upon the rate of the reaction on the electrode, i.e. upon the density of the polarizing current. The relationship between the hydrogen overvoltage η and the current density i is expressed by the Tafel equation:

$\eta = a + b \log i.$

The constant b is the same for all metals and is 0.18 V at room temperature. The constant a depends on the metal nature. The Tafel equation is valid within a wide range of current densities, from 10^{-8} to 10 A/cm^2.

5

5.1 Classification of Corrosion Processes

In service of power equipment, the metal destructs due to physico-chemical processes (electrochemical and chemical) occurring on the metal-to-medium interface, the metal-to-coolant interface in the case in question. Such deterioration of metals is called corrosion. The cost of metal lost in corrosion is high. In certain cases even minute corrosion defects may render a machine inoperative. About 1/3 of the annual output of metal is lost for technical utilization because of corrosion. About 2/3 of this amount is regenerated in scrap remelting. Still 1/10 of the annual output of metal is an irretrievable loss. The USA alone loses by corrosion approximately 45 000 million dollars each year.

In nuclear power plants, for example, corrosive destruction of fuel element cladding, heat exchangers, channels may lead to reactor shutdown. More than that, the release of corrosion products into the primary circuit, their activation in the core zone and subsequent deposition on the structural components hinder the reactor maintenance and repair. Many failures leading to the nuclear power plant shutdown are accounted for by corrosion. Therefore, much attention should be given to a high corrosion resistance of the structural materials employed in nuclear power plant engineering.

Most commercial metals are thermodynamically unstable in the metallic state. Therefore, they are found in nature as salts and oxides. Only noble metals Pt, Au, and partially Ag, Hg and Cu occur natively. The change in free energy in transition of 1 mole of metal to the ionic state exceeds zero for noble metals, while it is below zero for most commercial metals. Thermodynamics, however, determining the possibility of corrosion reactions, says nothing of their kinetics. An actual resistance of a metal to corrosion attack without taking into account the environmental conditions cannot be evaluated in terms of an absolute number as the case may be with mechanical properties of metals and alloys.

As to the mechanism of corrosion, it can be classified into chemical and electrochemical. The *chemical corrosion* follows the laws of chemical heterogeneous reactions involving no electrical current, e.g., corrosion in dry gases and nonelectrolytes. A metal oxidizes and the medium oxidant reduces simultaneously. The *electrochemical corro-*

sion takes place in electrolytes. A metal ionizes and the medium oxidant reduces not in one event. The electrochemical corrosion follows the laws of electrochemical kinetics and involves an electric current.

As to the conditions under which corrosion proceeds, the electrochemical corrosion is classified into: (1) corrosion with complete, partial, and alternating immersion in an electrolyte; (2) crevice and contact corrosion; (3) stress corrosion.

Depending on the kind of corrosion damage, it is convenient to classify corrosion into *grain face (general) corrosion* and *local attack*. In the former case, corrosion attacks the entire surface of a metal, in the latter, only part of it. If the attack is confined to individual fixed areas not so deep and relatively large, *spot corrosion* takes place. *Pit corrosion* is a localized type of deep attack on a small area. Sometimes the attack is in the form of *pitting*. *Intergranular corrosion*, as the name suggests, is the attack that occurs along metal grain boundaries. Corrosion cracking involves *transcrystalline cracks*. *Selective corrosion* occurs due to dissolving preferentially one of alloy constituents, an example is dezincification of yellow brass, in which zinc dissolves leaving a porous residue at copper and corrosion products.

As a rule, local corrosion is more dangerous compared to grain face corrosion and often results in loss of strength or tightness. Grain face corrosion is not rarely objectionable from the standpoint of coolant contamination with corrosion products.

Rate of grain face corrosion is evaluated in terms of metal loss $[mg/(m^2 h)$ or $g/(m^2 day)]$ and also of corrosion penetration depth (mm/year) characteristic of metal thinning. In cases when corrosion products are well bonded to the metal, the attack rate is estimated by metal gain in weight, i.e. by the amount of oxygen combined in oxides. In case of local corrosion its rate is evaluated (mm/year) by the depth of pits.

According to the rate of attack in a given medium, metals and alloys are classified by their corrosion resistance into a number of groups. The reactor structural materials should belong to resistant or perfectly resistant groups, i.e. their uniform corrosion depth should not exceed 0.01 mm/year, and they should not be liable to local attack.

In electrochemical corrosion, two interrelated but to some extent individual reactions occur: (1) *anodic*, in which some metal passes into a solution in the form of hydrated ions leaving an equivalent quantity of electrons in the metal; and (2) *cathodic*, in which excessive electrons released by the anodic process are assimilated by depolarizers (atoms, molecules, ions) reduced at the cathode.

If the cathodic and anodic reactions are separated by space, i.e. take place on different electrodes or different areas of the metal or alloy, corrosion takes a heterogeneous course. Corrosion proceeds

8*

homogeneously when the cathodic and anodic processes occur on the
same area of metal alternating only in time.

The influence of water coolant on the service life of the nuclear
power plant equipment can be evaluated only when taking into
account the processes occurring at the metal-to-water interface where
an electrical double layer forms.

5.2 Electrical Double Layer

The contact to water molecules affects the properties of the metal
surface. Water molecules are oriented randomly with respect to the
surface as shown in Fig. 5.1a. The Coulomb interaction of the metal
electrons found in the conductivity zone with the positive charge
of a water molecule (which is a dipole) forms a negatively-charged
layer in the metal. Oriented in position a, positive charges of water
molecules form a positively-charged layer. The two layers form a
flat capacitor or an electrical double layer. Lack of electrons occurs
on that area of the metal surface whereof electrons have gone to form
a negatively-charged layer (the inner Helmholtz plane, IHP) and,
from an energy standpoint, a double layer formed with the water
molecules as in position b will be advantageous. The double layer
contains no substance between the metal atoms and water molecu-
les forming the outer Helmholtz
plane, OHP. In view of this, the
Coulomb forces between the charges
of the metallic surface and water
molecules are not weakened, and
the dielectric constant may be taken
equal to unity.

The *capacitance of the electrical
double layer* (μF cm^{-2}) is determin-
ed by the relationship character-
istic of a flat capacitor at $D = 1$:

$$L = D/9 \cdot 10^5 \cdot 4 \cdot \pi\delta = 8.85$$
$$\times 10^{-8}/\delta, \qquad (5.1)$$

where δ is the distance between
the capacitor plates (between the
layers), cm.

With a negative charge of the
metal, the distance from the metal
surface to the centre of positive
charges in the water molecule (ac-
cording to the Rowlinson model) is

$$\delta = \delta_4 + \delta_3; \qquad (5.2)$$
$$\delta_3 = \delta_1 - \delta_2. \qquad (5.3)$$
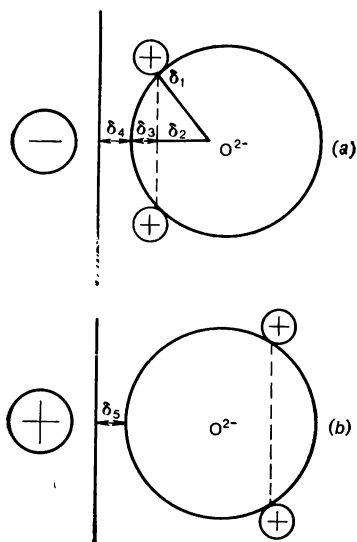
Fig. 5.1 Orientation of water mo-
lecules in electrical double layer
at negative (a) and positive (b)
charges of metal

The distance between the hydrogen atom and the centre of the water molecule is $\delta_1 = 0.096$ nm. The distance between the centre of the positive charges and the centre of the water molecule $\delta_2 = 0.059$ nm. Hence, $\delta_3 = 0.037$. To determine δ_4, use the uncertainty principle:

$$\Delta x = \hbar/\Delta P. \tag{5.4}$$

When considering the interaction with a surface atom, one should take into account the water molecule energy per one degree of freedom. Hence

$$P_{H_2O} = (2m_{H_2O}\, kT)^{0.5} = 1.1\cdot10^{-18} \text{ g cm s}^{-1}, \tag{5.5}$$

where $m = 18\cdot1.67\cdot10^{-24} = 3\cdot10^{-23}$ g is the mass of water molecules; $k = 1.38\cdot10^{-23}$ J deg^{-1} is the Boltzmann constant.

Water molecule collides in thermal vibration with a metal atom having momentum P_{Me}. The electrical double layer is best studied on mercury.

From the law of conservation of momentum, the velocity of a water molecule and a metal atom after collision is

$$\begin{aligned} V &= (P_{H_2O} + P_{Hg})/(m_{H_2O} + m_{Hg}) \\ &= (1.1\cdot10^{-18} + 3.66\cdot10^{-18})/(3\cdot10^{-23} + 3.34\cdot10^{-22}) \\ &= 1.31\cdot10^4 \text{ cm s}^{-1}. \end{aligned} \tag{5.6}$$

After collision the momenta of the water molecule and mercury atom are:

$$\begin{aligned} \Delta P'_{H_2O} &= m_{H_2O}\, V = 3\cdot10^{-23}\cdot1.31\cdot10^4 \\ &= 3.93\cdot10^{-19} \text{ g cm s}^{-1}; \end{aligned} \tag{5.7}$$

$$\begin{aligned} \Delta P'_{Hg} &= m_{Hg}\, V = 3.34\cdot10^{-22}\cdot1.31\cdot10^4 \\ &= 4.38\cdot10^{-18} \text{ g cm s}^{-1}. \end{aligned}$$

Taking into account (5.4) along the coordinate perpendicular to the metal surface, we obtain:

$$\begin{aligned} \delta_4 &= \Delta x_{H_2O} = \hbar/\Delta P'_{H_2O} = 1.05\cdot10^{-27}/(3.93\cdot10^{-19}) \\ &\approx 0.27\cdot10^{-8} \text{ cm}; \end{aligned} \tag{5.8}$$

$$\begin{aligned} \Delta x_{Hg} &= \hbar/\Delta P'_{Hg} = 1.05\cdot10^{-27}/(4.36\cdot10^{-18}) \\ &\approx 0.02\cdot10^{-8} \text{ cm}. \end{aligned} \tag{5.9}$$

For a negatively charged surface:

$$\begin{aligned} \delta_- &= \delta_4 + \delta_3 + \Delta x_{Hg} = 0.26\cdot10^{-8} \\ &\quad + 0.37\cdot10^{-8} + 0.02\cdot10^{-8} = 0.65\cdot10^{-8}; \end{aligned} \tag{5.10}$$

and taking into account (5.1):

$$L_-^0 = 8.84 \cdot 10^{-8}/(0.65 \cdot 10^{-8}) \approx 14 \ \mu F \ cm^{-2}. \qquad (5.11)$$

With a surface having a positive charge (see Fig. 5.1b)

$$\delta_5 = \delta_4 + \Delta x_{Hg} = 0.27 \cdot 10^{-8} \ cm; \qquad (5.12)$$

$$L_+^0 = 8.84 \cdot 10^{-8}/(0.27 \cdot 10^{-8}) \approx 33 \ \mu F \ cm^{-2}. \qquad (5.13)$$

The negative charge in the double layer of the metal surface ($C \ cm^{-2}$):

$$q^- = q_0 S_- pF, \qquad (5.14)$$

where $q_0 = 0.66$ of the electron charge, is the charge in the water molecule dipole; S_- is the surface occupied by water molecules found in position a (see Fig. 5.1); $p \approx 10^{-9}$ mole cm^{-2} is the number of water moles in the electrical double layer per $1 cm^2$; $F \approx 10^5 \ C \ mole^{-1}$ is the Faraday constant.

The positive charge:

$$q^+ = q_0 S_+ pF, \qquad (5.15)$$

where S_+ is the surface occupied by the water molecules found in position b (see Fig. 5.1).

Under certain conditions the sums of positive and negative charges in the double layer on the metal surface are equal. Then

$$S_- = S_+ = 0.5.$$

The surface of the metal is neutral, since the net charge of the surface equals zero. This corresponds to the *zero-charge potential*.

Each water molecule and a charge corresponding to it in the metal form a charged capacitor at the molecular level. If the neighboring molecules of water are arranged with respect to the surface as shown in Fig. 5.1, the energy of these dipole molecules, owing to the Coulomb interaction, is lower than in any other arrangement. From this follows that the configurations are stable.

As is seen from Fig. 5.1, the capacitors form at the molecular level a circuit of series-connected capacitors. At the potential of zero charge, when molecules are in position a, the net capacitance per $1 \ cm^2$ at the molecular level is

$$L_- = 0.5 L_-^0 \qquad (5.16)$$

and when they are in position b

$$L_+ = 0.5 L_+^0. \qquad (5.17)$$

The total capacitance of the double layer at the potential of zero charge $L_{z.c.}$ with the capacitors connected in series is

$$1/L_{z.c.} = 1/L_- + 1/L_+ = 1/0.5 L_-^0 + 1/0.5 L_+^0. \qquad (5.18)$$

Hence $L_{z.c.} = 4.9 \ \mu F \ cm^{-2}$.

The capacitance of the electrical double layer evaluated for mercury by this model agrees well with the experimental data tabulated below (Table 5.1).

It should be noted that, according to the Boltzmann distribution law, part of water molecules in the electrical double layer may have an energy other than $(3/2) RT$. Therefore, these molecules may be separated from the surface by a distance greater than δ_5. The electrical double layer is then blurred owing to thermal vibrations. The compact part of the double layer is realized at a distance less than

TABLE 5.1 Capacitance of Electrical Double Layer on Mercury, μF cm^{-2}

Surface condition	Calculated	Experimental
Positively charged	33.0	37.0
Negatively charged	14.0	17.0
Potential of zero charge	4.9	5.0

δ_5 from the metal surface. At a distance greater than δ_5 the so-called diffusion layer forms. The potential drop across this part of the electrical double layer is designated ψ_1. With a potential gradient, the liquid of the electrical double layer moves (electroosmosis), or solid particles in the solution migrate (electrophoresis).

Thus, to a first approximation the metal surface may be treated as one of the capacitor plates formed by the electrical double layer whose capacitance varies with potential. At the potential of zero charge, the capacitance of such a capacitor is close to $5 \cdot 10^{-6}$ F cm^{-2}. An 0.1 V increase in the metal potential increases the positive metal charge on half of the surface with the water orientation as in Fig. 5.1b by $+ \Delta q$:

$$+\Delta q = S^{+}L_{+}^{0} (\varphi - \varphi_{z.c.}) = 0.5 \cdot 3.7 \cdot 10^{-5} \cdot 0.1$$
$$= 1.85 \cdot 10^{-6} \text{ C } cm^{-2}. \tag{5.19}$$

The charge changed because part of water molecules went over from position a to position b. In this connection $+ \Delta q = - (- \Delta q)$ and the absolute change in the charge per 1 cm^2 to a first approximation is

$$\Sigma \Delta q = 2 \cdot \Delta q = 3.7 \cdot 10^{-6} \text{ C } cm^{-2}. \tag{5.20}$$

The charge of 1 cm^2 of the surface

$$S^0 = 0.66 \cdot 10^{-9}/10^{-5} = 6.6 \cdot 10^{-5} \text{ C } cm^{-2}.$$

Hence, the area of metal corresponding to position a changes by

$$\Delta S = \Sigma \Delta q/S^0 = 3.7 \cdot 10^{-6}/(6.6 \cdot 10^{-5}) = 5.6 \cdot 10^{-2} \text{ } cm^2. \tag{5.21}$$
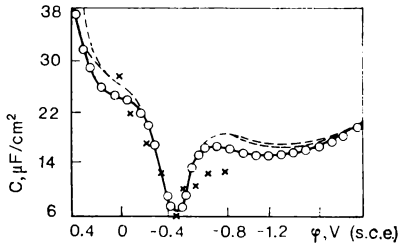
Fig. 5.2 Capacity of electrical double layer versus mercury potential in 10^{-4} N solution of NaF

o—experiment; x—calculated by proposed method; dashed line—calculated by the Green method

The capacitance then changes by

$$\Delta L = \Delta S L_0^0 = 5.6 \cdot 10^{-2} \cdot 3.7 \cdot 10^{-5} = 2.07 \cdot 10^{-6} \text{ F cm}^{-2}. \quad (5.22)$$

The 0.1 V increase in the potential increases the capacitance as follows:

$$L_{0\;1} = 5 \cdot 10^{-6} + 2.07 \cdot 10^{-6} = 7.07 \cdot 10^{-6} \text{ F cm}^{-2}.$$

Note that, since we speak about a capacitor with the capacitance equivalent to that of the electrical double layer, we mean the *integral capacitance*.

The integral capacitance L_i relates to the *differential capacitance* L_d being measured as follows:

$$L_i = (1/\varphi) \int_0^\varphi L_d d\varphi$$

When the potential varies from the potential of zero charge by 0.5 V, L_i linearly depends on L_d. To a first approximation, with

$$\Delta\varphi = \varphi - \varphi_{z.c} = 0.5 \text{ V},$$

$$L_i \approx (1/\varphi) [0.5 (L_d - L_{z.\,c.}) \varphi + L_{z.c}\varphi]$$

$$= 0.5 L_d + 0.5 L_{z.c.}$$

$$= 0.5 L_d + 2.5 \cdot 10^{-6} \text{ F cm}^{-2}; \quad (5.23)$$

$$L_d = 2 L_i - 2.5 \cdot 10^{-6} \text{ F cm}^{-2}. \quad (5.24)$$

Using this technique, we may obtain at $\Delta\varphi = 0.1$ V $L_d = 1.2 \cdot 10^{-5}$ F cm^{-2}. This accords well with an experimental value of $1.14 \cdot 10^{-6}$ F cm^{-2}. The same technique has been used to calculate the differential capacitance when $\Delta\varphi$ varies from $+0.5$ to -0.5 V. As Fig. 5.2 shows, the calculated and experimental values

agree well. The statistical processing of the data with the use of the Student t distribution shows that the experiment and calculation differ insignificantly.

5.3 Kinetics of Cathodic Processes

The metal corrosion, i.e. the transition of metals into an ionic state under the influence of corrosive medium, comprises two interrelated processes: anodic involving the metal ionization and the accumulation of an equivalent quantity of electrons in the metal, and cathodic in which the electrons interact with molecules or ions of a corrosive medium.

Hydrogen Depolarization. In deaerated aqueous media typical of nuclear power engineering and also in acid media, the cathodic process consists in the discharge of the hydrogen ions:

$$H^+ + e \rightarrow H \rightarrow 0.5H_2$$
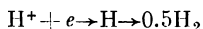
with the formation of first atomic and second molecular hydrogen. With this the attack involves *hydrogen depolarization*.

The equilibrium potential of the *hydrogen electrode* is

$$\varphi_{H^+} = \varphi^0 + (RT/F) \log C_{H^+} - (RT/F) \log P_{H_2}^{0.5},$$

where $\varphi^0 = 0$ is the normal potential of the hydrogen electrode. Taking into account that $P_{H_2} = 0.1$ MPa and pH $= 0$

$$-\log C_{H^+} = pH; \quad \varphi_{H^+} = - (RT/F) pH = - 0.059 \ pH.$$

Then, the hydrogen electrode potential varies with pH as follows:

pH	0	7	14
φ_{H^+}	0	−0.42	−0.84

In order to evaluate the service life of reactor materials, one has to know, in certain cases, the absolute *rate of the hydrogen ions discharge*. The hydrogen ion owing to a small size associates in aqueous media with a water molecule forming the hydronium ion H_3O^+. The energy of the hydronium ions at the metal surface, like that of any other charged particle, depends on the potential drop across the electrical double layer:

$$dQ = \varphi dq$$

With a flat capacitor $\varphi = q/L$, hence

$$dQ = q dq/L;$$

$$Q = (1/L) \int q dq = (1/L) \ (q^2/2) = q\varphi/2 = L\varphi^2/2. \tag{5.25}$$

Designating the number of charges of a particle as n, we obtain in kJ/g-eq

$$Q = 0.5nF\varphi = \alpha nF\varphi,$$

where $\alpha = 0.5$.

Outside the electrical double layer, $C_1 = C \cdot 2.36 \cdot 10^{-8} \cdot 10^{-3}$ g-ion of hydronium is found in the monolayer per 1 cm^2, where C, g-ion/l is the hydronium ion concentration in the volume; and $2.36 \cdot 10^{-8}$ cm is the diameter of hydronium ion.

The energy of these ions is independent of the potential of the double layer. The quantity of the hydronium ions in the monolayer per 1 cm^2 found directly near the metal surface (C_s) and those found outside the double layer (C_1), mole cm^{-2}, are interrelated as follows:

$$C_s \exp \{-[Q + \alpha nF (\varphi_{z.c.} - \varphi)]/RT\} = C_1 \cdot 10^{-Q/RT},$$

where Q is the hydration energy; $F = 96.5$ kJ eV^{-1} is the factor for conversion from an electron-volt per atom (eV/atom) to a kilojoule per mole (kJ mole^{-1}); ($\varphi_{z.c.} - \varphi$) is the potential drop across the electrical double layer; $\varphi_{z.c.}$ is the zero charge potential.

Taking into account the above-mentioned:

$$C_s = C \cdot 2.36 \cdot 10^{-11} \quad \exp \quad \{[\alpha F (\varphi_{z.c.} - \varphi)]/RT\}. \tag{5.26}$$

Knowing the size of a water molecule and the number of water molecules in 1 l, we may find, as a first approximation, that 1 cm^2 of the monolayer contains 10^{-9} water moles. Then, for a not too acid medium, (5.26) shows that at $\varphi_{z.c.} - \varphi \leqslant 0.5$ V the hydronium ions do not form a monolayer. Both the water molecules and the hydronium ions are found directly near the metal surface.

In hydrogen depolarization, the hydronium ion interacts with the electrons which have escaped the metal by means of the tunnel effect. Proceeding from the quantum mechanical notions, the probability of this event W_t is as follows:

$$\log W_t = - 0.44aE^{0.5}, \tag{5.27}$$

where $a \cdot 10^{-8}$ cm is the width of the barrier tunnelled by the electron; E, eV, is the height of the barrier or a work done by an electron on escaping the metal.

The width of the barrier may be evaluated taking into account the Fermi level E_F, i.e. the level of maximum energy in the metal. For most commercial metals, E_F approaches 10 eV $= 1.6 \cdot 10^{-18}$ J.

The uncertainty principle defines the position of an electron in the metal accurate to $\Delta x = 0.55 \cdot 10^{-8}$ cm.

In order to participate in the cathodic depolarization of the hydrogen ions an electron leaving the metal must cover a distance δ_- according to (5.10) equal to $0.64 \cdot 10^{-8}$ cm. Hence,

$$a = \Delta x + \delta_- = 0.55 \cdot 10^{-8} + 0.64 \cdot 10^{-8} = 1.19 \cdot 10^{-8} \quad \text{cm}.$$

For most commercial metals $E = 4.2$ eV. Then, according to (5.27):

$$\log W_t = -0.44 \cdot 1.19 \cdot (4.2)^{0.5} \approx -1.$$

The quantity of negatively charged particles (electrons) in the metallic plate of the double layer, q, g-eq cm^{-2}, according to (5.22), is

$$q = L\Delta\varphi/F.$$

Real media always contain a certain amount of cations and anions. Then $L \approx 2.3 \cdot 10^{-5}$ F cm^{-2}.

For $\Delta\varphi = 0.5$ V,

$$q = 2.3 \cdot 10^{-5} \cdot 0.5 \cdot 10^{-5} = 1.15 \cdot 10^{-5} \text{ g-eq cm}^{-2}$$

The probability that an electron leaves 1 cm^2 of the metal surface is:

$$W_m = qW_t = 1.15 \cdot 10^{-10} \cdot 10^{-1} \approx 10^{-11}.$$

As stated above, the hydronium ions in the electrical double layer do not form a monolayer. Therefore, the probability that an electron which has left the metal collides with the hydronium ion is not equal to unity but is proportional to C_s [see (5.26)]. The electron escape from the metal surface and the electron interaction with a hydronium ion are independent events. The probability of electron-to-hydronium interaction is

$$W = W_m C_s.$$

When a hydrogen ion interacts with an electron to form a hydrogen atom, it gives off energy equal to the ionization potential of hydrogen, 13.59 eV. This energy exceeds the hydration energy of a hydronium ion, and the hydronium ion dehydrates.

The rate of the cathodic process of the hydrogen ions discharge in A cm^{-2} is

$$i = vF'W_m C_s = 10^{13} \cdot 10^5 \cdot 10^{-11} \cdot C_1 \cdot 2.36 \cdot 10^{-11}$$

$$\times \exp \{[\alpha F (\varphi_{z.c.} - \varphi)]/RT\}$$

$$= C_1 \cdot 2.36 \cdot 10^{-4} \exp \{[\alpha F (\varphi_{z.c.} - \varphi)]/RT\}, \qquad (5.28)$$

where $v = 10^{13}$ s^{-1}; $F' = 10^5$ C/g-eq. At $C_1 = 1$, for 293 K

$$\varphi = 4RT/0.5F + \varphi_{z.c.} - (RT/0.5F) \log i$$

$$= \varphi_{z.c.} - 0.47 - 0.118 \log i.$$

At $C = 1$, the equilibrium potential of hydrogen electrode $\varphi^0 = 0$, and the overvoltage is

$$\eta = \varphi^0 - \varphi = 0.47 - \varphi_{z.c.} + 0.118 \log i. \qquad (5.29)$$

In the Tafel equation relating the hydrogen overvoltage to the current density of the cathodic polarization

$$\eta = a + b \log i, \qquad (5.30)$$

constant $b = 0.118$, which accords with (5.29). From (5.29) and (5.30)

$$a = 0.47 - \varphi_{z.c.}. \qquad (5.31)$$

The potential of zero charge and the work done by an electron to escape the metal, $e\varphi$, are related as follows:

$$\varphi_{z.c.} = e\varphi - 4.7. \qquad (5.32)$$

Hence

$$a = 5.17 - e\varphi. \qquad (5.33)$$

The values of a found by (5.33) and determined experimentally differ by not more than 20%. In order to evaluate quantitatively the rate of hydrogen depolarization, we may use in a first approximation the relationship that follows from (5.28):

$$\log i = \log C_{H^+} - 3.62 + [(\alpha F(\varphi_{z.c.} - \varphi)/RT]. \qquad (5.34)$$

The zero charge potentials for a series of commercial metals are tabulated below:

Metal	Al	Cr	Cu	Fe	Hg	Ni	Pb	Ti	Zr
$e\varphi$, V	-0.19	-0.45	-0.03	-0.37	-0.2	-0.25	-0.65	-0.7	-0.8

Oxygen Depolarization. In media containing oxygen, e.g. on the walls or in the circuit of boiling reactors, corrosion may take place with *oxygen depolarizaticn*. The cathodic reaction of the oxygen ionization is as follows:

$$0.5O_2 + H_2O + 2e = 2OH^-.$$
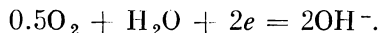
The equilibrium potential of the oxygen ionization varies with pH:

pH   0   7   14
q_{O_2} 1.23   0.82   0.40

The kinetics states that it is the single-electron stage that controls the reaction. The electron migration to oxygen coincides with chemisorption. In this an energy is given off equal to the affinity of oxygen for electron: 1.47 eV/mole = 141.3 kJ/mole.

The addition of a second electron to the oxygen atom involves an energy absorption $Q_1 = 6.8$ eV/mole $= 656$ kJ/mole. The energy of oxygen adsorption, at high degree of filling, is $Q_2 = 41.8$ kJ/mole. The hydration energy of OH^- is $Q_3 = 919$ kJ/mole.

The algebraic sum of Q_1, Q_2, Q_3, i.e. the energy given off in the elementary event of the oxygen ionization, is enough to compensate for the energy binding water molecules to other molecules or to the metal surface.

Since the slowest single-electron stage of the oxygen ionization controls the rate of the reaction, the concentration of oxygen participating in the cathodic process depends on the potential. By analogy with hydrogen depolarization, the quantity of oxygen per 1 cm^2 is

$$C_s = C_{O_2} (d/A)\, 10^{-3} \cdot 10^{-11} \exp\{[\alpha F(\varphi_{z.\,c.} - \varphi)]/RT\}$$

$$= C_{O_2} \cdot 4.6 \cdot 10^{-15} \exp\{[\alpha F (\varphi_{z.\,c.} - \varphi)]/RT\}, \qquad (5.35)$$

where C_{O_2} is the concentration of oxygen, mg/l; $\alpha = 1.46 \cdot 10^{-8}$ cm is the atomic diameter of oxygen; $A = 32$ is the molecular weight of oxygen.

Even in an aerated water coolant $(C_{O_2} = 10$ mg/l) at $\varphi_{z.\,c.} -$ $- \varphi = 0.5$ V, $C_s \approx 10^{-10}$ g-mole/cm^2, i.e. oxygen does not form a monolayer at the metal surface. Hence, the probability of the electron-to-oxygen interaction is $W_0 = W_m C_s$.

As a first approximation, we may assume $W_m = 10^{-11}$, i.e. as with the hydrogen depolarization. Hence the *rate of the cathodic reaction of oxygen ionization* is

$$i = \nu F' n W_m C_s = C_{O_2} 10^{13} \cdot 10^5 \cdot 2 \cdot 10^{-11}$$

$$\times\, 4.6 \cdot 10^{-15} \exp\{[\alpha F(\varphi_{z.c.} - \varphi)]/RT\}$$

$$= C_{O_2} 10^{-7} \exp\{[\alpha F(\varphi_{z.c.} - \varphi)]/RT\}, \qquad (5.36)$$

where $n = 2$ is the number of electrons participating in the oxygen depolarization.

$$\log i = \log C_{O_2} - 7 + \{[\alpha F(\varphi_{z.c.} - \varphi)]/RT\}. \qquad (5.37)$$

The overvoltage of the oxygen ionization calculated by (5.36) for 14 metals in an aerated medium with pH $= 9.2$ at a current density of 0.001 A cm^{-2} differs from the experimental values by not more than 10%.

Concentration Polarization. When a current flows through an electrode, the electrochemical reactions change the composition of a solution near the electrode. With an equilibrium electrode, the

equilibrium is disturbed. This gives rise to diffusion directed towards equalizing of the arising concentrations differences: the reactants are delivered to the electrode surface and the reaction products are removed thereof. The electrode potential may assume a value other than equilibrium. This is known as the *concentration polarization*. A layer next to the electrode wherein the solution concentration varies from the electrochemical reactions on the electrode surface is called the *diffusion layer*. Its thickness δ is 10^{-3}-$5 \cdot 10^{-2}$ cm in non-agitated media.

Suppose that the solution contains along with ion A taking part in the electrode reaction excessive ions of the same sign which mainly ensure the current passage, but do not participate in the electrode reactions. The current-induced migration of ion A may be neglected. As the electrochemical reaction proceeds, the concentration of ion A at the electrode surface decreases. The concentration gradient of ion A and its delivery to the surface owing to diffusion increase. With time an equilibrium establishes: the amount of ions participating in the electrode reaction equals the amount of ions delivered to the electrode owing to diffusion. The number of ions diffusing in unit time to 1 cm² of the electrode surface is equal to DdC/dx. The current density corresponding to this quantity of ions

$$i = nFD dC/dx,$$

and in case of a stationary process

$$i = nFD \ (C - C_s)/\delta,$$

where C_s is the concentration at the electrode surface and δ is the thickness of the diffusion layer.

With an increase in the current density, C_s may vary from the starting value C to zero. In the latter case, the current density reaches a certain value known as the *limiting diffusion current*:

$$i_d = nFDC/\delta.$$

The value of δ can be calculated only for a rotating disk electrode:

$$\delta = 1.62 D^{1/3} \nu^{1/6} \omega^{-1/2},$$

where ν is the kinematic viscosity; and ω is the angular velocity.

If the electrode polarizes, i.e. changes its potential owing to a passage of current, because a stage of the electrochemical reaction proceeds deceleratingly (e.g. the electron migration from the metal in the cathodic process), the process is referred to as kinetic or chemical. When the reactant delivery to the metal surface is limited the metal potential changes and the electrode polarizes. This is known as the concentration polarization. It is accounted for by diffusion limiting the delivery of reactants to the electrode surface.

5.4 Kinetics of Anodic Processes

Active Area. The anodic process converts metal into an ionic state. If the rate of the anodic process

$$Me \rightarrow Me^{n+} + ne$$

rises with potential, the metal dissolves in the *active region* of the anodic polarization curve (portion *B-C* in Fig. 5.3). In the metal dissolution a surface atom leaves the lattice. The activation energy necessary to produce an elementary event of the atom migration from the metal surface layer (Q) is, according to the Eyring rule, $Q = 0.25 E_{cr}^{surf}$, where E_{cr}^{surf} is the lattice energy of the surface atom equal to half the lattice energy E_{cr} for an atom in a three-dimensional lattice, i.e.

$$Q = 0.125 E_{cr}. \tag{5.38}$$

The probability that an atom leaves the metal surface is as follows:

$$W_{cr} = \exp(-0.125 E_{cr}/RT). \tag{5.39}$$

The lattice energy is the quantity of energy required to convert one mole of metal from a gas consisting of the nonionized atoms into a metallically bonded array.

Only a nonionized atom after having received an energy of $0.125 E_{cr}$ as a result of thermal vibrations may leave the lattice. For bivalent metals, the probability that both electrons are in the atom when it leaves the lattice is

$$W_1 = 0.5 \cdot 0.5 = 0.25;$$

$$\log W_1 = -0.6. \tag{5.40}$$

Only that atom may leave the lattice which in thermal vibrations moves away from the surface in the direction normal to it.

The probability of this

$$W_2 = 1/6 \cdot 10^{-1}; \quad \log W_2 = -0.78.$$

In a close-packed lattice an atom has six neighbors in the surface layer and three neighbors in the underlying layer. An atom may leave the lattice only when its neighbors in the surface layer are oriented in thermal vibrations neither along the normal to the surface towards the medium, nor in the direction of the atom
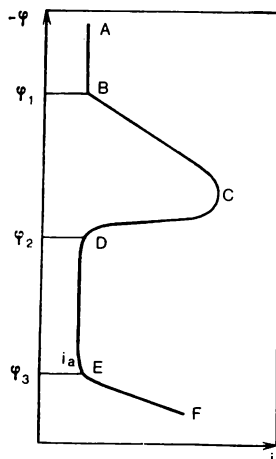
Fig. 5.3 Anodic polarization curve of passivating metal

leaving the lattice. The probability of such a situation

$$W_3 = (2/3)^6 \approx 8 \cdot 10^{-2}.$$

The underlying atoms at this moment must move inward the crystal, or aside. The probability of this

$$W_4 = (2/3)^3 = 3.7 \cdot 10^{-2}.$$

The product of probabilities *2*, *3*, and *4*

$$\Pi W_{cl.} = 1.6 \cdot 10^{-1} \cdot 8 \cdot 10^{-2} \cdot 3.7 \cdot 10^{-2}$$

$$\approx 4.7 \cdot 10^{-4}.$$

For a cubic nonclose-packed lattice

$$\Pi W_{ncl.} \approx 10^{-2}.$$

We may assume the following value as the average:

$$\Pi W = 10^{-3}. \tag{5.41}$$

An atom which has left the lattice for a corrosive medium will be hydrated only if it is ionized. In the ionization of the atom, electrons leave it (the tunnel effect) with a probability of

W_I and $\log W_I = -0.44a\sqrt{E}.$

The hydration must proceed following the ionization. Only then the ion would not return immediately into the lattice. When a bivalent ion adds two water molecules, the ion energy decreases by $q_1 = 83.6 \cdot 2 \cdot 2 = 334$ kJ. For most commercial metals, the ion energy decreases by 280 to 400 kJ, when an ion returns to the lattice. Therefore, the addition of even two water molecules prevents an ion from returning to the crystal.

To realize an elementary event of hydration, thermal vibrations should make a water molecule collide with the neighboring ion. The probability that a water molecule moves in the prescribed direction is 1/6. The probability that two molecules participate in the process is as follows:

$$W_5 = (1/6) \cdot (1/6) = 2.8 \cdot 10^{-2}; \quad \log W_5 = -1.55.$$

In the anodic dissolution of a metal, first an atom migrates into the medium and then the atom is ionized. This is proved by the following observation. The interaction of potassium with cold water not containing even traces of oxygen produces a blue solution. The water irradiation with electrons gives the same color. The first stage of dissolution involves the potassium atom migration into the water where it is ionized to form a hydrated electron.

The surface atoms of a metal exchange electrons. In the anodic polarization ($\Delta\varphi \approx 0.5$ V) and position of the water molecules as in Fig. 5.1b, the number of electrons per atom decreases by

$$\Delta n = \Delta q/1.6 \cdot 10^{-19} \cdot 10^{15} = L_+^0 \Delta\varphi/1.6 \cdot 10^{-4}$$
$$= 3.7 \cdot 10^{-5} \cdot 0.5/1.6 \cdot 10^{-4} \approx 0.12, \tag{5.42}$$

where $1.6 \cdot 10^{-19}$ C is the charge of the electron; 10^{15} is the number of atoms per 1 cm^2.

In a bivalent metal, such a change in the number of electrons leaves only 0.12 of the unit positive charge of the nucleus uncompensated.

Coulomb forces are not saturated. Therefore, the energy of the electrons shielding the positive charge of the atomic nucleus increases because of the interaction with the water molecule found in position b (see Fig. 5.1). For a bivalent metal, the number of electrons per atom, $n = 2 - 0.12 = 1.88 \approx 2$. The energy of electrons increases by $\Delta Q = \alpha n F \Delta\varphi$.

At room temperature practically all electrons in a metal are degenerated, i.e. have a minimum energy. Therefore, they give energy ΔQ imparted to them to the lattice atoms. The activation energy of the atom leaving the crystal lattice decreases by this very value.

Taking into account the above-stated, the *rate of the anodic dissolution* of a bivalent metal at an equilibrium potential, i.e. at the *exchange current*, is

$$i_e = n v F' C_s \Pi W W_{I_1} W_{I_2} W_1 W_5 \exp \{ -[0.125 E_{cr}$$
$$- \alpha n F (\varphi^\circ - \varphi_{z.c.})]/RT \}, \tag{5.43}$$

where n is the valency; $v = 10^{13}$ s^{-1}; $F = 96.5$ kJ/eV; $F' = 10^5$ C/g-eq is the Faraday constant; $C_s = 3 \cdot 10^{-9}$ g-eq/cm^2 is the surface concentration of the dissolved metal; W_{I_1}, W_{I_2} are the probabilities of the electron tunnelling corresponding to the first and second ionization potentials.

Calculated by (5.43), the exchange current for Ag, Cd, Hg, Pb exceeds 10-100 A cm^{-2}. The exchange currents are limited obviously by the anodic diffusion current which at room temperature is 10^{-2} to 10^{-1} A cm^{-2}. The expression (5.43) gives for iron:

$$\log i_e = 0.9 + 13 + 5 - 8.5 - 3$$
$$- 0.44 \cdot 1.19 \sqrt{7.87} - 0.44 \cdot 1.19 \sqrt{16.18} - 0.6 - 1.55$$
$$- \frac{0.125 \cdot 405 - 0.5 \cdot 2 \cdot 9.65 [-0.44 - (-0.37)]}{5.68} \approx -8.4.$$

Table 5.2 gives the calculated and experimental values of the exchange current.

In anodic polarization, i.e. at potentials more positive than $\varphi_{z.c.}$, the number of negative charges, i.e. electrons in the metallic plate

TABLE 5.2 Calculated and Experimental Values of Exchange Current
(log i_e, A cm^{-2})

Metal	Ag	Cd	Co	Cu	Fe	Hg	Ni	Pb	Zn	Cr
Calculated	—1 to —2	—1 to —2	—9.1	—3.35	—8.4	—1 to —2	—8.28	—1 to —2	—4.65	—13.1
Experimental	—2 to —2.5	—1.7 to —1.9	—6.1	—1.3 to —4.7	—8	—0.3	—8.7 to —9.1	—1	—3.2 to —4.7	—12

of the electrical double layer, decreases. As follows from the funda-
mentals of the band theory of solids, the Fermi energy decreases and
so does the energy of the crystal lattice. The latter is related to the
number of electrons per 1 cm^2 of surface (q, C cm^{-2}) through the fol-
lowing empirical dependence (kJ mole^{-1}):

$$E_{cr} = 148.4 + 7.5 \cdot 10^5 \, q. \tag{5.44}$$

Taking into account (5.19):

$$E_{cr} = 148.4 + 7.5 \cdot 10^5 \, L\varphi. \tag{5.45}$$

When the potential differs from $\varphi_{z.c.}$ by less than 0.3-0.5 V
$L \approx 2.5 \cdot 10^{-5}$ F cm^{-2}.

Hence

$$\Delta E_{cr} = 148.4 + 18.8 \, (\varphi - \varphi_{z.c.}). \tag{5.46}$$

Taking into account the above-stated, it follows from (5.43) that the
rate of the anodic process in the active region (i_a, A cm^{-2}) depends
on the potential as follows:

$$i_a = K \exp \{[\alpha n F(\varphi - \varphi_{z.c.}) + 18.8 \, (\varphi - \varphi_{z.c.})]/RT\}; \tag{5.47}$$

$$\log i_a = \log K + (\alpha n F/RT) \, (\varphi - \varphi_{z.c.})$$
$$+ (18.8/RT)(\varphi - \varphi_{z.c.}), \tag{5.48}$$

where

$$K = n v F C_s \Pi W \Pi W_{I_i} \, W_1 W_5 \exp \left[-(0.125 E_{cr} - 148.4)/RT \right]. \tag{5.49}$$

For bivalent metals (5.48) gives:

$$d \, (\varphi - \varphi_{z.c.})/d \log i = RT/(\alpha n F + 18.8)$$
$$= 2.3 \cdot 8.27 \cdot 298 \cdot 10^{-3}/(0.5 \cdot 2 \cdot 96.5 + 18.8) \approx 4.9 \cdot 10^{-2}. \tag{5.50}$$

The experimental value for iron is 0.042 ± 0.008 which approaches the calculated value (5.50). Neglecting the last term of the right-hand side of (5.48), we obtain 0.059.

Thus, in semilogarithmic coordinates the relation of the metal potential to the rate of metal dissolution in the active region is expressed by a straight line:

$$\log i = a + b\varphi, \tag{5.51}$$

where b equals the value of (5.50).

At a considerable anodic polarization in the active state, the rate of dissolution depends on the rate of the metal ions removal from the surface into the depth of solution. Since the rate of diffusion is independent of the potential, the *critical anodic diffusion current* does not depend on the potential and at 293 K is equal to 10^{-2} to 10^{-1} A cm^{-2}.

Passive Region. The *passivity* is an abrupt drop in the rate of the anodic process and, hence, in the rate of corrosion of a metal under conditions when it is thermodynamically unstable. Essential contribution to the theory of passivity has been made by the Soviet scientists V. A. Kostyakovskiy, G. V. Akimov, B. V. Ershler, Ya. M. Kolotyrkin, N. D. Tomashov, and others.

The passivity is attributed to the formation of a protective film on the metal surface. The surface atoms spend part of the energy to bond with oxygen of the protective layer. As a result, the activation energy necessary for the bond cleavage in the metal dissolution rises, and the rate of the anodic process and corrosion decreases.

The DE section of the anodic polarization curve in Fig. 5.3 corresponding to the passive state is known for a low rate of the anodic process (10^{-8} to 10^{-5} A cm^{-2}) and the independence from the potential. The potential corresponding to point D is called the *potential of complete passivity* or the Flade potential (φ_F). At this potential, the following reaction takes place

$$Me + H_2O = Me^+O^{2-} + H^+_{ads} + H^* + e. \tag{5.52}$$
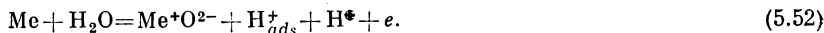
The Flade potential is determined by the following relation:

$$\varphi_F = \Delta G/F = 0.01 \, G_{Me^+O^{2-}} - 0.059 \, \text{pH} + a, \tag{5.53}$$

where ΔG is the change of the thermodynamic potential of (5.52); $G_{Me^+O^{2-}} = G_{Me_{\frac{m}{n}}^+O_P}$, kJ/g-eq is the thermodynamic potential of the lower oxide of metal referred to gram-equivalent.

For example,

$$G_{Cr^+O^{2-}} = G_{Cr_2O_3}/2 \cdot 3 = 1057/6 = 176 \ \text{kJ/g-eq.}$$

The values of a are as follows:

$a = 2.46$ for Al, Zr, Ti, V, Nb, Mn, U, Be, Ta, Si, Bi;

$a = 1.89$ for Cr, Fe, Ni, Co, Tc, Ga, In, Ge, Zn, Mg, Sn, Cd, W;

$a = 1.16$ for Ag, Cu, Hg, Pd, Au, Ru.

In order to take part in the formation of a passive film, a water molecule must break off the neighboring molecules. The activation energy of this process, Q_p, increases with potential, as in the electrical double layer the energy of water molecules decreases with potential by (5.25) as follows:

$$\Delta Q_p = \alpha n F \varphi = \alpha F L \varphi^2.$$

Hence, the rate of forming a passive film is

$$v_p = K \exp \left[-(Q_p + \alpha F L \varphi^2)/RT \right].$$

When an anodic reaction takes place on a metallic surface coated by a passive film, the latter decomposes. As a first approximation, the fraction of a metallic surface coated by a passive film, S_p, is proportional to the rate of the reaction of its formation:

$$S_p = K_1 v_p = K_2 \exp (-\alpha F L \varphi^2 / RT).$$

At the potentials of the passive region, most of the metallic surface is coated by a passive film. Hence, the rate of metal dissolution in the passive state is

$$i_p = K_3 S_p 10^{\alpha n F \varphi / RT}.$$

The metal ions of the passive film form one of the plates of the electrical double layer. Their energy depends on potential. Taking into account (5.43), we may write:

$$i_p = K_3 K_2 \exp (-\alpha F L \varphi^2 / RT) \exp (\alpha F L \varphi^2 / RT) = \text{const.}$$

The rate of the anodic process in the passive region should be independent of potential, which is observed in practice.

The more negative the φ_F, the greater is the probability that the corrosion potential of a metal or alloy corresponds to the passive region and the rate of corrosion is low.

When a metal is held in an aqueous medium for a long period of time, a phase oxide film forms on the metal surface. This also reduces the rate of corrosion:

$$2Cr^+O^{2-} + H_2O = Cr_2O_3 + 2H^+ + 4e.$$
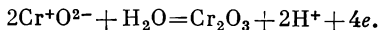
At 473-573 K the oxide films form on the metal surface at a greater rate. In particular, protective magnetite films Fe_3O_4 form on iron and steels of the perlitic class. The oxide layers grow following the laws of the solid phase surface diffusion. To a first approximation,

the thickness of oxide, δ (cm), may be evaluated by the following relation:

$$\delta^2 \approx D_0 \exp (-Q_s/RT) \, \tau,$$

where $D_0 \approx 10^3$; the activation energy of surface diffusion $Q_s = 0.35$ to $0.45Q$ (Q is the activation energy of volume diffusion); τ (s) is the time.

Under the service conditions of nuclear power plants, the stainless steels and aluminum and zirconium alloys operate at a corrosion potential in the passive state. This accounts for their high corrosion-resistance.

Repassivation. When the potential is raised to E (see Fig. 5.3), the reaction leading to the formation of a readily soluble ions of higher valency becomes thermodynamically possible.

In a neutral medium the following reaction takes place:

$$Cr_2O_3 + 4H_2O = Cr_2O_7^{2-} + 8H^+ + 6e. \tag{5.54}$$

In an alkaline medium

$$Cr_2O_3 + 10OH^- = 2CrO_4^{2-} + 5H_2O + 6e. \tag{5.55}$$

The EF portion of the anodic polarization curve (see Fig. 5.3) is known as the *repassivation region*, and the potential corresponding to point E, as the repassivation potential φ_{rp}.

The equilibrium potential for (5.55) at pH $= 14$ is equal to -0.07 V. Hence, the equilibrium potential for this reaction $\varphi = -0.07 + (0.059 \cdot 10/6)$ pH $= -0.07 + 0.098$ pH $\approx -0.07 + 0.1$ pH.

In alkaline media at pH $= 12$ to 13, in the presence of an oxidizer, $KMnO_4$ for example, the corrosion potential for stainless steel corresponds to the repassivation region. The oxide film formed on the stainless steel surface naturally dissolves. All substances deposited on the surface of oxides, including compounds containing radioactive isotopes of cobalt, iron, manganese, etc., pass into the medium. This deactivates the equipment and improves the radioactive situation.

In acid and neutral media, repassivation proceeds by (5.54). At pH $= 7$, the equilibrium potential of the reaction is close to 0.9 V. At this potential the passive state of the austenitic Cr-Ni stainless steels is disturbed.

Pseudopassive State. In media containing no activators, chlorides, for example, in particular in chemically demineralized water, at potentials more negative than those of the active dissolution region, the rate of the anodic process is independent of potential and is low (portion AB in Fig. 5.3). This makes it resemble the passive state, and hence the name, *pseudopassive state*. The onset of the pseudopassive state at potentials more positive than $\varphi_{z.c.}$ is associated with the adsorption of H_2O. Within the potential region in question,

where water molecules are oriented according to Fig. 5.1*b*, the metal is charged positively. In adsorption, the H_2O molecule gives an electron to the metal.

$$Me + H_2O = (H_2O)_{ads.\ Me};$$
$$\Delta G \approx \Delta H = -Q = -41.8 \ \text{kJ/mole.}$$
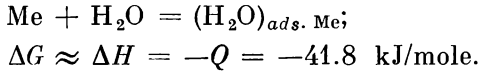
Hence,

$$G_{H_2O_{ads.\ Me}} = \Delta G + G_{H_2O} = -41.8 - 237.0 = 278.8 \ \text{kJ/mole.}$$

In sections where water molecules are oriented as in Fig. 5.1*a*, the metal is negative. These areas adsorb O_2, and the metal gives off an electron.

Adsorption releases energy. The energy of the metal surface atoms decreases. This decreases the rate of the anodic process to a value close to the rate of the anodic process in the passive state and, therefore, decreases the rate of corrosion. Thus, in chemically demineralized water containing 0.2 mg/l oxygen the rate of corrosion attack on perlitic steels at 293 and 353 K is 0.020 and 0.065 g/(m² day). If oxygen in the medium is combined with, say, hydrazine no oxygen adsorption takes place, and the corrosion rate increases three- to fourfold.

As the reaction

$$(H_2O)_{ads.\ Me} = Me^{n+} + H_2O + ne$$

proceeds, the pseudopassive state is disturbed. The potential of this reaction

$$\varphi_d = (G_{Me^{n+}} + G_{H_2O} - G_{(H_2O)_{ads.\ Me}})/n \cdot 96.5 = (G_{Me^{n+}}/n \cdot 96.5)$$
$$+ 41.8/n \cdot 96.5 = \varphi^0_{Me^{n+}} + 0.43/n. \qquad (5.56)$$

For iron, the calculated value of φ_d is -0.22 V and the experimental, -0.25 V. At potentials more positive than φ_d, iron and other metals dissolve in the active state.

In the presence of chlorides, the pseudopassive state is not realized. In view of this, to reduce the rate of the perlitic steel corrosion under the conditions of, say, the condensate feed circuit, the content of the chloride ion in the condensate should not exceed 0.02 mg/kg, and the electrical conductivity lie within 0.1-1.0 μS/cm.

5.5 Local Corrosion

Pit corrosion is another type of corrosion that is localized. When crossing the boundaries of three grains, in places of dislocation pile-ups the surface atoms possess an increased energy. The rate of the anodic

process here is greater than at the neighboring areas. This creates pits on the metal surface. The base diameter of such a pit is comparable to its depth.

The oxygen dissolved in the medium filling up the pit is consumed in the cathodic reaction taking place on the pit walls. Therefore, the metal at the pit bottom following some time contacts practically dearated medium. In chemically demineralized water, the pseudopassive state is realized and the rate of attack sharply decelerates. The pit stops to grow. In chemically demineralized water, the pit depth does not exceed 0.3 to 0.4 mm. In media containing chlorides, the latter retard the onset of the pseudopassive state. Pits continue to grow and may reach several millimeters in depth.

Stress Corrosion. Chlorides in a medium disturb not only the pseudopassive state, but also the passive state. When the passive state is disturbed the following reaction takes place on stainless steels:

$$Cr^+O^{-2} + 3Cl^- = CrCl_3 + 0.5O_2 + 4e.$$

The normal potential of this reaction (*break-down potential* φ_{bd}) is close to 0.2 to 0.3 V. Interacting with water $CrCl_3$ forms readily soluble complexes.

In places where dislocations pass out to the surface, the ions forming a passive film $(Cr^+O^{2-})_{disl}$ are displaced and their energy exceeds by 41.8 kJ/mole that of the ions in the areas with a perfect lattice. Hence

$$G_{(Cr^+O^{2-})_{disl}} = G_{(Cr^+O^{2-})} + 41.8$$

and accordingly

$$\varphi_{bd\ disl} = \varphi_{bd} - (41.8/4 \cdot 96.14) \approx \varphi_{bd} - 0.11.$$

The corrosion potential of stainless steel φ_c may be such that $\varphi_{bd\ disl} < \varphi_c < \varphi_{bd}$.

Then the metal surface with a perfect lattice is in the passive state, while the places, where the dislocations pass out to the surface, become active. So, the *active-passive cells* are formed. At sites, where the passive state is disturbed, the metal dissolves in the active state, the surface atoms being given an extra energy:

$$Q_{act} = \alpha nF\ (\varphi_c - \varphi_{z.\ c.}). \tag{5.57}$$

Passing out to the surface, the dislocations form a slip step. Its formation requires energy equal to $b^2\gamma$, where b is the Burgers vector and γ is the surface energy. Therefore, the surface slows down the movement of dislocations. To form a passive film, part of the energy of surface atoms is spent in bonding to the oxygen of the passive film. The energy of the surface atom, the dislocated atom including, also reduces. When reaction (5.56) disturbs the passive state, the slip step formed by the escaped dislocation dissolves owing to the

anodic process. The energy of the surface dislocated atoms increases by

$$\Sigma Q = b^2 \gamma + \alpha n F \, (\varphi_c - \varphi_{z.c.}).$$

At sites, where the metal dissolves in the active state, the surface does not decelerate the movement of dislocations but even accelerates it because the surface atoms receive extra energy Q_{act}. The activation energy of dislocation movement decreases by Q_{act} in (3.31) and (3.32), and dislocations move at a greater rate. Hence, a flat dislocation pile-up, which is a crack embryo, forms in smaller time interval. Cracks in this case cross the metal grains. This is transcrystalline stress corrosion or corrosion cracking.

The *time to the appearance of a crack embryo* in corrosion cracking can be determined using (3.32) and (5.57):

$$\log \tau = \log \tau_0 - [\alpha n F \, (\varphi_c - \varphi_{z.c.})]/RT. \qquad (5.58)$$

To estimate the effect of the O_2 and Cl^- content in the medium on time τ, use the following relationship taking into account (5.57) and (5.58):

$$d \log \tau = (\partial Q_{act}/\partial \log C_{O_2}) \, d \log C_{O_2}$$
$$+ (\partial Q_{act}/\partial \log C_{Cl^-}) \, d \log C_{Cl^-}. \qquad (5.59)$$

In the right-hand side of (5.57), φ_c depends on the oxygen concentration. Determine φ_c as a function of $\log C_{O_2}$. The value of $\mathbf{b}$ in the Tafel relation describing the rate of the anodic process of steel dissolution in the active region and potential at room temperature is close to 0.04. At 573 K, $\mathbf{b}$ equals $0.04 \cdot 573/298 = 0.077$. For the cathodic polarization curve, we obtain $-0.118 \cdot 573/298 = -0.23$. Taking into consideration that the rate of the cathodic process is directly proportional to the oxygen concentration, the rates of the cathodic and anodic processes at 573 K at active regions are as follows:

$$\varphi_a = K_a + 0.077 \log i;$$
$$\varphi_c = K_c - 0.23 \, \log i + 0.23 \log C_{O_2}.$$

The rates of the cathodic and anodic processes at the corrosion potential, φ_c, are equal. Hence,

$$\varphi_c = K + 0.06 \log C_{O_2}. \qquad (5.60)$$

From (5.59) and (5.60), at 573 K:

$$d \log \tau/d \log C_{O_2} = -\alpha n F \cdot 0.06/RT$$
$$= -0.5 \cdot 2 \cdot 96.5 \cdot 0.06/2.3 \cdot 8.27 \cdot 573 \cdot 10^{-3} = -0.53.$$

The experimental value is close to -0.5. In the right-hand side of (5.57), n in compliance with (5.42) depends on the capacitance of

the electrical double layer L_1 which in turn depends on concentration:

$$L_{Cl} = a + K \log C_{Cl^-};$$
$$n_{Cl} = n_0 L_{Cl}/L_0 = n_0 \left[(a/L_0) + (K/L_0) \log C_{Cl^-}\right]$$
$$= n_0 (a_1 + K_1 \log C_{Cl^-}). \tag{5.61}$$

In chemically demineralized water, i.e. in the absence of Cl^-, $L_0 = 5$ µF cm^{-2}. At $C_{Cl^-} < 10^{-3}$ N, $K = 3$ µF cm^{-2} by the experimental data and, accordingly, $K_1 = 0.6$, and $\varphi_{z.c.} = -0.41$ V is practically independent of the chloride concentration.

From (5.59) and (5.61), at $C_{O_2} = 0.1 - 0.3$ mg/l, $\varphi_c \approx -0.1$ V, and $n_0 = 2$:

$$d \log \tau/d \log C_{Cl^-} = -(\alpha n_0 F/RT)(\varphi_c - \varphi_{z.c.}) K_1 = -1.65. \tag{5.62}$$

The experiment gives the value close to -1.5. Taking into account (5.58), (5.62), (3.31), and (3.32), we obtain at 573 K and $\sigma \approx \sigma_y$:

$$\log \tau = 3.3 - 0.5 \log C_{O_2} - 1.5 \log C_{Cl^-}. \tag{5.63}$$

This relationship quantitatively evaluates the influence of the O_2 and Cl^- content in the medium on the time to the generation of cracks caused by stress corrosion of the austenitic Cr-Ni stainless steel, grade 08X18H10T, at 573 K.

From (3.31) and (3.32) at 573 K, σ in MPa, we have:

$$\Delta \log \tau/\Delta \sigma = -v\gamma/RT = -1.64 \cdot 10^{-3} \cdot 150/19 \cdot 0.573$$
$$= -2.26 \cdot 10^{-2},$$

which is close to the experimental values. This relation quantitatively predicts, as a first approximation, the effect of the stress level on the time to the appearance of cracks.

In service, the concentration of the chloride ion on the surface where boiling takes place may increase. Thus, the deposits of corrosion products have pores forming a system of capillaries. Part of these capillaries pass coolant to the heat transferring surface where evaporation occurs. The forming steam is removed through other capillaries. At temperatures close to 573 K, chlorides dissolve in steam only slightly. Therefore, the concentration of chlorides in the evaporation zone increases and, depending on the thickness of the layer of corrosion products, may increase K times compared to the volume concentration:

Thickness of deposits, µm	22	50	75	100
K		25	485	10^4	$2.3 \cdot 10^5$

Chlorides may concentrate in the evaporation zone of a direct flow low-pressure steam generator, in low-pressure steam generators with impaired circulation and heat exchange, in crevices, etc.

Leaking water may find its way to pipes heated to above 373 K and evaporate on their surface. Even if the water is chemically demineralized, chlorides concentrate on the surface of pipework.

To reduce or avoid stress corrosion, the aluminum coating 0.1 to 0.2 mm thick is applied to the surface of pipes.

Another way to prevent stress corrosion is to reduce the concentration of Cl^- and O_2 in the coolant to 0.02 mg/kg and decrease the concentration of corrosion products to cut down the thickness of deposits. Elimination of leaks, crevices, fissures, etc., also serves for the purpose.

To raise the resistance of stainless steels to stress corrosion, the content of nickel in them is increased. Steels containing 40% Ni do not practically suffer from intergranular corrosion cracking. An increase in the nickel content increases the energy of stacking faults and facilitates cross slip of dislocations and their passing from one slip plane to another. The probability of forming plane dislocation pile-ups naturally reduces. In high-nickel alloys containing 50-60% Ni, the cross slip of dislocations is so easy that they migrate through the grain and accumulate at the grain boundaries. Embryo cracks form at the grain boundary, and high-nickel alloys are liable to intergranular corrosion cracking.

Aluminum alloys also have a high stacking fault energy. This facilitates dislocations cross slip. Therefore, aluminum alloys, like high-nickel alloys, are prone to intergranular corrosion cracking.

Stainless steel containing 7-8% Ni becomes austenitic-ferritic rather than austenitic. In the ferritic component (α-phase) having a BCC-lattice, the cross slip of dislocation is easier. This makes austenitic-ferritic steels more resistant to stress corrosion than steel 08X18H10T.

When a metal is subjected to a combined effect of a corrosive medium and alternating stresses, it fails from *corrosion fatigue*. A number of alternating stress cycles (10^7 to 10^8) a metal can withstand in the absence of corrosive medium is called the *endurance limit* or *fatigue limit*. As the number of cycles grows, the stress goes down approximating asymptotically the fatigue limit (AA in Fig. 5.4). In a corrosive medium, the metal has no fatigue limit. Even in the absence of alternating stresses, the specimen fails within a sufficiently long period of time from corrosion. The calculations use a conditional fatigue limit (B in Fig. 5.4) which is a minimum alternating stress producing metal failure within a certain number of cycles, 10^7 for instance. Material contribution to the investigation of corrosion fatigue has been made by the Soviet scientists A. V. Ryabchenkov, I. D. Tomashov, G. V. Karpenko and others.

The corrosion fatigue control includes generation of compressive stresses, e.g. shot peening of the metal surface (this reduces the detrimental effect of alternating tensile stresses), or application of protective coatings, and use of electrochemical protection. Under alternating loads responsible for the fatigue failure of metal, the deformation in each stress cycle does not exceed 0.1-0.2%.

In reaching the full power output and in a shutdown cooling, and also in changing the power output, the nuclear power plant assemblies, in places where, say, pipes are welded to the drum-separator, may suffer from stresses exceeding the yield point. The deformation naturally exceeds 0.1% and may reach 0.5 and even 1%.

Number of reversals of stress

Fig. 5.4 Wöhler diagram
1—fatigue; *2*—corrosion fatigue; *AA*—fatigue limit; *B*—conventional limit of corrosion fatigue

The number of reactor starts and stops when such a situation may arise, is limited. The metal failure under alternating stresses 10^3 to 10^4 cycles involving deformation above 0.1 to 0.2% is known as the *low-cycle fatigue*.

As has been mentioned earlier, the formation of oxide films on the steel surface in contact with water is preceded by the oxygen dissolution in the metal. Oxygen, diffusing with time into the depth of metal, forms the Cottrell atmospheres around a dislocation. They lock dislocation movement, hinder their passage to other slip planes, and promote the formation of flat dislocation pile-ups and, hence, embryo cracks. Therefore, the contact with even chemically demineralized water at about 573 K reduces the number of cycles to failure because of the small-cycle fatigue to 1/3 to 1/5 of its former value. The activation energies of the oxygen diffusion in austenite and ferrite are 170.54 and 99.07 kJ/mole, respectively. At 573 K, the coefficient of oxygen diffusion in austenitic steels is $1.7 \cdot 10^3$ times less than in perlitic steels. Therefore, failures from small-cycle fatigue are to be expected when nuclear power plants employ steels of the perlitic class. Surface cladding, for example, of the drum-separator or headers with the austenitic stainless steel practically eliminates the risk of cracking due to small-cycle fatigue.

In service, the equipment parts may rub against each other. Friction causes damage to the oxide protective films. This is known as *fretting corrosion*. Fretting corrosion may cause failure of the zirconium alloys.

Heating in welding may separate carbides in the austenitic stainless steels close in composition to Cr_4C. The content of Cr and C in

the austenite at the grain boundaries decreases. Carbides precipitate mainly at grain boundaries. Chromium and carbon diffuse from the center of grain towards the boundaries. The diffusion coefficient of C is by several orders of magnitude greater than that of Cr. Therefore, C diffused to the grain boundaries binds new portions of Cr into carbides facilitating in this way the austenite depletion of chromium. The content of Cr may drop to less than 8%, i.e. below the first threshold of resistance equal to 12%. When at the corrosion potential, the austenite containing 18% Cr is in the passive state, while the grain boundaries depleted of chromium are in the active state, intergranular corrosion may develop. As a rule, it takes place in acidic media.

To control the intergranular corrosion, the austenitic Cr-Ni stainless steels are alloyed with Ti and Nb which combine with carbon to produce strong carbides. Another way is to reduce the carbon content in steels, but this is rather expensive and not adaptable to production.

5.6 Influence of Various Factors on Corrosion of Reactor Materials

External Factors. The external factors of corrosion include corrosive medium, its composition, pH, temperature, pressure, contacts with other materials, etc. Internal factors include the composition and structure of the metal, surface condition, presence of mechanical stresses.

Effect of pH. There is no general rule which makes it possible to evaluate the effect of pH on the resistance of all materials. In each particular case one has to consider the influence of pH on the kinetics of the cathodic and anodic processes and, hence, on the rate of corrosion. In a neutral aerated medium iron corrodes in the active state with oxygen depolarization limited by diffusion.

The change of pH from 4 to 10 has no effect, other things being equal, on concentration and diffusion, i.e. it does not affect the rate of both the cathodic and the anodic process. Therefore, the rate of iron corrosion remains practically constant within pH 4-10. With pH below 4, the concentration of the hydrogen ions rises, the equilibrium potential of the hydrogen electrode increases so that the rate of hydrogen depolarization increases and becomes comparable to the rate of oxygen depolarization and exceeds it. Thus, the corrosion potential increases. This, according to the anodic polarization curve of the iron dissolution in the active state, increases the rate of iron corrosion with a decrease in pH. At pH above 11.3, iron passivates in aerated solutions at the corrosion potential. Hence, the rate of corrosion sharply decreases. When pH increases above 14, the hydroxide protective films dissolve at elevated temperatures. The result is that at pH above 14 the iron corrosion accelerates.

It is easier to predict the behavior of amphoteric metals, such as aluminum and zinc, at varying pH. The rate of corrosion increases both when pH becomes less and when it becomes greater than the neutral value. Nickel, cobalt, and cadmium are not effective in acidic media, while in alkali solutions the rate of their corrosion is low owing to the formation of protective oxide and hydroxide films. A number of metals, e.g. tantalum, molybdenum, and tugsten, are, on the contrary, resistant in acidic media and ineffective in alkali solutions. Their oxides being anhydrides of corresponding acids are soluble in alkalis and offer no protection in high pH media. The rate of corro-sion of noble metals, gold, platinum, and silver, is practically inde-pendent of the pH medium.

Effect of oxidizers. By their influence on the corrosion resistance of metals oxidizers may be divided into two groups: (1) those increas-ing the rate of the cathodic process and practically having no effect on the kinetics of the anodic process, and (2) those increasing the rate of the cathodic process and decelerating the anodic process of metal dissolution.

The first group includes, for instance, ions of ferric iron and biva-lent copper. The presence of the oxidizers in the medium accelerates the cathodic process and, hence, increases the metal potential. There-fore, an increase in the content of oxygen or oxidizers increases the corrosion rate, if the corrosion potential corresponds to the active region of metal dissolution. If, with an increase in the content of oxygen or oxidizers, the corrosion potential converts the metal from the active into the passive state the rate of attack decreases. If in changing the concentration of oxidizers the corrosion potential re-mains within the passive region, the corrosion rate does not vary. At a very high concentration of oxidizers, the corrosion potential goes from the passive region to the repassivation region which increases the rate of corrosion. Thus, an increase in the concentration of oxi-dizers having no effect on the rate of the anodic process may diffe-rently affect the corrosion resistance of passivating materials.

Permanganates, nitrites, and chromates may be referred to the se-cond group. Interacting with the metal surface these oxidizers dece-lerate the anodic process passivating the metal. Therefore, such oxi-dizers are called the anodic passivators, or anodic inhibitors of corro-sion; often they are known as *inhibitors*. Metal passivates by inhibi-tors owing to the formation of the adsorption or phase protective films on its surface.

To reduce materially the corrosion rate of iron or steel at tempe-ratures up to 353 K, the passivator concentration should be 1-5 g/l. Used as inhibitors of steel corrosion are chromates, nitrides, silica-tes, water glass, molybdates, and aluminates. When the concentra-tion of inhibitor is insufficient, part of the metal surface does not passivate and remains in the active state. This involves the risk of

pitting attack. Often this is observed in crevices not accessible for the inhibitor because of the diffusion limitations. The presence of activators in the medium, say, chlorides, raises the risk of pitting when the inhibitor is lacking. Generally speaking, the higher the concentration of activator, the higher the inhibitor concentration.

Note that inhibitors protect only the metal in contact with the solution. They provide no protection along the waterline and above it. To do this use is made of the so-called vapor-phase inhibitors, e.g. nitrites, carbonates and benzoates of dicyclohexylamine and monoethanolamine. They possess a high vapor pressure. The molecules of these compounds convert into the gaseous phase and therefrom the metal surface adsorbs them. The resultant adsorption layer slows down the metal corrosion. The volatile inhibitors find application, in particular, for corrosion protection of water shielding tanks and for preassembly preservation of the carbon steel items when they are kept packed. The container where the volatile inhibitors are utilized must naturally be air-tight. For the same purpose the item surfaces are treated with aqueous solutions of a nitrite with appropriate thickening agents. After the treatment a nitrite film forms which protects the item against corrosion.

When pickling metals for cleaning the surface of corrosion products and scale, high-molecular organic compounds containing sulfur and nitrogen are added to the acids. Such compounds are known as corrosion inhibitors.

Effect of oxygen. Now let us consider the effect of oxygen dissolved in water on the corrosion resistance of iron, and carbon and low-alloyed steels.

When the concentration of O_2 is less than 0.2 mg/kg the steels of perlitic class in chemically demineralized water are in the pseudo-passive state within 293-353 K and the rate of their corrosion is low, 0.02 to 0.06 g/(m² day). With an increase in the oxygen concentration, the rate of the cathodic process increases and, hence, the corrosion potential starts to operate in the region of active dissolution. So, an increase in the oxygen concentration increases the rate of attack.

At a sufficiently high rate of the anodic process the concentration of corrosion products at the metal surface materially increases. The rate of their removal from the metal surface inward the solution, which is determined by the diffusion rate, controls the anodic process of metal dissolution. The latter is then independent of the potential and is determined by the critical diffusion current i_d. At room temperature, $i_d = 10^{-2}$ A cm^{-2}. This corresponds to dissolving an iron layer $3.6 \cdot 10^{-7}$ cm thick in 1 s.

In order that a protective oxide film be formed on the metal surface, oxygen should diffuse in 1 s into the metal to a depth in excess of $3.6 \cdot 10^{-7}$ cm. Note that an increase in the corrosion potential due to an increase in the oxygen concentration involves an increase in

the energy of surface atoms and an appropriate decrease in the activation energy of diffusion. The coefficient of the oxygen diffusion in α-Fe is:

$$D = 3.7 \cdot 10^{-2} \cdot 10^{-(99 - \alpha n F \Delta \varphi)/RT}.$$

The displacement of the diffusion front δ (cm) can be evaluated by the relation

$$\delta^2 \approx D \tau.$$

For a protective film to be formed, the following equality must be satisfied:

$$(3.6 \cdot 10^{-7})^2 \approx 3.7 \cdot 10^{-2}$$
$$\times 10^{-(99 - 0.5 \cdot 2 \cdot 96 \Delta \varphi)/(19 \cdot 298 \cdot 10^{-3})}. \tag{5.64}$$

From (5.64)

$$\Delta \varphi = \varphi_c - \varphi_{z.c.} = \varphi_c - (-0.37) = 0.35.$$

Hence $\varphi_c \approx 0.00$ V.

The corrosion rate of steel 20 considerably decreases at $\varphi_c = 0.1 - 0.11$ V, which corresponds to $C_{O_2} = 16$-40 mg/kg (Table 5.3).

TABLE 5.3 Effect of Oxygen on Corrosion Rate of Steel 20

Oxygen concentration, mg/kg	φ_c, V	K, g/(m² day)	Oxygen concentration, mg/kg	φ_c, V	K, g/(m² day)
4	—0.3 to —0.4	0.18	16	—0.11	0.53
8-10	—0.2	2.9	40	0.1	0.17

In certain instances, the presence in the medium of substances other than oxidizers may affect the intensity of forming the protective layers and, consequently, the corrosion resistance of metals. This occurs when substances interacting with metal form *soluble complexes*. Naturally, no protective layers form and the metal dissolves in the active state. Under certain conditions (e.g. with the temperature rise), the complex compounds decompose and the metal atoms form oxides. The latter deposit on the metal surface and yield in a short time a protective passivating film reducing the metal corrosion.

Effect of temperature. The rate of the anodic process in the active and passive states grows with temperature. The rate of the cathodic process of hydrogen depolarization also increases with temperature. Oxygen depolarization does not always increase with temperature. The effective convection agitation of a hot solution decreases the thickness of the diffusion layer. Note that in a system communicat-

ing with the atmosphere the solubility of oxygen drops with tempe-
rature. Therefore, the critical diffusion current and corrosion rate in
an open system pass with temperature through maxima. In a closed
system, the critical diffusion current and corrosion rate continuously
grow with temperature. At 293 K, the oxygen and hydrogen branches
of the cathodic polarization curve are separated by 0.5-1.0 V. With an
increase in temperature, both branches approach each other and at
473 K merge, i.e. the ionization of oxygen and the discharge of the
hydrogen ions take place at practically equal potentials.

The corrosion of all reactor materials in water and vapor grows with
temperature. Especially abruptly increases the corrosion of perlitic
steels at temperatures above 673 K. It should be noted, however, that
increasing temperature intensifies the oxygen diffusion into the metal
and, consequently, the growth of protective oxide films. In saturated
steam, the rate of corrosion is the same as in water at the same tem-
perature. In superheated steam, the corrosion is less intensive than
in water at the same temperature.

Changes in the pressure of water and steam have no effect on the
corrosion resistance of perlitic and stainless steels. The rate of cor-
rosion of the aluminum alloys increases with steam pressure.

If one region of a metal is heated to a high temperature whereas
the other is at a low temperature, a potential difference arises be-
tween them and a thermogalvanic macrocouple forms. An anode is the
hotter region. The thermogalvanic macrocouple operates, as a rule,
with the cathodic control limited by diffusion. The *thermogalvanic cor-
rosion* may be a serious hazard with a small area of anode, large area
of cathode, and intensive medium agitation.

Effect of medium motion. Water motion thins the diffusion layer
and intensifies corrosion limited by diffusion.

Erosion takes place where the inner diameter of piping changes, pi-
pes bend or hydrodynamic characteristics of flow are affected. The
destruction of a protective oxide film by erosion renders the equip-
ment inoperative. Such failures are observed at bends and where
tubes are expanded in a tube plate in low- and high-pressure preheat-
ers at 403 to 473 K. At these temperatures the intensity of oxygen
diffusion into iron is still small, and so the rate of increasing the
magnetite protective oxide film is also low. Adding oxygen to che-
mically demineralized water in an amount not in excess of 0.2 mg/kg
facilitates the growth of the protective oxide film and materially
increases the corrosion resistance of the equipment of the condensate-
feed system.

An increase in the water rate does not practically affect the corro-
sion resistance of stainless steels at the corrosive potential in the pas-
sive state. Copper and brass are washed out from tubes at water velo-
cities of 5 to 10 m/s. Alloying brasses with arsenic increases their cor-
rosion resistance in flowing water.

Contact corrosion. In nuclear power plants it is practically impossible to avoid contacts between various materials differing in electrochemical characteristics and, first of all, in the corrosion potential. A metal more negative in a galvanic couple becomes an anode and fails because of contact corrosion. An aluminum alloy and stainless steel furnish an example of such a corrosion couple. When a current flows in a galvanic couple the electrode potentials vary. This is known as the *polarization of electrodes.*

In the simplest case a change in the electrode potential is in direct proportion to the density of polarizing current. Let us consider the *effectiveness of the galvanic couple.* To this end, evaluate the couple current and the amount of dissolved metal. When a galvanic couple operates, current I flows through it. This current producing polarization of electrodes changes their potential by $\Delta\varphi$. The relation between the potential and current is expressed through the polarization resistance R:

$$\Delta\varphi = IR.$$

The difference between the potentials of cathode and anode φ_c^0 $-\varphi_a^0$ is equal to the sum of potential drops in the galvanic circuit:

$$\varphi_c^0 - \varphi_a^0 = \Delta\varphi_c + \Delta\varphi_a + \Delta\varphi_{Me} + \Delta\varphi_R,$$

where $\Delta\varphi_{Me}$ is the ohmic potential drop in the metal equal to zero due to perfect metal conductivity; $\Delta\varphi_R$ is the ohmic potential drop in the electrolyte equal to IR (where R is the electrolyte resistance); $\Delta\varphi_c = R_c I$ is the change in the cathodic potential produced by polarization; $\Delta\varphi_a = R_a I$ is the change in the anodic potential produced by polarization.

The above equation may be written as follows:

$$\varphi_c^0 - \varphi_a^0 = R_c I + R_a I + IR$$
$$= I (R_c + R_a + R) = \Delta\varphi^0,$$

hence,

$$I = \Delta\varphi^0/(R_c + R_a + R).$$

This is graphically shown in Fig. 5.5a. When a conductivity of a solution is high, R is close to zero, and

$$I = \Delta\varphi^0/(R_c + R_a).$$

In the simplest case, $R_a = \tan \alpha$ and $R_c = \tan \beta$ (see Fig. 5.5b). If $R \to 0$, the system is completely polarized and the potentials of both electrodes become equal to φ (see Fig. 5.5b). A change in the potential of an electrode when a current is passed through it, i.e. in polarization, can be represented by polarization curves (see Fig. 5.5). The most simple case is the linear dependence of the poten-
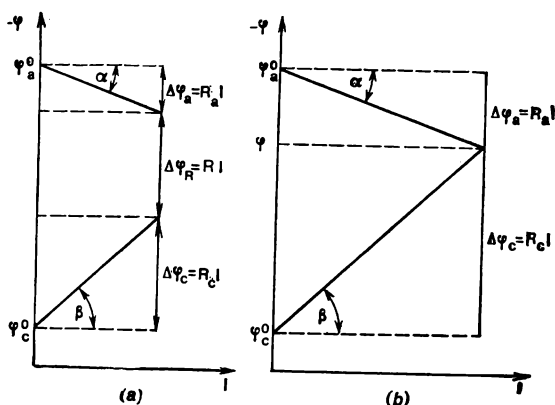
Fig. 5.5 Corrosion diagram of partially (*a*) and completely (*b*) polarized galvanic couple

tial variation on current, or current density. In a number of cases the linear relationship is observed in semilogarithmic coordinates ($\varphi - \log I$) (Fig. 5.6). The polarization resistance proportional to the tangent of the polarization curve determines the rate of the electrode process. The greater the slope of the curve, the slower the process, and vice versa. It should be recalled that the rates of the electrode reactions should be compared at equal potentials.

The set of cathodic and anodic polarization curves represent a *corrosion diagram* of a given corrosion process. Since the rates of cathodic and anodic processes should be equal, the intersection of the cathodic and anodic curves corresponds to the corrosion potential of the system and the rate of the electrode processes proper. If the process is characterized by polarization curves OA and MN (see Fig. 5.6), the corrosion proceeds with oxygen depolarization, with kinetic limitation of the cathodic process. With polarization curves OAL and KL corrosion proceeds with oxygen depolarization limited by diffusion. With polarization curves $OALBC$ and ST corrosion proceeds with hydrogen depolarization. In practice the critical diffusion current by hydrogen ions is only seldom reached. Corrosion of most commercial materials in neutral media proceeds with oxygen depolarization limited by diffusion. The thickness of the diffusion layer in artificially non-agitated electrolytes is usually taken equal to 0.05 mm.

As mentioned above, the emf of a corrosion cell is spent to overcome the ohmic and polarization potential drops: $\Delta\varphi^0 = \Delta\varphi_c + \Delta\varphi_a + \Delta\varphi_R$. Depending on the relation between these quantities the corrosion proceeds with any of the control types (ohmic, cathodic, or anodic control), or with a mixed control. The ratio of the potential
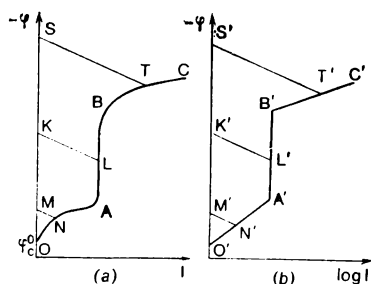
Fig. 5.6 Corrosion diagram in Cartesian (a) and semilogarithmic (b) coordinates

drop of one type to the initial potential difference in per cent characterizes the degree of control:

$(\Delta\varphi_c/\Delta\varphi^0)\cdot 100$ is the degree of cathodic control;

$(\Delta\varphi_a/\Delta\varphi^0)\cdot 100$ is the degree of anodic control;

$(\Delta\varphi_R/\Delta\varphi^0)\cdot 100$ is the degree of ohmic control.

In completely polarized systems, when the ohmic drop of potential is small, corrosion proceeds with cathodic, anodic, or mixed control. The difference between the corrosion and initial potentials of the cathode and anode ($\Delta\varphi_c$ and $\Delta\varphi_a$), which can be readily obtained from the corrosion diagrams, gives us a clear knowledge of the control type in a given corrosive process.

A process is called controlling, if a change in its rate affects the corrosion. As follows from the corrosion diagram shown in Fig. 5.6, the slope of the straight line KL varying in a wide range, i.e. a change in the rate of the anodic process, has no effect on the rate of corrosion, since in the range of potentials AB the rate of the cathodic reaction is independent of potential. In this case, the corrosion is mainly cathodically controlled.

In order to control the contact corrosion one has to increase the resistivity of the water coolant, i.e. decrease the salt content of water, reduce its conductance, and lower the content of oxygen. The contact corrosion in the aluminum alloy-stainless steel couple may be reduced by forming an oxide film on the aluminum alloy surface by anodizing. The most effective is an oxide film 50 to 60 μm thick obtained by the thick-film technique. It is also good practice to separate aluminum and steel parts with a replaceable spacer, often called protector, made of aluminum, or Zr and Ti alloys. As a rule, remedial measures are used to control the contact corrosion.

A crevice formed when parts of the same material contact each other accumulates the corrosion products most often in the form of

hydroxides. The diffusion exchange between the liquid in the crevice and the medium outside is difficult.

As a rule, hydroxides are poorly soluble compounds. Nevertheless, their dissociation in the crevice alkalifies the medium to pH = = 8.5-9.0. At this pH, the corrosion accelerates. Thus, crevices in aluminum alloys intensify corrosion.

Internal Factors. Alloying. The corrosion resistance of the reactor materials considerably depends on their *composition* and *structure*. In the majority of cases of practical importance, alloys of homogeneous structure, solid solutions, for instance, are more corrosion-resistant than the heterogeneous alloys. The structural components of the heterogeneous alloys have different electrochemical properties.

Intermetallic Compounds. In aluminum alloys utilized in reactor engineering at temperatures up to 473 K the content of Fe, Ni, Cu is 0.5 to 1% each. These elements form with aluminum the intermetallic compounds, $FeAl_3$, for instance. The energy of its crystal lattice is:

$$E = - \Delta H = - (\Delta H_{FeAl_3} - H_{Fe} - 3H_{Al})$$
$$= 1456 \text{ kJ/mole} = 364 \text{ kJ/g-at,}$$

where $\Delta H_{FeAl_3} = - 112$ kJ/mole; $H_{Fe} = -405$ kJ/mole is the enthalpy in the atomic state; $H_{Al} = - 313$ kJ/mole, while the energy of the Al crystal lattice is $E_{Al} = 313.5$ kJ/mole.

According to the empirical dependence, the electronic work function $e\varphi$ and the energy of the lattice (kJ/mole) are interrelated as follows:

$$\Delta e\varphi = 2.4 \cdot 10^{-3} \Delta E.$$

As is evident from (5.30) through (5.36), the zero charge potential, $\varphi_{z.c.}$, and, hence, the overvoltage and the absolute rate of oxygen and hydrogen depolarization depend upon the electronic work function. In particular, the difference in overvoltage, $\Delta\eta$, of the reactions at the intermetallic compound and aluminum is:

$$\Delta\eta = - 2.4 \cdot 10^{-3} \Delta E = -2.4 \cdot 10^{-3} (364-313) = - 0.12 \text{ V.}$$

A decrease in the overvoltage and, consequently, an increase in the rate of the cathodic reactions raise the corrosion potential. If the alloy is in the active state, the rate of its corrosion increases. At 473 K and above, when the diffusion coefficient increases and, consequently, the protective oxide films grow at a faster rate, an increase in the corrosion potential facilitates the formation of the protective oxide layers. In fact alloying aluminum alloys with Fe, Ni, and Cu increases their corrosion resistance at high temperatures and decreases it at 363 K.

Solid Solutions. The energy of an alloy lattice may decrease by q_2 [see (3.24)] owing to the lattice deformation in producing *substitu-*

tional and *interstitial* solid solutions. This increases the rate of the anodic reaction in the active region. The alloying element atoms also change the energy of the crystal lattice.

At the same time, introducing into the alloy the element with a greater affinity for oxygen facilitates the alloy passivation. The radii of the iron and oxygen ions are equal to 0.08 and 0.14 nm, respectively. Therefore, oxygen can block only two atoms. In order that the characteristics of the passivating layer be changed essentially, one of the atoms must be that of the alloying element. In the crystallographic plane (100), $(1/8)\cdot 4 = 0.5$ atom is per unit cell of the BCC α-Fe. The plane (100) should contain 0.25 atom of the alloying element. A unit BCC cell has $(1/8)\cdot 8 + 1 = 2$. If the activity of an alloying atom is X, the following relation should be satisfied:

$$X\cdot 2 = 0.25.$$

Hence, $X = 0.125$, and the atomic content of the alloying element, at which the corrosion resistance of the alloy essentially rises, must be 12.5%. In fact, the so-called first threshold of corrosion resistance is obtained at the Cr content of steel equal to 13%. In the stainless steels containing 13-14% Cr, the Flade potential is close to the potential of pure Cr. At the 25% Cr content, the entire plane (100) consists of Cr atoms. Steels of grade X25 (containing 25% Cr) are known in practice.

In certain instances the surface condition of a metal may have an effect on its corrosion resistance. Polishing decreases the true area of the surface and thus lowers the corrosion losses referred to unit area. This manifests itself in the first hours of the medium-to-metal interaction. After a film of corrosion products has been formed on the metal surface, the preliminary surface treatment ceases to produce any effect. It should also be noted that production defects are more readily revealed on the surfaces of perfect finish (electrolytic polishing, for example).

5.7 Effect of Radiation on Corrosion

Changes in the electrochemical and corrosion characteristics of metals exposed to radiation mainly occur owing to radiolytical, radiation-electrochemical and destructive effects.

The *radiolytical effect* is accounted for by changes in the composition of a corrosive medium brought about by its radiolysis. The *radiation-electrochemical effect* is a result of increased energy of the atom surface layer following the radiation energy absorption, and the *destructive effect* is produced by changes in the structure (destruction, formation of microdefects) of the protective oxide film exposed to irradiation with high-energy particles.

Radiolytical Effect. The ionizing irradiation produces in an aerated chemically demineralized water oxygen, hydrogen peroxide and short-lived radicals. The concentration of stable products (O_2, H_2O_2) reaches 0.001 M. At room temperature an aerated water contains about 10 mg/l ($3.10 \cdot 10^{-4}$ M) of oxygen.

Perlitic steels corrode in an aerated water with diffusion control. At an increase in the concentration of oxidizers the corrosion accelerates $10^{-3}/(3.1 \cdot 10^{-4}) \approx 3.2$ times. At room temperature, irradiation at the neutron flux 10^{12} cm^{-2} s^{-1} increases the corrosion rate of steel 20 owing to the radiolytical effect 3 to 5 times. The radiolysis increases the oxygen content in the circuit water of boiling reactors to 0.3 mg/kg. Under the reactor core conditions stainless steels and zirconium alloys are in the passive state, and increasing the oxygen concentration only slightly affects their corrosion resistance. Steels of perlitic class at temperatures of the order of 573 K become coated with a phase protective oxide film. An increase in the oxygen content to 0.1-0.3 mg/kg has only little effect on their corrosion resistance.

Radiation-Electrochemical Effect. In the core of modern reactors, metal atoms, surface atoms including, receive energy of an order of 10^{-5} eV/(at s). In a deaerated chemically demineralized water at 573 K, perlitic steel at the bottom of pores in the oxide film is in the active state. The activation energy of the anodic reaction in the active state may be assumed as equal to 5 kcal/mole = 0.22 eV/at = = 20.9 kJ/mole. If even all the energy received by the surface atoms in the irradiation field is consumed to increase their energy, then an atom gets 0.22 eV/at in $\tau = 0.22/10^{-5} = 2.2 \cdot 10^4$ s.

A monolayer contains 10^{-8} moles in 1 cm^2. As a first approximation we may assume that all surface atoms take part in the anodic reaction at regular intervals of $2.2 \cdot 10^4$ s forming bivalent ions. The rate of the anodic reaction is:

$$i = 10^{-8} \cdot 10^5 \cdot 2/(2.2 \cdot 10^4) \approx 10^{-7} \text{ A cm}^{-2},$$

where 10^5 C mole^{-1} is the Faraday constant. This corresponds to the corrosion rate of $2.8 \cdot 10^{-2}$ g/(m^2 day). The area of pores is 1-3%, i.e. corrosion from the radiation-electrochemical effect should not increase by more than 10^{-3} g/(m^2 day). In a 10^4-hour test the rate of corrosion is close to 0.01 g/(m^2 day). Thus, the corrosion rate of perlitic steel may increase from the radiation-electrochemical effect by nearly 10%. In practice, the corrosion rate of perlitic steels exposed to irradiation may increase several times.

Destructive Effect. Irradiation produces defects in the protective oxide film formed on the metal surface.

At 573 K, the corrosion behavior of reactor materials in aqueous media is determined by the surface diffusion transfer of the metal and oxygen ions through the protective oxide film. As a first approximation, we may assume that the oxygen ions form a closed-packed lattice

in an oxide film. The radius of octahedral pores $r = 0.414\ r_0 = 0.414 \cdot 0.14 \approx 0.06$, where $r_0 = 0.14$ nm is the oxygen ion radius.

Irradiation distorts the crystal lattice. The oxygen ion occupies an octahedral void. Taking into account (3.47), the maximum lattice deformation is:

$\varepsilon = (r_0 - r)/2r_0 n = (0.14 - 0.06)/(2 \cdot 0.14 \cdot 3.6) \approx 0.08.$

The energy of the lattice distortion at $K \approx 10^{-3}$:

$Q = \varepsilon^2/K = 6.4 \cdot 10^{-3}/10^{-3} = 6.4$ kJ/mole.

The activation energy of diffusion reduces by this value. Hence, the ratio of the rate of the diffusion-controlled corrosion through the oxide film in irradiation and that without it is as follows:

$K_{ir}/K = 10^{(0.5 \cdot 6.4)/(19.1 \cdot 573 \cdot 10^{-3})} \approx 2.$

At temperatures close to 573 K, the corrosion rate of perlitic and stainless steels and zirconium alloys, i.e. the materials coated with an oxide film, increases 1.2 to 4.4 times when exposed to irradiation.

At a fluence of 10^{20}-10^{21} cm^{-2}, the number of radiation defects in stainless steel and thus the number of atoms having increased energy is considerable. This affects the dislocation motion and increases the liability of austenitic stainless steels to corrosion cracking.

6

Water Radiolysis

6.1 Nuclear Reactor Radiation

A nuclear reactor is a powerful source radiating neutrons, γ-quanta, β- and α-particles, and fission fragments. Radiation passing through a medium ionizes it and, hence, is called ionizing.

The off-system unit, electronvolt (eV), serves as the unit of the *ionizing radiation energy*. An electronvolt is the energy acquired by an electron in falling freely through a potential difference of one volt. Nuclear engineering extensively uses megaelectronvolt: $1 \text{ MeV} = 10^6 \text{ eV}$.

Gamma radiation is often characterized by the wave length. Wave length λ and the radiation energy E are related as follows:

$E = 12\ 400/\lambda.$

Radiation dose characterizes the field of radiation and determines its ionizing ability.

One should distinguish between the absorbed and the so-called exposure doses of radiation. The *exposure dose* is a measure of X- or gamma-radiation to which a body is exposed. It is equal to the total charge collected on ions of one sign produced in unit mass of dry air by all secondary electrons liberated in a volume element by incident photons stopped in that element. The unit is Coulomb per kilogram.

The *intensity of directional radiation* is taken to be the radiant energy passing in 1 s through 1 cm² of area perpendicular to the direction of flow. It is measured in watts meter^{-2} second^{-1}; the off-system unit is electronvolt centimeter^{-2} second^{-1}.

The measure of the intensity of neutrons is the neutron flux defined as the number of neutrons passing per second through one square centimeter of area normal to the direction of flow and integral (with respect to time) flux. They are measured in neutrons per square centimeter per second and neutrons per square centimeter, respectively.

The *absorbed dose* is the energy of ionizing radiation absorbed per unit mass of an irradiated medium. The unit is Joule per kilogram, or gray (Gy).

The ionizing radiation in the definition of the absorbed dose means that when electrons are absorbed by a medium we must take into account only losses by ionization and that portion of radiation losses that corresponds to braking radiation absorbed by the medium proper.

In absorbing neutrons, the ionization is produced not only by recoil nuclei, but also by the capture gamma rays.

Absorbed dose rate is the absorbed dose of radiation referred to a unit time. It is measured in watts per kilogram and gray per second.

Basic units of radioactivity and ionizing radiations are listed in Table 6.1.

Radiation-chemical yield is the basic quantitative characteristic of any reaction taking place under the ionizing radiation. It is designated by G. The radiation-chemical yield is the number of atoms, ions, radicals, or

Fig. 6.1 Concentration C of released hydrogen versus absorbed dose D in irradiating 1 N solution of sodium hydroxide saturated with nitrogen. Tangent to the curve (dashed line) determines starting radiation-chemical yield

molecules formed or decomposed after a chemical system has absorbed 100 eV of ionizing radiation. The subscript is the chemical formula of the corresponding substance. For example, G_{H_2} stands

TABLE 6.1 Conversion Factors

1 disintegration $s = 27.027 \cdot 10^{-12}$ Ci $= 10^{-6}$ Rd (rutherford) $= 1 Bq$ (becquerel)
 $1 erg = 10^{-7}$ J $= 6.24 \cdot 10^{5}$ MeV $= 6.24 \cdot 10^{11}$ eV
 $1 cal = 4.185 \cdot 10^{7}$ erg
 $1 eV = 1.602 \cdot 10^{-12}$ erg
 $1 C kg^{-1} = 3.87672 \cdot 10^{3}$ R (roentgen)
 $1 R = 257.976 \cdot 10^{-6}$ C kg^{-1}
 $1 R = 0.877$ rad in air $= 0.98$ rad in soft tissue $= 0.96$ rad in water (the energy of gamma-quanta ≈ 1 MeV)
 $= 2.08 \cdot 10^{9}$ pairs of ions in 1 cm^3 of air $= 1.61 \cdot 10^{12}$ pairs of ions in 1 g of dry air
 $1 A kg^{-1} = 3.87672 \cdot 10^{3}$ R s^{-1}
 $1 W m^{-2} = 10^{3}$ erg cm^{-2} s$^{-1} = 6.24 \cdot 10^{14}$ eV cm^{-2} s^{-1}
 $1 J kg^{-1} = 10^{4}$ erg g$^{-1} = 100$ rad
 $1 W kg^{-1} = 10^{4}$ erg g^{-1}s$^{-1} = 100$ rad s^{-1}

for the number of hydrogen molecules initially formed after the system has received 100 eV of radiation. This is the starting yield because it does not characterize the reaction in whole. The net radiation yield is designated as $G_{(H_2)}$ (the chemical formula is in the parentheses). If the formula is preceded by minus, this means that the given substance decomposes under irradiation. For example, $G_{(-H_2O)}$ shows the number of water molecules which decompose under 100 eV of radiation energy.

The radiation-chemical yield depends primarily on the type of nuclear reaction. In non-chain reactions the radiation yield is small, up to 10-15 molecules per 100 eV. In chain reactions, the yield may

reach hundred thousand molecules per 100 eV. In order to determine G, one has to know the absorbed dose and the concentration of formed or decomposed products. And vice versa, knowing the radiation yield and the absorbed dose, one can determine a change in the reactant concentrations. In practice, use is made of the kinetic curves illustrating the dependence of the reactant concentration on the absorbed dose. Used in calculations is the initial portion of the curve. If the very first experimental points deviate from linearity, G is calculated by a tangent to the experimental curve drawn from the origin of coordinates (Fig. 6.1). The values of G are given in Table 6.2.

TABLE 6.2 Radiolysis of Pure Water : Radiation Yield, Molecules/100 eV

Radiation	Initial LET value, eV/nm	Radiolysis products							
		H_2O	H_2	$H + \bar{e}_{aq}$	H	$\bar{e}_{aq}$	H_2O_2	HO_2	OH
β, γ	0.2	3.74	0.44	2.86	0.55	2.31	0.70	0.00	2.34
Fast neutrons	40.0	2.97	1.12	0.72	0.36	0.36	1.00	0.17	0.47
$^{10}B\,(n,\alpha)^7Li$	240.0	3.30	1.70	0.20	0.16*	0.04*	1.30	0.30	0.10

* Calculated values.

In nuclear chemistry, the absorbed dose is generally measured in electronvolts per milliliter or per gram, and the absorbed dose rate, in electronvolts per milliliter, or per gram, per second.

6.2 Interaction of Radiation with Matter

When passing through a medium the ionizing radiation gives it all its energy or part of it. Let us consider the interaction of electrons, heavy charged particles, electromagnetic radiation, and neutrons with matter.

Electrons interact with matter by several mechanisms which reduce the electron energy. These include: bremsstrahlung, inelastic and elastic collisions. At low energy of electrons elastic scattering, in which the kinetic energy is conserved and the direction of motion changes, gains essential importance.

Charged particles decelerated by a nucleus give off electromagnetic radiation (bremsstrahlung). A particle moving through a substance loses its energy. The rate of the energy loss per unit length of path in a matter is directly proportional to the particle mass. Therefore, energy losses in radiation are greater for light particles interacting with a substance having a large atomic number. Below 0.1 MeV radiation losses are inconsiderable. They, however, abruptly increase with the

energy and become prevalent within 10-100 MeV. If the braking radiation is not absorbed by the material it produces no essential changes in it. If the energy of electrons is so small that no bremsstrahlung arises, the energy of the particle is spent on elastic and inelastic collisions.

Elastic scattering prevails when low-energy electrons interact with a substance having a large atomic number. The electrons are repulsed by the electrostatic field of atomic nuclei (the Coulomb repulsion). The scattering is elastic, if the interaction of electron with atoms or molecules of the medium only increases the kinetic energy of the latter, and inelastic, if the potential energy of the atoms and molecules changes. In elastic scattering, the sum of the kinetic energy of electron and atom is the same after the scattering as before, and only the electron direction changes. The greatest deflection is observed when electrons come very close to the nucleus.

In *inelastic scattering*, the electron energy is lost as a result of its interaction with the atom electrons. This produces excitation and ionization of atoms and molecules. The greater the initial energy of electron the greater the probability of the atom excitation. If the energy of the excited atom is passed to a valent electron, the latter may be knocked out of its energy level and leaves the atom. The dislodged electron is able to cause ionization and make a secondary trajectory with a stronger ionization than in the initial, faster electron. The number of secondary electrons formed per unit length of trajectory increases with a decrease in the energy of the primary electron. In excitation an atom does not lose electrons; some electrons only jump to higher energy levels. Usually the energy of electrons consumed in ionization and excitation of atoms and molecules of a medium is referred to as the ionization loss. The total loss of electron energy is equal to the sum of ionization and radiation losses. Gradual deceleration of electrons in an absorbing medium depends mainly on their interaction with electrons of atoms.

The *penetrating power of electrons* depends first of all on their initial energy. The thickness of a layer of complete electron absorption is determined by the number of inelastic collisions of an electron and atom electrons in a unit volume, i.e. by the electron density of a substance. The absorption of electrons is described by the exponential relation:

$$I = I_0 \exp (-\mu d),$$

where I_0 is the intensity in the absence of absorber; I is the intensity after passing through a layer of absorber d (cm) thick; μ is the total coefficient of absorption, cm^{-1}.

The absorption coefficient shows a fraction of electrons absorbed on a unit length of path in a given medium. The absorption coefficient is proportional to the density ρ of the absorbing medium. Ratio

μ/ρ called the mass absorption coefficient is nearly constant for various substances. In this case

$$I = I_0 \exp \left(-\mu Q/\rho\right),$$

where Q is the thickness of the absorbing layer, g cm^{-2}.

The radiation intensity decreases to half its value when passing through a layer of a thickness:

$$x = \ln 2/\mu.$$

The relation between the thickness of the layer and the maximum energy of the β-spectrum, $E_{\max}$, is approximately expressed by the empirical relation

$$E_{\max} = x^{0.75}.$$

Heavy charged particles (protons, deutons, α-particles and the like) interact with matter like electrons do, i.e. lose energy in bremsstrahlung, elastic and inelastic collisions. The bremsstrahlung prevails only at very high energies, of the order of 1000 MeV, while elastic collisions play in this case only a minute role. In practice one has to take into consideration only inelastic collisions with the absorber electrons. Heavy particles lose far more energy than light particles on the same lengths of path in the absorbing medium. For example, the density of ions along an α-particle track is several hundred times that along a track of electrons having the same energy.

When γ-*radiation passes through* a medium the radiation intensity attenuates and the radiation energy converts into other forms of energy. Passing through a medium γ-quanta interact with electrons of atoms, nucleus, and field of electrical charges. The medium may absorb γ-quanta or scatter them elastically and inelastically. In the former case the energy of γ-quanta completely converts into other forms of energy. In elastic (coherent) scattering, only the direction of radiation changes without changing the energy of γ-quanta. Inelastic (Compton) scattering changes the direction of γ-quantum and partial absorption of its energy. γ-Radiation loses its energy because of the photoelectric effect, Compton scattering, and pair production.

γ-Quanta of low energy are absorbed by matter mainly owing to the *photoelectric interaction*. The energy of gamma photon, $h\nu$, goes to one of the atom electrons (Fig. 6.2a). The kinetic energy of this electron is

$$E = h\nu - j,$$

where j is the ionization potential of the initially occupied level. At low energy of γ-quantum, the photoelectron is ejected mainly perpendicularly to the starting direction of γ-quantum. The higher the energy of γ-quantum, the more the directions of photoelectron

and γ-quantum coincide. The photo-electron scatters its energy in ionization and bremsstrahlung.

γ-Quanta of higher energy knock out electrons from the levels most tightly bound to the atom, i.e. the K-shell electrons. If the energy of γ-quantum is greater than the binding energy of K-electrons, then 80% of photoelectrons are knocked out of the K shell. The remaining γ-quanta interact with the electrons of the L shell. Electrons from the outermost shells occupy the free sites in the K and L shells emitting characteristic X-rays. In elements with low atomic number, the binding energy of electrons in the inner shells is relatively small. For water it is of the order of 500 eV. Therefore, a secondary characteristic radiation with low energy is absorbed in the direct vicinity

Fig. 6.2 Kinds of gamma-electron interactions
a—photoelectric effect; b—Compton scattering; c—pair production

of the initial interaction. Photoelectric absorption markedly increases, if the energy of γ-quantum becomes greater than the binding energy of electrons in the K shell. Since the photoelectric effect obeys the law of conservation of energy and angular momentum, an atom which has lost an electron also receives a certain pulse (recoil atoms). Thus, free electrons are incapable of the photoelectric interaction.

In *Compton scattering* γ-quantum interacts either with an orbital or free electron. Compton scattering is observed when the energy of γ-quantum exceeds 0.01 MeV.

γ-Quantum gives part of its energy to an electron. As a result the electron is ejected from the atom and gains kinetic energy E equal to the difference between the energies of the initial and scattered γ-quanta (Fig. 6.2b). γ-Quantum changes the initial direction and becomes a secondary γ-quantum having a lower energy. Scattered γ-quanta interacting with the atom electrons lose their energy as they pass through matter, and their absorption usually ends in a photoelectric interaction.

The Compton electrons are characterized by a continuous energy spectrum ranging from minute to maximum values observed in the case when electrons are ejected in the direction of the primary γ-quantum. Thus, the energy loss of Compton scattering is equal to the energy carried away by electrons and scattered energy of secondary γ-quanta. When the energy of primary γ-quanta is equal to 1.6 MeV,

these values are about the same. At higher energy of γ-quanta, the energy carried away by electrons exceeds that lost in scattering. In water, Compton scattering is the most important absorption mechanism at an energy of primary γ-quanta within 0.03 to 20 MeV.

Pair production, i.e. the conversion of a gamma photon into a positron and an electron, takes place in the immediate vicinity of the atomic nucleus under the influence of its field. The energy of γ-quantum partially goes into the rest mass of the positron and electron $(2m_0c^2)$ and partially into the kinetic energy of the pair. No pairs can be produced when the energy of γ-quantum is below $2m_0c^2 = 1.02$ MeV. The produced positron is slowed down like an ordinary electron, or interacts with an electron (both particles annihilate) giving two γ-quanta having an energy of 0.51 MeV.

Interaction of Neutrons with Matter. Having no charge, neutrons do not ionize matter directly and interact only with nuclei. The medium can be ionized by the products of the neutron interaction with a nucleus: protons, heavy ions, γ-radiation. The neutron interaction with the atomic nucleus includes: elastic and inelastic scattering, radiative capture, nuclear reactions with emission of charged particles (protons, α-particles and the like), and nuclear fission. The nature of interaction depends primarily on the neutron energy. By the energy neutrons are generally divided into slow neutrons (with an energy of 0 to 1 keV, thermal neutrons, 0.025 eV, including), intermediate neutrons (1-100 keV), fast neutrons (100 keV-14 MeV), ultrafast neutrons ($>$14 MeV). It should be noted that the classification of neutrons by their energy is not strictly defined.

Elastic scattering is a most probable interaction for fast neutrons. It is also of importance for the interaction of intermediate neutrons with matter. When colliding with nuclei, the energy of neutrons is distributed among scattered neutrons and recoil nuclei according to the law of conservation of energy and angular momentum. The maximum energy that can be given by a neutron to a nucleus having an atomic weight A can be determined by the relation:

$$(\Delta E/E_0)_{\mathbf{max}} = 4A/(A + 1)^2$$

where ΔE is the given energy; E_0 is the neutron initial energy.

In the case of hydrogen ($A = 1$), all energy of a neutron may be given to a hydrogen atom. The resultant recoil proton ionizes and excites molecules of the scattering substance, say, water. In inelastic scattering, the neutron is absorbed by a nucleus and then reemitted but with a lower energy. For some time the nucleus remains excited and changes over to the basic state with releasing one or several gamma-quanta. Inelastic scattering is not observed, if the energy of neutrons is below the minimum energy of an excited nucleus, which is usually of the order of 100 keV. The probability of the process

rapidly increases with the energy of neutrons. At an energy of the order of 10 MeV, elastic and inelastic scattering are equally probable.

Nuclear capture is characteristic of slow neutrons. The capture produces an unstable nucleus which converts emitting gamma-quanta or charged particles. Examples of such reactions are: $H(n, \gamma)D$, $^{16}O(n, \gamma)$ ^{17}N, ^{10}B (n, α) ^{7}Li. Heavy elements undergo fission reactions. The fission products possess high energy and are able to ionize and excite the medium.

Particles of high energy ionize and excite the molecules along their path. An excited state arises when electrons in atoms or molecules receive extra energy and jump to higher levels. In ionization, atoms and molecules lose electrons, having received energy higher than in excitation.

The absorption of whatever radiation forms *tracks of excited and ionized particles*. Products of the radiation interaction with matter are mainly independent of the type and energy of radiation. All kinds of ionizing radiation produce chemical effects of the same quality. Radiations of different type and energy lose their energy in matter at a different rate, and the density of primary products in tracks depends on the type of radiation. The chemical effect depends on the density of primary products in tracks, particularly in liquids, where migration of primary products from the track is impeded by the surrounding molecules. In gases, primary products relatively easily leave tracks; therefore, the yields of the radiation-chemical reactions only slightly depend upon the type of radiation.

The electrons dislodged from atoms or molecules due to primary ionization can produce ionization and excitation if they possess enough energy. If the energy of the secondary electrons is less than 100 eV, their paths in liquids are small and the secondary ionization products are found very close to the primary products, forming the so-called spurs of excited and ionized atoms and molecules. Certain secondary electrons having enough energy may migrate over considerable distances from the place of their origin producing their own tracks branching from the primary tracks. These electrons are called β-rays. They account for about half of the ionization products at an electron energy above 100 eV.

A spur contains on the average 2-3 pairs of ions or molecules of water. If a particle possesses a high ionization density along its path (α-particle, for instance), spurs then recombine and form columns of ions and excited particles along the tracks (column ionization). For fast secondary electrons formed when water absorbs γ-radiation, the distance between spurs along the electron track is 10^3 nm and their initial diameter is about 2 nm. Decelerated electrons having an energy of about 0.025 eV are likely to directly neutralize a positive ion or to be captured by a neutral molecule to produce a negative ion which then neutralizes a positive ion.

Linear Energy Transfer (LET). It has been said above that the rate at which the ionizing particle loses energy when passing through a unit length of matter is characterized by the braking ability of the latter (dE/dx). In nuclear chemistry this is called the linear energy transfer (LET). It is measured in kiloelectronvolts per micrometer, or electronvolts per nanometer. When passing through a medium

TABLE 6.3 Initial Values of LET in Water for Various Kinds of Radiation

Radiation	Energy, MeV	LET, eV/nm
γ-radiation of ^{60}Co	1.25 (average)	0.200
Electrons	1 or 2	0.200
	0.48	0.207
	0.10	0.417
	50.00	0.670
β-radiation	0.046 (average)	0.700
X-rays	0.250 (maximum)	1.000
	0.010	2.000
Electrons	0.010	2.300
X-rays	0.008	2.800
β-radiation of tritium	0.0055 (average)	3.600
Deutons	20.000	4.500
Protons	10.000	4.670
	5.000	8.160
Deutons	8.000	10.000
	5.200	13.000
Protons	2.000	17.000
Helions	38.000	22.000
	32.000	225.000
Protons	1.000	30.000
	0.900	30.000
Helions	12.000	50.000
Protons	0.300	54.000
α-particles of ^{210}Po	5.300	88.000
Nuclear reaction products of Li (n, α)T	2.050 (α) and 2.730 (T)	100.000
α-particles	3.400	120.000
Nuclear reaction products of ^{10}B (n, α) ^{7}Li	1.500 (α) and 0.850 (Li)	170.000

charged particles gradually lose their energy. Therefore, LET varies along the particle track. This is particularly true of charged particles. Table 6.3 gives the initial values of LET in water subjected to ionizing radiation of different types.

6.3 Theory of Free Radicals

The radiolysis of water is best explained by the theory of free radicals. Ionizing radiation acting on water produces free radicals H$^{\cdot}$ and OH$^{\cdot}$:

$$H_2O \rightarrow H^{\cdot} + OH^{\cdot}. \qquad (6.1)$$
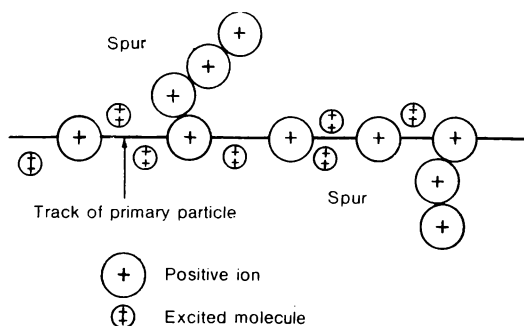
Fig. 6.3 Processes taking place in track of ionizing particle 10^{-18} to 10^{-16} s following its passage through water

These radicals arise as follows. An energetic particle ionizes a water molecule located near its trajectory:

$$H_2O \rightarrow H_2O^+ + e^-. \qquad (6.2)$$

Secondary electrons ionize several other water molecules. The resultant ions form spurs. Some other molecules of water located farther from the track become excited, because they receive energy not sufficient to produce the ionization. The processes are schematically shown in Fig. 6.3. There exist two hypotheses as to the further behavior of the secondary electron. According to Samuel and Maggi, the secondary electron loses its energy in inelastic collisions with water molecules, then returns and interacts with the parent ion which has been formed from a water molecule as a result of the electron loss. The formed neutral molecule of water is strongly excited (the excited state is marked with an asterisk) and decomposes into radicals:

$$H_2O^* \rightarrow H^{\cdot} + OH^-. \qquad (6.3)$$
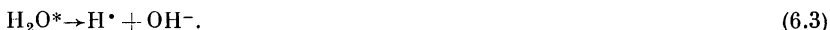
According to Lee and Gray, the secondary electron having lost its energy cannot add to the ion and solvates, somewhat removed from it, to produce the hydrogen radical:

$$e^- + H_2O \rightarrow H^{\cdot} + OH^-. \qquad (6.4)$$

The H_2O^+ ion dissociates forming $OH^{\cdot}$:

$$H_2O^+ \rightarrow H^+ + OH^{\cdot}. \qquad (6.5)$$

According to Samuel and Maggi, the radicals $H^{\cdot}$ and $OH^{\cdot}$ formed from an excited water molecule are close to each other, while Lee and Gray state that $OH^{\cdot}$ is near the track of the ionizing particle and $H^{\cdot}$ is at a certain distance from it. At present it is difficult to decide between two hypotheses.

The hydration of electrons ejected in ionization may cause the formation of the hydrated electrons e^-_{hydr}. The latter may be represented

as an electron surrounded by the oriented molecules of water. One of hydrogens of the H_2O molecule is directed towards the hydrated electron. The hydrated electron is a powerful reducing agent. The activation energy of reactions of the hydrated electron is small. The hydrated electron is extremely reactive: it reacts in a number of cases at each collision with a particle.

The ionization and radical formation proceed very quickly. Depending on the particle energy, the ionization takes 10^{-18} to 10^{-16} s. The ion is transformed into $OH^{\cdot}$ in 10^{-12} to 10^{-11} s. The secondary electron loses energy and is captured with subsequent formation of $H^{\cdot}$ in approximately the same time.

Radiolysis Products. The formed radicals $H^{\cdot}$ and $OH^{\cdot}$ recombine at sites of their high concentration:

$$H^{\cdot} + H^{\cdot} \rightarrow H_2; \tag{6.6}$$

$$OH^{\cdot} + OH^{\cdot} \rightarrow H_2O_2; \tag{6.7}$$

$$H^{\cdot} + OH \rightarrow H_2O. \tag{6.8}$$

It is these reactions that yield most molecular products H_2 and H_2O_2. It is not improbable, however, that a certain amount of H_2 and H_2O_2 is formed as a result of direct water decomposition, say, by the reaction:

$$H_2O + H_2O^* \rightarrow H_2 + H_2O_2. \tag{6.9}$$

The hydroperoxide radical $HO_2^{\cdot}$ may appear in spurs by the following reactions:

$$H_2O_2 + OH \rightarrow HO_2 + H_2O; \tag{6.10}$$

$$2OH \rightarrow HO_2 + H. \tag{6.11}$$
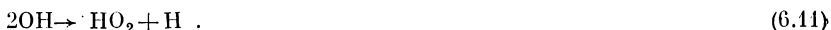
The probability of recombination with the formation of a water molecule from $H^{\cdot}$ and $OH^{\cdot}$ in the liquid phase is 0.1, while in the gaseous phase under 10 MPa, 10^{-3} only. Therefore, the recombination in steam and steam-and-water mixture is more sluggish than in water, and the radiolysis of water in a boiling system is greater than in the condensed. The maximum radiation yield of water decomposition in the gaseous phase, $G_{(-H_2O)_{max}}$ is equal to 12 molecules.

The initial yield of the water decomposition products G_H, G_{OH}, G_{H_2}, and $G_{H_2O_2}$ differs from the measured yields of $G_{(H_2)}$ and $G_{(H_2O)}$, as the radiolysis of water is accompanied by the recombination. Taking the radiation yields of primary products of radiolysis as the stoichiometric coefficients, the water decomposition may be represented as follows:

$$G_{(-H_2O)}H_2O \rightarrow G_{H_2}H_2 + G_{H_2O_2}H_2O_2 + G_H H^{\bullet} + G_{OH}OH^{\bullet} + G_{HO_2}HO_2^{\bullet}. \tag{6.12}$$
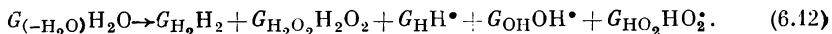
The yield of $HO_2^{\cdot}$ is very small and in most cases we may neglect its formation as a primary product. It should be noted that this radi-

cal easily forms when water contains oxygen:

$$H^{\cdot} + O_2 \rightarrow HO_2^{\cdot}. \tag{6.13}$$

Formulating a *material balance equation* one has to take into account the number of water molecules consumed to form one or another product of radiolysis. One molecule of water gives $H^{\cdot}$ and two molecules are needed to produce H_2. Therefore,

$$G_{(-H_2O)} = G_H + 2G_{H_2}.$$

Accordingly, one molecule of water is used to form the hydroxyl radical and two molecules, to form hydrogen peroxide:

$$G_{(-H_2O)} = G_{OH} + 2G_{H_2O_2}.$$

Inasmuch as one molecule of water produces both $H^{\cdot}$ and $OH^{\cdot}$, combining these equations we obtain a material balance equation widely used in the study of the kinetics of water radiolysis:

$$G_{-H_2O} = G_H + 2G_{H_2} = G_{OH} + 2G_{H_2O_2}. \tag{6.14}$$

Taking into account the formation of $HO_2^{\cdot}$ from $H^{\cdot}$ [see (6.13)] and from $OH^{\cdot}$ [see (6.11)] the material balance equation of water radiolysis takes the form:

$$G_{(-H_2O)} = G_H + 2G_{H_2} - G_{HO_2} = G_{OH} + 2G_{H_2O_2} + 2G_{HO_2}. \tag{6.15}$$

The products of water radiolysis, except for H_2, and, in particular, free short-lived radicals, are very reactive. The atomic hydrogen, as a rule, is a reducer. Its reducing capacity enhances with pH of the medium. In acid media, $H^{\cdot}$ may display the oxidizing properties. The radical $OH^{\cdot}$ possesses the oxidizing properties. At pH > 9, it dissociates by the reaction

$$OH^{\cdot} \rightarrow H^+ + O^-. \tag{6.16}$$

Molecular hydrogen, as a rule, does not react directly with the dissolved substances. It may, however, interact with $OH^{\cdot}$ by the reaction:

$$H_2 + OH^{\cdot} \rightarrow H^{\cdot} + H_2O. \tag{6.17}$$

The radical $HO_2^{\cdot}$ is able to dissociate into the following ions:

$${}^{\cdot}HO_2 \rightarrow H^+ + O_2^-. \tag{6.18}$$

This radical is a strong oxidizer.

When 0.5 M sulfuric acid aqueous solution is subjected to gamma-radiation of ^{60}Co, the yields of radiolysis products are as follows: $G_H = 3.65$, $G_{OH} = 2.95$, $G_{H_2} = 0.45$, $G_{H_2O_2} = 0.80$, and $G_{(-H_2O)} = 4.55$.

The theory of free radicals applies to solutions diluted so that the direct effect of radiation on the dissolved substance is negligibly small.

Interaction with dissolved substance. It is expected that any radical which has avoided recombination and diffused into the depth of solution, finally reacts with the dissolved substances even if its concentration is below 10^{-4} M. In the absence of the dissolved substance, the molecular products react with radicals:

$$H_2O_2 + {}^{\bullet}H \rightarrow OH^{\bullet} + H_2O. \qquad (6.19)$$

Therefore the concentration of a molecular product increases only to a certain constant value. The presence of the dissolved substance reacting with radicals prevents the molecular products from the reverse reactions. The concentration of the dissolved substance enough to completely suppress the reverse reactions depends on the nature of the substance and is 10^{-5} to 10^{-3} M.

For example, a bromide ion interacts with $OH^{\bullet}$ as follows:

$$Br^- + OH^{\bullet} \rightarrow Br + OH^- \qquad (6.20)$$

and thus suppresses (6.17). In radiolysis of thoroughly purified water, the concentration of resultant H_2 and H_2O_2 is very low. Radicals $H^{\bullet}$ and $OH^{\bullet}$ interact with molecular products H_2 and H_2O_2 reproducing water [(6.17) and (6.19)]. Therefore, the stationary concentrations of molecular products of radiolysis under gamma-radiation are 10^{-6} to 10^{-5} M. In the case of heavy charged particles, these concentrations are higher.

Now, let us consider the reactions with the participation of radicals in more detail:

$$H^{\bullet} + H_2 \rightarrow H_2 + H; \qquad (6.21)$$

$$H^{\bullet} + O_2 \rightarrow OH^{\bullet} + O. \qquad (6.22)$$

The kinetics of these reactions is studied only in gaseous media. Particles can interact only when they are at a distance from each other not exceeding the displacement in thermal vibrations, i.e. not greater than $l = 10^{-9}$ cm. If the particle radii (cm) are r_1 and r_2, the volume with two particles spaced at l is $V_0 \approx (r_1 + r_2)^3$.

As a first approximation, we may assume $r_1 + r_2 = 5 \cdot 10^{-8}$ cm. Then $V_0 \approx 10^{-22}$ cm^3. The concentration of particles in the medium is C_1 and C_2, mole/h. Volume V_0 contains the following number of molecules of substance *2*:

$$n_2 = V_0 C_2 N_A \cdot 10^{-3} = C_2 \cdot 10^{-22} \cdot 6 \cdot 10^{23} \cdot 10^{-3} = C_2 \cdot 6 \cdot 10^{-2},$$

where N_A is the Avogadro number.

The probability that a molecule of substance *1* encounters in volume V_0 a molecule of substance *2* in the process of thermal vibrations is as follows:

$$W = 1 \cdot n_2 = C_2 \cdot 6 \cdot 10^{-2}. \qquad (6.23)$$

For an interaction to take place, a molecule of substance *2* must move towards a molecule of substance *1*. The probability of this

event is

$$W_1 = 1/6 \approx 0.16.$$

The rate of the bimolecular reaction (mole l^{-1} s^{-1}) is:

$$v = C_1 \nu W W_1 \exp(-Q/RT) = C_1 \cdot 10^{13} \cdot C_2 \cdot 6 \cdot 10^{-2} \cdot 0.16 \exp(-Q/RT)$$
$$= C_1 C_2 \cdot 10^{11} \exp(-Q/RT), \tag{6.24}$$

where $\nu = 10^{13}$ s^{-1} is the frequency of thermal vibrations; Q is the activation energy.

In order that (6.21) takes place, the hydrogen molecules must dissociate. The activation energy of the hydrogen molecule dissociation is:

$$Q_{H_2} = 0.25 E_{bH_2} = 0.25 \cdot 434.8 = 108.7 \quad kJ/mole,$$

where E_{bH_2} is the bond energy in H_2.

From the law of conservation of momentum, the momentum of a hydrogen molecule after its collision with a hydrogen radical is:

$$p'_{H_2} = [m_{H_2}/(m_{H_2} + m_{H\cdot}] (p_{H\cdot} + p_{H_2}). \tag{6.25}$$

The energy of $H\cdot$ is

$$E_{H\cdot} = 217 \quad kJ/mole = 3.6 \cdot 10^{-12} \text{ erg/at} = 3.6 \cdot 10^{-19} \text{ J/at};$$

$$E_{H_2} = 1.5 \; kT = 6.2 \cdot 10^{-14} \text{ erg/at} = 6.2 \cdot 10^{-21} \text{ J/at}. \tag{6.26}$$

$$p_{H\cdot} = \sqrt{2 m_{H\cdot} \cdot E_{H\cdot}} = \sqrt{2 \cdot 1.6 \cdot 10^{-24} \cdot 3.6 \cdot 10^{-12}} = 3.4 \cdot 10^{-18};$$

$$p_{H_2} = \sqrt{2 \cdot 2 m_{H_2} E_{H_2}} = \sqrt{2 \cdot 2 \cdot 1.6 \cdot 10^{-24} \cdot 6.2 \cdot 10^{-14}} = 6.30 \cdot 10^{-19}. \tag{6.27}$$

From (6.25) through (6.27), we obtain:

$$p'_{H_2} = (2/3) \cdot (3.4 \cdot 10^{-18} + 6.3 \cdot 10^{-19}) = 2.7 \cdot 10^{-18}.$$

After a collision with $H\cdot$ the energy of the hydrogen molecule increases by:

$$E'_{H_2} = (p'_{H_2})^2/4m = (2.7 \cdot 10^{-18})^2/(4 \cdot 1.6 \cdot 10^{-24})$$
$$= 1.14 \cdot 10^{-19} \text{ erg/at} = 68.5 \quad kJ/mole.$$

The activation energy Q_{H_2} decreases by this value. The effective activation energy is

$$Q'_{H_2} = 108.7 - 68.5 = 40.2 \quad kJ/mole.$$

Reaction (6.22) usually occurs at a temperature of the order of 1000 K. In this case

$$E_{O_2} = 2.07 \cdot 10^{-20} \text{ J/mole}; \quad p_{O_2} = 4.6 \cdot 10^{-18} \text{ g cm s}^{-1}.$$

According to (6.25):

$$p'_{O_2} = 8.0 \cdot 10^{-18} \text{ g cm s}^{-1}.$$

The energy received by a water molecule after collision $E'_{O_2} =$ $= 37.6$ kJ/mole.

The activation energy of the oxygen molecule dissociation equal to 123.3 kJ/mole decreases by this value. Hence, the effective activation energy of the reaction is 85.4 kJ/mole.

The rate of the reaction may be represented as follows:

$$v = C_1 C_2 A \exp(-Q/RT).$$

The calculated and experimental values of the pre-exponential factor A and activation energy Q are in good accord (Table 6.4).

TABLE 6.4 Calculated and Experimental Values of A and Q, kJ/mole

Reaction	A		Q	
	Calculated	Experimental	Calculated	Experimental
$H^{\bullet} + H_2 \to H_2 + H$	10^{11}	$5 \cdot 10^{12}$	40.2	35.6
$H^{\bullet} + O_2 \to OH^{\bullet} + O$	10^{11}	$2.5 \cdot 10^{12}$	85.4	75.2

The radiolysis of pure water yields, in addition to H_2 and H_2O_2, oxygen in minute concentrations. Its occurrence is associated with the formation of $^{\bullet}HO_2$ by (6.10) and its subsequent interaction with the radical and molecular products of radiolysis:

$OH^{\bullet} + {}^{\bullet}HO_2 \to H_2O + O_2;$

$H_2O_2 + {}^{\bullet}HO_2 \to H_2O + {}^{\bullet}OH + O_2;$

$^{\bullet}HO_2 + {}^{\bullet}HO_2 \to H_2O_2 + O_2.$
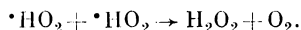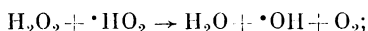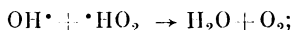
Inasmuch as the molecular products are initially formed as a result of the radical recombination, the stationary concentrations of H_2 and H_2O_2 are obviously proportional to the square root of the dose rate. The presence of oxygen in water exposed to irradiation affects the stationary concentration of hydrogen peroxide. The oxygen protects the peroxide against reacting with $H^{\bullet}$. Interacting with $H^{\bullet}$ by (6.13), the oxygen forms hydroperoxide radicals $HO_2^{\bullet}$. These interacting with each other by (6.23) form H_2O_2. Thus, at a dose rate of $5 \cdot 10^{20}$ eV ml^{-1} s^{-1}, 0.5 and 9.0 μM of hydrogen peroxide form respectively in deaerated and oxygen-saturated water. If in a deaerated water 0.5 μM is already a stationary concentration, in an oxygen-saturated water the peroxide concentration is proportional to the dose rate.

When water is hydrogen-saturated, the peroxide does not form, as it is immediately decomposed by $H^{\bullet}$ according to (6.19). The radicals $H^{\bullet}$ are produced in water radiolysis (6.1) and in (6.17). Molecular hydrogen in circuit I accumulates owing to radiolysis and corro-

sion with hydrogen depolarization. This suppresses the further radio-
lysis of water when hydrogen concentration reaches a stationary
value of 5 cm³l $^{-1}$. The water must naturally be deaerated before filling
the circuit. When otherwise, the presence of oxygen augments the
radiolysis and formation of hydrogen peroxide. The radiochemical
reactions with the participation of nitrogen produce the nitrate ion,
and (6.5) and dissociation of hydrogen peroxide

$H_2O_2 \rightarrow HO_2^- + H^+$

acidify the medium to pH $= 3$ to 4. This is known as an acid well.
Therefore, the deaeration of circuit I water is absolutely imperative.

Temperature enhances the recombination. Therefore, the water
radiolysis decelerates with temperature.

6.4 Radiolysis in Nuclear Reactors

In *pressurized water reactors*, PWR, a high temperature (and hence
a considerable rate of recombination) and also accumulation of
hydrogen prevent water radiolysis. No oxygen is detected in circuit
I in water having electrical conductivity of 10^{-1} µS cm^{-1} at H_2
concentration of 25 to 50 cm³/kg. If oxygen finds its way to circuit
I with feed water, it is consumed in the reaction with H_2 and in
corrosion. Within 12 minutes oxygen concentration drops to half its
initial value. To reduce the rate of steel corrosion, ammonia is added
(in doses) to water in circuit I of water-cooled and moderated power
reactors. It is also a source of hydrogen.

Boric acid is added to the primary circuit of a water-cooled and
moderated power reactor for mild control. Alpha-particles having
an energy of 0.49 MeV and gamma-rays having an energy of 2.3 MeV
resulting from ^{10}B (n, α) ^7Li enhance the radiolysis.

If circuit I contains excess oxygen it combines with H_2 and N_2
dissolved in water to produce HNO_3. The pH may drop to 3.5. This
is the so-called acid well. In certain cases pH is decreased by mete-
ring out oxygen into the circuit water. Therefore, neither air, nor
nitrogen are inert under irradiation. Promising is the use of inert
gases He, Ne, Ar, Kr, Xe in the volume compensators. They, however,
except for helium and neon, produce radioisotopes in a radiation
field. Xenon has about 15 radioisotopes having a half-life from 1 s to
36.4 days; argon has 3 radioisotopes with a half-life from 109 min to
265 years. Krypton also has long-lived isotopes. Helium and neon
produce no isotopes, but they are expensive. Besides, helium is of
high fluidity and it is difficult to keep it in the circuit at high pres-
sures. Therefore, the best gas for volume compensators used in pres-
surized water circuits allowing pH of water to be increased is nitrogen.

Oxygen is usually removed from the circuit water by thermal deae-
ration. Remaining oxygen combines with hydrazine. As this happens,

gaseous nitrogen remains in the water. Another source of nitrogen may
be a gas volume compensator filled with nitrogen. Nitrogen from the
volume compensators is transferred to the primary circuit mainly
through the transfer of nitrogen-saturated water at high pressure due
to a change in the coolant volume when the temperature varies and
insignificantly through diffusion.

Ammonia is synthesized in water from nitrogen and hydrogen in
the reactor operation. The rate of ammonia formation is proportional
to the reactor capacity and concentration of nitrogen in water, but
is practically independent of the hydrogen concentration. Ammonia
decomposes in the core zone. When a reactor operates for a long period
of time, the equilibrium establishes between the synthesis and
decomposition at pH of 8 to 9. The ammonia synthesis takes place
in the absence of oxygen in the coolant.

In *boiling single-circuit reactors* the radiolysis proceeds more vigo-
rously than in pressurized water reactors. As mentioned before,
recombination is more sluggish in the steam phase than in the con-
densed phase. Moreover, in compliance with the water-and-steam
distribution ratio, the radiolytic hydrogen goes mainly to steam and
is discharged from the system through the condenser ejector. Hydro-
gen does not accumulate in the system. The hydrogen content in the
feedwater is 0.02 ml/kg and at the inlet to the reactor, 0.02 ml/kg.
Therefore, intensive water radiolysis takes place in the core zone of
a vessel-type BWR and the oxygen concentration in the circulating
water is 0.03 to 0.3 mg/kg, in the water-and-steam mixture, 6 to
10 mg/kg, and in steam, 30 to 40 mg/kg. Inasmuch as the circulation
water is not deaerated, the presence of oxygen in it enhances the
radiolysis. The rate of water decomposition in a BWR is 2.5 to
3.5 mole MW^{-1} h^{-1}. The radiolytic gas contains 30% of oxygen,
60% of hydrogen, and 10% of inert gases. The yield of oxygen depends
on the power reactor:

Specific power,
    kW/l of core zone   7   27   50
Yield of oxygen,
    l of O_2 MW^{-1} h^{-1} 9   11   14

The yield of oxygen is close to 30-50 l MW^{-1} h^{-1}. The content of
hydrogen and oxygen in the saturated steam is 36 and 18 l/kg of
steam, respectively. Note that the intensity of radiolysis and, hence,
the oxygen content in water depend on the BWR type. In a vessel-
type BWR, water serves as both the coolant and the moderator.
The radiation energy the water receives is obviously greater than in
a channel-type BWR where graphite is the moderator.

The relative release of radiation energy in the coolant (a fraction
of the reactor total power) in BWRs of different types varies within

a wide range. In vessel-type BWRs up to 1.6-2% of the reactor total power may be liberated in the coolant. About 0.2% of the power capacity of the evaporating channels is released in the coolant in the Beloyarsk atomic power plant named after I.V. Kurchatov and not more than 0.01% of the power capacity of the steam reheating channels is given off to the steam cooling these channels.

In a *channel-type* graphite-moderated reactor equipped with rod-type fuel elements the energy given to the coolant is about 0.6% of the capacity.

The rate of oxygen formation in a vessel-type reactor is higher ($0.4 \text{ l MW}^{-1} \text{ min}^{-1}$) for the BK-50 series reactor than in a channel-type reactor ($0.1 \text{ l MW}^{-1} \text{ min}^{-1}$) for unit II of the Beloyarsk APS and $0.23 \text{ l MW}^{-1} \text{ min}^{-1}$ for the RBMK series reactor.

The oxygen concentration in steam generated by nuclear power plants furnished with vessel-type reactors may reach 25 to 35 mg/kg. In channel-type reactors the concentration is 5 to 15 mg/kg. In nuclear steam superheating, the concentration of radiolytic gases does not increase. Therefore, the oxygen content of water in a channel-type water-cooled graphite-moderated reactor is lower than in a vessel-type reactor and is 0.1 mg/kg. The content of H_2O_2 is 30 mg/kg in operation and 1.5 mg/kg in shut-down.

The radiolysis in a single-circuit boiling water reactor may be suppressed by continuous metering-out of hydrogen or ammonia into the coolant. Thus, injection of hydrogen in an amount of 160 ml/l into the feed water reduces the oxygen content in steam to 1/8-1/10 th of its former value. A further increase in the hydrogen content to 3 000 ml/l has practically no effect on the oxygen concentration in steam. Continuous adding of hydrogen requires its considerable flow-rate and is economically objectionable.

Increasing pH of reactor water to 8 on account of ammonia injection decreases the oxygen content in steam by a factor of 3 to 5. With a channel-type reactor, the oxygen content in steam is 5 to 6 mg/kg. The oxygen yield is $6.2 \text{ l MW}^{-1} \text{ h}^{-1}$. The degree of ammonia decomposition per 1 MW of reactor power lies within 8.5 to 9%. Nitrates and nitrites 0.05 g/h form per 1 MW of reactor power. Their content in the reactor water reaches 0.1 mg/l. To fully suppress the radiolysis in a BWR, the ammonia content in water should be not less than 10 mg/kg. The ammonia supply to compensate for its losses should be 4% of the amount required to suppress the radiolysis.

It should be remembered that the injection of ammonia in such an amount into the water of a boiling reactor requires that the pipe assemblies of condensers and heaters be made of stainless steel. When pipe assemblies are made of copper alloys, their corrosion rate is high. Moreover, the presence of copper in water intensifies the scale formation. This is particularly detrimental to the fuel elements.

Zinc being a product of brass corrosion, increases the activity of coolant and equipment.

In *pool research reactors* having power of up to 18 MW, the content of radiolytic hydrogen in water does not exceed 4.5 ml/kg and that of hydrogen peroxide, 10 mg/kg. The volume concentration of hydrogen in air volumes of the reactor is below 1%, the explosive concentration being 4%. The hydrogen content in water is independent of power at its high values. This is associated with that an increase in the water-absorbed dose increases the specific density of radicals and, consequently, the intensity of recombination. Increasing the temperature by one degree similarly decreases the hydrogen concentration by 0.03 ml/kg. The concentration of hydrogen peroxide varies only slightly at temperatures up to 323 K and abruptly drops because of its decomposition at above 323 K. The concentration of dissolved hydrogen is practically independent of the water flow velocity in the core zone. The experience gained in operation of pool-type reactors with power up to 18 MW has confirmed the possibility of the long-term operation without degassing systems. In cases of necessity, however, the explosive mixture is burnt: oxygen catalytically interacts with hydrogen to form water. Gas-and-air mixture is explosive within 3.3 to 81.5%. The lower limit of the volume content of explosive mixture with steam depends on pressure and is 33 and 16%, respectively, for pressures of 0.005 and 0.1-3 MPa.

When the coolant enters the core in an emergency, the radiolytic hydrogen forms. In the analysis of emergency situations involving the loss of coolant, due consideration should be given to that hydrogen may be produced in the reactor building in explosive concentrations.

7.1 Physical and Mechanical Properties of Uranium

Physical Properties. Uranium is a chemical element, atomic number 92. Uranium in nature is a mixture of three isotopes: ^{238}U, ^{235}U, and ^{234}U. The natural occurrence of the latter two isotopes is 0.7 and 0.005%, respectively. All natural isotopes of uranium emit α-particles having an energy of 4.21-4.76 MeV. Half-lives of the isotopes are $2.44 \cdot 10^5$ y for ^{234}U, $6.85 \cdot 10^8$ y for ^{235}U, and $4.5 \cdot 10^9$ y for ^{238}U. A number of man-made isotopes of uranium are known.

Uranium exists in three allotropic modifications: low-temperature α-modification, β- and γ-modifications. The crystal structure of uranium in all modifications and the critical temperature of conversions are given in Table 7.1. Fig. 7.1 gives the arrangement of atoms in the lattice of α-uranium. The lattice of α-uranium contains corrugated layers of uranium atoms parallel to plane (010). The coordination number for α-uranium is 12. Four atoms, however, lie at lower dis-
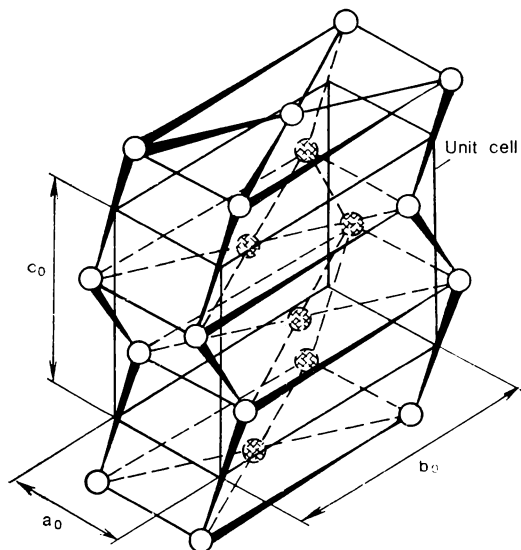
Fig. 7.1 Crystal lattice of α-uranium

TABLE 7.1 Physical Properties of Uranium

Atomic number	92
Atomic weight	238.03
Density, g/cm³	19.05
Melting point, K	1402-1403
Specific heat at 298 K, kJ mole⁻¹ deg⁻¹	27.6
Boiling point, K	4086
Electrical resistivity at 298 K, μΩ cm	30
Crystal structure	α-phase is orthorhombic up to 940.7±1.3 K; β-phase is tetragonal up to 1047.8 ±1.6 K γ-phase BCC above 1049 K
Parameters of lattice, nm	α-phase: $a = 0.2852$ $b = 0.5865$ $c = 0.4955$ β-phase: $a = 1.0759$ $c = 0.5656$ γ-phase: $a = 0.3524$
Coefficient of linear expansion within 293-773 K along crystallographic axes, 10⁻⁶ deg⁻¹	$a = 39.2$ $b = -6.3$ $c = 27.6$

tances than the other. The atoms are spaced at 0.28539 and 0.27544 nm within the layer. The distances between the atoms lying in different layers are 0.32631 and 0.33423 nm. The interatomic forces decrease with an increase in the interatomic distance. Therefore, the interatomic forces within the layer are stronger than those between the layers.

TABLE 7.2 Strength and Ductility of Uranium in Tensile Tests at Room Temperature

Machining	$\sigma_{0.2}$, MPa	σ_u, MPa	δ, %
Casting	190-280	380-480	4-6
γ-Hot rolling with quick cooling	250	400	⩾ 5
γ-Annealing (after α-rolling)	180	390	5
Quenching from γ-region (after casting)	460	600	4
Quenching from β-region (after α-rolling)	250	580	9
Quenching from β-region (after casting)	460	580	4
α-Rolling (at 773 K with 25% reduction)	540	630	9
α-Rolling (at 773 K with 50% reduction)	600	710	7
Rolling at 573 K with 28% reduction (total content of impurity < 0.05% by mass)	—	980	35
α-Rolling and annealing at 823 K	220	620	12
α-Rolling at 773 K with 50% reduction and annealing at 873 K	430	600	7
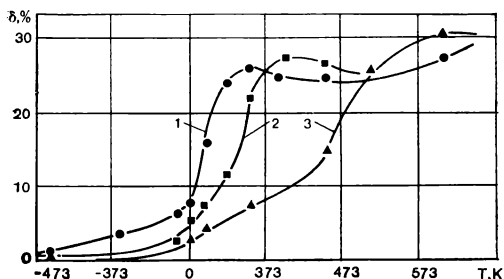
Fig. 7.2 Effect of small iron and aluminum additives on temperature of transition from brittle to ductile state for uranium annealed in β-region

1—0.005% Fe, 0.006% Al, grain size 0.45 mm; *2*—0.05% Fe, 0.025% Al, grain size 0.30 mm; *3*—0.1% Fe, 0.02% Al, grain size 0.12 mm
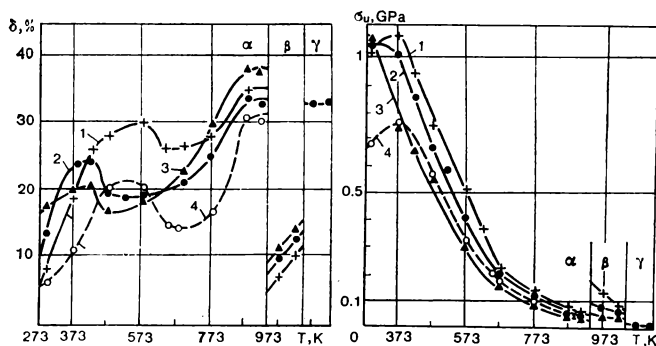
Fig. 7.3 Effect of temperature on mechanical properties of uranium

1—grain size $d = 20$ μm, deformation rate $v_{def} = 1$ cm/min; *2*—$d = 20$ μm, $v_{def} = 0.1$ cm/min; *3*—$d = 20$ μm, $v_{def} = 0.003$ cm/min; *4*—$d = 130$ μm, $v_{def} = 0.1$ cm/min

Table 7.1 covers also the physical properties of uranium. The properties of uranium to a considerable extent depend on its purity. A low symmetry of the rhombic lattice of α-uranium produces anisotropy of its physical and mechanical properties.

Mechanical Characteristics. A pure monocrystal of α-uranium is highly ductile. Commercial uranium is not too ductile but rather hard and brittle. Uranium machining proceeds with certain difficulties. The grain orientation determined by the item fabrication and thermal treatment materially affects its mechanical characteristics.

Even minute variations in the content of nonmetallic impurities affect the mechanical properties of uranium. Uranium is strongly strain-hardened. This interferes with its machining by cutting. Its mechanical properties essentially depend on temperature and thermal treatment (Table 7.2). Within 373 to 77 K, the ductility of ura-
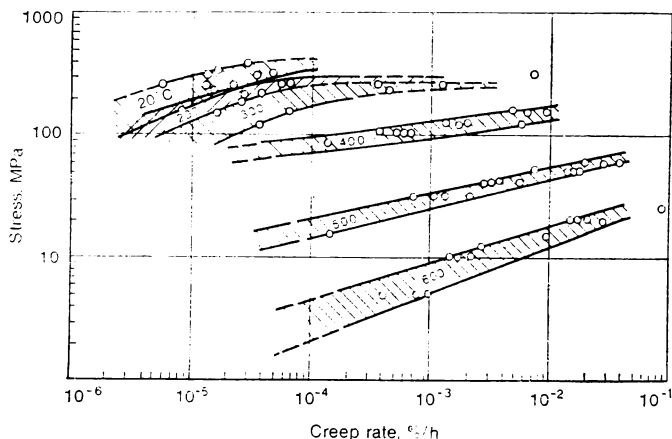
Fig. 7.4 Stress versus creep rate of hot-rolled uranium

nium abruptly drops with a decrease in the testing temperature
(Fig. 7.2). Concurrently its ultimate strength decreases. Uranium
becomes brittle. The critical point depends on the content of impu-
rities, grain size and the like. The uranium ductility at room tempe-
rature may be increased by vacuum annealing. The best results are
obtained by 24-h annealing at 623 to 673 K. With an increase in
temperature, the uranium strength decreases and its ductility rises
(Fig. 7.3). With coarse grains the ductility and ultimate strength
are lower.

Figure 7.4 illustrates the uranium creep rate. When the tempera-
ture exceeds the lowest temperature of recrystallization (643-703 K)
the uranium creep rate abruptly increases. Quenching from tempera-
tures of β- and γ-phases increases the resistance to creep at a tempe-
rature below 673 K, but decreases it at higher temperatures. When
temperature varies cyclically, the rate of creep increases. This should
be attributed to the internal stresses arizing from the anisotropy
of thermal expansion of α-uranium in temperature change. The inter-
nal stresses increase to the yield point and cause plastic deformation
of grains. The uranium ultimate strength in fatigue tests depends on
the metal purity and machining and is of 100-280 MPa at room tem-
perature.

Thermal cycles (regular variations in temperature) change the
size of uranium items. The highest rate of growth (increase in the
item length) of uranium is noticed at the greatest difference between
the temperatures of thermal cycle (the greatest effect is produced by
the upper temperature), low rate of heating, and high rate of cooling.
As the temperature changes within the thermal cycle, items of

polycrystalline uranium somewhat swell (their density decreases),
the surface becomes rough and even cracks.

The uranium growth in thermal cycles is associated with that in two
adjacent differently oriented grains having different coefficients of
thermal expansion in a certain direction, heating produces internal
stresses. They after reaching a certain value relax by slip or twinning
at a lower temperature and by flow along the grain boundary at a
higher temperature. The interaction between the grains generates
plastic deformation accumulating with the number of cycles.

The mechanism of uranium growth in thermal cycles with phase
transitions is different. The uranium grows owing to differences in
density and strength of crystalline modifications of uranium. The α-
β-and β-γ-transformations increase the volume by about 1%. This
generates internal stresses exceeding the yield point of all uranium
modifications at the boundary between the phases. Plastic deforma-
tion of less strong α- and β-phases changes the uranium shape.

7.2 Radiation Growth of Uranium

Irradiation changes the shape and size of items made of uranium.
Below 673 K, these phenomena are accounted for by the radiation
growth of uranium. In fine-grained polycrystalline uranium, a low
burnup makes the item surface rough. The so-called orange peel effect
takes place. In coarse-grained uranium high burnup increases surface
irregularities, ridges and dents form. This is known as "chewed
surface". At the same time items may deform, e.g rods of uranium.

The examination of an irradiated monocrystal of uranium has
revealed the elongation in direction [010] and reduction along axis
[100] (in direction [001] the monocrystal does not change). Changes
in dimensions are expressed through the radiation growth coefficient,
G_i, the non-dimensional value which is the elongation at a small
change in length referred to the burnup: $G_i =$ the length change,
%/burnup, %.

In a more general case, the radiation growth coefficient is expressed
as follows:

$$G_i = \ln (l/l_0)/(\Delta m/m),$$

where l and l_0 are the final and starting lengths; Δm is the number of
atoms which underwent fission of the total number of atoms m.

The radiation growth coefficient of a uranium crystal irradiated
at 373 K is $+420 \pm 20$, -420 ± 20, and 0 ± 20 for directions [010],
[100] and [001], respectively.

The behavior of a polycrystalline uranium exposed to irradiation
essentially depends on the grain size, perfection of grain structure,
and nature of texture. With an increase in the degree of cold defor-
mation, the radiation growth coefficient increases. With a rise in
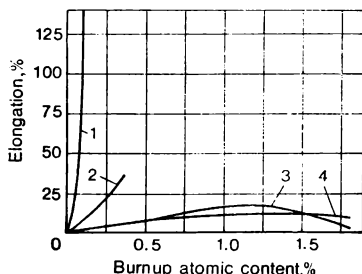
Fig. 7.5 Changes in length of uranium specimens versus burnup
1—rolling at 573 K; 2—at 773 K; 3—at 573 K (hardening from γ-phase); 4—at 573 K (hardening from β-phase and recrystallization)

temperature of α-rolling, it decreases. Quenching from the β-region to a considerable extent approaches the structure to the quasi-isotropic. Thus, for uranium rolled at 573 K and irradiated to 0.5% burnup, G is 690. After quenching from the β-phase, G for the same metal is equal to 25. Fig. 7.5 shows changes in the length of uranium specimens after thermal treatment against the burnup.

A change in the uranium shape in radiation growth may be represented as the transfer of atoms from plane (100) to plane (010). The transfer must proceed either by migration of individual atoms or by their cooperative motion. Several theories have been proposed to explain the radiation growth of uranium.

The *thermomechanical theory* attributes the uranium growth to thermal spikes arising in fission and to the anisotropy of the plastic properties of α-uranium. In uranium that fissions, local regions 4 to 8 nm in diameter have temperatures of several thousand degrees during 10^{-10} to 10^{-11} s. Within the thermal spike region, the metal should expand, which is hindered by the surrounding cold metal. This produces homogeneous compressive stresses causing local plastic deformation by twinning in direction [010].

The *Cottrell theory* bases on the anisotropy of the uranium growth coefficient and in its essence is nothing more than the above-mentioned thermomechanical theory. When a local field of stresses arises in the thermal spike zone due to the anisotropy of the thermal expansion coefficient, part of the atoms move from planes (100) and (001) to plane (010). A new layer of atoms appears along axis [010]. It should be kept in mind that the spike volume cannot increase as the cold part of the crystal surrounding it prevents this. Therefore, the local plastic deformation involves the displacement of atoms.

When the metal having an ideal lattice is cooled in the spike zone, the process progresses in the reverse direction, and no radiation growth takes place. If spikes occur on the line of edge dislocation, the

reverse process does not take place. Then dislocation loops form in plane (010). They lead to the growth in direction [010], and the extra planes forming dislocations with the Burgers vector in plane [100] annihilate in the fission peak. This reduces the dimension along axis [100].

The *theory of correlative impact processes* bases on that the regular arrangement of atoms in the uranium lattice makes impact processes (energy transfer to the lattice atoms from fast neutrons and fission fragments) correlative, i.e. they depend in a certain manner on the impact energy and direction, and also on the mechanism of atom-to-atom energy transfer in the chain of uranium atoms. A rough model of the process may be represented by a billiard ball striking a "triangle", i.e. a triangular close-packed group of balls. Recoiled at an angle to the impact direction is an outer ball of the triangle rather than that which has been struck. Therefore, an impact may be transmitted along a chain of atoms in directions [100] and [010]. Atoms are closely packed in direction [100]. With each new impact in the atomic row in direction [100], the angle between the impact direction and the atomic row becomes less and focusing takes place. With such a focusing impact, the energy imparted to the last atom of the chain is enough to knock it out of the lattice. The displaced atom gets to the boundary of an adjacent grain, subgrain boundary, or dislocation. The atom reaches the zone of a lattice defect and leaves the atomic chain. As a result, the atomic row loses an atom and the length decreases. The calculations show that focusing of displaced atoms takes place in the close-packing direction [100].

The situation differs when an impact is produced in direction [010]. The packing in this row is loose. As a result, a reverse effect takes place, a crowdion forms instead of focusing. The angle between the impact direction and the atomic row increases with each impact. Finally collisions of a chain atom with surrounding atoms result either in knocking atoms out of the row outside a given grain and transforming them into interstitial atoms, or, what is more probable, the crowdion process is retained at the grain boundary, and no atom goes outside the grain. The atoms accumulated at the boundary form a new corrugated layer in direction [010], which causes radiation growth of uranium in this direction.

As it follows from the analysis of the α-uranium crystal lattice, the third direction [001] entirely lacks the close-packed chains of atoms. Energetic particles cannot give off their energy through correlative dynamic processes, like the formation of focusons or crowdions. The result is that the dimensions in this direction do not change.

The *diffusion theory* is based on the anisotropic diffusion of vacancies and interstitials. Irradiation with fast neutrons having an energy of 1 to 2 MeV and fission fragments with an energy about 100 MeV produces in uranium up to 10^{18} to 10^{19} point defects (vacancies and

interstitials) per second. Burnup of 0.07% of the total number of atoms makes each atom of natural uranium displace from its position 17 times. About 98% of displaced atoms recombine with vacancies and occupy sites in the lattice nodes, and 1% of displaced atoms are absorbed by dislocations. The remaining atoms and vacancies migrate to the boundaries of grains and subgrains. In an anisotropic diffusion, displaced atoms form additional planes. This increases dimensions in one direction. Vacancies are subtracted from the lattice, thus causing shrinkage in other direction.

The coefficients of vacancy diffusion in directions [100], [010], and [001] are in the ratio 1 : 0 : 0.8, while the diffusion of displaced atoms in these directions is practically isotropic (0.9 : 0.9 : 1). Therefore, the fluxes of vacancies and displaced atoms in these directions are inhomogeneous. Only displaced atoms diffuse in direction [010]. Therefore, the dimensions increase in this direction. Diffusing in direction [100] are predominantly vacancies, for which reason shrinkage takes place in this direction. It should be noted that neither theory explains all the experimental facts.

The *Buckley theory* provides the best agreement with the experimental data. According to Buckley, the radiation growth is accounted for by the formation of far spaced groups of vacancies and displaced atoms in the field of elastic stresses of fission peaks. Displaced atoms are far spaced from a fission peak owing to focusing collisions and crowdions. Stresses resulting from heating in a thermal spike favor the condensation of displaced atoms and vacancies at different atomic planes. The elongation arising from flat aggregations of displaced atoms in plane (010) proceeds in the direction of the lowest thermal expansion. The shrinkage in the direction of the greatest thermal expansion should be attributed to the aggregation of vacancies in plane (100). This is facilitated by a small Burgers vector in direction [100]. The Burgers vector in direction [001] is greater. Therefore, no flat aggregates generate in plane (001), though elastic stresses favor their formation.

Flat aggregates of displaced atoms and vacancies are limited by dislocations loops. The number of survived displaced atoms depends on the radiation temperature and dislocation structure of uranium. Focusing impacts and crowdions move the atoms in direction [110] considerably away from the fission peak, propagating in other directions in the lattice only by several interatomic distances. In a perfect crystal lattice formation of complexes must be homogeneous. In irradiation, the probability of homogeneous formation is small and most displaced atoms annihilate at flat aggregates of vacancies. The resulting growth is small. As the dose of radiation increases, the probability of homogeneous nucleation of displaced atom aggregates increases, the probability of annihilation decreases, and the coefficient of growth rises. Polycrystalline specimens and imper-

fect monocrystals probably contain enough dislocations to catch most migrating displaced atoms. Therefore, the growth rate is very high up to the moment the number of vacancy complexes is such that is able to screen the dislocation sinks. Then, the growth rate decreases to a constant value.

7.3 Gas Swelling

Gas swelling is the change in the uranium geometry with a large decrease in density. In case of radiation growth the density change is the lowest. The rate of radiation growth reaches its maximum at 473 K, decreases with further increase in temperature, and becomes equal to zero at 733-773 K. Gas swelling occurs at a temperature above 623 to 773 K. The radiation growth and swelling may overlap, i.e. the growth may still continue at the lower temperature of gas swelling.

Gas swelling is accounted for by gas bubbles filled with fission fragments, mainly gaseous xenon and krypton. Under normal conditions, 4.73 cm^3 of inert gas forms in 1 cm^3 of uranium irradiated to 1% burnup. The solubility of xenon and krypton in α-uranium is minute. Atoms of the inert elements do not combine chemically with uranium, its impurities, and fission fragments, and leave the lattice occupying the sites where it is distorted. These sites may be micropores, dislocations, twin boundaries, boundaries of grains and subgrains, metal layers surrounding intermetallic compounds, nonmetallic inclusions. Atoms of xenon and krypton may evidently be captured by individual vacancies and groups of vacancies, i.e. by volumes giving birth to pores. At a high temperature, the accumulated gas builds up a high pressure in the pores under which the metal deforms plastically. Small gas bubbles grow, unite and form large bubbles. This produces an increase in the uranium volume, i.e. gas swelling takes place.

Gas swelling increases with temperature because the material creep resistance decreases with temperature. At 848 K, an increase in the burnup from 0.2 to 0.5% leads to a practically linear increase of the uranium volume from 1 to 7%. As a first approximation, the following relationship is true:

$$\Delta V = -3.6 + 19.4 \text{ (burnup percentage).}$$

A burnup of 0.27 to 0.3% increases the uranium volume at 973 and 1073 K by 11.5 and 84.5%, respectively. In gas swelling, destruction may occur intragranularly or along grain boundaries.

An improvement of strength characteristics of uranium at an elevated temperature, creep resistance in particular, decreases gas swelling. This is attained by alloying uranium with molybdenum, niobium, and zirconium. Thus, an alloy containing 10% Mo does not

swell up to 873 K at a 2% burnup. Iron and aluminum added to
uranium form finely divided intermetallic compounds. Bubbles
formed on them are too fine to merge with one another. In combina-
tion with quenching from the γ-phase, alloying eliminates swelling at
burnups up to 0.7%. The use of devices compressing the nuclear fuel
also contributes to the reduction of gas swelling.

7.4 Effect of Radiation on Mechanical Properties of Uranium

Irradiation of metals with neutrons causes radiation damage involv-
ing an increase in the electrical resistivity, yield point, and ulti-
mate strength, a decrease in the ductility and impact elasticity,
a shift of the cold brittleness threshold towards high temperature.
In uranium, these effects sharply manifest themselves as its lattice
is subjected not only to fast neutrons but also to fission fragments
having an energy up to 100 MeV. Of most practical importance are
the irradiation-caused changes in the mechanical properties and
heat conductivity. Thus,at irradiation within 423-573 K and 0.08%
burnup, the yield point of uranium increases from 270 to 560 MPa.
The ultimate strength somewhat decreases with an increase in fluence
and then increases. Most characteristic is an abrupt decrease in elon-
gation (from 19 to 0.3-0.5%) with an 0.02% burnup. The impact
strength of uranium at a neutron fluence of 10^{19} cm^2 reduces from
20-30 to 6-9 J cm^{-2}. The uranium *embrittlement* under irradiation
starts at small fluences (10^{16} cm^2). Irradiation at 573-673 K yields
the same results.

   Annealing irradiated uranium recovers to a certain extent the
ultimate strength and yield point but does not restore its ductility.
Radiation damage cannot be remedied by annealing. This is not only
because foreign atoms intrude into the uranium lattice, but mainly
because of microcracking. Microcracks at the boundaries and in the
bulk of polycrystalline uranium grains evidently generate from the
anisotropic radiation growth of individual grains. Impurity atoms
that are fission products harden the metal and prevent from relaxa-
tion of internal stresses by plastic deformation. Grains of irradiated
polycrystalline uranium have a great number of twins and slip bands.
The grains deform. The interaction of randomly oriented grains re-
sults in their plastic deformation and the so-called *radiation hardening*
of metal.

   An important mechanical property of uranium under radiation is
supercreep, or *radiation creep*. In a field of neutrons the creep of
quenched, annealed and grain-oriented uranium exceeds its creep
outside the neutron field dozens and hundreds of time. At a neutron
flux density of $6 \cdot 10^{12}$ cm^{-2} s^{-1}, uranium creeps at 493 K at a stress
of 0.02 MPa. At the same temperature with no irradiation uranium

shows no creep. When exposed to irradiation at 373 K, uranium creeps at a rate of $10^{-5}\%$ h^{-1} under a load constituting 1% of the normal yield point of uranium at a given temperature. As has been suggested, supercreep results from the radiation growth in which uranium grains press against one another thus increasing the stress to the yield point. The application of even a minute external load leads to a considerable creep, as the radiation growth in direction [010] constantly increases stress with deformation. Enhanced creep is often associated with the formation of stacking faults and with the motion of atoms in the thermal spike zone. Supercreep may deform fuel elements, as happened in the reactors of the power station at Calder Hall.

7.5 Uranium Alloys

The use of pure uranium for the fabrication of the fuel element metallic rods is restricted because of the changes in the uranium properties produced by irradiation. Thermal and thermomechanical working of uranium producing a more resistant fine-grained and quasi-isotropic structure cannot completely solve the problem of obtaining fully resistant metallic nuclear fuel. The resistance of nuclear fuel in the fuel elements with metallic rods may be improved through alloying.

Uranium alloys must provide the lowest parasitic neutron capture. To this end, the alloying elements must have a minimum neutron absorption cross section. When operating in a reactor, the alloys must preserve the size and shape, possess high strength and ductility. The alloy must be compatible with the fuel element cladding. The diffusion interaction of the alloy with the cladding materials is impermissible, as diffusion may result in damage of cladding and destruction of fuel elements. In long-term operation, the fuel element clads may become unsealed. As a result, the fuel may contact the coolant. To prevent the wash-out of uranium and its corrosion products into the coolant, the alloys must be highly resistant to corrosion and erosion.

Uranium alloys to be used as a nuclear fuel may be divided into two groups: alloys having an α-phase structure in which a small amount of alloying elements promote the formation of a fine-grained metal without grain orientation; and alloys having a γ-phase structure to which the alloying elements are added in an amount enough to stabilize partially or fully the cubic γ-phase. Alloys of the first group based on natural or slightly enriched uranium are used mainly in thermal reactors. These are uranium alloys with 0.4% Al, 0.5-2.0% Mo, 2.0% Zr, and 0.1% Cr. Alloys of the second group are more universal. A high content of alloying elements, however, necessitates their considerable enrichment. Examples are alloys of systems U-Mo, U-Zr, U-Nb, and ternary alloys of system U-Zr-Nb with a considera-

Fig. 7.6 Uranium corner of U-Fe phase diagram

Fig. 7.7 U-Al phase diagram

ble quantity of alloying components. Of interest are compositions
based on intermetallic compounds U_3Si, UAl_4 and the like.

Alloys with Iron. Alloying uranium with small amounts (hun-
dredth parts of a per cent) of iron improves service reliability of
metallic rods of fuel elements. Quenching produces a fine-grained
structure and improves the mechanical properties of uranium. This
makes the radiation roughening of the fuel element rod surfaces
milder.

Figure 7.6 shows the uranium part of the U-Fe constitution dia-
gram. A series of uranium intermetallic compounds form in this
system. The critical solubility of iron in α-uranium is close to zero,
and is 0.5 and 1.8% in the β- and γ-uranium, respectively.

Alloys with Aluminum. Aluminum is practically insoluble in
α-uranium. The ultimate solubility of aluminum in β- and γ-phases
is 0.18 and 0.60%, respectively. Three intermetallic compounds form
in the U-Al system.

Figure 7.7 gives the constitutional diagram of the U-Al system.
Alloying uranium by small additions of aluminum is used to obtain
fine-grained metal with the α-phase structure. Alloys containing up
to 0.15 to 0.50% aluminum have inclusions of the intermetallic
compound UAl_2. An alloy containing 0.4% aluminum recrystallizes
very quickly and acquires a fine-grained polyhedral structure with
grains 10-20 μm in size. Grains with preferable orientation are prac-
tically absent. The alloy possesses high resistance to thermal fatigue
and is far more resistant to changes in the shape at cyclic heating
and irradiation compared with pure uranium.

Of certain interest as to the use in reactors are uranium-aluminum
alloys containing less than 35% U. In a 14-16% U alloy much of alu-
minum is in the form of UAl_4. The alloy consists of crystals of pri-
mary compound UAl_4 dispersed in the eutectic matrix Al-UAl_4.

Among three intermetallic compounds, UAl_4 acquires the highest
importance for dispersion fuel elements. The spheroidal shape of
inclusions of this compound does not violate the matrix structure
and involves no difficulties in fabricating fuel elements.

Alloys with Silicon. Fig. 7.8 demonstrates the U-Si constitutional
diagram. Silicon practically does not dissolve in α-uranium. The
silicon solubility in β- and γ-uranium (atomic per cent) is 2.58 and
3.75%, respectively. Alloying uranium with 0.5 to 1.5 silicon redu-
ces the temperature of γ-β- and especially β-α-transformations.
The β-phase fixes complete in alloys containing 0.25 to 1.5% Si.

As to preservation of β-phase in quenching silicon is more effective
than aluminum and iron. Alloying uranium with silicon decreases
the grain size in uranium quenched from γ- and β-phases.

The U_3Si phase contains 3.78% Si. In extruded and irradiated
rods of U_3Si the ultimate strength and yield point are 703 and
420 MPa, respectively. Cast specimens have smooth surface and are
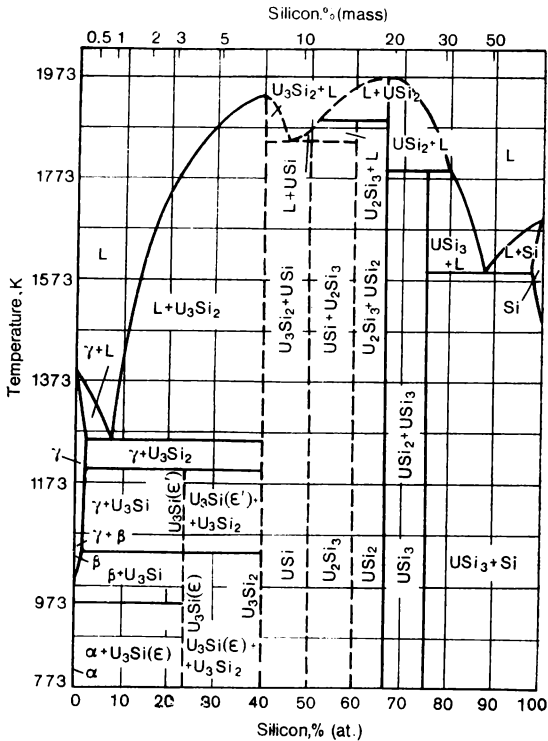
Fig. 7.8 U-Si phase diagram

stable when exposed to irradiation. Extruded' specimens notably elongate when irradiated. The accumulation of the gaseous products of fission produces swelling at a temperature below 773 K. At a burn-up in excess of 600 MW day t, a maximum increase in volume due to swelling is 7%. A non-irradiated alloy displayed a high corrosion resistance in water at 588 K.

Alloys with Chromium. One of the most considerable effects achieved by alloying uranium is the size reduction of grains in uranium-chromium alloys. The size of grains decreases with content of the alloying element. Hence, at chromium contents of 0.067, 0.4, and 0.9%, the grain size is 0.050, 0.035, and 0.030 mm, respectively. The ultimate solubility of chromium in uranium modifications is as follows: α-U, 1.5% at.; β-U, 1.5%; and γ-U, 4.5%. Alloying with chromium drastically decelerates the phase transformations. Uranium alloys containing less than 0.3% Cr may be subject to isothermal treatment in which the β-α-transformation takes place at a constant temperature. Small additions of chromium increase the strength of uranium.
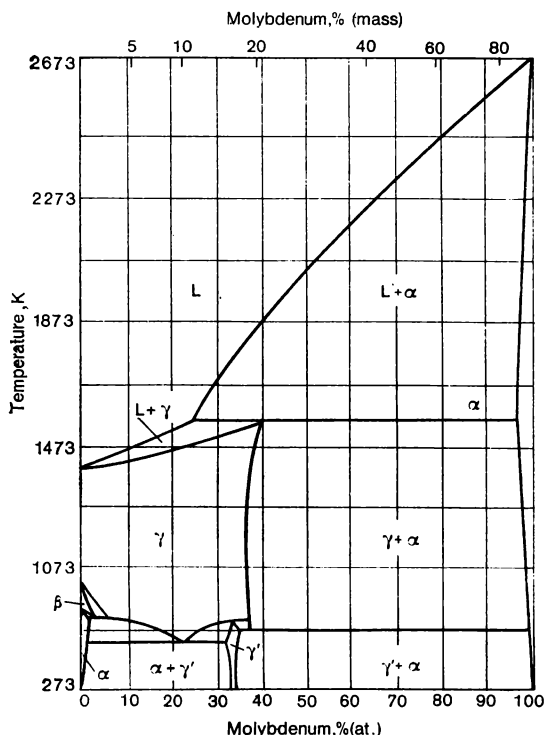
Molybdenum,% (mass)

Fig. 7.9 U-Mo phase diagram

Alloys with Molybdenum. Fig. 7.9 presents the U-Mo constitution-al diagram. Quenching of these alloys gives intermediate metasta-ble phases and also β- and γ-phases. When a molybdenum content is about 1% quenching preserves the β-phase at room temperature. When quenching alloys containing 3% Mo a gamma-solid solution fully transforms into the α'-phase, i.e. a molybdenum-supersaturated solid solution based on the α-phase of uranium. In alloys containing more than 3% Mo the inhibition of the γ- α'-transformation starts, which is completely effected when the content of Mo reaches 11% (at.).

The ultimate strength and yield point of quenched alloys pass through their maxima at 5% Mo and are 1300 and 900 MPa, respecti-vely. The elongation is 8%. The radiation resistance of the alloys increases with the molybdenum content.

A 10% Mo alloy irradiated in the γ-condition has the highest radi-ation resistance. After water quenching irradiation at 513 K to a 0.09% (at.) burnup did not change the geometry of specimens. The

dimensions of cold-worked and sintered alloys having the same content of molybdenum at 0.18-1.02% (at.) burnup changed by 0.5 to 1.2%.

Uranium-molybdenum alloys resist gas swelling better than pure uranium does. The alloy stability grows with the molybdenum content. At a 2.5-3.0% (at.) burnup, alloys containing 10-13% Mo increase in volume by 2-4%. Such an increase in volume is observed in pure uranium as early as at a burnup of 0.2-0.5%. Uranium-molybdenum alloys containing 10-12% Mo when tested in water of high purity at 573 K display a sufficiently high corrosion resistance.

Alloys with Zirconium. Zirconium dissolves in γ-uranium in considerable amounts and inhibits the structural transformation. However, the stabilization of the γ-phase at room temperature requires a considerable quantity of zirconium. Adding niobium decreases the zirconium content in the alloy necessary to fix the γ-solid solution at room temperature. Thus, a uranium alloy containing 5% Zr and 1.5% Nb was successfully utilized in a BWR in the USA. The temperature of the fuel elements surface was 553 K and the corrosion resistance of the alloy in water was satisfactory at 573 to 623 K. The greatest radiation resistance of an alloy having a growth coefficient of 17 is achieved after isothermal transformation at 893-923 K which produces spheroidal particles of α-uranium.

Fissium. Pyrometallurgical processing of a waste nuclear fuel removes highly volatile rare-earth elements in reasonable amounts. Some elements, uranium fission products, remain with uranium. They, Mo (3.42%), Ru (2.6%), Tc, Rh, Pd (0.3 to 0.9% each), are called fissium Fs. The stability of gamma-uranium increases with increasing the fissium concentration.

In a 5% Fs alloy the gamma-phase is readily fixed at room temperature. The ultimate strength and yield point of this alloy at 813 K are 22-30 and 80-100 MPa, and elongation, 8-13%. A uranium alloy containing 5% Fs has a high radiation stability. At 633-863 K, the radiation growth coefficient is 1-2. At 873 K, gas swelling increases the volume by 8% per atomic per cent of burnup. Promising is the metallic fuel of, say, the following composition: U-15% Pu-10% Fs.

Fuel Diluents. Recently attention has been drawn to highly diluted uranium alloys containing less than 50% U. They are prepared on the basis of Al, Zr, and Nb, elements with small absorption cross-sections.

7.6 Uranium Compatibility with Cladding Material and Uranium Corrosion

In service, the fuel element of uranium and its alloys contact the cladding material for a long period of time. The interaction between the cladding and fuel may unseal the fuel elements.

Aluminum. Many thermal reactors utilize metallic uranium fuel elements clad with aluminum or its alloys. The rate of uranium interaction with aluminum depends on temperature by the Arrhenius equation. With an increase in temperature from 484 to 993 K, the reaction accelerates 10^4 times. The diffusion layer formed between the uranium and aluminum consists mainly of the intermetallic compound UAl_3. The intensive interaction of uranium with aluminum starts as early as at 523 K. At 573 K, the metals are separated by a layer of intermetallic compounds which in 2000 h grows to a 0.025 mm thickness.

The diffusion rate depends on pressure. It is supposed that pressure impairs the continuity of oxide films on aluminum and uranium, and this favors the diffusion. Under unfavourable conditions the diffusion layer consisting of intermetallic compounds passes out to the surface of the aluminum cladding. The result is the interaction with the reactor coolant and the unsealed fuel element. To improve the resistance of fuel elements of uranium clad with aluminum use is made of an intermediate layer often of nickel. The uranium interaction with aluminum decelerates, and the cladding is tightly bonded to the fuel material. The same effect is produced by an intermediate layer of the aluminum-silicon eutectic.

Zirconium. Zirconium is compatible with unalloyed uranium and its alloys containing 10% Mo approximately up to 773 K and with uranium alloys containing 2-80% Zr or 80-90% Nb approximately up to 973 K. Zirconium is poorly compatible with uranium alloys containing 75 to 84% Al. Their interaction starts as early as at 773 K.

Magnesium. Magnesium is compatible with uranium and its alloys up to 773 K.

1X18H10T Steel. The compatibility of the austenitic stainless steel, type 1X18H10T, with uranium is as follows. At 773 K, a layer of uranium-containing intermetallic compounds 0.03-0.04 mm thick forms in the steel. At 873 and 973 K, the layer thickness is 0.25 and 0.5 mm, respectively. Such a drastic increase in the interaction rate with temperature and the risk of local overheating in the cladding make us either reduce the nominal design temperature, or isolate the steel from uranium by oxidizing the latter, or with a layer of sodium-potassium eutectic. Fuel elements with a sodium or sodium-potassium layer between the fuel and steel cladding were used in the "Enrico Fermi" reactor. However, this isolation is unreliable and now it is not recommended to use fuel elements with uranium rods and stainless steel cladding.

Electrochemical Behavior of Uranium. Uranium is among the metals that passivate in neutral media. In air-saturated aqueous media containing no activators uranium remains passive at a corrosion potential. The uranium passivation is associated with a dark-brown film of uranium dioxide formed on its surface. The crystal

lattices of uranium dioxide and uranium structurally correspond. Thus, crystallographic plane (110) of uranium dioxide is parallel to plane (100) of uranium. In the presence of oxygen in water, a more dense film of corrosion products forms. It features better protective properties. In the deaeration of water, the corrosion potential of uranium shifts into the negative direction and corresponds to an active region. The rate of corrosion naturally increases. The presence of strong oxidants in the medium in considerable amounts, chromates or permanganates for instance, displaces the uranium corrosion potential towards the repassivation region, which enhances corrosion. In low concentrations (0.1-1 g/l) such oxidants as chromates and nitrites act as passivators. The corrosion potential of uranium then corresponds to a passive region.

Corrosion of Uranium. In a neutral air-saturated medium, corrosion of uranium proceeds with oxygen depolarization, in deaerated media, with hydrogen depolarization. In the latter case, corrosion products contain hydrides. The presence of nitrates and sulfates in the medium in concentrations up to 0.1-1 g/l does not affect the uranium resistance. Chlorides even in an amount of 0.01 to 0.1 mg/l depassivate uranium and enhance uranium corrosion generating pits.

Decreasing pH of the medium enhances the uranium corrosion. Acid media, containing a considerable amount of oxidant, are used to dissolve uranium in fuel reprocessing. With an increase in temperature, the uranium corrosion enhances in compliance with the Arrhenius equation. At 373 K, the attack proceeds with hydrogen depolarization at a rate of 2 to 5 mg cm^{-2} h^{-1}. Hydrogen peroxide as a strong oxidant passivates uranium and reduces the rate of its corrosion.

In wet steam, the resistance of uranium is the same as in water at the same temperature. In superheated steam the rate of uranium corrosion increases with pressure. The presence of crevices intensifies the uranium corrosion therein as the oxygen ingress to crevices is hindered. In case of unsealed cladding, water finds its way in-between the fuel and the cladding. The intensive attack accumulates uranium oxides and hydride. This results in swelling of the cladding and formation of the so-called blisters.

Corrosion resistance of uranium may be improved by alloying. Most effective are : (1) alloys with the structure of γ-solid solution, (2) alloys with the structure of supersaturated α-solid solution of the martensite type, and (3) composition based on the intermetallic compounds.

The first group includes, in particular, a series of alloys of the U-Mo system containing 13-20% of molybdenum. Within 373-473 K, the efficiency of such alloys is dozens of times the resistance of unalloyed uranium. Even after the optimal thermal treatment these

alloys destruct in water at 573 K in 30 to 100 days. The second group
has somewhat less resistant uranium alloy containing 5% Zr and
1.5% Nb quenched to martensite from the γ-region. The third group
covers compositions having 3.8% Si. These are reasonably resistant
in water at 533 K. The composition containing 3.8% Si can be uti-
lized at a higher temperature than the alloys with the structure of
γ-solid solution and α-martensite. When aged for a long period of
time at a high temperature the latter two groups undergo structural
transformation with the formation of a stable α-phase of low corro-
sion resistance.

Atmospheric Corrosion of Uranium. Metallic uranium interacts
with air at room temperature. In wet air a darkbrown oxide film
consisting of uranium dioxide coats the metal. The oxide compo-
sition may differ from the stoichiometric composition in that it
has excessive oxygen. The rate of uranium corrosion at room tempe-
rature in dry air is not high and equals several microns per year.
Increasing the humidity and temperature enhances the uranium oxi-
dation. The uranium corrosion then follows the linear law. At high
humidity and at $T > 343$ K, the oxide film provides no protection.
Heating in the air to 773-973 K may ignite uranium which is more
pyrophoric than zirconium. At low temperatures, uranium does not
interact with helium, nitrogen, carbon dioxide, and hydrogen de-
prived of moisture and oxygen. At 643 K, however, uranium reacts
with dry nitrogen and at 773 K, with carbon dioxide.

Uranium Resistance in Liquid Metals. Uranium is sufficiently
resistant in sodium and Na-K eutectic cleared from oxygen. The
presence of oxygen in alkali metals enhances the uranium corrosion.
The affinity of uranium for oxygen is greater than that of sodium
(-1030.8 and -751.6 kJ/mole, respectively) and, therefore, urani-
um reduces sodium oxide oxidizing to uranium dioxide. The urani-
um corrosion rate is equal to 0.8 mg cm^{-2} h^{-1} in a flow of sodium
containing 0.005% oxygen at 873 K. Up to 773 K, uranium practi-
cally does not react with alkali metals cleared off oxygen. Irradiation
has no effect on the intensity of uranium interaction with alkali
metals up to 873 K. Even in case of damage to the continuity of the
fuel element cladding, the interaction of uranium rod with alkali
metals does not lead to a bad contamination of the reactor coolant.

Uranium Resistance in Organic Coolant. In diphenyl, uranium is
far more resistant than in water at the same temperature. The ura-
nium corrosion resistance considerably depends on the purity of or-
ganic coolants. In a purified diphenyl, uranium is efficient at least
6 months. In the case of unsealed claddings, the contact between
uranium and organic coolant does not contaminate the latter essen-
tially.

Protective Coatings. To protect against corrosion and as an inter-
mediate layer between the fuel rod and metallic cladding of the

fuel element, coatings are applied to uranium. They are applied by electroplating, chemical methods, diffusion, hot methods, decomposition of volatile compounds in the gas phase, or by forming a protective oxide or nitride film. The quality of coatings essentially depends on whether the uranium surface is clean, in particular, whether it is free from oxides. Uranium readily oxidizes in the air, therefore, cleaning of its surface presents certain difficulties. Most of protective coatings protect uranium against corrosion in boiling water for a short period of time. They are mainly used as an intermediate layer between uranium and cladding.

7.7 Plutonium and Its Alloys

Physical Properties. Pu is the 94th element of the periodic table. The principal isotope of importance is ^{239}Pu. Plutonium practically does not exist in nature, although traces of ^{239}Pu are found in uranium ores ($5 \cdot 10^{-12}$% of the uranium content). Plutonium is produced in nuclear reactors by nuclear processes. Irradiating natural uranium to a burnup of 0.5% ^{235}U forms 0.28% ^{239}Pu. To recover plutonium from the irradiated uranium, the latter is dissolved in nitric acid. Uranium and plutonium are extracted from the solution by organic solvents. The main bulk of fission products remains in the aqueous solution. Then, plutonium is separated from uranium. Metallic plutonium is prepared by thermal reduction of its compounds,

TABLE 7.3 Structure of Plutonium Modifications

Phase	Tempera-ture range of exis-tance, K	Density, g/cm³	Unit cell		Num-ber of atoms in cell
			Lattice	Parameters	
α	Below 392	19.816 (298 K)	Monoclinic	$a = 0.61835$ nm (294 K), $b = 0.48244$ nm $c = 1.0973$ nm $\beta = 101.81°$	16
β	392–491	17.82 (406 K)	Body-centered monoclinic	$a = 0.9284$ nm (463 K) $b = 1.0463$ nm $c = 0.7859$ nm $\beta = 92.13°$	34
γ	491–583	17.14 (508 K)	Face-centered or-thorhombic	$a = 0.31587$ nm (506 K) $b = 0.57682$ nm $c = 1.0162$ nm	8
δ	583–723	15.92 (593 K)	Face-centered cubic	$a = 0.46371$ nm (593 K)	4
η	723–745	16.0 (720 K)	Face-centered tet-ragonal	$a = 0.4701$ nm (738 K) $c = 0.4489$ nm $c/a = 0.955$	4
ε	745–913	16.48 (783 K)	Body-centered cu-bic	$a = 0.36361$ nm (763 K)	2

halides, for instance. The best reducer is calcium forming no alloys with plutonium.

Depending on duration of uranium irradiation, 11 isotopes of plutonium may be obtained (from ^{232}Pu through ^{243}Pu) in reactors with half-lives from 35 min to $9 \cdot 10^5$ years. The half-life of ^{239}Pu [is 24 060 years. Isotope ^{239}Pu decays by α- and γ-emission.

The melting point of metallic plutonium is 913 K. Its boiling point is 3500 K. Plutonium is known to exist in six allotropic forms within the temperature range from room temperature to melting point. Table 7.3 gives the temperatures of phase transitions, types of crystal lattice, and densities of plutonium crystalline modifications. The plutonium δ-modification having a close-packed lattice has the least density. Depending upon the crystallographic modification, the thermal expansion coefficient varies from $56 \cdot 10^{-6}$ deg^{-1} for the α-modification to $-57.9 \cdot 10^{-6}$ deg^{-1} for the η-modification. A negative thermal expansion coefficient for δ- and η-phases of plutonium, i.e. contraction of linear dimensions on heating, is unusual for metals with a simple lattice and so far has not found a reasonable explanation.

The transition of one crystalline modification of plutonium into another involves a change in volume and corresponding heat effects

TABLE 7.4 Volume Changes and Latent Heat of Allotropic Transitions of Plutonium

Transition	$\alpha \to \beta$	$\beta \to \gamma$	$\gamma \to \delta$	$\delta \to \eta$	$\eta \to \varepsilon$	$\varepsilon \to$ liquid
Volume change, %	8.9	2.4	6.7	—0.4	—3.0	~ 0.1
Latent heat of transition, J/g	13.4 ± 2.0	2.9 ± 0.4	3.3 ± 0.4	0	6.70 ± 1.25	14.0 ± 2.0

(Table 7.4). Allotropic transitions of plutonium may occur both with increasing and decreasing the volume.

Allotropic transitions followed by essential changes in the metal properties change the shape of items made of plutonium at cyclic heating and cooling.

Mechanical Properties of Plutonium. At room temperature, the ultimate strength of plutonium is 356 MPa, yield point 225 MPa, and elongation 0.068%. At 598 K, they are 14.1 MPa, 11.5 MPa, and 50.1%, respectively. At room temperature, plutonium possesses high strength and low ductility, i.e. it is brittle. Owing to a low ductility of the α-phase, the volume changes taking place in plutonium cooling generate internal stresses and hence microcracks.

As a result of its α-activity metallic plutonium selfheats in the compact form.

A high chemical activity, a great number of allotropic transitions involving material changes in volume, and a low ductility of α-plutonium complicate the fabrication of plutonium items. A high reactivity of plutonium limits the number of refractory metals applicable to fabrication of foundry equipment. Tantalum, tungsten, calcium oxides or fluorides, magnesium oxide, and cerium sulfide are most suitable for the purpose. To prevent the oxidation of plutonium, melting and casting must be carried out under a high vacuum.

Plutonium hardly lends itself to deformation in the region of α-phase because of its high brittleness. In the δ-region (583-723 K), plutonium is ductile and can be subject to all sorts of press working: pressing, forging, stamping, extruding. When cooled down from δ-phase to room temperature, three phase transitions take place. Therefore, ready items may distort and crack in cooling. As melting and casting, working of plutonium must be accomplished in vacuum or in an inert atmosphere.

Corrosion Resistance of Plutonium. Plutonium is chemically more active than uranium and possesses a higher affinity for oxygen, hydrogen, and nitrogen. Plutonium reacts with carbon dioxide at a relatively low temperature reducing it to carbon monoxide and to graphite at excess of plutonium. At room temperature, plutonium readily reacts (in particular at 473 K) with hydrogen to form hydrides. Plutonium weakly interacts with nitrogen even at a temperature of 1073 to 1273 K.

The compatibility of plutonium with alkali metals is not studied well. Lithium does not form with plutonium solid solutions and intermetallic compounds. Plutonium reduces potassium and sodium oxides, but does not reduce lithium oxide.

In the form of powder and chips, plutonium is pyrophoric and readily ignites in the air forming aerosols of oxide. A nonadherent oxide film covers compact plutonium kept in the air. In a moist atmosphere at a temperature up to 323 K, the film consists of plutonium dioxide and is yellow. The plutonium oxidation in the air enhances with temperature and proceeds up to 478 K following the law close to linear. At a higher temperature, the oxidation follows the parabolic law and produces a black protective film well adhered to the metal. In water plutonium corrodes to form hydroxide. The rate of its interaction with water is relatively low. In boiling water, the process considerably accelerates. The presence of oxygen in water decreases the rate of corrosion. This points to that plutonium is a passivating metal.

Corrosion resistance of plutonium approximates that of uranium. In many cases data on corrosion resistance of uranium gives us information on the plutonium behavior under similar conditions. The

corrosion products of plutonium offer a serious health hazard. Plutonium poorly dissolves in sulfuric acid and dissolves but little in nitric acid, though its dioxide and hydroxide are readily soluble in the concentrated acids. Alloying plutonium with elements stabilizing the δ-phase improves its resistance to attack, as is the case with uranium based on the γ-phase.

Plutonium Alloys. Alloying plutonium with aluminum, zirconium, titanium, cerium, thallium, and thorium with subsequent quenching from the temperature corresponding to δ-phase, allows the ductile δ-phase to be fixed at room temperature. For example, quenched plutonium-aluminum alloys (2-13% at. Al) have a δ-phase structure. When a plutonium alloy containing less than 5% Al is rapidly cooled down, the segregation of the latter produces an objectional α-phase. Annealing within the temperature region corresponding to the α-phase fully restores the alloy homogeneity. Iron, cobalt, and nickel materially reduce the melting point of plutonium, forming low-melting eutectics which may be utilized as liquid fuel. Specifically, plutonium-uranium alloys can be used as a nuclear fuel in fast-neutron reactors. Additionally alloying these alloys with molybdenum (14%) improves their stability at 773-873 K. Uranium alloyed with 15% Pu and 20% Mo has a structure stable to 823 K.

Radiation Stability. Radiation stability of plutonium is low. Irradiation of unalloyed plutonium at 623-673 K (region of δ-phase) with 44 cycles of cooling to a temperature of γ- and β-phases (423-473 K) destructed the specimen and demonstrated that the metal cannot be used as a nuclear fuel when it is unalloyed. Alloying various metals with plutonium is usually done when plutonium is to be uniformly distributed either in breeder materials (uranium or thorium), or in structural materials to obtain a radiation stable alloy. Uranium-plutonium alloys are radiation unstable because of radiation growth and gas swelling. Thermal working allows one to avoid radiation growth. After irradiation, however, the metal surface becomes too rough because of resultant coarse grains. Radiation stability of uranium-plutonium alloys (up to 10-15% Pu) increases when they are additionally alloyed with molybdenum in an amount of 28% at. Radiation stability of the Th-Pu alloys is higher than that of U-Pu alloys.

Aluminum alloys containing from 0.5 to 20% Pu are satisfactorily radiation stable. These alloys have good foundary properties and can be machined. Alloys with high contents of plutonium have a two-phase structure: individual grains of a brittle intermetallic compound $PuAl_4$ are dispersed in a ductile aluminum matrix. When a liquid-metal fuel based on plutonium is used, no radiation stability problem arises. Then, however, we face a problem of choosing structural materials compatible with the nuclear fuel. Tungsten

13-0816

and tantalum dissolve in liquid uranium at a lower rate than other refractory materials. Perhaps, they are compatible with plutonium and its alloys at high temperatures and long exposure.

7.8 Thorium and Its Alloys

Physical Properties. This is a radioactive chemical element of the actinium series, symbol Th, atomic number 90. Unlike uranium and plutonium, thorium itself is not a fissile material. Irradiating natural thorium with thermal neutrons forms ^{233}U which can be extracted and utilized as a fissile material.

Thorium when freshly prepared is silvery white but turns dark gray on exposure to air. At 1673 K, the low-temperature α-modification of thorium with a FCC-lattice transforms into the β-modification with a BCC-lattice. The melting point of thorium is 1968 K, its density is 11.71 g/cm³. Coefficient of thermal expansion within the range of 303-873 K is $12 \cdot 10^{-6}$ deg⁻¹. Natural thorium consists of practically pure isotope having atomic weight of 232. In addition, five natural and seven man-made isotopes of thorium are known.

Mechanical Properties. Pure thorium is ductile and readily deforms in cold state. Relatively small amounts of impurities affect its mechanical properties. Depending upon the preparation techniques, its ultimate strength lies within 140 to 220 MPa, yield point, within 80 to 130 MPa, and elongation, within 20 to 50%. Additions of most elements, in particular carbon, notably harden thorium, and impurities of oxygen and nitrogen only slightly affect its mechanical properties. Thorium strength rapidly drops with temperature.

Corrosion Resistance. Thorium is more corrosion resistant than uranium and plutonium. Its cut surface remains unoxidized for a long period of time. With an increase in temperature the rate of thorium oxidation in the air grows. At 1123 K, thorium oxidizes following the linear law to form thorium dioxide. In distilled water, thorium is efficient to 273 K. A protective film forms on the metal surface. With a further increase in temperature, the rate of attack in water drastically increases. Alloying with titanium, zirconium, and beryllium adds to its corrosion resistance.

Radiation Stability. In liquid metal coolants, thorium is efficient. Contaminating the liquid metals with oxygen decreases their stability. Metallic thorium undergoes no allotropic transformations and up to 1673 K has an isotropic FCC-lattice. In view of this, one should not expect dimensional instability and anisotropic properties under irradiation, which are characteristic of uranium. Thus, irradiation with a neutron fluence of 10^{21} cm⁻² increased the diameter of thorium blocks by 0.02%. Thorium alloys with uranium are radiation stable, and resist well gas swelling. Thorium-plutonium alloys also show good dimensional stability.

TABLE 7.5 Characteristics of Compounds of Uranium, Plutonium, and Thorium

Compound	Crystal lattice	Parameters, nm	Theoretical density, g/cm3	Melting point, K	Content of U, (Pu, Th)		Cross-section, 10^{28} m2	
					by mass, %	g/cm3	fission	capture (cross-section of fission included)
UO_2	Cubic, type CaF_2	$a = 0.54704$	10.97	3153	88.2	9.68	1.40	2.56
U_3O_8	Orthorhombic	$a = 0.67198$ $b = 0.39830$ $c = 0.41462$	8.38	2773	84.8	7.11	1.16	2.11
PuO_2	Cubic, type CaF_2	$a = 0.53900$	11.46	2513	88.0	10.11	240	339
ThO_2	Cubic, type CaF_2	$a = 0.55597$	9.82	3573	87.8	8.62	—	2.31
UC	Cubic, type NaCl	$a = 0.49610$	13.63	2643	95.2	13.00	2.10	3.85
UC_2	α-UC_2 (up to 2100 K) tetragonal, type CaC_2	$a = 0.35240$ $c = 0.59990$	11.68	2743	90.8	10.60	1.39	2.54
	β-UC_2 (> 2100 K) cubic, type CaF_2	$a = 0.54500$	—	—	—	—	—	—
PuC	Cubic, type NaCl	$a = 0.49700$	13.60	2123	95.0	12.91	358	505
ThC	Same	$a = 0.53380$	10.64	2898	95.1	10.11	—	3.51
ThC_2	Monoclinic	$a = 0.65300$ $b = 0.42400$ $c = 0.65600$ $\alpha = 1040$	9.30	2928	90.8	8.45	—	2.36
UN	Cubic, type NaCl	$a = 0.48891$	14.32	3123	94.4	13.50	2.10	4.79
PuN	Same	$a = 0.49050$	14.23	3123	94.5	13.92	366	517
US	Same	$a = 0.54905$	10.87	2723	88.1	9.60	2.10	4.14

Note. Calculations of cross-sections for uranium compounds were based on the corresponding values of natural uranium cross-sections.

13*

7.9 Ceramic and Dispersion Nuclear Fuel

Compounds of uranium, plutonium, and thorium with nonmetals (oxygen, carbon, nitrogen, etc.) having a high melting point, considerable density of fuel material, low thermal neutron absorption cross-section, good radiation stability are usually combined into one group known as ceramic nuclear fuel. This fuel finds ever increasing application, especially in high temperature reactors. The materials may be subdivided into three principal groups. The first group includes ceramics based on uranium, thorium, plutonium oxides, and their mixtures. Use is also made of mixtures of oxides of fissile and nonfissile materials. The second group covers ceramic materials other than oxides, such as carbides, nitrides, sulfides, phosphides and other compounds of uranium, plutonium, and thorium and their mixtures, and also their mixtures with other compounds containing no fissile isotopes. The third group consists of ceramic materials dispersed in graphite or other matrix. The dispersed phase (nuclear fuel) may be any compound of uranium, plutonium, thorium, or their mixtures.

Uranium Dioxide. Of oxide materials uranium dioxide is the most extensively employed. The uranium dioxide has a FCC-lattice of the type of calcium fluoride (fluorite). Table 7.5 gives the lattice parameters and some other properties of uranium dioxide. It should be noted that the melting point of uranium dioxide depends on its stoichiometric composition. Within 299-1273 K, the coefficient of thermal expansion of uranium dioxide is $10.52 \cdot 10^{-6}$ deg^{-1}.

An essential drawback of uranium dioxide is its low thermal conductivity: at 873 and 1273 K, it equals 0.033 and 0.026 J cm^{-1} s^{-1} deg^{-1}, respectively. In service this accounts for high temperature gradients across sections and may cause cracking or even melting of UO_2. To avoid this, one tries to make items of uranium dioxide as thin as practicable.

Mechanical properties of uranium dioxide depend on the fabrication techniques and testing temperature. Breaking strength at room temperature is far lower than at a high temperature. Uranium dioxide of stoichiometric composition, brittle at 1273 K, becomes ductile at 1873 K. Compact $UO_{2.06}$ of nonstoichiometric composition plastically deforms at 1073 K. Compressive strength of uranium dioxide lies within 420 to 980 MPa.

Compatibility. One of important characteristics of a nuclear fuel is its compatibility with the cladding material. For the data on the compatibility of uranium dioxide with various materials refer to Table 7.6.

Uranium dioxide does not react with water at 573 K. At 773 K, 0.005% of uranium dioxide dissolves in water. Uranium dioxide does not dissolve in hydrochloric acid and alkalis, but reacts with

TABLE 7.6 Compatibility of Compact UO_2 with Various Materials

Material	Temperature, K	Notes
Al	about 773	Relatively slow interaction with formation of UAl_2 and UAl_3
Be	873	Reaction with formation of intermetallic compound
Zr	873	Slow reaction, zirconium embrittles
Stainless steel	1673	No interaction
Ni	< 1673	Reacts mildly
Si	< 2173	At 2173-2373 K, USi_3 forms
SiO_2	< 1873	No interaction
Al_2O_3, MoO, BeO	< 2073	Same
C (fine powder)	1573	Slow reaction at 1473 K, rapid reaction at 2073 K
Nb, Ta, Mo	1473	During 1000 h no reaction is observed
W	2273	No interaction
H	3153	Reduces to stoichiometric composition, UO_2, at $T > 873$ K; no other reactions occur
Water (degassed) with neutral or increased pH	613	Stable during 30 days
Steam	673	Same
CO_2	1173	Sufficient stability
Na, Na-K	873	Sufficient stability of highly dense UO_2

aqua regia, nitric, and hydrofluoric acids. At room temperature, uranium dioxide oxidizes but slightly. With a grain size less than 0.5 μm, uranium dioxide is pyrophoric. When heated in the air it absorbs oxygen the more intensive the higher the temperature.

Radiation Stability. For nuclear fuel changes in its properties and size under irradiation are essential.

Swelling and resultant changes in volume are caused by (1) aggregation of atoms of fission products having a greater volume than the fissioned atoms, (2) growth of individual grains produced by knocking atoms out of lattice nodes and introduction of atoms of fission products into the lattice, (3) formation of pores due to merging of migrating vacancies, (4) increase in the volume of pores due to gaseous products of fission accumulated therein, (5) increase in the size of pores due to their merging in migration.

Depending on the irradiation temperature the relative weight of the above processes varies. As a general guide we may distinguish three regions of temperature:

1. Temperatures below $0.3 T_{mel}$ (823-873 K). Swelling is mainly determined by atom aggregates of fission products and slightly depends on temperature.

2. Temperatures within $0.3-0.5T_{mel}$ (933-1523 K). Swelling is determined by atom aggregates of fission products, pores formed in merging of vacancies, and pore volume increased under pressure of gaseous fission products.

3. Temperatures above $0.5T_{mel}$ (above 1373-1673 K). Swelling is determined by increasing the volume of pores under internal pressure of gaseous fission products in combination with pores merging and increasing in size as a result of their migration in the field of temperature gradient.

Pores found in the field of temperature gradient displace towards the higher temperature (towards the fuel rod center). The matter in this case moves in the opposite direction, following the mechanism: evaporation—condensation, surface and volume diffusion.

Fuel swelling makes the fuel rod compress in the inner zones and expand in the outer zones.

An increase in the diameter of a fuel rod due to radiation swelling leads to a mechanical contact between the fuel and the fuel element cladding. In service radial cracks occur in the fuel rod. If the adhesion (friction) force between the fuel and the cladding is enough, the cladding deforms in the zone of crack location. At cyclic changes of power (start and shut-down of the reactor), the arising stresses damage the cladding.

When the reactor operates at a load above 350 W/cm^2 under stationary conditions with oxide fuel, radial cracks may heal because in evaporation matter is transferred from the central heated zones and condenses in the cold zones. Radial mass transfer reduces the clearance between the fuel rod and the cladding up to its complete elimination. This improves heat removal from the outer layers of the fuel rod.

The center zones of the UO_2 pellets are heated to a higher temperature and undergo far greater thermal expansion than the claddings and outer layers of the UO_2 pellets. This generates stresses and strains along the fuel element axis (Fig. 7.10). The result of this is the development of "chewed" cladding, elongation of the fuel element, or, finally, destruction of the fuel element cladding along a circle perpendicular to the cladding element.

As to the chemical properties, the fission products in oxide fuel may be divided into several groups:

(a) noble gases Kr and Xe slightly soluble in UO_2 and forming gas bubbles and pores;

(b) chemically active Rb, Cs, Te, Br, and I which, in particular, may react with the fuel element cladding;

(c) Ru, Rh, Pd, Mo, Te, Sr, and Ba released in the metallic or oxide phase;

(4) Y, Zr, Nb, and rare earth elements whose oxides partially dissolve in UO_2.
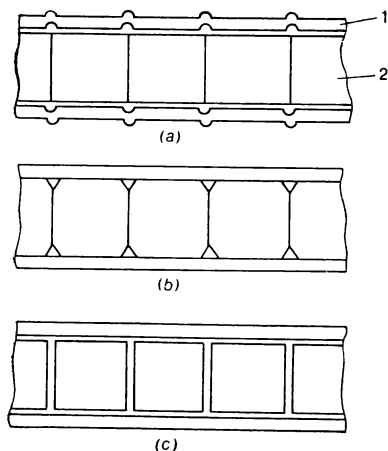
Fig. 7.10 Development of "chewed" cladding
a—in cooling; *b*—in operation; *c*—before irradiation; *1*—cladding; *2*—pellet of UO_2

Isotopes of Xe and Kr form in an amount about 0.25 atom of noble gas per one fissioned atom of ^{235}U. They make up 12-15% of the total amount of fission fragments.

The yield of gaseous products of fission increases with burning up. With the center of the UO_2 pellets at 1523 K, the relative gas emission linearly depends on burnup up to 20 MW day kg^{-1} and makes up 0.075% per each 9 MW day kg^{-1}. At a higher burnup, the gas emission abruptly increases. At a burnup of 50 MW day kg^{-1} it makes up as much as 7.9%.

Below 1773 K, UO_2 mainly swells because it retains bubbles of Xe and Kr. Their growth highly depends upon temperature. In a relatively cold fuel, swelling increases with temperature, approximating a certain maximum in the region of 1773 K, and decreases with diffusion and release of the gaseous products of fission.

Generally, uranium dioxide permits a high burnup without notable swelling and distortion of geometrical dimensions of fuel elements. Hence, at a burnup up to 15.5% (at.), an increase in the volume does not exceed 8%. The upper limit at a burnup up to 9% makes 0.33% per 1% of burnup atoms and is independent of temperature within 1033-2253 K. At a burnup in excess of 9% swelling enhances and the volume changes on the average by 0.7% per 1% of burnup atoms. Decreasing the uranium dioxide density to 81% of the theoretical reduces swelling. Swelling, however, is small, far lower than in the case of metallic alloys of uranium, and can be readily taken into account in designing the fuel elements. If in exposure to radiation, the temperature in the centre exceeds the melting point of ura-
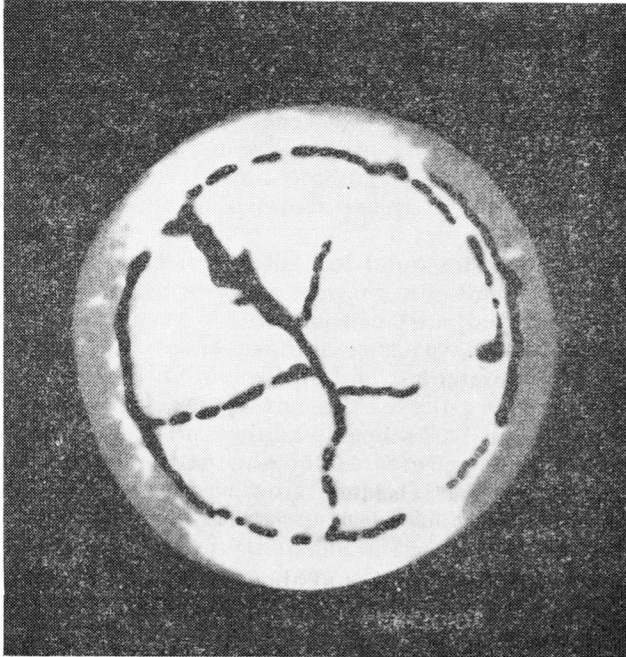
Fig. 7.11 Pattern of cracking of uranium dioxide pellets

nium dioxide, the volume expansion materially increases. When
more than 70% of the cross-section area of a uranium dioxide fuel rod
melts, swelling reaches 5-7% per 1% of burnup atoms. Part of the
gaseous products of fission is retained in the dioxide and part is
released into the fissures between the fuel rod and the cladding, or
into special cavities for collection of gases provided for the purpose
inside the fuel elements. Gas emission into the fissures increases
the internal pressure and involves the risk of damage to the cladding.
Moreover, this changes the composition of the gas in the fissures.
In fabrication the fissures are often filled with helium having a
better heat conductivity compared with air and argon. Gas emission
into the fissures affects the heat transfer between the fuel and the
cladding and increases the fuel temperature.

Irradiation reduces heat conductivity of uranium dioxide low
as it is. A low heat conductivity and high thermal strains accounted
for by it may cause cracking in the uranium dioxide due to a high
temperature gradient. Cracking as a rule, occurs in the radial di-
rection (Fig. 7.11) and may damage the pellets of uranium dioxide.
Irradiation often involves changes in the dioxide structure, the
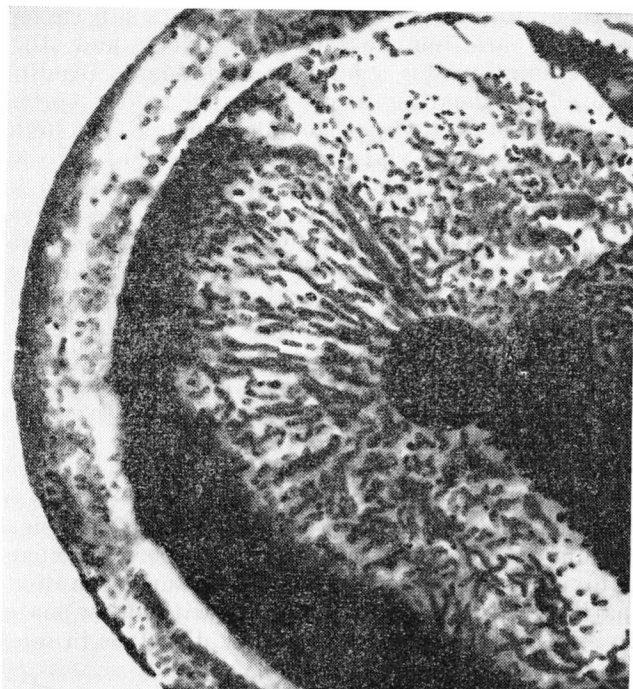
Fig. 7.12 Columnar crystals and central channel in irradiated uranium dioxide

formation of columnar crystals which account for up to 70% of the entire cross-sectional area of pellets. Deviation from the stoichiometry enhances the grain growth in uranium dioxide.

Irradiation forms a cavity (Fig. 7.12) in the centre of cylindrical uranium dioxide pellets in the zone of the highest temperature. Increasing the temperature in the centre up to the melting point facilitates the formation of the cavity. At about 1173 K, irradiation of loosely filled in or compacted (not sintered) uranium dioxide causes intensive sintering of particles.

When the continuity of the fuel element claddings is disturbed, water during reactor shut-down periods, or during operation into low loads find its way to pores in uranium dioxide. With the operating temperature being reached, the evaporation of water increases the pressure in the pores and destructs uranium dioxide. A similar effect is observed in the case of a liquid metal coolant.

Fabrication of Items of Uranium Dioxide. Compact uranium dioxide is prepared either by cold pressing with subsequent sintering to increase the compactness and strength, or by packing the fuel

element cladding with uranium dioxide powder with its subsequent
compacting. In pressing, paraffine, polyethylene glycol, and other
organic compounds are employed as a binding component. Binding
components are removed by heating after pressing before sinter-
ing. The latter is accomplished in a hydrogen atmosphere. The high-
est density of item is achieved at a sintering temperature of 1973 K.
The content of carbon in powder-like uranium dioxide must be li-
mited as it affects the item fabrication and stability in service.
Dioxide powder is compacted in a fuel element cladding by vibra-
tion, compressing, or by extruding together with the cladding.
Not sintered compacted dioxide has lower coefficient of heat transfer,
corrosion resistance, and resistance to swelling.

Uranium Mixed Oxide. U_3O_8 has limited application compared
with uranium dioxide. It is utilized in dispersion type fuel elements,
in particular, in mixture with aluminum in contact with which
uranium dioxide is thermodynamically unstable.

Plutonium Dioxide. In the form of a solid solution with uranium
dioxide plutonium dioxide is used to fabricate the fuel elements in
fast neutron breeder reactors. Table 7.5 presents certain physical
properties of plutonium dioxide. The coefficient of thermal expan-
sion of plutonium dioxide is comparable with that of uranium diox-
ide. For the compatibility of plutonium dioxide with other mate-
rials refer to Table 7.7. Plutonium dioxide poorly dissolves in most

TABLE 7.7 Compatibility of PuO_2 with Various Materials

Material	Tempera-ture, K	Notes
Th	1073	Partial reduction to Pu_2O_3; at 1273, partial reduction to metallic Pu forming a solid solution with Th
U	1073	Partial reduction to Pu_2O_3
Zr	1433	No interaction; partial reduction to Pu_2O_3
Fe	1573	Same
Al	873	No interaction
Mg	773	Partial reduction to Pu_2O_3; at 873 K, signs of reduction to metallic Pu
C	1273	Partial reduction to Pu_2O_3; at 1473 K, slow formation of monocarbide PuC; at 2123 K formation of PuC and Pu_2C_3

media. Phosphoric, nitric, and hydrofluoric acids dissolve it most
readily. Compact items of plutonium dioxide are fabricated by the
techniques described for uranium dioxide. Radiation stability of
plutonium dioxide is close to that of uranium dioxide.

Thorium Dioxide. In many aspects thorium dioxide resembles
uranium dioxide. It has a high melting point (see Table 7.5) and

does not oxidize in the air. Thorium dioxide is a brittle material. Its compressive strength at 293 K is 24.5 MPa. Sintered thorium dioxide does not interact with carbon dioxide and is stable in water to 573 K. Heat conductivity of thorium dioxide is low and decreases with temperature approximating that of uranium dioxide. Fuel in the form of a mixture of uranium and thorium dioxides is of great importance to the uranium-thorium cycle reactors. Mixture of the oxides may be sintered in the air. A solid solution of thorium dioxide and uranium dioxide, when exposed to radiation, behaves like uranium dioxide.

Nonoxidic Fuel Materials. Carbides of fissile materials may be used as nuclear fuel.

Uranium Monocarbide. UC is one of the promising nuclear fuels because of its high fuel content (25-30% more than in uranium dioxide) and increased heat conductivity (8-10 times that of uranium dioxide). The use of uranium monocarbide allows one to raise heat release, reduce gas emission and temperature in the fuel element center at the same core charge. The isotropic cubic structure of the monocarbide ensures its good radiation stability at high temperatures and heavy burnup.

A number of properties of the uranium monocarbide and carbides of other fissile materials are given in Table 7.5. The coefficient of linear expansion of uranium monocarbide within 293-773 K is $11.6 \cdot 10^{-6}$ deg^{-1}. Monocarbide of the stoichiometric structure dissolves slowly in concentrated acids and rapidly in diluted acids. It is pyrophoric in the air at above 573 K. In carbon dioxide, it oxidizes at 773 K to uranous oxide-uranium oxide. Monocarbide reacts with water at a high rate at 293-333 K. In organic coolants it is relatively unstable at a high temperature and inert in melts of sodium and potassium. For the compatibility of uranium monocarbide with various materials refer to Table 7.8.

Uranium Dicarbide. UC_2 has a lower density by uranium than monocarbide and undergoes allotropic transformation at 2103 K. Corrosion resistance of dicarbide in the air and carbon dioxide is close to that of monocarbide. Dicarbide starts to react with most structural materials at a higher temperature than monocarbide. Heat conductivity of dicarbide is close to that of monocarbide and increases with temperature.

Heat conductivity of plutonium monocarbide is far lower than that of uranium monocarbide (see Table 7.5). A solid solution (U, Pu) C has a higher heat conductivity. This carbide is inert to sodium and potassium and is compatible with a Zr-1% Nb alloy up to 873 K. It is stable under irradiation.

Uranium Nitrides. Of three uranium compounds with nitrogen (UN, U_2N_3, UN_2) uranium mononitride is most promising as a nuclear fuel (see Table 7.5). Compatibility of uranium mononitride

TABLE 7.8 Compatibility of UC with Various Materials

Material	Tempera-ture, K	Notes
Al	773	Reacts to form UAl_3 and UAl_4
Be	873	Reacts to form UBe_{13}
Cu	1273	No interaction for 24 h
Zr	1073	No interaction; at 1273 K, quick reaction with formation of ZrC + U
Stainless steel	1173	No interaction for 100 h; at 1243, for 6000 h. Slightly interacts with monocarbide of overstoichiometric composition
Nb	1373	No interaction for 100 h; at higher temperature (> 1473 K) interacts to produce niobium carbide and uranium carbide
Nb + 1% Zr	1273	No interaction
Mo	< 1273	Compatible; at > 1473 K interacts to produce Mo_2C and U
W	2073	No interaction for 838 h
Re	2123	Simple eutectic; Re does not produce carbides, therefore, it should not react
C	1473	Reacts to form UC_2 and U_2C_3

with many materials is higher than that of uranium monocarbide. Mononitride has a sufficiently high heat conductivity. It well resists deformation at a high temperature and possesses a good radiation stability. Uranium mononitride is stable in deaerated water up to 523 K, in alkali metals up to 1073 K, and in organic coolants up to 623 K. Uranium mononitride is compatible with aluminum, zirconium alloys, and stainless steel up to 673, 873 and 1573 K, respectively. When heated to above 1973 K mononitride decomposes. Increasing the nitrogen pressure decelerates the process. Hence, at a nitrogen pressure of 10^{-5} MPa the decomposition temperature of uranium mononitride is 2353 K. In order to completely prevent decomposition up to the melting point, the nitrogen pressure must be increased to 0.25 MPa.

Uranium Monophosphide and Uranium and Thorium Sulfides. They have a high melting point, are relatively stable at high temperatures, compatible at a high temperature with many materials, and are rather efficient in many reactor coolants. Because of all this the above-mentioned compounds are promising as a nuclear fuel.

Dispersion Nuclear Fuel. In a dispersion nuclear fuel, a fuel phase is dispersed in a nonactive matrix. Each particle of nuclear fuel may be considered as a microelement surrounded by matrix. Ceramic materials, whose high melting point and radiation stability combine with strength, ductility and high thermal conductivity, may be used as dispersed fuel. The fission processes and resultant

radiation damage are concentrated in the fuel part dispersed in the matrix. The matrix itself is mainly subjected to the action of neutrons which produce radiation damage not so heavy as that of fission fragments. However, the part of the matrix contacting the nuclear fuel is also damaged by fission fragments. The depth of damage is independent of the size of dispersed particles and equals the distance the fission fragments cover in the matrix. The strength of dispersion system greatly depends on the ratio between the damaged and intact parts of the matrix. At a constant ratio between the fuel part and the matrix, the size of dispersed particles may be different. The finer the grains, the greater their surface, and the larger the zone of the matrix damage. Al, Be, Mg, Zr, Nb, W, and stainless steel may be used as a matrix material. Various uranium compounds, uranium intermetallic compounds with aluminum, beryllium, oxides, carbides, and nitrides of uranium and other fissile materials are used as a dispersion fuel phase. To increase the radiation stability of dispersion fuel the distance between dispersed particles should exceed the doubled path of fission fragments. The dispersion nuclear fuel should be compatible with the matrix material during fabrication and in service, have enough strength, and be uniformly distributed in the matrix.

The matrix material must possess high strength and ductility in order to withstand swelling of dispersed fuel particles when solid products of fission accumulate in them and withstand the pressure of gaseous products of fission without damage. It should also have good heat conductivity, not undergo structural transformations within in the entire range of operating temperatures, and be corrosion resistant with regard to coolant and compatible with materials of the fuel element cladding.

A system of 30% UO_2 dispersed in a matrix of the austenitic stainless steel possesses a high radiation stability at a burnup up to 15% U when the temperature in the fuel element center is 700-1144 K.

The matrix absorbs strains produced by irradiation in the space filled by the fuel until the strains do not exceed the maximum strength of the matrix material. Note that the matrix strength reduces from brittle ceramic inclusions. To determine the strength of the system is quite a complicated problem.

At 873 K, the materials of the dispersion uranium dioxide-aluminum system interact forming the intermetallic compounds of uranium and aluminum, and aluminum oxide. The volume changes by 20-30%. When uranium dioxide is replaced with uranium-uranous oxide, the volume changes under similar conditions only by 4%. Used as a dispersion system is fiber glass containing uranium-uranous oxide. The uranium monocarbide-aluminum system is employed up to 773 K (at 873 K, carbide is incompatible with aluminum and

completely decomposes). A system of the intermetallic compounds of uranium and aluminum dispersed in a matrix of aluminum alloy or aluminum powder operates well.

7.10 Fuel Elements of Nuclear Reactors

The *fuel element* is a contrivance designed to arrange nuclear fuel in the reactor core zone following a certain order, generate the main bulk of heat energy produced in the core and transfer it to the reactor coolant. Fuel elements may also accumulate secondary nuclear fuel, ^{239}Pu and ^{233}U.

The fuel element consists of a rod containing nuclear fuel materials, cladding, end caps, and spacing parts. As to shape, the fuel elements may be cylindrical, rod-like, ring-type, tubular, plate, band, ball-type, prismatic, etc. The cladding isolates the nuclear fuel from the reactor coolant in order to prevent the contamination of the latter. The end caps seal the fuel element and together with the spacing parts fix it in the required position. To be loaded into a reactor, the fuel elements are assembled into: bundles, assembled units, packs, blocks with holes for fuel pins. The fuel assemblies arrange the coolant flow in the reactor core.

A trouble-free operation of the fuel elements is ensured by a proper choice of materials and coolant, service maintenance of prescribed composition of reactor coolants and temperature, and selection of the fuel elements structure and supporting mechanism. The simplicity and low cost of fuel elements and also the possibility and simplicity of the nuclear fuel regeneration are another important problem.

Checking. After fabrication, a fuel element must be checked for proper arrangement of the fuel rod inside the cladding, quality of the cladding itself, its leak-proofness, connection between the cladding and the rod, dimensions, and surface finish.

Conventionally the methods of the fuel element control may be divided into two groups:

(1) control in the fuel element fabrication and assembly;

(2) testing of fuel elements on experimental stands under conditions similar to the reactor service conditions.

In fabrication, fuel elements undergo nondestructive testing. It does not affect the properties of parts in their further operation. The tests may be divided into: leak tests under pressure, penetrant inspection, visual inspection, thermal, radiography, acoustic, electrical, and eddy-current. Different methods only supplement one another.

Defects to be detected by nondestructive testing may be classified into three groups:

(1) primary defects in the source material: changes in the chemical composition, surface and internal cracks;

(2) defects generated in making the fuel elements (preparation of blanks, machining, thermal treatment): porosity, ruptures, blow-holes and contraction cavities;

(3) defects produced in assembly: porosity, lack of fussion in welded seams, no bond between the cladding and the fuel rod. In the latter case the thermal contact is affected.

Thermal Contact. Local overheating may take place because of the poor contact between the fuel rod and the cladding.

A reliable contact between the fuel rod and the cladding, in particular, when bonding ceramic materials to metals, is accomplished with much difficulty. In certain cases, however, it is advisable to leave a clearance between the fuel rod and the cladding and pack it with a heat conducting material. The bonding between the rod and the cladding may be accomplished "metallurgically". This connection is obtained by heating the contacting surfaces. The metallurgical bond comprises all types of bonding in metallic systems, including chemical interaction, diffusion, etc. If the fuel rod and the cladding are made of the same material, e.g. uranium dioxide dispersed in a matrix of stainless steel and the cladding of the stainless steel, the rod and the cladding to form a metallurgical bond should be brought in contact and heated to a certain temperature.

In other cases compatible materials, uranium and aluminum, for instance, form intermetallic compounds when heated. The corrosion products exceed in volume the uranium and aluminum consumed to form them. Volume changes in the intermediate layer and formation of brittle compounds may damage the entire fuel element. To prevent this, an intermediate diffusion barrier is created. To create a diffusion barrier, the fuel rod is coated with a layer of Ni, Nb, Si, and other metals 8–20 μm thick. When heated, the intermediate layer forms diffusion pairs facing the fuel rod and cladding. Aluminum from the cladding may diffuse through a nickel interlayer, but this takes considerable time. If the contact between the fuel rod and the cladding is purely mechanical, the mating parts must thoroughly fit one another. This requires precise machining or reduction. The coefficients of thermal expansion must be taken into account.

As has been mentioned already, it is advisable in certain cases to leave a clearance between the fuel rod and the cladding, since the fuel volume increases in service. The clearance is filled with a substance having good thermal conductivity. Helium is generally used as a gas interlayer, because of its high thermal conductivity. Then, no problem of metal wetting arises. The liquid metal interlayer is usually Na, Pb, and alloys Na-K and Pb-Bi. The fuel rod-to-cladding bonding is obtained through joint rolling, pressing, extrusion, rotation forging (reduction from all sides), etc. Tightness of the fuel element is of prime importance. The most widely used technique of

sealing is arc welding in a protective atmosphere. Recently, electron-beam welding has found wide application.

Damage. Changes in the shape and size of fuel rods due to radiation growth, swelling, thermal cycles and allotropic transformations, damage to the cladding because of corrosion and erosion, diffusion interaction between the fuel and the cladding materials, and over-heating of individual cladding portions due to deposits, rank among the main service defects of the fuel elements.

Claddings may damage from pressure produced either by thermal expansion, or release of gaseous products of the nuclear fuel fission. Temperature gradients in nuclear fuel distort the fuel elements, and, hence, the claddings crack. Nonuniform expansion of the cladding and fuel produces swelling of the fuel element. Local corrosion attack

TABLE 7.9 Failure of Fuel Elements and Its Control

Cause	Remedial Measures
Hydrogenation of inside of cladding, fuel contamination (moisture)	Increasing pellet density, vacuum hot drying of fuel elements, limiting impurity contents in nuclear fuel
Local deformation in mechanical interaction between fuel and cladding; loss of ductility under irradiation	Increasing cladding annealing temperature, increasing wall thickness, optimizing pellet geometry and diametral clearance, reducing clearance tolerances, using lubricants, counterpressure, and reducing l'near loads
Consolidation of fuel at beginning of operation, clad crumpling	Use of counterpressure, increasing pellet density, use of stable uranium dioxide
Embrittlement of welded seams	Improvement of welding process
Bending of fuel elements	Thorough selection of materials for fuel assembly components, proper choice of axial clearanc`
Corrosion cracking of cladding	Increasing cladding annealing temperature to raise ductility
Local power increase of fuel assemblies in overload	Optimization of overloads
Load cycling	Choice of most smooth mode of reaching required power output and control
Fretting corrosion	Elimination of vibration source (in particular, reduction of flow velocity in clearance between fuel assemblies)

results in disturbed cla ding. Listed in Table 7.9 are the causes of the fuel element failures and remedial methods.

Hydrogenation damages fuel elements at relatively small burnups, up to 11 000 MW day t^{-1}. The hydrogenation control of the fuel element inside surfaces is done by observing the moisture content of the UO_2 pellets. The ability of uranium dioxide to absorb moisture depends upon its density. In view of this, it is good practice to employ UO_2 of high density (10.5 to 10.6 g cm^{-3}). The assembled fuel elements are vacuum-dried directly prior to sealing. In addition to this, a getter is placed in the fuel element to absorb hydrogen. When the measures are taken, not more than 0.02% of the fuel elements fail during the first period of operation.

Damage due to mechanical interaction of metal with the UO_2 pellets takes place at a burnup 6000-27 500 MW day t^{-1}. Damage in this case is mainly controlled by increasing the initial ductility of the cladding material. With Zr alloys, this increases the annealing temperature to a temperature of complete recrystallization. A resultant decrease in the yield point is compensated for by an increase in the cladding thickness. It is considered that decreasing the ratio of height to diameter of the UO_2 pellets, chamfers, reducing the linear load (W cm^{-1}), decreasing the fuel elements diameter with a simultaneous increase of their number in a fuel assembly and smoothly changing the power output materially add to the serviceability of fuel elements. Abrupt changes in the power output of certain fuel assemblies during fuel recharging may damage the fuel elements.

An increase in the power output of fuel assemblies is, in particular, dangerous to fuel assemblies that have been operating at lower loads for a long period of time.

In service, pellets may become seized and subsequently destruct. Chemical interaction of UO_2 with a Zr alloy at great burnups or linear loads forms a diffusion layer containing Zr, U, O, Cs. At burnups of 22 500 MW day t^{-1} a diffusion layer forms at linear loads of 300 W cm^{-1} and more.

If use is made of porous UO_2 of reduced density, the fuel element cladding may become crumpled. In the first (2-5) 10^3 h the fuel column decreases by 1-3%. Seizure of certain pellets produces gaps between the individual parts of the fuel column. This results in local energy surges and crumpling of claddings. The use of the fuel elements with the internal counterpressure prevents the crumpling of claddings. Increasing the temperature of sintering of the UO_2 pellets along with increasing their density improves the radiation stability of pellets.

Fission fragments (iodine) cause corrosion of the fuel elements and render them inoperative. The fuel element vibration and fretting corrosion may also render them inoperative. Reduction of the water flow velocity in passages between the fuel assemblies eliminates the vibration.

The main aspects of improving the reliability of the fuel elements with UO_2 are listed in Table 7.10.

Fuel Elements. Figure 7.13 shows the fuel element utilized in the Hanford natural-uranium reactor. A uranium rod 35.5 mm in diameter and 204 mm long is placed in aluminum cladding which is

TABLE 7.10 Main Aspects of Improving Fuel Elements

Improvement	Result
Hot vacuum drying of fuel elements	Removal of moisture from fuel, prevention of hydrogenation
Use of uranium dioxide pellets of increased density	Decreasing moisture sorption in manufacture, reduction of fuel consolidation in initial period of irradiation, prevention of gaps in fuel column
Increasing ductility of cladding (as a result of elevated annealing temperature)	Increased resistance to destruction in mechanical interaction of pellets with cladding, increased resistance to iodine corrosion
Use of internal counterpressure in fuel elements	Prevention of cladding crumpling, reduced interaction between fuel and cladding
Increased thickness of cladding	Compensation for loss of strength in high-temperature annealing of cladding, increase in rigidity of cladding and its preventive effect on deformation of fuel pellets
Optimization of pellet geometry on the basis of special design models	Decreased local deformation of cladding in mechanical interaction with pellets

soldered to the fuel rod with silumin solder. The cladding thickness including an 0.25 mm solder layer is 1.05 mm. At the ends the cladding is thickened to 8.9 mm (the dead end) and 8.4 mm (the end stopped with a welded on disk).

To fabricate a fuel rod a turned ingot of natural unalloyed uranium is forged to form a rolling billet. This breaks the casting structure. A rolling billet may be also prepared by pressing in the γ-phase region. Rolling into bars 37-38 mm in diameter is accomplished in the α-phase with heating. The bars are then straightened, cut, and after quenching from the β-phase brought up to the required size. Checked are the grain size and surface defects: cracks, pits, roughness, scores, tightness, gas-holes, poor soldering, solder-corroded areas on aluminum cladding, brittleness of the solder layer.

Fuel elements of gas-cooled reactors employ metallic uranium in the form of rods 29.2 mm in diameter and 1020 mm long, the thick-
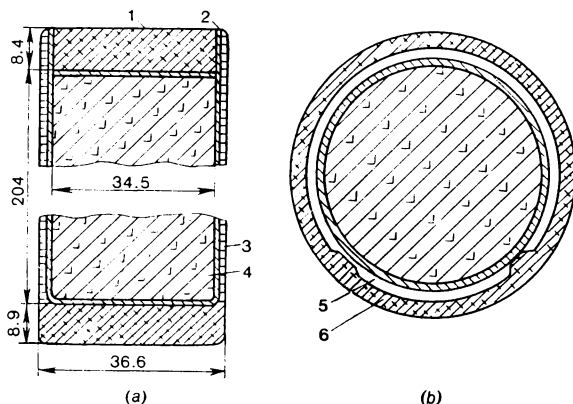
Fig. 7.13 Fuel element (a) and fuel assembly (b) of Hanford reactor
1—top cover; 2—welded seam; 3—aluminum cladding; 4—uranium block; 5—circular slit
for coolant (2.18 mm); 6—aluminum tubing

ness of magnox cladding is 1.83 mm. To improve heat transfer, clads
are made with helical fins 10.4 mm high. The end caps welded to the
clad are used to align the fuel element with the channel axis. In
service, the fuel element slightly increases in length and diameter.
Generally, these fuel elements are reliable in operation to the burnup
of several kilograms per ton of uranium.

The *fuel elements of water-cooled and moderated reactors* are assem-
bled into hexagonal bundles (see Fig. 1.5). In the reactors of the
BBЭP-210 and BBЭP-440 series, the fuel assemblies comprise an
outer casing and fuel elements spaced and supported by an upper
and lower tie plates of stainless steel. Spacer grids to suppress vibra-
tions are arranged between the top and bottom plates. The bail hand-
le is attached to top heads to withdraw the fuel assemblies out of
the reactor and lower them into it. The bottom ends have shanks to
fit and secure them in the barrel bottom. The upper plate allows
endwise motion of the fuel elements to compensate for thermal ex-
pansion. The fuel elements are filled with pellets of sintered UO_2
with free space at top to compensate for thermal expansion of the
fuel.   Starting with block I of the Kolsk APS series-production
BBЭP-440 reactors employ 312 operating fuel assemblies. Each
operating fuel assembly contains 126 cylindrical fuel elements 9.1 mm
in diameter arranged in a triangle plate and spaced at 12.2 mm, the
thickness of the tubular cladding is 0.6 mm. The fuel assembly with
fuel elements is given in Fig. 1.5. The burnup in the BBЭP-440
series reactors under stationary conditions is, on the average, 28.6 MW
day kg^{-1} at three partial refuelings per operating period. The clad-
ding material is an alloy of Zr with 1% Nb.

The core of the BBЭP-1000 series reactors is assembled of 151
hexagonal fuel assemblies 238 mm in width across flats. Each assem-

bly contains 317 fuel elements 9.1 mm in diameter with the UO_2 pellets and 12 guide tubes 7 mm in the outer diameter for absorbers. The burnup under stationary conditions is, on the average, 27 MW day kg^{-1} at two refuelings per operating period. Provision has been made to use in future a burnup up to 40 MW day kg^{-1} at three refuelings per operating period.

Fuel elements of channel-type reactors of Beloyarsk APS. The fuel channels (see Fig. 1.4) contain tubes and fuel elements arranged in graphite and metallic tubes forming a cylinder 75 mm in diameter, 13.6 m in length at evaporating channels and 12.9 m long at steam superheating channels. A channel contains six fuel elements. The outer diameter of the fuel element is 20 mm, the dimensions of an internal tube passing the reactor coolant are 9.4×0.6 mm for the first reactor and 12.0×0.6 mm for the second. The cladding material is stainless steel. The nuclear fuel is an alloy of U with 9% Mo with magnesium aggregate to provide a thermal contact. The average burnup is 22.2 MW day kg^{-1}.

Fuel assemblies of Leningrad APS. This fuel assembly consists of 18 fuel elements with a heat release part 3.5 m long. The fuel element is a tube of zirconium alloy with 1% Nb, 13.6 mm in the outer diameter and 0.9 mm thick filled with the UO_2 pellets. The burnup is 18.5 MW day kg^{-1}.

Fuel elements of fast neutron reactors. In the neutron reactors, the fuel elements operate under very severe conditions. The neutron flux in fast neutron reactors is 10^{15}-10^{16} cm^{-2} s^{-1}, and the neutron fluence is 10^{23} cm^{-2}. The heat flow density reaches $1.25 \cdot 10^7$ kJ m^{-2} h^{-1} and the burnup is 5-10%. Operating media may be liquid metals moving at a flow rate of 7-10 m/s at 773-873 K.

The core of the БH-350 series commercial fast reactor comprises hexagonal bundles 96 mm in width across flats. The core bundles include fuel elements filled with oxide of enriched uranium to a height of 106 cm (by fuel). The top and bottom of the bundle carry the end shield elements containing oxide of depleted uranium. The total height of a bundle is 3.5 m. The fuel elements are made of stainless steel in the form of tubes 5 mm in diameter with a wall thickness of 0.4 mm. The cladding has strength sufficient to withstand thermal and tensile stresses arizing from internal pressure generated by the gaseous products of fission at the end of the operating period.

The fast neutron reactor "Enrico Fermi" utilizes the radiation-stable γ-phase of U-10% Mo alloy as a nuclear fuel material. The fuel elements are made by joint extrusion of the fuel and cladding of a zirconium alloy.

Thermoelectric and thermionic fuel elements. Recently methods have been developed to convert heat energy of fission directly into electric energy. With this method, semiconductor thermocouple elements assembled into batteries are built into the core. In the

"Romashka" series reactor, the thermocouples based on semiconductors of silicon-germanium alloys utilize heat of the fuel element cladding. Heat from the cold end of the thermoelectric battery is removed via a finned sink. In reactors of other design, thermoelectric batteries receive heat from coolant of circuit I.

In reactors with thermionic energy conversion, the cathode emitting electrons when heated to 1773-2473 K is a fuel element operating at a cesium vapor pressure of 0.013-0.133 Pa. The cathode material should have high conductivity, low rate of evaporation, good emission characteristics, high corrosion resistance in vapors of cesium, and sufficient strength. When monocarbides of uranium and zirconium were used as solid solutions without cladding, swelling and cracking of the cathode and evaporation of uranium carbide were observed. Tungsten and molybdenum claddings improve the operation of plants employing thermionic converters. An essential role in the reliability of the plants play the insulation materials, and also the corrosion resistance of insulating and cladding materials in the cesium vapor.

Serious problems arise in selecting the materials and design of fuel elements, when a nuclear reactor is used for heating up plasma in magnetohydrodynamic generators.

Fuel elements of nuclear rocket engines operate under severe conditions. In the reactors, the working medium is hydrogen heated to a temperature above 2273 K. The fuel element material must be radiation stable and corrosion resistant, have enough strength at operating temperatures, and be capable of standing up abrupt changes in temperature inavoidable in rapid starts of nuclear rocket engines.

The most refractory materials may be divided into three classes: metals, refractory (ceramic) materials, and graphite. Refractory metals are Ta, Mo, W, Re, Os, and others. Metals of the platinum group (Os and others) are expensive and not susceptible to manufacture; Ta absorbs hydrogen at 620-920 K and embrittles. Tungsten and molybdenum recrystallize at a temperature relatively low with regard to their melting point. The recrystallization leads to grain growth and embrittlement. The maximum operating temperature for molybdenum is 2073 K. Adding uranium dioxide to tungsten, decelerates diffusion through the boundaries between grains and suspend their growth. The strength of tungsten must drop abruptly at a temperature above 2223 K.

Nitrides of refractory metals are brittle below 1673 K. Above 2493 K they tend to decompose and carburize. Tungsten and zirconium borides are stable to 2773 K and can be utilized as structural materials operating in compression. Natural boron contains, however, nuclide ^{10}B having a large cross-section of thermal neutron capture. Carbides of refractory metals are stable in a reducing atmosphere at a high temperature. The melting point of tantalum and zirconium

carbides is above 3153 K. Niobium carbide may be used at 3503 K.

At room temperature, graphite is less strong and ductile than metals. However, it remains strong to about 2773 K, and at this temperature its strength approximates that of tungsten. Graphite becomes more and more ductile with temperature and does not melt to the sublimation temperature equal to 4198 K at the atmospheric pressure. At this temperature its strength drops to zero. Graphite has good thermal conductivity and high specific heat.

The fuel elements of the "Kevy L." engine are graphite plates 203 mm long, 6.3 mm thick, and 195-203 mm wide containing dispersed uranium dioxide. The plates are made from a mixture of uranium dioxide and unsintered graphite. In other reactors, the fission matter in the form of uranium carbide particles 10 to 20 μm in size is protected by a coating of pyrolitic graphite and dispersed in a matrix of graphite. The matrix is protected by a coating of niobium carbide applied by thermal decomposition of niobium chloride.

8

8.1 Beryllium

Physical Properties. The whole complex of the physical properties makes beryllium one of the most attractive and promising reactor materials. It has a low thermal-neutron absorption cross section (Table 8.1). The combination of low absorption cross section and

TABLE 8.1 Physical Properties of Beryllium

Atomic number	4
Atomic weight	about 9
Thermal-neutron absorption cross section, m^2	$9 \cdot 10^{-31}$
Density, g/cm^3	1.85
Melting point, K	1556
Coefficient of linear expansion, deg^{-1}	$11.6 \cdot 10^{-6}$
Boiling point, K	3243
Coefficient of thermal conductivity, $W\ m^{-1}\ K^{-1}$	180
Crystal structure	α-phase, HCP up to 1513 K β-phase, BCC above 1513 K
α-Phase lattice parameters, nm	$a = 0.228$ $c = 0.358$

high scattering cross section and a great number of atoms per 1 cm^3 makes beryllium an excellent moderator and reflector material. Its use decreases a critical fuel charge. Its wide use, however, is limited by a number of circumstances. Beryllium is a scarce and costly metal. Its cost is almost one hundred times that of aluminum, magnesium, and steel. Beryllium is brittle. Irradiation causes embrittlement and swelling. The manufacture of thin-walled claddings of fuel elements from beryllium and, in particular, their sealing are very difficult. Its positive properties include a low density, a relatively high melting point, and a low coefficient of thermal expansion (see Table 8.1). Up to 1513 K, beryllium does not undergo allotropic transformations and crystallizes in the HCP lattice. The absence of structural modifications within a wide temperature range makes beryllium insensitive to cyclic changes of temperature. Beryllium and its compounds are extremely toxic. Metallic beryllium
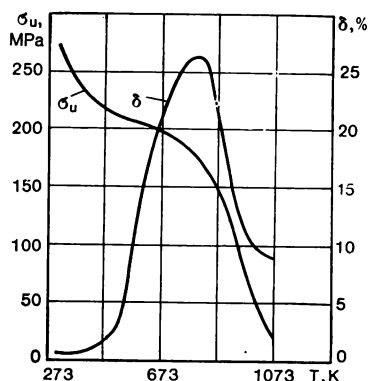
Fig. 8.1 Ultimate strength σ_u and elongation δ of hot-worked beryllium versus temperature. Grain size 50 μm

is prepared by thermal reduction of beryllium oxide with magnesium, or by electrolysis.

Beryllium items are made by metalloceramic metallurgy. Powders are hot pressed into blanks which are then extruded, hot rolled, rotary swaged into bars, tubes, sheets and other shapes.

Mechanical Properties. Mechanical properties of beryllium, especially its ductility, depend essentially on temperature (Fig. 8.1). Its ductility abruptly drops when the temperature decreases below 573-473 K. This is the so-called *cold shortness threshold*. The threshold may be displaced by 323-373 K to a lower temperature by removing impurities from beryllium and mainly by obtaining finer grains. However, whatever the technique, the cold shortness threshold of quasiisotropic polycrystalline beryllium cannot be displaced below room temperature, i.e. we cannot prepare beryllium ductile at room temperature. Prolonged annealing at 1023-1073 K and very slow cooling down eliminates the ductility drop at 873-1073 K. This releases the beryllium intermetallic compounds at the grain boundaries.

In extruding beryllium, the basal planes of the hexagonal lattice orient parallel with the direction of extrusion. Such a texture causes drastic anisotropy of beryllium properties. The beryllium ductility increases along the extrusion axis and decreases in the transverse direction. Tubes of beryllium can be manufactured from cast blanks by impact extrusion. After recrystallization annealing to fine grain, the tubes have high longitudinal ductility and sufficient (1-2%) transverse ductility. Alloying beryllium with calcium in an amount of 0.4% somewhat improves the properties of tubes. Because of low ductility the components of moderators and reflectors are not designed to withstand considerable loads. The decrease of beryllium ductility under irradiation is not so dangerous.

Radiation Stability. Irradiation of beryllium causes nuclear reactions with the formation of gaseous products:

$^9Be + n \rightarrow {}^4He + {}^6He;$

$^6He \rightarrow {}^6Li + \beta^-;$

$^6Li + n \rightarrow {}^4He + {}^3H.$
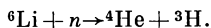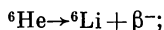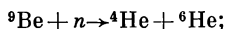
Helium and tritium may accumulate in pores and form gas bubbles causing gas swelling. The intrusion of helium and tritium into the crystal lattice of beryllium affects its ductility. Table 8.2 illu-

TABLE 8.2 Effect of Irradiation at 703 K on Mechanical Properties of Beryllium (fast neutron fluence 10^{21} cm^{-2})

Testing temperature of irradiated and starting specimens, K	σ_y, MPa		δ, %	
	starting	irradiated	starting	irradiated
298	340	670	3	0
473	300	560	35	5
573	270	440	45	26
703	190	350	40	25
873	130	190	17	5

strates changes produced in beryllium by irradiation. Irradiation increases strength and decreases ductility of beryllium.

At a neutron fluence of 10^{20} cm^{-2} and irradiation temperature of 973 to 1023 K, gas swelling is small and does not exceed 1-2%. At 1073-1173 K, gas swelling is 3-5%. At the above neutron fluence, beryllium may be used in reflectors and moderators up to 973-1073 K.

Compatibility. When the oxide film covers uranium and beryllium they are compatible to 873 K. When the oxide film on beryllium is not continuous the metal is compatible with uranium up to 773 K. At 773 K, beryllium is incompatible with Fe, Ni, Zr and compatible with Al and Mg.

Corrosion Resistance. The normal potential of beryllium is —1.85 V. The corrosion potential of beryllium is —0.8 V. This indicates that beryllium is capable of passivating. In neutral media containing no chlorides and sulfates, beryllium passivates within a wide range of potentials. In water of high purity beryllium is stable. The corrosion product is beryllium oxide white in colour. It well stands out on the metal surface making an impression that beryllium has badly corroded. Water in motion washes away the products of corrosion, creating an impression that a water flow essentially adds to the beryllium resistance. In highly pure water, beryllium is efficient to 423-473 K. At this temperature, a dark oxide film forms on the metal surface. At 573 K, the beryllium resistance decreases

and becomes essentially dependent on the metal quality. As this happens, pitting takes place. Alloying beryllium with iron somewhat increases its resistance to attack. When beryllium is used at a water temperature of 573 to 623 K, it is canned with zirconium alloys. The presence of chlorides and sulfates in water, and also an increase in pH of the environment to 10-12 abruptly reduce the beryllium resistance. Contacting aluminum practically has no effect on the beryllium resistance to corrosion, whereas the contact to stainless steel somewhat decreases it. In highly purified water, the cyclic changes in temperature produce beryllium stress corrosion. The formation of oxide films on beryllium surface by the anodic oxidation technique adds to beryllium resistance.

At a pressure of a few dozen megapascals beryllium is efficient in dry oxygen up to 923 K, in steam and wet oxygen up to 873 K, and in carbon dioxide up to 973 K. At 773 K, beryllium is resistant in sodium containing up to 0.01% O_2. At 873 K, beryllium is efficient in lithium and eutectic Pb-Bi.

Beryllium Oxide. Beryllium oxide may find its application as a reflector material. Its melting point is high, 2823 K. Beryllium oxide is a good insulator. As the case is with most of ceramic materials, the compression strength of beryllium oxide is several times its tensile strength. Its relatively high thermal conductivity improves the thermal resistance. Items of beryllium oxide are made by pressing, extrusion, and casting. Uncalcinated beryllium oxide is cut by wetted abrasive wheels, sintered beryllium oxide, by diamond wheels. Beryllium oxide is resistant in water at 573-623 K, does not interact with air and carbon dioxide up to 773-873 K. At 873 K, sodium impregnates an insufficiently dense beryllium oxide and destructs it. Neutron irradiation produces gas swelling in and cracking of beryllium oxide accounted for by the accumulation of helium and tritium. Beryllium oxide is used in research reactors as a moderator and reflector.

8.2 Graphite

Graphite is one of the crystalline modifications of carbon. The latter exists in the form of two stable isotopes with mass numbers 12 (98.892%) and 13 (1.108%).

Physical Properties. Graphite is widely utilized in thermal neutron reactors as a moderator and reflector. The thermal-neutron absorption cross section of graphite is less than that of beryllium and magnesium (Table 8.3). Preparation of the reactor-grade graphite is not a difficult problem from the technical point of view. Graphite possesses good thermal properties, sufficient strength and good machinability. High thermal conductivity and low coefficient of linear expansion enable graphite to resist well the thermal shocks.

TABLE 8.3 Physical Properties of Graphite

Atomic number	6
Atomic weight	12
Thermal-neutron absorption cross section, m^2	$4.5 \cdot 10^{-31}$
Density, g/cm^3	1.65-1.75
Melting point, K	Sublimate at 0.1 MPa and 3923 ± 25 K
Coefficient of linear expansion, deg^{-1}	$(28-44) \, 10^{-7}$
Coefficient of thermal conductivity, $W \, m^{-1} \, K^{-1}$	263.8-523.5
Crystal structure	Atoms are hexagonally arranged in planes
Parameters of crystal lattice, nm	$a = 0.246$ $c = 0.670$

Its application is hindered, however, by a low resistance to oxidation and high brittleness. Besides, neutron irradiation damages the graphite lattice, which affects its physical properties.

The graphite properties essentially depend on the source material and preparation technique. The graphite purity considerably depends upon the purity of the source products. The reactor-grade graphite must contain ash not more than 0.054-0.16% and boron, not more than $4 \cdot 10^{-5}$%. In case of gas purification these values may be reduced to $5 \cdot 10^{-4}$ and $6 \cdot 10^{-6}$%, respectively. Treating graphite with gaseous chlorine increases the chlorine content in graphite. This contaminates the reactor interior in service with chlorine. At a high temperature graphite sublimates rather than melts. The lattice of graphite does not change till the sublimation point.

The perfect crystals of graphite consist of parallel atomic layers (Fig. 8.2). In each layer graphite atoms form a hexagonal network. The interatomic distance in a layer is equal to 0.142 nm. The layer-to-layer distance is 0.335 nm. The layers are shifted in their plane so that above and under the center of each hexagon in the adjacent layers lies an atom of graphite. Any hexagon in each third layer is above the corresponding hexagon in the first layer. The lattice parameters of graphite are given in Table 8.3. The laminar structure of graphite forms in the graphitization annealing at about 3353 K. The crystalline layers move sufficiently freely relative to one another. Therefore, the graphite properties essentially depend on the crystallographic direction.

The theoretical density of graphite is 2.27 g/cm^3, while the density of the reactor-grade graphite lies within 1.65-1.75 g/cm^3. This difference is accounted for by the porosity of the reactor graphite which makes up about 20 to 30%. As a rule, pores communicate with one another, and for this reason graphite passes gases. The thermal conductivity of graphite differs but little from that of many metals. Heat

0.1nm
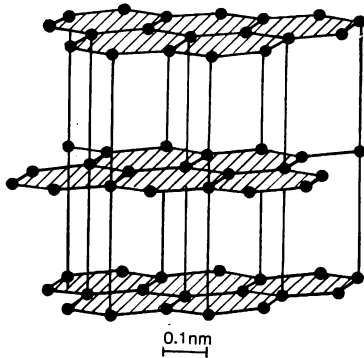
Fig. 8.2 Graphite structure

flows in graphite mainly along the basal planes located predominant-
ly parallel with the axis of extrusion.

Mechanical Properties. The mechanical properties of gra hite
depend essentially on the crystallographic stress. In the close-packed
planes carbon atoms are bonded to one another by strong covalent
bonds, while the planes themselves are bonded only by relatively
weak forces.

In uranium-graphite reactors, the graphite blocks are arranged so
as to leave space for channels running through the graphite. There-
fore, the main requirement imposed on the reactor graphite is that
it must have enough compression strength to withstand the weight
of the above arranged graphite blocks. Thus, the compressive strength
(σ_u, MPa) of graphite prepared by the electrode technology with
finely divided filler depends on density (γ, g/cm^3) as follows:
$\sigma_u = 232 + 166\gamma$. Its tensile strength at room temperature varies
from 7 to 21 MPa and bending strength, from 7 to 30 MPa. The com-
pression strength is generally 21-35 MPa. The graphite strength
increases with temperature. Up to 2273 K, the strength grows ap-
proximately linearly. At 3073 K, the strength reaches its maximum
and is about twice that at room temperature. An increase in strength
with temperature is associated with the removal of heavy internal
stresses arising in graphite following cooling from the graphitiza-
tion temperature. The stresses arise from a great difference in the
coefficients of thermal expansion along axis c and across it. The
higher the graphite density, the greater its strength.

In the region of high temperatures, items of graphite deform under
sustained stresses, i.e. graphite creeps. The creep rate of graphite
is high at temperatures close to 2273 K. Under irradiation, however,
graphite noticeably creeps at lower temperatures. In short-term tests
at a constant temperature, the creep rate is proportional to the square
of the stress applied. Removal of stress partially recovers the speci-

men length. Removal of stress restores about 30% of the total amount of deformation attained in testing at 2836 K.

The test medium has a material effect on the results obtained. In particular, decreasing the argon pressure abruptly increases the creep rate. The rate of steady-state creep (v, cm^{-1}) may be evaluated by the following dependence:

$$v = 40 \ (\sigma/\sigma_u)^{3.8} \exp \ (-Q/RT),$$

where σ is the tensile stress; σ_u is the ultimate strength; $Q = 209$ kJ/mole.

Graphite Oxidation. At high temperatures, graphite is sufficiently reactive. Graphite, however, is compatible with solid substances up to high temperatures, when carbon notably diffuses into metals and carburizes the metals and alloys, or reduces them in chemical interaction. The problem of graphite compatibility reduces to the problem of its interaction with the reactor coolant. The rate of graphite interaction with gases is usually determined by the relative change in the mass of the specimens. The influence of specific surface is neglected, though it is known that it changes in oxidation. The most popular and promising gases for cooling reactors are helium, nitrogen, carbon dioxide and air. Helium does not interact with graphite even under irradiation. At about 2273 K, a helium flow transfers the mass of graphite because of the graphite particles spalling. Such erosion usually stops when all loose particles have been removed from the bulk material. Impurities in helium, e.g. oxygen, may cause graphite corrosion.

Graphite corrosion is a complex physicochemical process which may be conventionally divided into several stages: (1) delivery of an oxidant to the graphite surface by means of the molecular convective diffusion; (2) adsorption of the oxidant molecules on the graphite crystals; (3) interaction of the adsorbed oxidant with the surface atoms of carbon at active centres with the formation of the complex C_xO_y; (4) decomposition of the complex C_xO_y with the formation of CO and CO_2 and their removal into the gaseous atmosphere.

Below 773 K, the rate of corrosion is determined by the rate of chemical reaction. When oxygen freely reaches the reaction surface, the gas flow velocity produces no essential effect. At $T > 973$ K, the rate of graphite burning begins to be limited by the oxidant diffusion towards the reaction surface. Then, the graphite oxidation rate K (g cm^{-2} s^{-1}), depends but little on temperature. Thus, with commercial graphite, the following data have been obtained at an oxygen concentration of 0.1% and gas flow rate of 3.8 l/h:

T, K	723	823	873	973	1073
$\log K$	−9.50	−8.50	−8.30	−8.08	−8.05

In the diffusion stage, the reaction products (CO_2 and CO) accumulate at the graphite surface displacing oxygen. Therefore, increasing the velocity of the gas medium movement enhances the oxygen delivery towards the surface and hence augments the graphite oxidation rate. This is illustrated by the data obtained at 1000 K and oxygen concentration of 0.005%:

Gas flow rate, l/h	0.85	1.7	2.9
$\log K$	−9.6	−9.3	−9.1

At 1073 K and gas flow rate of 3.8 l/h, the oxidation rate of graphite versus the oxygen concentration in the gas phase (C_{O_2}, %) is expressed by the following equation:

$$\log K = -7 + 0.95 \log C_{O_2}$$

The graphite oxidation rate decreases with density in the same manner, as impurities of Fe, V and Na intensify the graphite oxidation with an increase in temperature of thermal treatment. In the presence of impurities oxidation proceeds locally. Increasing the degree of graphite purity decreases the rate of its oxidation.

Graphite does not practically interact with molecular nitrogen. The basic product of graphite interaction with hydrogen at 573-1273 K is methane. In the presence of graphite, the equilibrium concentration of methane decreases with temperature and approximates zero at 1273 K and 0.1 MPa. Irradiation ionizes hydrogen and facilitates the methane formation. The presence of water vapors in the reactor medium enhances the graphite oxidation.

Sometimes to evaluate the resistance of a graphite stacking to oxidation use is made of burnup equal to the fraction of oxygen that has reacted with carbon when passing over the graphite surface. In helium containing 0.22% (by volume) O_2, with the graphite surface area of 0.22 m² and gas flow rate of 1.1 l/min, the burnup at 673 and 973 K is 0.1 and 0.8, respectively.

Graphite reacts with CO_2 as follows:

$$C + CO_2 = 2CO.$$
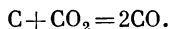
If some other reaction makes the CO concentration exceed the equilibrium concentration of the reaction in question, the intensification of the reverse reaction

$$2CO \rightarrow C + CO_2$$
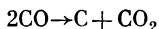
produces carbon deposition. At 673 to 773 K, the graphite deposition is inconsiderable.

When irradiated at 323 K by a neutron fluence of $5 \cdot 10^{20}$ cm⁻² graphite oxidizes in the air at 873 K seven times as quickly as the non-irradiated. Irradiation at 573 to 623 K by a fluence of $1.5 \cdot 10^{21}$ cm⁻² does not increase the rate of oxidation. Above 1073 K,

preirradiation of graphite has no effect on the oxidation rate. This is associated with the annealing of the radiation defects.

Irradiation of the gaseous atmosphere ionizes molecules, which also affects the kinetics of graphite oxidation. This is observed at a γ-radiation dose rate of above 154.8 Ci kg^{-1} s^{-1}. The oxidation rate becomes 2.6 times its previous value.

Protection from Oxidation. To protect the graphite stacking of a reactor operating at 973-1073 K against corrosion, one has to reduce the volume content of oxygen in the gaseous atmosphere to 0.05-0.10%. The H_2O content should not exceed 1%. It is also recommended to inject at regular intervals into the gas the compounds liable to pyrolysis, such as CO, CH_4, illuminating gas. The pyrolysis produces a protective layer preventing oxidation.

The oxidation reaction involves primarily the graphite energetic atoms. In other words, oxidized first are active sites in the lattice. If they are occupied, for example, by the adsorbed atoms of certain elements, these sites will be excluded from further interaction. To this end, various phosphorous-containing substances may be suggested for use. When heated to a certain temperature, they decompose leaving adsorbed phosphorous on active places of the lattice, and this decreases the oxidation rate. Generally, items of graphite are impregnated with a phosphorous-containing substance and quickly calcinated at 1073-1473 K in an inert atmosphere. Used as phosphorous-containing substances are both organic and inorganic compounds: phosphoric acid, trimethylphosphate, etc. This treatment reduces graphite mass losses in oxidation to 1/2 to 1/3 of its previous value.

To increase the graphite resistance to oxidation use may be made of mixtures composed of compounds of the phosphate glass type. To form phosphate glass, the graphite items are treated at the temperature of phosphate glass formation following the impregnation with a solution containing the required constituents. A film of phosphate glass protects graphite well against oxidation within 773-1223 K. The oxidation rate reduces nearly by two orders. Under irradiation, protective coatings of phosphates are ineffective. This is associated evidently with an increase in the activity of the gas-oxidant under irradiation. As a result, it may interact with carbons located not only in active places. After irradiation has been ceased, the coatings start again to protect the graphite from oxidation, which indicates that the coating remains intact under irradiation.

Graphite practically does not interact with eutectic Pb-Bi below 973 K. When liquid sodium is used as a coolant in a reactor with a graphite moderator, two problems arise: transfer of graphite mass and penetration of sodium into pores of graphite.

When interacting with graphite, sodium forms a compound with a laminated structure. Sodium, evidently, occupies the space between

the close-packed layers, each eighth interplane space being occupied. The average distance between the close-packed planes increases by 5%. This causes graphite expansion and cracking. Carbon transfer by sodium produces the carburization of the austenitic stainless steel, or the carbon precipitation from the coolant in the colder parts of the system. If graphite is not treated as required, or its surface is not protected against ingress of sodium, the latter must be separated from graphite by a metallic cladding, say, of a zirconium alloy. In this case one should take into account the gas formation in the cladded blocks of graphite.

Radiation Stability. Irradiation of graphite with energetic parti- cles affects its physical and mechanical characteristics and size. This is associated with the deformation of the graphite crystal lattice. Irradiation produces vacancies and interstitials. They form complex- es of 3 to 6 atoms each. Dislocation loops also form. This increases the size of the graphite unit cell in direction c and decreases the latti- ce parameter a in proportion to the irradiation fluence. An increase in the lattice, constant along axis c in irradiation of graphite is asso- ciated with the introduction of interstitials or their complexes into the interplanar space of graphite. Compression of the lattice along axis a is caused, probably, by its relaxation at vacancies. Increasing the irradiation temperature eliminates the radiation defects, i.e. vacancies, and interstitials recombine. This decreases the deforma- tion of the graphite lattice. Thus, at a neutron fluence of $2 \cdot 10^{20}$ cm^{-2}, an increase in the irradiation temperature from 333 to 573 K, decreas- es the elongation along axis c to 1/50th of its previous value. At a low temperature, the relative change of parameter c under irradia- tion does not exceed 15%.

The main consequence of the graphite lattice deformation under irradiation is a change in its macrodimensions. In polycrystalline graphite rods manufactured by extrusion with subsequent sintering, axis c is generally arranged in the radial direction and axis a, in the longitudinal direction. Changes in the parameters of lattice under irradiation lead to anisotropic changes in the dimensions of graphite items. Macroscopic swelling corresponds, but not completely, to the increasing of graphite lattice, since the crystallographic expan- sion is partially compensated for by filling of existing pores. When the temperature is increased up to 673-773 K and more, pore filling and additional sintering exceed the growth of crystal cell and com- press the polycrystalline graphite. The effect of irradiation temperatu- re manifests itself in relative swelling of graphite bricks over the height of reactor stacking (Fig. 8.3). Though the neutron flux density is the greatest in the middle of the stacking height, swelling here is the lowest because of a higher temperature. The highest growth is observed at the inlet, colder end of the stacking. Another specific feature is that the radiation defects aggregate in the graphite bulk
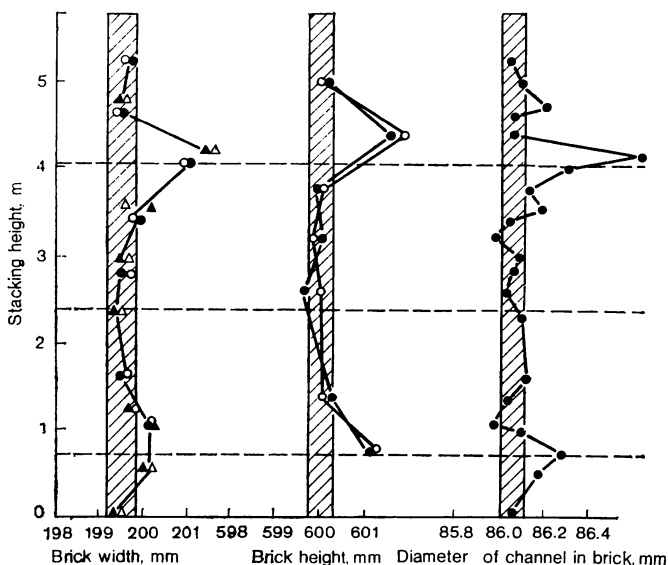
Fig. 8.3 Deformation of graphite in reactor channels

non-uniformly. Defects form predominantly on the side adjacent to the source of fast neutrons, i.e. fissile uranium. In the graphite layers neighboring the fuel element, thermal conductivity decreases to 1/40th of its previous value.

Irradiation increases the graphite creep. In the absence of irradiation graphite does not creep below 423 to 473 K. In irradiation with a neutron fluence of 10^{20} cm^{-2} at 353 K, creep at 10 MPa is 0.7-0.8%. Irradiation decreases the graphite thermal- and electrical conductivity.

Wigner Energy. Irradiation displaces atoms from their normal positions in the lattice. As a result, latent energy accumulates in graphite. This is known as the Wigner effect. The energy may be released as heat, when graphite is heated to a temperature which exceeds the temperature of irradiation. In this case, temperature increases in annealing graphite irradiated at a lower temperature. Graphite annealing in low-temperature reactors is accomplished in order to remove the radiation defects, for, say, deformation of the graphite stacking or bushings may interfere with the reactor operation. Radiation defects may be corrected by simple heating. This may be accomplished in several ways:

(1) Changing the coolant circulation to increase the graphite temperature within certain limits.

(2) Increasing the graphite temperature by nuclear or electrical

heating until energy starts to release by itself, and this gradually involves the whole moderator.

(3) Slowly heating and removing a certain amount of released energy in order to avoid its spontaneous liberation. It should be remembered that, if heating at 373 to 473 K occurs too rapidly and the released energy is not removed, the graphite stacking may overheat considerably.

Radiation damage to the graphite lattice changes the graphite mechanical properties. With an increase in the neutron fluence, the compression and bending strengths pass through their maxima, increasing at a fluence of 10^{20} cm^{-2} 3-3.5 times and at a fluence of $2 \cdot 10^{20}$-10^{21} cm^{-2}, 2-2.2 times as compared with the initial value. The highest increase in the mechanical characteristics at small fluences should be attributed to blocking of dislocations having the Burgers vector located in the basal plane. This interferes with the displacement of crystal parts relative to one another. The dislocation blocking is evidently caused by the defects of a small size. The higher the irradiation temperature, to the lesser degree the graphite strength increases at the same fluence of neutrons. It is supposed that at a higher temperature some vacancies recombine and interstitials aggregate. Both factors reduce the probability of the dislocation blocking, and this decreases the graphite strength.

8.3 Control and Shielding Materials

To the elements having high absorption cross sections may be referred Gd, Sm, Eu, B, Cd, Dy, Ir, Hg, In, Er, Rh, Tm, Lu, Hf, Au, Re, and Ag. By no means all of them may be used in the control system of power reactors. Cadmium possesses bad mechanical properties; Au, Re, Rh, and Ir are too expensive. Mercury is a liquid and its utilization in a control system involves a number of difficulties. Hafnium may be used in the elementary form; silver to improve physical and mechanical properties is employed in the form of an alloy with indium and cadmium. The other elements find their applications as oxides or oxide mixtures usually dispersed in a metallic matrix. Boron is used as a carbide in a metallic or ceramic matrix, and also as an alloying element to be added to stainless steel, zirconium, and titanium. In most cases, control rod materials can operate in the reactor core only in a cladding. Hafnium and stainless steel alloyed with boron can be utilized without protective coverings. At present, the control rods most often use boron in the form of carbides and alloys, boron-alloyed steel, hafnium, silver alloy with indium and cadmium, rare earths dispersed in metallic matrices.

Boron Compounds. Of boron compounds boron carbide B_4C is used most often. This is a high-melting material of a theoretical

density of 2.51 g/cm³. Its actual density is 2.4 g/cm³. Boron carbide is brittle but possesses a high resistance to heat. In case of damage to the cladding, carbide slowly dissolves in water. Defects of the carbide lattice caused by irradiation with neutrons are partially annealed at 973-1173 K. The introduction of helium produced by the nuclear reaction

$$^{10}B + n \rightarrow {}^7Li + {}^4He$$
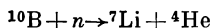
into the crystal lattice also distorts it.

Helium accumulating in pores at high temperatures locally increases pressure in the gas space and generates local stresses and cracks. Another product of the reaction is lithium. Lithium present in a boron-containing material affects its resistance to corrosion as it actively reacts with water.

When boron is added to alloyed steel its amount should not exceed 3%. A higher content of boron makes steels extremely brittle and poorly machinable. For example, adding 2% of boron to steel reduces its elongation to about 1/10th of the initial value . The accumulation of helium under neutron irradiation may cause cracking of steel alloyed with boron. Up to 90% burnup of boron, stainless steel is sufficiently corrosion resistant and radiation stable and may be used without a protective coating. Somewhat lower is the corrosion resistance of titanium alloys boron-alloyed to 1.7%. Zirconium alloys alloyed with 2% of boron are not resistant in water at 573-633 K. Alloying with boron reduces ductility of titanium and zirconium. Irradiation enhances this effect.

Along with alloys, dispersion materials are widely used for the manufacture of control rods. Dispersion materials include boron carbide dispersed in aluminum (boral), stainless steel, titanium, and zirconium. Compared to alloys, dispersion materials possess a higher radiation stability.

Hafnium. Hafnium and its alloys may be used in control rods without claddings. Corrosion resistance of hafnium surpasses that of zirconium. Hafnium is more ductile than zirconium and excels it in strength. It is advisable to use hafnium for the absorption of epithermal neutrons. Its thermal neutron absorption cross section is relatively small. Therefore, to absorb a considerable amount of neutrons relatively bulky rods are required.

Silver Alloys. A silver alloy containing 15% In and 5% Cd can be used as an absorbing material. As a neutron absorber, the alloy is comparable with hafnium and surpasses the Ag-30% Cd alloy. When absorbing neutrons, silver is converted into cadmium, part of cadmium into indium, and indium, into tin. Therefore, prolonged irradiation changes the composition of the alloy. The alloy is resistant in water having pH = 9-10.5 at 538 K. No contact corrosion of this alloy paired with stainless steel is observed. After irradiation

15*

with a neutron fluence of $1.4 \cdot 10^{21}$ cm^{-2}, the dimensions of specimens and their structure do not change.

Rare Earths. A rare earth element europium is advisable to be used for the manufacture of control rods effective for a long period of time. Nuclides formed following capture of neutrons in such a rod have a large absorption cross section. Therefore, the rods containing europium are effective for a long period of time. However, it should be noted that europium is extremely expensive.

Gadolinium may be added as an alloying element to stainless steel and titanium alloy. The alloys with a gadolinium content of up to 25% are highly corrosion-resistant in water up to 633 K. The hardness and brittleness of stainless steels containing gadolinium increase with the content of the latter. The corrosion resistance of titanium alloys lowers with increasing the concentration of rare earth elements.

For reasons of economy it is advisable to use rare earth elements in the form of less expensive oxides. A mixture of rare-earth element oxides is least costly. Rods of oxides of rare earth elements are made by the powder metallurgy technique: extrusion with subsequent sintering. Rods of rare earths usually operate in claddings of stainless steel.

Rare-earths may be dispersed in a matrix of stainless steel. Along with oxides, borides of rare-earth elements may be utilized in control rods. These compounds are inert and very hard.

Burnable Poisons. Materials having a large neutron absorption cross section are used as burnable poisons and for power control. They may be introduced into the reactor core for life. As the reactor operates, the nuclear fuel is consumed and the number of absorber nuclei decreases as a result of nuclear reactions proceeding with the absorption of neutrons. Two processes take place concurrently: decrease in the total level of reactivity due to a burnup of nuclear fuel and release of excess reactivity compensated for at first by a surplus amount of absorber. At a certain rate of the absorber burnup, the reactor becomes critical following prolonged operation of the core. A smaller fraction of reactivity should be compensated for by means of control rods. In most cases, ^{10}B serves as a burnable poison. Its compounds are dispersed in aluminum, stainless steel, graphite, etc. In addition to boron, Hf, Eu, Gd, Sm, Cd, Hg may perform the functions of an absorber. A burnable poison homogeneously mixes with a nuclear fuel. This, however, may produce an objectionable change in the nuclear fuel and hinder its subsequent regeneration.

Shielding Materials. A nuclear reactor is a source of neutron, α-, β-, and γ-radiations. Therefore, measures must be taken to protect the personnel. To this end, the reactor must be shielded with the materials capable of absorbing the radiation energy. Protection

against α- and β-radiations is not difficult. The path of these partic-
les in the solid matter and in the air is so short that no special pro-
tection is required. Quite different is the case with neutron- and
γ-radiations as their penetrating power is high. The ability of ma-
terials to absorb neutrons essentially depends upon the energy of
neutrons. To capture neutrons, their energy must be reduced com-
pared with that of neutrons released in fission of nuclear fuel.

The reactor shielding system must meet the following require-
ments:

(1) It must thermalize the neutrons.

(2) It must absorb moderated neutrons (if the thickness of the
shielding layer is the lowest, the shielding materials must have
a considerable thermal neutron absorption cross section).

(3) It must effectively absorb penetrating γ-rays.

When selecting shielding materials one must take into account
not only their physical properties, but also economic indices and
susceptibility to manufacture. To provide effective absorption of
γ-rays it is advisable to use high-density metals.

Therefore, the reactor shielding must provide attenuation of
neutron energy, and absorption of neutron- and gamma-radiations.
The neutron energy attenuation is their moderation. The character-
istics of the moderator materials have been considered above. From
the theoretical standpoint any material, that is an effective modera-
tor of neutrons, may be utilized in the reactor shielding system. When
solving actual problems one has to take into account not only the
physical properties but also other characteristics of materials.

High moderation ability, convenience of use in the shielding
system, and low costs make hydrogen an especially suitable compo-
nent of materials utilized in shielding systems. In swimming-pool
reactors, water performs a twofold function of moderation and
shielding. A number of power reactors employ water shielding tanks.
In certain cases, however, the use of water as a material shielding
the reactor is limited, as the thickness of a water shield must be
considerable and this affects the overall dimensions of the reactor.
Increasing the reactor power output involves an increase in the
temperature of the water used in the shielding system. Therefore,
this and a number of other reasons advise sometimes to replace water
with other hydrogen-containing materials (hydrides, hydrocarbons).
The use of these materials and also beryllium and graphite in the
shielding system should be determined basing on economic indices,
susceptibility to manufacture, and radiation stability. The cha-
racteristics of materials having high thermal neutron absorption
cross sections have been considered in the foregoing sections. Compo-
site materials containing boron, in particular, boron-alloyed perlitic
steel, are most often used for the purpose in shielding systems.
Such steels containing 1-2% of boron can be rolled into sheets.

Increasing the boron percentage makes the steel not liable to ma-
nufacture. Their rolling is difficult and often even impossible.

Neutron radiation shielding system utilizes boral. This is a metal-
ceramic composite material consisting of fine particles of boron carbi-
de dispersed in an aluminum matrix. Boral sheets 6 mm thick are
cladded on both sides with aluminum to a thickness of 0.5 mm.

The thermal shield is intended mainly to prevent thermal neutrons
from getting into the biological shield. The energy given off, when
the neutrons are absorbed, heats the thermal shield material. In
view of this one has to choose materials of appropriate properties
and cool the thermal shield. The thermal shield is generally made
of cast iron alloyed with 14% Ni, 5% Cu, and 1-4% Cr to prevent
cast-iron growth in heating. The gray cast-iron grows because decom-
posing iron carbide produces free carbon. Low-carbon steel not sus-
ceptible to growth can be used for the same purpose. However, the
preparation of large castings of it presents certain difficulties. It is
more advisable to assemble the thermal shield of individual forgings
whose size is dictated by economy. Generally, boron-containing
composite materials and steels find their applications in reactor
shielding where the shield size and mass are at a premium.

If the mass and dimensions of shielding are not the limiting
factors, cement and concrete are used as the main shielding materials.
This is the case at most of power plants and research reactors. The
cost of concrete shielding is determined not only by the cost of the
cement and aggregates, but also by the method of shield manufactu-
re, presence and layout of holes in it, etc. The degree of attenuating
the neutron fluence intensity by the biological shield depends to
a great extent on the water content in the shielding material. This
in turn is determined by the type of concrete utilized and the method
of its preparation. Neutron absorption by a concrete shield may be
considerably increased by adding boron to the shielding material.
To build up shielding systems use is made of cements containing
about 1% B. The cost of concrete in this case increases 2 to 3 times.
The ability of a concrete shielding layer to attenuate gamma radia-
tion depends on the density of the shielding material. Depending
on the composition of cement and aggregate, the concrete density is
from 2.4 to 6.6 g/cm^3. Concrete has the least density when it utilizes
sand and gravel aggregates, and the greatest, with steel balls, lengths
of steel wire, and steel scrap. In the latter case the cost of concrete
is 40 to 50 times that with sand and gravel.

Depending upon the application, concrete shielding may be either
monolithic or comprising individual prefabricated blocks. Monolithic
shielding is used on large reactors. The block-type design is advisable
in case of small research reactors providing free access to the core
and less dangerous as sources of radiation.

The monolithic concrete shielding of a reactor is expensive because

it utilizes reinforcing cages. When placing concrete, the aggregate of high density, say, steel balls, should be distributed uniformly.

When shielding is assembled of prefabricated blocks, special attention should be given to the block-to-block joints to provide good protection against radiation. If the reactor design allows a thick shield of concrete, water and other nonmetallic materials to be used, they may offer a simultaneous shielding against neutron radiation and gamma rays. If the size and mass of shielding are limited, it is advisable to use high-density metals to attenuate gamma rays. The material most effectively attenuating gamma rays of high energy is lead. Its use is limited by a low melting point. If the shielding material is subject to high temperatures, use should be made of tungsten and tantalum in place of lead. They are extremely expensive and their use for shielding commercial reactors is inexpedient.

8.4 Magnesium and Its Alloys

Physical Properties. Magnesium and its alloys hold much promise as cladding materials. It is abundant and not expensive. Disadvantages of magnesium as a material for cladding and other parts of the core are its low corrosion resistance, ability to self-ignite, low melting point, and poor mechanical properties at an elevated temperature. Magnesium alloys despite their shortcomings are widely used as cladding materials in dual-purpose graphite- or heavy-water-moderated reactors utilizing natural uranium as the fuel and carbon dioxide as the reactor coolant. Examples are Calder Hall Nuclear Power Station, Bradwell reactors in Great Britain, a number of French reactors operating at a carbon dioxide temperature of 623 to 673 K.

As to the thermal neutron absorption cross section, magnesium is inferior only to beryllium. Physical properties of magnesium are given in Table 8.4, while compositions of certain magnesium alloys for claddings are listed in Table 8.5.

TABLE 8.4 Physical Properties of Magnesium

Atomic number	12
Atomic weight	24.32
Thermal neutron absorption cross section, m^2	$5.9 \cdot 10^{-30}$
Density, g/cm^3	1.74
Melting point, K	924
Boiling point, K	1393
Coefficient of linear expansion, deg^{-1}	$26 \cdot 10^{-6}$
Thermal conductivity, $W\ m^{-1}\ K^{-1}$	158.30
Crystal structure	HCP
Lattice parameters, nm	$a = 0.32$
	$c = 0.52$

TABLE 8.5 Magnesium Alloys

Alloy	Mass content of alloying elements and impurities, %										
	Be	Si	Al	Th	Fe	Mn	Ni	Cu	MgO	Ca	Zr
USSR:											
ПМБ	0.50-3.20	—	0.04	—	0.04	—	0.001	0.005	0.2-0.3	—	—
МБ-3	0.04	0.5	—	—	0.01	0.001	0.001	0.005	—	—	—
МБ-4	0.08-0.15	0.7	—	—	0.01	0.001	0.001	0.005	—	—	—
Mg-Al-Be	0.04	—	0.50	—	0.01	0.001	0.001	0.005	—	—	—
Mg-Th-Be	0.04	—	—	3	0.01	0.001	0.001	0.005	—	—	—
Mg-Ca-Zr-Be	0.04	—	—	—	0.01	0.001	0.001	0.005	—	0.5	0.50
Great Britain:											
Magnox AL-80	0.01	—	0.80	—	—	—	—	—	—	—	—
ZA (+Be)	0.01	—	—	—	—	—	—	—	—	—	0.55
Magzan-2	—	—	—	—	—	0.150	—	—	—	—	0.55
Magzan-4	—	—	—	—	—	0.400	—	—	—	—	0.60
AM 503 (S)	—	—	—	—	—	0.700	—	—	—	—	—
AM 503	—	—	—	—	—	1.400	—	—	—	—	—

Natural magnesium consists of the following isotopes: 78.8% ^{24}Mg, 10.14% ^{25}Mg, 11.06% ^{26}Mg. Under neutron irradiation only ^{26}Mg is activated. The reaction (n, γ) forms ^{27}Mg with a half-life of 9.46 min. Magnesium and its alloys are utilized in fuel element claddings of uranium-graphite and heavy-water reactors using natural uranium as the fuel and carbon dioxide as the coolant. In Great Britain magnesium alloys are used in the Calder Hall, Birkeley and other reactors. Fuel elements with claddings of a magnesium-beryllium alloy are used in the A-1 Czechoslovakian nuclear power station created by the joint Soviet-Czechoslovakian project. The CO_2 temperature in the reactor core is from 623 to 723 K.

In fuel elements cladded with Mg alloys, the mechanical strength is ensured by the uranium metal rod. The cladding protects the fuel rod against the corrosive attack of the coolant. In addition to high corrosion resistance, the basic requirement imposed on magnesium alloys is not heat resistance (resistance to creep and destruction) but rather sufficient ductility preventing unsealing of the fuel element cladding following deformation of the fuel rod.

Mechanical Properties. Pure magnesium is poorly ductile below 373 K. Its elongation lies within 5 to 10% and varies materially depending on the grain size and texture. When holding the metal for 100 to 200 h at 670 to 720 K, the grain size in pure magnesium increases hundreds and thousands of times. This accounts for further reduction of ductility at room temperature to elongation of 2-4%.

Fine stable grains in magnesium may be prepared by alloying it with Zr, Al, Mn, and Th. Thus, adding 0.55 % Zr to magnesium

increases its elongation 2.5 to 3 times. This also hardens magnesium. Table 8.6 gives mechanical properties of the Soviet-made magnesium alloys.

TABLE 8.6 Mechanical Properties of Mg and Mg-Be
Alloys at Various Temperatures, K

Material	σ_u, MPa			σ_y, MPa		δ, %		
	293	573	773	293	573	293	573	773
Magnesium	180	18	4	90	14	9	52	78
МБ-4	220	38	9	150	19	6	48	82
МБ-3	200	29	8	130	17	8	58	90
ПМБ-2	260	80	28	190	48	5	16	52
ПМБ-5	240	75	30	190	50	5	15	49

A number of magnesium alloys are prepared of powder by the metal-ceramic technique. The resultant alloy contains oxides. Such materials (ПМБ-2 and ПМБ-5, see Table 8.6) are less ductile than cast and wrought alloys but are stronger and more resistant to heat.

In deformation and plastic flow, large pores and voids form along grain boundaries in magnesium and its alloys. This reduces ductility of magnesium alloys and involves the risk of gas swelling. In the alloys used in reactor engineering, this phenomenon is practically eliminated, and at 673 to 773 K claddings of these alloys are sufficiently effective.

Radiation Stability. The recrystallization temperature of magnesium is low. Therefore, irradiation should not materially affect the mechanical properties of magnesium and its alloys. Thus, when irradiated with a neutron fluence of 10^{18} cm^{-2} at 318 K the ultimate strength and yield point of an alloy containing zirconium increase by 0-11 and 2-18%, respectively, and its elongation decreases by 10-35%. Higher fluences must have a more essential effect on the ductility of magnesium alloys. It should be noted that in a gas-cooled reactor, components and parts of magnesium alloys operate at a temperature not below 423-473 K. At these temperatures, the ductility of magnesium alloys is sufficiently high and radiation damage does not reduce it to a dangerous value.

Compatibility. Magnesium compatible with uranium to a temperature of 773 K reduces oxides of nearly all metals. Therefore, mutual diffusion of metals depends on the penetration of magnesium oxide. Small amounts of alloying elements practically have no effect on the penetration of magnesium oxide and the magnesium compatibility with other metals. Below 720-850 K, magnesium and its alloys do not interact with alloys of Zr, Cr, Ti, Ni, and Pt. Magnesium com-

bines with aluminum above 673 K. Low-alloyed perlitic steels do not react with molten magnesium.

Resistance to Corrosion. Alloys containing 2% Be are resistant in dry carbon dioxide at 5 MPa and 853 K. Alloys of the magnox series are resistant under 793 K. Corrosion proceeds following a parabolic law. Water vapors enhance oxidation. At 773 K and 1.4 MPa, alloys of the magnox type are resistant in carbon dioxide containing up to 1% CO and up to 0.03% water. Increasing the water content up to 2%, as well as increasing the air content up to 50%, does not cause the black way corrosion. With an increase in the carbon dioxide pressure, the corrosion rate increases. Irradiation with a neutron fluence of $2 \cdot 10^{18}$ cm^{-2} only slightly affects the oxidation rate.

With an increase in temperature, magnesium alloys ignite in carbon dioxide. Thus, at 1 MPa, the ignition point is 913 K. The material fully burns up owing to self-heating not below 888 K. The fuel element claddings of sintered powder magnesium alloys are not inferior in corrosion resistance in carbon dioxide to claddings made of other cast and wrought alloys.

In neutral media, distilled water including, magnesium and its alloys are not resistant. The normal potential of magnesium is —2.38 V, i.e. magnesium is very electronegative and extremely active corrosively. Irradiated fuel elements cladded with magnox alloys are kept in water during the time required to reduce the activity of short-lived products of fission. Heavy corrosion of magnesium alloys may lead to a contact between uranium and water with the resultant contamination of the cooling pond. Cleaning the water of chlorides and carbonates to their content of 0.02 mg/l and increasing pH of the medium above 11 nearly completely suppress the magnox corrosion. The contact of magnesium alloys with stainless and low-alloyed steels, and graphite enhances corrosion and causes pitting. The contact with aluminum and its alloys does not promote corrosion of magnesium alloys.

Magnesium and its alloys are not resistant to atmospheric corrosion. To protect items of magnesium alloys use is made of coatings. Claddings of magnesium alloys are welded by the argon-arc and electron-beam techniques.

8.5 Aluminum and Its Alloys

Physical Properties. The physical properties of aluminum are listed in Table 8.7. The small thermal neutron absorption cross section and low density make aluminum a very promising material for reactor engineering. The melting point of aluminum is low. Aluminum undergoes no structural transformations up to its melting point.

The natural aluminum consists of stable isotope ^{27}Al. Aluminum interacting with neutrons according to reaction (n, γ) forms radioiso-

TABLE 8.7 Physical Properties of Aluminum

Atomic number	13
Atomic weight	26.98
Thermal neutron absorption cross section, m²	$2.15 \cdot 10^{-29}$
Density, g/cm³	2.7
Melting point, K	933
Boiling point, K	2600
Coefficient of linear expansion at 293-873 K, deg^{-1}	$28.7 \cdot 10^{-6}$
Thermal conductivity at 373-473 K, W m^{-1} K^{-1}	210-233
Crystal structure	FCC
Parameters of lattice, nm	$a = 0.405$

tope ^{28}Al with a half-life of 2.24 min. Aluminum and its alloys are used in the manufacture of the fuel element claddings, channel tubes, pipes, shells of tanks, etc. When aluminum having a low thermal neutron absorption cross section operates in the core, the reactor may be run on natural uranium with a considerable burnup.

In addition to pure aluminum (0.0002% of all impurities) aluminum alloys are widely used in reactor engineering. They may be divided into several groups:

commercial aluminum, grade АД, (and aluminum, grade 1100, produced in the USA) contains about 0.5% impurities, mainly Fe and Si;

alloys with additions of nickel and iron (X8001, X8003, A288, Table 8.8). The alloys are used to manufacture the fuel element claddings operating under 473 K;

TABLE 8.8 Aluminum Alloys Used in Reactor Engineering in the USA

Alloy	Mass content of alloying elements and impurities, %						Alloy	Mass content of alloying elements and impurities, %					
	Ni	Fe	Cu	Si	Mg	Cr		Ni	Fe	Cu	Si	Mg	Cr
X8001	1.0	0.5	—	0.1-0.3	—	—	A288	1	0.5	—	0.003	—	—
X8003	1.5	1.5	—	0.003	—	—	6061	—	—	0.25	0.6	1.0	0.25

stronger alloys, type 6061, (see Table 8.8) are used to manufacture fuel channels.

Aluminum can be considerably hardened by adding aluminum oxide to it. Items of such composite materials are made by the powder metallurgy methods, by pressing with subsequent sintering of finely dispersed aluminum powder. The composite materials of the САП type contain 8-10% aluminum oxide. The САП composite materials comprise aluminum grains partially enveloped with oxide

films. Ceramic oxide is highly hard and strong. Enveloping aluminum grains, the oxide prevents them from fusing together into large grains and hence limits creep. High hardness of the САП alloys is achieved at the expense of their ductility.

Certain alloying elements considerably dissolve in solid aluminum at elevated temperatures. Their solubility drops with a decrease in temperature. To obtain an aluminum alloy having a structure of a solid solution, the alloy is heated to a temperature providing complete dissolution of the alloying element and then rapidly cooled. This operation, hardening, fixes a nonequilibrium solid solution at room temperature. Since the solid solution is unstable, it decomposes as a result of ageing. Ageing can be accelerated by heating to 393-443 K during 4 to 12 h. This is known as artificial ageing, or dispersion hardening. Ageing improves the hardness characteristics of aluminum alloys. To remove strain-hardening, aluminum alloys are annealed at 623 to 673 K for 0.5-2 h.

Aluminum alloys, except for metal-ceramic, are sufficiently ductile and susceptible to manufacture. Items are readily made of them by pressing and extruding. Welding aluminum alloys is somewhat difficult. This process, however, is mastered well and finds wide use in manufacturing fuel elements. Items of aluminum alloys can be soldered and cemented. Favourable physical, mechanical and technological properties of aluminum alloys provide their wide use in the manufacture of the fuel element claddings and other components of the core. The first uranium-graphite reactor for plutonium production utilized aluminum, grade 1100. Fuel elements cladded with aluminum alloys are used in research reactors, plutonium-producing reactors in Hanford and Savannah River, USA, and in experimental boiling reactors.

The requirement of high ductility is imposed on the alloys used in the manufacture of the fuel element claddings. The alloys used for making the fuel channels and other components of the core should be strong.

Mechanical Properties. Pure aluminum is very ductile and weak. Its ultimate strength is 50-60 MPa. A small amount of impurities present in commercial aluminum improve its strength. After annealing at 673 to 723 K, extruded and cold-drawn or cold-rolled tubes of commercial aluminum have the following characteristics:

Ultimate strength, MPa	80-110
Yield point, MPa	30-50
Elongation, %	20-30

The USA alloy 6061 approximating the Soviet-made aluminum-magnesium alloys, type АМг, has a somewhat higher strength. After

annealing in tubes its properties are as follows:

	293 K	473 K
Ultimate strength, MPa	120-150	90-100
Yield point, MPa	40-60	30-40
Elongation, %	25-30	45-60

The strength of an alloy decreases whereas its ductility increases with temperature.

The strength of alloys, type X8001, made on the basis of commercial aluminum lies between those of commercial aluminum and alloy 6061. The rate of creep of commercial aluminum at 373 K and a stress of 100 MPa is $10^{-2}\%$ h^{-1}. The same rate of creep is observed at 523 K and a stress of 10 MPa.

The cladding materials must be compatible with the nuclear fuel. Uranium and aluminum start to interact at 523 K. A 2000-h interaction at 573 K produces a layer of intermetallic compound 0.025 mm thick. Uranium dioxide is compatible with aluminum up to 533 K, and uranium carbide and nitride, up to 813 K.

Radiation Stability. Radiation damage to aluminum and its alloys is insignificant because of their low recrystallization temperatures. The yield point and ultimate strength increase on the background of sustained (for prehardened materials) or reduced (to a tolerable level) ductility.

Neutron fluence, 10^{21} cm^{-2}	0	2	7	27	38
σ_u, MPa	140	180	200	220	240
σ_y, MPa	125	160	170	180	200
δ, %	22	25	22	22	24

So, one may conclude that neutron irradiation improves rather than worsens the mechanical properties of aluminum and its alloys.

Corrosion Resistance. The highest temperature at which aluminum alloys can be utilized in water-cooled reactors is dictated by their resistance to corrosion. It seems quite attractive from the economy and nuclear physics points of view to use aluminum alloys for the manufacture of fuel element claddings and fuel channels of boiling reactors. The solution of this problem is hindered by a low corrosion resistance of aluminum alloys in water and steam-water mixture at 523-573 K. Long-term and reliable operation of components made of aluminum and its alloys in water-cooled reactors below 523 K should be attributed to a great extent to their corrosion resistance. The latter considerably depends on water quality, structural peculiarities (presence of crevices and stagnant areas, contacts to other materials), composition of alloys, irradiation, etc. A troublefree operation of a reactor employing aluminum alloys in the core zone

may be achieved only when all the above-mentioned considerations are taken into account.

The normal potential of the anodic reaction

$$Al \rightarrow Al^{3+} + 3e$$
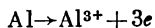
is equal to -1.663 V. This points to a high chemical activity of aluminum. The first millisecond after immersion in an aqueous medium, the potential of newly filed aluminum is close to normal. With time, the aluminum potential becomes more positive till reaching -0.5 to 0.0 V. This is associated with the oxide film formation on its surface. Damage to the continuous oxide film on a metal immersed in a solution abruptly shifts the aluminum potential into a negative direction. A drastic change in the electrochemical characteristics of aluminum upon formation of an oxide film along with other factors gives us reason to suppose that aluminum can passivate.

Composition and structure of oxide films. Let us consider the composition and structure of oxide films formed on aluminum in the process of corrosion. In contact with air, the so-called air-oxide coating 0.01 μm thick builds up on aluminum. This film consists of two layers. The inner layer facing the metal (a barrier layer) is compact, whereas the outer layer is of a more penetrable oxide.

When aluminum 99.995% pure contacts the aerated distilled water at 363 K, the metal surface becomes coated with an amorphous film of aluminum oxide covered in turn with a layer of boehmite $Al_2O_3 \cdot H_2O$ (orthorhombic lattice) and a layer of bayerite $Al_2O_3 \cdot 3H_2O$ (monoclinic lattice). The coating is a few tenths of a millimeter thick; and the thickness depends on particular conditions. Above 373 K, the oxide film on aluminum and its alloys consists mainly of boehmite.

An oxide coating formed on aluminum is not uniform. Its thickness varies and the film has pores. It is in the pores that the anodic reaction mainly proceeds. Being 5 to 10 nm thick, the aluminum oxide film has a sufficiently low electrical resistance, and the cathodic process may take place therein. The film areas of considerable thickness practically do not pass electrons and, therefore, are inert. Neither cathodic, nor anodic reactions occur on these areas. A phase oxide film covering the aluminum surface passivates the metal. The anodic polarization curve of aluminum (Fig. 8.4) points to the aluminum passivation within the potential range from -0.4 to -0.75 V.

When the continuity of a passivating oxide coating is disturbed, for example, in stirring the medium containing particles of corundum, aluminum activates and the anodic polarization curve has no passive region. The formation of an oxide film following aluminum oxidation in the air or anodic oxidation increases the passive area to a potential of 2.0 V. At room temperature, corrosion of alu-

minum and its alloys proceeds main-
ly with oxygen depolarization limited
by diffusion. The critical diffusion
current on aluminum is a tenth of
that on iron and copper, as no catho-
dic reaction proceeds on most of the
aluminum surface. At room tempera-
ture, Al and its alloys at a corrosion
potential are in the passive state. The
corrosion rate is small and makes
0.002 g m^{-2} day^{-1} after 30-day testing.
With increasing temperature to 353 K,
the corrosion rate grows to 0.03 g m^{-2}
day^{-1}.

Increasing the temperature enhan-
ces the formation of phase protec-
tive layers. This decelerates cor-
rosion in time. At 373 K, 10 to 20
days after the beginning of a test the

Fig. 8.4 Anodic polarization of
aluminum in deaerated 0.1 N
solution of potassium nitrate

thickness of an oxide film δ (cm) depends on time τ (s) as follows:

$$\log \delta = -7 + 0.5 \log \tau.$$

When the test duration exceeds 10 days, aluminum, the АД alloy
type, corrodes at 353-373 K following a linear law. After a certain
thickness has been achieved, the oxide film on a metal surface grows
only slightly, and its thickness as a first approximation may be
taken as constant. The corrosion rate is determined by the rate of
diffusion through the oxide film and in this case approximates
0.03 g m^{-2} day^{-1}.

At temperatures close to 473 K, corrosion produces blisters on the
aluminum surface. They are filled with aluminum hydroxide, parti-
cles of noncorroded aluminum, and hydrogen.

In a deaerated medium (corrosion above 373 K, as a rule, occurs
in a deaerated medium) the cathodic process involves the discharge
of the hydrogen ion. Part of hydrogen dissolves in the metal. Recom-
bining into molecules in micropores and microporosities, hydrogen
increases the pressure in them, forms blisters on the metal surface,
destroys the oxide protective film, and thus drastically enhances
the corrosion. This disturbs the lattice order at grain boundaries.
Discontinuities of the oxide protective coating evidently concentrate
in these areas. Therefore, aluminum corrosion should be more inten-
sive at grain boundaries, and this is observed in practice. Iron and
nickel poorly soluble in aluminum form with it intermetallic com-
pounds even when present in low concentrations. Hydrogen overvolt-
age on the intermetallic compounds of iron and nickel is less than
on aluminum. Therefore, the cathodic reaction of the hydrogen

ions discharge proceeds mainly on the surface of the intermetallic compounds. The recombination into molecules should also be expected on the same areas. As a result, hydrogen dissolves less in aluminum alloyed with iron, nickel and copper. The protective properties of the oxide film are accordingly higher. Thus, an increase in the iron content of aluminum reduces the hydrogen overvoltage at 473 K as follows:

Content of Fe, %	0.25	0.5	1	5
Hydrogen overvoltage,V	1.34	1.14	0.85	0.74

Note that hydrogen overvoltage decreases mostly when iron is added to aluminum in an amount of up to 1%. Evidently, the aluminum corrosion rate decreases most effectively when the content of iron increases to 1%. A further increase in the iron content has a far less effect on the aluminum corrosion resistance. In fact, increasing the iron content from 0.5 to 0.8% and from 0.8 to 5% reduces the corrosion rate by a factor of 1.7 and 1.5, respectively.

Therefore, aluminum alloys that are corrosion resistant at about 573 K should contain alloying elements such as iron and nickel in an amount close to 1%. In particular, the alloy, grade X8001, recommended for operation at 573 K contains this amount of nickel. The corrosion rate of this alloy at 473 and 573 K is 0.1 and 0.25 g m^{-2} day^{-1}, respectively, and decreases with time τ (days). At 573 K, the following relation is valid:

$$\log K = 0.58 - 0.42 \log \tau.$$

Precipitating on the surface of oxide layers, the aluminum corrosion products that are present in the reactor coolant prevent the corrosion products from going to the water. As this happens, the corrosion rate decreases. So, the larger the area of stainless steel in the circuit, the higher the corrosion rate of the aluminum alloys found in the same circuit.

It should be noted that pure Al is most corrosion resistant below 373 K. Above 373 K, a higher corrosion resistance is offered by alloys containing Fe, Ni, Cu.

At the initial stage, corrosion of aluminum and its alloys proceeds following a parabolic law. After a certain period of time, usually called an incubative period, the corrosion rate increases (Fig. 8.5) and then takes the linear course.

With aluminum purified to 99.5%, the duration of incubative period τ (h) of corrosion in water depends on temperature as follows:

$$\log \tau = -18.78 + (1.4 \cdot 10^4/T).$$

As a first approximation, the relation evaluates the incubative period of the aluminum alloys corrosion. The pH of the medium

has an essential effect on the alum-
inum corrosion resistance.

The passive state on aluminum
may be disturbed by the following
reactions.

$$Al + O^{2-} + 2H^+ = Al^{3+} + H_2O + 2e;$$

$$Al + O^{2-} + OH^- = HAlO_2 + 2e.$$

Fig. 8.5 Corrosion of alumin-
um alloy, grade M388, versus
time in water at 636 K
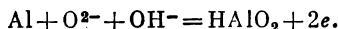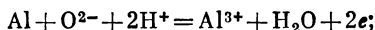
The lowest rate of aluminum cor-
rosion should evidently correspond
to the lowest rate of one or another
reaction. This becomes a fact when the
rates of the reactions are equal. To
a first approximation, this is expressed by the equality:

$$C_{H^+}^2 \exp{(\alpha n F \Delta\varphi/RT)} = C_{OH^-} \exp{(\alpha n F \Delta\varphi/RT)}.$$

On the other hand, the ion product of water is

$$W = C_{H^+}C_{OH^-}.$$

Combining these equations we obtain that the lowest rate of the
aluminum corrosion corresponds to pH $= -\log W/3$.

The ion product of water varies with temperature. Therefore, the
range of pH values corresponding to the lowest corrosion rate of alu-
minum alloys also varies with temperature:

T, K	333-373	398-473	523-573
pH	5.8-6.5	4.5-5.0	3.0-3.5

At 473 to 573 K, water acidification with phosphoric acid reduces
the corrosion rate of aluminum alloys. Hence, at 588 K and a flow
rate of 5.4 m/s gain in weight ΔG (g/m²) versus time τ (day) for alloy
X8001 is expressed as follows:

pH 5.5 log $\Delta G = 0.3 + 0.8 \log \tau$,

pH 3.5 log $\Delta G = -0.6 + 0.7 \log \tau$.

The oxygen content affects the rate of cathodic reaction and corro-
sion potential. Within a wide range of potentials, aluminum and
its alloys are in the passive state. Therefore, increasing the oxygen
concentration from 0.02 to 8 mg/kg has not practically changed the
rate of anodic reaction on aluminum 99.99% pure at a potential
of -0.3 V.

A change in the oxygen concentration should not have a noticeable
effect on the corrosion resistance of aluminum and its alloys. Hydro-
gen peroxide produces nearly the same effect. The presence of chlo-
rides in the medium affects the electrochemical and corrosion behavior
of Al and its alloys.

At a potential of 0.05 V and at 333 K, the rate of anodic process does not practically change on a specimen held for 72 h in water chemically demineralized to a chlorine ion concentration of 0.5 mg/l. With a further increase in the concentration of the chlorine ion the corrosion rate grows linearly with its concentration.

If the sulfate ion is present in water in an amount of 5 mg/l, the chloride ion does not increase the rate of anodic process under the same conditions to a concentration of 2 mg/l. The sulfate ion itself does not increase the rate of anodic process to a concentration of 5 mg/kg.

Inhibitors of the aluminum corrosion are silicic acid and chromates.

Contact corrosion. In any structure different metals contact. When aluminum alloys contact stainless steels, the corrosion potential of aluminum alloys is shifted into the region of repassivation, and the corrosion rate of aluminum increases. Only with certain alloys at a strictly defined ratio between the surfaces of aluminum and stainless steel, the corrosion potential corresponds to the passive region. To reduce the contact corrosion on aluminum items, a protective coating of aluminum oxide is formed by the anodic oxidation method. With the so-called ordinary anodic oxidation, the oxide film is 10 to 20 µm thick, and with thick-layer coating, 50 to 100 µm. In the latter case the film is black and hence the name of the method. The oxide film with the thick-layer anodic oxidation possesses good antifriction properties. After ordinary anodic oxidation the oxide films are usually soaked with chromates and are green.

To prevent contact corrosion of aluminum, a separator of aluminum alloy is fitted between the item of aluminum and the stainless steel. The separator contacting the stainless steel deteriorates and is then replaced. In other cases items of aluminum and steel are separated by a part made of zirconium or titanium alloy.

In research reactors, tanks made of aluminum alloys contact concrete. Steel scrap is generally added to the concrete. In addition, it carries steel reinforcing bars. The concrete surface in contact with an aluminum tank is coated with a protective coating. Usually, several coatings of coal-tar varnish are applied. If the protective coating is not continuous, the aluminum may contact the concrete and reinforcement and scrap embedded in it. Moisture contained in concrete may have pH = 13 to 14.

In the place of contact to concrete, intensive pitting develops on the aluminum. This may produce a through damage in few years of service. The most effective control of this type of corrosion is by applying a high-quality protective coating to the concrete surface.

The corrosion rate of aluminum alloys is appreciably enhanced by a contact to graphite. Thus, the corrosion rate of an alloy, grade 6061, in contact with graphite in chemically demineralized and

river water has increased more than 20 times. Anodic oxidation adds to the corrosion resistance of aluminum alloys.

Crevice corrosion. In real structures, it is difficult to completely avoid crevices and other areas of stagnation formed by similar materials. Crevice corrosion takes place when two components of aluminum alloys contact.

With two metallic surfaces tightly contacting each other the width of a clearance or crevice is usually of 0.005 cm.

The oxygen from the medium filling a crevice is consumed in the course of corrosion. New oxygen may find its way to the crevice only by diffusion. The aluminum ions passing into a corrosive medium due to corrosion hydrolize in the crevice as follows:

$$M_{O_2} = DSC/l = 10^{-5} \cdot 5 \cdot 10^{-3} \cdot 10^{-6}/1 = 5 \cdot 10^{-14} \text{ mole/s,}$$

where $D = 10^{-5}$ cm^2/s is the oxygen diffusion coefficient; $S = 5 \cdot 10^{-3}$ cm^2 is the crevice cross section; $C = 10^{-6}$ g-eq/cm^3 is the volume concentration of oxygen.

Even at a distance of 0.1 cm from the crevice edge, the oxygen supply is only $5 \cdot 10^{-13}$ g-eq/s.

The corrosion potential of aluminum in aerated chemically demineralized water corresponds to the passive state. As the concentration of oxygen in a crevice decreases, the rate of the anodic process in the passive state, and, accordingly, the rate of attack, remain constant and close to $3 \cdot 10^{-3}$ g m^{-2} day^{-1}. This makes up $1.85 \cdot 10^{-11}$ g-eq cm^{-2}s^{-1}. The oxygen entering the crevice due to diffusion obviously cannot maintain the corrosion.

The hydrolysis

$$Al^{3+} + 3H_2O = Al(OH)_3 + 3H^+$$

produces the hydrogen ion which participates in the cathodic process. The diffusion coefficient of H^+ is approximately two orders higher than that of oxygen. So, the greater portion of the hydrogen ion formed in hydrolysis is removed from the crevice owing to the hydrogen ion diffusion. Therefore the medium in the crevice may become practically neutral.

Note that a neutral corrosive medium entering a crevice may cause an anodic reaction with the formation of aluminates. This reaction reduces the amount of Al^{3+} in the crevice. The hydrolysis and formation of H^+ are then suppressed.

In the situation under consideration, the aluminum corrosion products in a crevice are present as $H_2AlO_3^-$ and $Al(OH)_3$. The concentration of Al^{3+} may be assumed to be 10^{-6} mole/l. Proceeding from the solubility product of $Al(OH)_3$ equal to $2 \cdot 10^{-32}$, pH in the crevice should be 5.4, i.e. the medium is close to neutral.

Owing to a poor oxygen supply to the crevice, the medium therein

is deaerated. In a deaerated chemically demineralized water the corrosion potential of aluminum is equal to —0.7 V. In a neutral medium at this potential, the rate of hydrogen ion discharge is 10^{-9} A cm^{-2}, or 10^{-14} mole cm^{-2} s^{-1} which is 1/1000th of the rate of the aluminum supply to the crevice. Therefore, it may be supposed, that the anodic reaction in a crevice is compensated for by the cathodic reaction outside the crevice.

Hydrogen ions in a crevice are consumed in the cathodic process. Since the concentrations of H^+ and OH^- are related by the ion product of water, then, as a result of the dissociation of water molecules the hydroxyl ions go to the corrosive medium in the crevice. The pH of the medium in the crevice rises to 8. Alkalifying the medium in the crevice abruptly increases the rate of attack. Crevice corrosion is extremely intensive, when the crevice is formed by aluminum and stainless steel. The corrosion is then said to be contact-crevice.

In view of the above, the formation of crevices and stagnant areas in nuclear power plants employing aluminum and its alloys should be avoided. The aluminum sheets and tubes must be butt-jointed by welding rather than overlapped. Heating in welding promotes the formation of oxide films on the surfaces of aluminum alloys and stainless steel. The films reduce the current in the operation of an aluminum-stainless steel galvanic couple.

Passage of Aluminum Corrosion Products into Coolant. In aluminum corrosion, part of the corrosion products remains on the metal surface in the form of a protective oxide film, or in the form of deposits, and the other part goes to the reactor coolant. With no coolant flow, a smaller part of corrosion products goes to the coolant than in case of its motion. At a coolant-flow velocity of 3 to 6 m/s and 423 K, up to 50% of corrosion products go to the medium.

When the mass of aluminum in corrosion changes with time linearly most of corrosion products enter the solution.

Effect of irradiation. Let us consider the effect of irradiation on the corrosion resistance of aluminum alloys. As has been mentioned above, corrosion of aluminum and its alloys is controlled by surface diffusion. The lattice unit cells at the oxide surface are in general considerably distorted. This is because the interface itself is a fairly serious defect of the lattice. In view of this, it is hard to expect that the lattice defects produced by irradiation will in any way influence the surface diffusion and accordingly the corrosion resistance of aluminum alloys.

In a deaerated medium corrosion proceeds with hydrogen depolarization, and irradiation has no essential effect on the kinetics of the cathodic process. In an oxygen-containing medium, irradiation accelerates the cathodic process, but the corrosion potential of aluminum remains in the passive state and the rate of the anodic process does not change. Hence, a conclusion follows that irradiation

has no noticeable effect on the corrosion resistance of aluminum and its alloys.

Thus, corrosion of the aluminum alloys containing 0.5 to 2% Ni and 0.5% Fe subjected to a 700-h 533 K test decreased under reactor irradiation by 11.9% on the average compared with a similar test without irradiation. The test is accurate to within 10%. It may be that in the beginning, irradiation enhances the growth of oxide film. The diffusion path becomes longer and the corrosion rate somewhat decreases in the subsequent stages of testing. A certain decrease in the corrosion rate under irradiation is observed in testing alloy, grade M288, at 493-523 K. At 463 K, the corrosion rate of alloy, grade X8001, exposed to irradiation increases. At 473 K, the corrosion rate of alloys, grades X8001 and M288, is 0.2 to 0.3 g m^{-2}day^{-1} when tested in a chemically demineralized water for 2000 h. Their corrosion rate without irradiation was of the same order.

Increasing the rate of the cathodic process under irradiation in the oxygen-containing media increases the potential at the aluminum-to-stainless steel interface. This in turn enhances contact corrosion of aluminum and its alloys.

The movement of reactor coolant augments the corrosion rate of aluminum alloys. This is especially noticeable at 553 K and above. Thus, when testing alloys containing 2.5% Ni and 0.4% Fe at a coolant velocity of 2 m/s, the alloys showed an increase in the corrosion rate from 0.37 to 0.93 g m^{-2}day^{-1}. When the rate of water flow is 5-6 m/s, aluminum specimens display corrosion-erosion damage. On certain specimens, the depth of damage reaches 0.5-1.0 mm at the inlet and outlet of the testing bay following 2000 h. This should be evidently attributed to washing the corrosion products off the metal surface. In special experiments, specimens of aluminum alloys were kept at 623 to 673 K in water saturated with aluminum corrosion products during a week and a day, respectively. A process similar to sintering obviously took place. Following it testing with circulating coolant did not increase the rate of corrosion.

Increasing the flow velocity of superheated steam also reduces the corrosion resistance of aluminum alloys. An increase in the pressure of superheated steam raises its density. This, obviously, increases the corrosion rate of aluminum alloys. Vibration essentially reduces the corrosion resistance of aluminum alloys. In the end it should be noted that to provide a reliable operation of aluminum alloys (high corrosion resistance) much attention must be paid to the composition of water coolant and hydrodynamic factors. The data now available confirm that aluminum alloys can be efficient for a long period of time up to 473 K.

Claddings of fuel elements and structural components of experimental reactors are made of aluminum of high purity, inasmuch as the temperature of the air-saturated water does not exceed 313-343 K.

The water quality must meet the following ratings:

Electrical conductivity, μS/cm   1

Hardness, μg-eq/l   1-2

Content, mg/l:

    chlorides   <0.02

    sulphates   <0.05

    copper   <0.02

pH   5-7

Aluminum of high purity and alloys, type 6061, can be used in reactors cooled by river or lake water, at temperatures below 353 to 363 K.

At 443 to 473 K, use is made of alloys of the type A288, X8001 (see Table 8.8). The water quality ratings in this case differ from those specified for research reactors in the content of oxygen and pH. Water must contain not more than 0.02 mg/l of oxygen and its pH must be within 5.5 to 6.5.

8.6 Zirconium and Its Alloys

Physical Properties. At the present time, aluminum alloys are not used above 473 K, as at such a temperature their corrosion resistance and strength are insufficiently high. Of materials having low thermal neutron absorption cross section in this region a wide application has been found by zirconium alloys. The physical and mechanical properties (Table 8.9) and corrosion resistance of zirconium alloys make them fairly promising for the manufacture of the fuel element claddings.

TABLE 8.9 Physical and Mechanical Properties of Zirconium

Atomic number	40
Atomic weight	91
Thermal neutron absorption cross section, m^2	$1.8 \cdot 10^{-29}$
Density, g/cm^3	6.5
Melting point, K	2118
Boiling point, K	3873-3973
Coefficient of linear expansion, deg^{-1}	$5.8 \cdot 10^{-6}$
Thermal conductivity, $W\ m^{-1}\ K^{-1}$	23.7
Crystal structure	α-phase, HCP up to 1135 K β-phase, BCC above 1135 K
Lattice parameters, nm	α-phase: $a = 0.3232$ $c = 0.5147$ β-phase: $a = 0.316$

In channel-type reactors, zirconium alloys are the leading channel tube materials. The use of channel tubes made of zirconium alloys materially reduces neutron absorption as compared with channel tubes made of the austenitic stainless steels.

The fuel channel tubes of the Leningrad, Kursk and Chernobyl atomic power stations are made of Zr + 2.5% Nb alloys. Their fuel element claddings employ Zr + 1% Nb alloy. The same alloy is used to manufacture the fuel element claddings of water-cooled and moderated reactors. The maximum temperature (573 to 623 K) at which zirconium alloys are utilized in water-cooled reactors is dictated by their corrosion resistance. An alloy containing 1.2% Cr and 0.1% Fe is considered as promising for operation in the super-heated steam at above 623 K.

Neutron irradiation of zirconium produces three isotopes:

^{93}Zr with a half-life of $1.5 \cdot 10^6$ years and β-radiation energy 0.06 MeV;

^{95}Zr with a half-life of 64.05 days and γ-radiation energy 0.24 MeV;

^{97}Zr with a half-life of 17 h.

Metallic zirconium is prepared mainly by the iodide (the Van Arkel-de Boer process), electrolytic, and magnesium-reduction (the Kroll process) processes. The first method yields the most pure metal.

Zirconium alloys are used in the fuel channel sections operating in the core. Therefore, it becomes necessary to joint zirconium alloys with stainless steels. In addition to stresses generated by the cool-ant pressure, the steel-zirconium joints are also subjected to consider-able cyclic stresses produced by the difference in the coefficients of thermal expansion of zirconium ($5.8 \cdot 10^{-6}$ deg^{-1}) and stainless steel ($17.5 \cdot 10^{-6}$ deg^{-1}).

Welding produces brittle phases (eutectic and intermetallic com-pounds) in the welding area with the resultant cracking in the joints even in cooling after welding. To obtain steel-to-zirconium joints more promising are mechanical methods, diffusion welding, braz-ing, joint extrusion, beading, explosion welding, etc. Beading is the most promising technique.

Mechanical Properties. Pure zirconium is weak (Table 8.10), but has a high corrosion resistance. Impurities in zirconium, nitrogen in particular, affect its resistance. To eliminate the detrimental effect of nitrogen zirconium is alloyed with tin. For the same reasons the tin-iron-nickel (0.1 to 0.3% Sn, Nb, Fe and Ni each) alloy (ozhen-it) is also alloyed with tin. Increasing the strength characteristics of zirconium is achieved by alloying it with Nb, Fe, Ni, Cu, and others. Alloys improved by adding 2.5% Nb and alloys, type Zircal-loy-2, (1.2-1.7% Sn, 0.07-0.2% Fe, 0.05-0.15% Cr, and 0.03-0.08% Ni) approximate stainless steels in mechanical properties (see Table 8.10). The possibility of their use in reactors at 750-900 K in gas,

TABLE 8.10 Mechanical Properties of Zirconium and Its Alloys, Rate of Steady-state Creep

Material	σ_u, MPa 293K	473K	573K	673K	σ_y, MPa 293K	473K	573K	673K	δ, % 293K	473K	573K	673K	Rate of steady-state creep v, %/h, at σ, MPa
Iodide-refining, arc remelting zirconium	220	140	120	110	80	50	45	40	45	55	55	60	$583K, \sigma=88$; $588K, \sigma=67$; $673K, \sigma=176$ $\}$ $v=10^{-1}$ $\{\sigma=98;\ \sigma=84;\ \sigma=49\}$ $v=10^{-2}$ $\{\sigma=109;\ \sigma=95;\ \sigma=77\}$ $v=1$
Zircalloy-2 (USA)	480	250	200	170	310	150	100	70	22	34	35	36	$\log v = -9.75 + 2.15\sigma$; $98.4 < \sigma < 189.8$; $\log v = -246.95 + 90\sigma$; $189.8 < \sigma < \sigma_u$
Zr+0.5% Ta (USSR)	300	200	160	140	130	80	60	50	40	42	42	45	$623K,\ \sigma=50$ $v=0.4\cdot10^{-1}$; $\sigma=60$ $v=1.9\cdot10^{-2}$; $\sigma=80$ $v=4\cdot10^{-2}$
Zr+1% Nb (USSR)	350	260	200	180	200	160	120	90	30	31	33	38	$623K,\ \sigma=80$ $v=10^{-1}$
Zr+2.5% Nb (USSR)	450	320	300	270	280	220	200	180	25	24	23	22	$623K,\ \sigma=150$ $v=10^{-1}$
Alloy Ozhenit (USSR)	290	200	160	130	120	80	70	70	33	42	46	50	$623K,\ \sigma=60$ $v=0.3\cdot10^{-4}$
Zr+5% Nb (USSR)	650	570	530	480	—	—	—	—	20	17	17	16	$673K,\ \sigma=45$ $v=0.7\cdot10^{-4}$
Valloy	560	—	360	270*	400	—	310	240*	13	—	11	13*	

* At 773K.

liquid-metal, or organic coolants is determined by the corrosion resistance under the conditions of the coolant flow and irradiation, rather than by their strength. Thermal treatment affects the mechanical characteristics of zirconium alloys. Hardening from β-phase with subsequent ageing at annealing produces high mechanical properties of alloys containing 2.5% Nb. An optimal mode of thermal treatment should provide high strength and corrosion resistance of zirconium alloys. Table 8.11 illustrates the influence of thermal

TABLE 8.11 Mechanical Properties of Alloy Zr + 2.5% Nb (neutron-irradiated, $E > 0.5$ MeV)

Treatment	Neutron fluence, cm^{-2}	Test temperature, K	$\sigma_{0.2}$, MPa	σ_u, MPa	δ, % (per length of 2.54 cm)	ψ, %
Hardening from 1153 K and ageing at 773 K for 24 h	Non-irradiated	293	780	870	13	63
	10^{20} at 523 K	293	960	1000	10	—
	10^{21} at 543 K	293	1080	1100	8	45
	Non-irradiated	573	530	580	14	75
	10^{20} at 523 K	573	680	720	13	—
	10^{21} at 543 K	573	780	810	9	65
Hardening from 1233-1273 K and ageing at 773 K for 24 h	Non-irradiated	573	480	580	13	70
	10^{20} at 573 K	573	770	810	8	50
	10^{21} at 543 K	573	860	860	4	5
Slow cooling from 1073 K	Non-irradiated	293	410	530	27	53
	Non-irradiated	573	210	310	27	67
Rapid cooling from 973 K and cold working by 20 %	Non-irradiated	293	630	730	13	51
	Non-irradiated	573	410	480	15	55

treatment on the strength of the alloy containing 2.5% Nb.

It follows from Table 8.11 that for an alloy containing 2.5% Nb σ_y varies from 0.4 to 7.8 MPa depending on the mode of thermal treatment. In a specified mode of thermal treatment the properties of certain blanks, tubes and the like may vary within wide limits. Table 8.10 gives values close to the minimum values of mechanical properties.

Prolonged service increases the diameter of the fuel channel tubes of zirconium owing to *creep*. After 4 to 5-h annealing at 738-823 K, the creep rate of the 2.5% Nb-bearing alloy at 1 MPa and 623 K is $(1.7-4.3) \cdot 10^{-7}$ h^{-1}. High temperature annealing (at 973 K during 30 min) increases the creep rate nearly tenfold.

At 573 K, the creep rate of the alloy containing 2.5% Nb ($\dot{\varepsilon}$, h^{-1}) and the stress (σ, MPa) are related to a first approximation as fol-

lows:

$$\log \dot{\varepsilon} = -8 + 0.1\sigma.$$

At 0.9 MPa, the creep rate and temperature are interrelated in a first approximation as follows:

$$\log \dot{\varepsilon} = -12.6 + 1.8 \cdot 10^{-2}t.$$

The prolonged strength depends essentially upon temperature. At 2.4-2.55 MPa, zircalloy-2 fails at 561 and 616 K in 10 882 and 140 h, respectively. At 561 K, increasing the stress from 2.55 to 2.72 MPa reduces the time to failure by a factor of 6.

In service, fuel channel tubes, fuel element clads, joints between tubes of stainless steel and zirconium alloy, and other components made of zirconium alloys are subjected to alternating stresses produced by temperature changes in the reactor coolant, internal pressure changes, external forces, or those generated by the coolant flow. In a first approximation, the number of cycles to failure N for alloys of Zr bearing 1-2.5% Nb at 573 K is connected with the deformation per each cycle (%) by the following relationship:

$$\log N = 5.32 - 2.32 \log \varepsilon.$$

Irradiation Effect. Table 8.11 gives data on the irradiation effect on the alloy properties. After hardening from 1 150 K and ageing, the alloy possesses high mechanical properties, at 573 K including. Irradiation with a neutron fluence of 10^{21} cm^{-2} somewhat decreases the ductility. After hardening from the β-phase and ageing, irradiation with the same fluence reduces the elongation from 13 to 4%.

At 293 K and neutron fluence of 10^{21} cm^{-2}, σ_y and σ_u of the alloy containing 1% Nb decrease by 180 and 60 MPa, respectively. With 2.5% Nb-bearing alloy, the values decrease by 300 and 230 MPa at 293 K and by 230 MPa at 573 K. Irradiation with a fast neutron flux of $(2-3) \cdot 10^{13}$ cm^{-2} s^{-1} ($E > 1$ MeV) does not reduce the ultimate long-term strength of Zircalloy-2.

In service, the fuel channels made of zirconium alloys change their dimensions because of radial creep and radiation growth. At temperatures close to 573 K and with a neutron fluence below 10^{20} cm^{-2} ($E > 1$ MeV), the theory evaluates creep of zirconium alloys as follows:

$$\log \varepsilon \, (\%) = -7.83 - (4.38/T \cdot 10^{-3})$$
$$+ (8 \cdot 10^{-3}\sigma/T \cdot 10^{-3} + 0.585 \log \varphi$$
$$+ 1.085 \log \tau,$$

where ε is the deformation, %; σ is the applied stress, MPa; φ is the neutron flux density at $E > 1$ MeV, cm^{-2} s^{-1}; τ is the time, h.

The radial deformation of the fuel channels of the CANDU reactor calculated by the above relationship accords well with the experimental data:

log τ	3.08	3.5	3.8	3.9	4.0
log ε: calculated	−1.96	−1.5	−1.2	−1.1	−1.0
experimental	−1.70	−1.25	−0.94	−0.9	−0.8

At a neutron fluence above 10^{20} cm^{-2} and σ ⩽ 140 MPa, the deformation may be evaluated by the following relation:

$$\log \varepsilon \ (\%) = 3 - (3.96/T \cdot 10^{-3})$$
$$+ (8 \cdot 10^{-3}\sigma/T \cdot 10^{-3}) + 0.5 \log \tau.$$

Elongation of fuel channels owing to radiation growth l (%) may be evaluated as follows:

$$\log l = -21.7 + \log \varphi + 1.7 \log \tau.$$

The radiation growth of the fuel channels of the Pickering reactor calculated by this relation agrees well with the experimental data:

log τ	4.26	4.4	4.48	4.60	4.66
log l: calculated	−1.20	−0.9	−0.72	−0.62	−0.50
experimental	−1.13	−0.9	−0.73	−0.62	−0.50

Compatibility. The solubility of uranium in α-Zr and zirconium in β-U is limited. Below 873 K, the interaction of zirconium with metallic uranium proceeds rather slowly. The β-Zr and γ-U are completely soluble in each other. The prevailing diffusion of uranium into zirconium at $T > 1073$ K forms in the uranium zone adjacent to the interface aggregates of vacancies which, coagulating, form micropores. This affects the bond between the fuel rod and the cladding and heat transfer between them. Zirconium alloys are compatible with unalloyed uranium up to 873 K.

At 873 K, UO_2 slowly interacts with zirconium alloys to form ZrO_2. Zirconium becomes brittle. Zirconium and its alloys can be used as matrices for dispersion of uranium compounds in the fuel rods of dispersed fuel elements, and also as claddings of fuel elements including a solid ceramic fuel rod operating at 873 K.

Corrosion Resistance. The quantity of electricity passed through a specimen of zirconium alloy containing 2.5% Nb at 573 K at a constant potential is equivalent to the amount of metallic zirconium that has passed into the ionic state. This amount was determined by the gain in weight, i.e. by the amount of oxygen consumed in the ionization of zirconium in the course of formation of oxide film. This indicates that corrosion of zirconium and its alloys in water at 573 K is an electrochemical process.

Zirconium easily passivates. With time, oxygen diffusing through passivating metal dissolves in the metal. This produces an interstitial solid solution and the lattice of Zr distorts. At a certain concentration of dissolved oxygen, the lattice distorts so that it becomes more favorable from the energy standpoint to form a zirconium solid solution in zirconium dioxide. The oxygen is then lacking compared with the stoichiometric amount in ZrO_2. The formed black protective oxide film of nonstoichiometric composition may be represented as $ZrO_{1.998}$. The oxide film on the surface of zirconium and its alloys always contains pores.

In corrosion of zirconium the main source of oxygen is water. If monoatomic oxygen diffuses through an oxide film into the metal, the corrosion in water should not differ from that in the gaseous oxygen, i.e. it must follow the chemical mechanism.

In electrochemical corrosion, the oxygen ion must form from water, say, by the following reaction:

$H_2O \rightleftarrows 2H^+ + O^{2-}$.
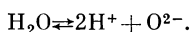
The oxygen ions diffuse through the oxide film towards the metal surface.

Similar to the electrochemical reaction, zirconium in the anodic process may ionize only when the oxygen interacting with the metal cannot accept an electron.

The oxide film of nonstoichiometric composition carries anionic vacancies. This facilitates the oxygen migration through the oxide film, and it proceeds at an activation energy of 120 kJ/mole. In water at 573 K, an increase in the mass of specimens of an alloy containing 2.5% Nb (ΔG, mg/dm^2) and the test duration τ (h) are connected by the following relation:

$\log \Delta G = 0.12 + 0.5 \log \tau$.

The corrosion follows a parabolic law. The amount of oxygen diffusing through the oxide film depends on its thickness and the concentration gradient. The oxygen concentration is constant in the saturated solution underlying the oxide layer. Hence, with an oxide film of a certain thickness corresponding to a gain in weight of 53.5 mg/dm^2, the oxygen content in the outer layers of the oxide film should correspond to a stoichiometric one, in order that the diffusing oxygen allows corrosion to occur. The oxide film of stoichiometric composition, ZrO_2, is white and has no protective properties. It falls off a black protective film underlying it. The thickness of the latter remains constant as corrosion proceeds. The corrosion in that follows a linear law.

In corrosion of niobium-bearing zirconium alloys, the rate of passage of the corrosion products into the coolant is close to 10^{-2} g m^{-2} day^{-1}.

With an increase in temperature, corrosion of zirconium alloys intensifies. Alloys containing 1 and 2.5 % Nb operate below 623 K. At higher temperatures, use is made of alloys, type valloy, with the addition of iron. At 673 K, in a medium containing 0.1 mg/kg oxygen the following relation is satisfied for this alloy:

$$\log \Delta G = 0.1 + 0.55 \log \tau.$$

When zirconium is contaminated with nitrogen, the latter finds its way to the interstitial sites and deforms the lattice. Oxygen diffusing in corrosion in the metal additionally deforms the lattice. The solid solution changes directly into zirconium oxide of the stoichiometric composition possessing no protective properties. The corrosion follows a linear law and proceeds at a high rate. To compensate for the detrimental effect of nitrogen, zirconium is alloyed with tin. The effect of carbon is similar to that of nitrogen.

When being adsorbed on the surface of oxide film, molecules of water-dissolved oxygen dissociate into the oxygen flow through the oxide film, and the rate of Zr corrosion increases.

When O_2 and NH_4OH are present in the medium together, NO_3^- may form. The reaction proceeds through an intermediate monoatomic nitrogen which dissolves in zirconium and reduces its corrosion resistance. Therefore, when both reagents are present in the coolant, the oxygen concentration should not exceed 0.1 mg/kg at an ammonia concentration corresponding to pH = 9.

At 573 K, 70% of the hydrogen released in corrosion diffuses through the bulk of components made of Zr alloys. The amount of hydrogen remaining in the metal is insufficient to form hydrides at 573 K. As the temperature decreases, the hydrogen solubility drops and at 293 K hydrides are fixed in zirconium alloys. At low temperatures, however, the coolant pressure is low too and accordingly the operating strain in the metal is not high. Therefore, the presence of hydrides should not affect the service life of equipment made of zirconium alloys.

The presence of chlorides and, especially, fluorides in the medium in an amount of 0.05 mg/kg reduces the corrosion resistance of zirconium alloys. The corrosion resistance of the zirconium alloy welded joints is raised by the mechanical and heat treatment. Items of zirconium alloys become more corrosion resistant after pickling in a mixture of nitric and hydrofluoric acids.

Irradiation produces radiation defects in the lattice of zirconium and its alloys. This increases the lattice energy and enhances the oxygen diffusion, which increases the rate of corrosion. A heat flow of $4.18 \cdot 10^6$ kJ m^{-2} h^{-1} enhances corrosion of zirconium alloys.

In a number of cases vibrating parts of zirconium alloys regularly contact one another and items of stainless steel. This may damage the protective oxide film on the surface of zirconium alloys. The

regular contact with stainless steel may hinder with the restoration of the oxide film. Fretting corrosion in this case enhances.

Requirements Imposed on Coolant of Boiling Reactors in Manufacturing Zirconium Fuel Element Claddings and Fuel Channels. The feed water must be deaerated. Decreasing the oxygen concentration in the feed water decreases the intensity of radiolysis and thus the oxygen concentration in the circulation water, which increases the corrosion resistance of the fuel element claddings, fuel channels, and other components of reactor core made of zirconium alloys.

Entrance of ammonia into the circulation circuit and its generation in the core zone must be excluded completely, for which reason extreme care must be exercised in using hydrazine for water deaeration purposes in the systems of boiling reactors.

In boiling water reactors, the concentration of the chlorine ion is rated at 0.1 mg/kg. This is not the optimal value from the standpoint of providing better corrosion resistance to the core materials and is associated with the specific operation of a single-circuit BWR. Because of the capillary effect in the corrosion product deposits, the concentration of the chlorine ion on the surface of the fuel element cladding may exceed 0.1 mg/kg. Therefore, the chloride ion content in the circulation water must be maintained at its minimum and never exceed it. The concentration of the fluoride ion should not exceed 0.02 mg/kg. Increasing the content of the fluoride ion and acidifying the medium should not take place simultaneously.

As follows from the above, it is good practice to use the ion exchanger for cleaning the circulation water. It is extremely objectionable to increase the content of corrosion products in the circulation water even for a short period of time, for instance, in starting, changing modes of operation, etc. The formation of deposits on the fuel elements increases the cladding temperature and concentrates water impurities affecting thus the corrosion resistance of zirconium alloys utilized in the manufacture of the fuel element claddings.

8.7 Austenitic Chrome-nickel Stainless Steel

Very severe corrosion-resistance requirements are imposed on the structural materials of the reactor circuit of nuclear power plants. This is of utmost importance for circuits employing light water and liquid metals as reactor coolants. Water, even highly purified, is a corrosive medium. Mass transfer is observed in liquid metals above 773 K.

The first years of building water- and liquid metal-cooled power nuclear plants yielded little data on the corrosion resistance of various materials in pure water and liquid metals, since the conventional power engineering did not resolve itself to the study of these problems. Studies were confined to highly resistant materials utili-

zed in allied industries. Much emphasis has been placed on the aus-
tenitic chrome-nickel stainless steel (Soviet, grades X18H9 and
X18H10T and American, grades 304 and 347). The steels of this
class are corrosion-resistant in water to 633 K, in gas coolant (in
carbon dioxide, for instance), to 873 K, and in superheated steam,
up to 923 K. Along with high corrosion resistance these materials
possess the required manufacturing characteristics.

Austenitic stainless steels are successfully used for manufacturing the
fuel element claddings and other components of reactor core in thermal
and fast reactors. Although they have a higher thermal neutron absorp-
tion cross section [$(2.7-2.9) \cdot 10^{-28}$ m² as compared with $0.19 \cdot 10^{-28}$ m²
in zirconium], which involves the use of a more enriched fuel, the
chrome-nickel stainless steels have a number of important advant-
ages over other materials. They are much cheaper than zirconium,
possess a better high-temperature strength and a higher heat resistance
up to 823 to 873 K, and are well weldable and susceptible to manu-
facture. Claddings of X18H10T steel are more favorable in fast-neu-
tron reactors, since they mainly employ the liquid metal coolants.

The composition of certain chrome-nickel steels and their alloys
is given in Table 8.12. The austenitic stainless steels have fairly high
mechanical properties up to 873 to 923 K (see Table 8.13). There-
fore, they may find application in reactors operating at high coolant
pressures. To raise the high-temperature strength of the austenitic
stainless steels, they should be additionally alloyed with molybde-
num and tungsten.

When use is made of the austenitic stainless steels, one must pay
regard to the compatibility of the steel with the fuel. The X18H10T
steel is highly compatible with uranium dioxide up to 1023 K. This
is especially important, when use is made of the liquid metal cool-
ants, as even with an unsealed fuel element cladding uranium diox-
ide does not interact with the liquid metal (sodium). These steels
interact with metallic uranium within 773-973 K to form the urani-
um-containing intermetallic compounds in a layer of 0.03 to 0.5 nm
thick.

Uranium monocarbide is highly compatible with the austenitic
stainless steels to 873 K. At a higher temperature, it usually interacts
with steel and is incompatible with water, and high-temperature and
high-pressure steam. The steels are fairly corrosion resistant in water
of high purity and in steam. High corrosion resistance of the steels
is accounted for by their ability to passivate.

Depending upon the composition of steels, their structure, pH
and presence of impurities, the austenitic stainless steels may suf-
fer from several types of corrosion: general (affecting uniformly the
entire surface), local (pitting and pointed corrosion), intercrystal-
line (along grain boundaries), and stress corrosion.

The *general corrosion* of the steels in distilled water at room tem-

TABLE 8.12 Chemical Composition of Chrome-nickel Stainless Steels

Steel or alloy	Mass				
	C	Si	Mg	Cr	Ni
X18H10T	0.08	0.8	1-2	17-19	9-11
X18H10T (ЭЯ1Т)	0.12	0.8	1-2	17-19	9-11
X18H12T	0.08	0.8	1-2	17-19	11-13
1X14H16Б (ЭИ-694)	0.07-0.12	0.6	1-2	14-17	14-17
X14H18B2Б (ЭИ-695)	0.07-0.12	0.6	1-2	13-15	18-20
TP304 (4301 FRG)	0.07	1.0	2	18-19	9-10.5
X12H20T3P (ЭИ-696)	0.10	1.0	1	10-12.5	18-21
XH35BTЮ (ЭИ-787)	0.10	0.6	1	14-16	35-38
304*	0.8	1.0	2	18-20	8-10
316*	0.8	0.75	2	16-18	11-14
321*	0.8	1.0	2	17-19	9-12
347*	0.8	1.0	2	17-19	9-13
X16H16M3Б	0.05-0.1	0.8	0.8	14-17	14-16
O8X18H9T	0.08	0.8	1-2	17-19	0.8-9.5
OX18H10T	0.08	0.8	1-2	17-19	9-11
OX18H9 (ЭЯО)	0.06	0.8	1-2	17-19	8-10
OX18H9T	0.06	0.8	1-2	17-19	9-11
1X18H9T (ЭЯ1Т)	0.12	0.8	1-2	17-19	9-11
1X18H10T	0.08	0.8	1-2	17-19	9-11
X17H13M2T (ЭИ-448)	0.10	0.8	1-2	16-18	12-14
X17H16M3T	0.08	0.8	1-2	16-18	15-17
OX23H28M2T (ЭИ-628)	0.06	0.8	0.8	22-25	26-29
OX18H12Б	0.06	0.8	1-2	17-19	11-13
OX21H5T	0.08	0.8	0.8	20-22	4.8-5.8
OX21H6M2T	0.08	0.8	0.8	20-22	5.5-6.5

* Alloys produced in the USA.

perature proceeds with oxygen depolarization. As the temperature rises, the rate of the hydrogen ion discharge increases, and at 573 to 633 K corrosion in the deaerated water proceeds with hydrogen depolarization. When oxygen is present in water, the steel may corrode with oxygen depolarization also at a high temperature. The corrosion rate of austenitic stainless steels in saturated steam is practically equal to its corrosion rate in water at the same temperature.

At 553 to 623 K in water under static conditions the rate of general corrosion is 0.8 to 4 μm/year, and in water-steam mixture containing oxygen at a temperature up to 873 K and pressure up to 3.5 MPa it is from 5 to 10 μm/year. In commercial power plants, the corrosion rate somewhat rises due to irradiation and water and steam circulation. However, to 873 K the steels are sufficiently corrosion resistant.

The presence of slag inclusions, cracks, pits, various impurities, and other inhomogeneities in steel produces local corrosion (pitting,

content %

Ti	Mo	W	B	Nb	Ce	S	P
5% C	—	—	—	—	—	0.02	0.035
(%C-0.03)5	—	—	—	—	—	0.02	0.035
(%C-0.03)5	—	—	—	—	—	0.02	0.035
—	—	—	—	0.9-1.3	—	0.02	0.035
—	—	2-2.75	—	0.9-1.3	—	0.02	0.035
—	—	—	—	—	—	0.03	0.045
2.6-3.2	1.1-1.4	—	—	—	—	0.02	0.035
1.1-1.5	—	4-5	0.005	—	0.025	0.02	0.035
—	—	—	—	—	—	—	—
—	2-3	—	—	—	—	—	—
—	—	—	—	—	—	—	—
—	—	—	—	0.8	—	—	—
—	2.5-3.5	2.0-2.7	—	0.45-0.85	—	0.02	0.030
(%C-0.03) 5-0.8	—	—	—	—	—	—	—
(%C-0.03) 5-0.8	—	—	—	—	—	0.02	0.035
—	—	—	—	—	—	0.02	0.035
0.3-0.6	—	—	—	—	—	0.02	0.035
(%C-0,03) 5.0.8	—	—	—	—	—	0.02	0.035
(%C-0.03) 5-0.8	—	—	—	—	—	0.02	0.035
0.3-0.6	1.8-2.5	—	—	—	—	0.02	0.035
0.3-0.6	2.8-3.5	—	—	—	—	0.02	0.035
0.4-0.7	1.8-2.5	—	—	—	—	0.02	0.035
—	—	—	—	0.5-0.8	—	0.02	0.035
0.3-0.6	—	—	—	—	—	0.025	0.035
0.2-0.4	1.8-2.5	—	—	—	—	0.025	0.035

TABLE 8.13 Mechanical Properties of Steel, Grade X18H10T, at Various Temperatures

T, K	σ_y, MPa	σ_u, MPa	δ, %	ψ, %	a_i, J/cm^2	E, 10^{-5} MPa
293	270	655	55.0	75.5	250	2.02
373	245	510	44.0	76.5	—	1.98
473	205	465	38.0	70.5	370	1.93
573	160	450	29.0	66.0	—	1.85
673	180	445	26.5	64.0	317	1.77
773	170	430	30.0	64.5	365	1.69
823	180	455	40.5	61.0	365	1.64
873	160	360	28.5	64.5	360	1.60
923	160	355	30.0	68.3	—	1.55
973	180	275	29.5	57.5	340	1.50
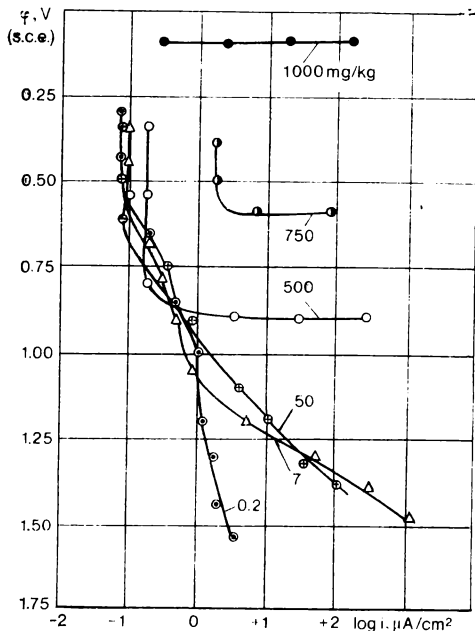
Fig. 8.6 Anodic curves of steel, grade 1X18H9T, in neutral medium (water) with different contents of chlorine ions

point- or spot-corrosion). This type of corrosion is particularly dangerous to thin-walled claddings of fuel elements, as a hole in the cladding admits the coolant to the nuclear fuel, which places the reactor under emergency conditions. Various inhomogeneities in the metal produce microgalvanic corrosion couples. This results in local depassivation of metal. Local corrosion is facilitated also by the presence of the chlorine ion in water, which enhances depassivation of the metal surface. This is illustrated by anodic curves in Fig. 8.6. As the concentration of the chlorine ions in the solution increases, the area of passivity contracts, and at a concentration of chlorides of 1000 mg/kg the metal activates completely. Therefore, the permissible amount of chlorides in the reactor water should not exceed 0.1 mg/kg. Local corrosion of the steels is more intensive in stagnant areas, crevices, etc., in other words, in places where evaporation increases the content of impurities. These steels are used in the reactor core as materials for fuel assemblies, supports, spacing parts, thermal shields. When parts are made of different metals, say, stainless steel and aluminum, the net rate of aluminum corrosion increases because the difference in their potentials may generate macrogalvanic couples.

The austenitic stainless steels may also suffer from local corrosion, i.e. intercrystalline corrosion. Heating the steels to 823-923 K forms chromium carbide which precipitates along grain boundaries. The boundary regions become depleted of chromium, and this affects their electrochemical stability. As has been observed, steels rich in carbon are more liable to intercrystalline attack, as at this temperature carbon intensively diffuses towards the grain boundaries.

Increasing the nickel content of the austenitic stainless steels has no effect on its susceptibility to this sort of destruction. Sometimes an increased content of chromium, or its additional alloying with molybdenum adds to the passivity of depleted boundaries and thus improves the resistance of steels to intercrystalline corrosion. This, however, is not the optimal way to control the corrosion. The best results yields alloying, or as it is said, stabilization, of the austenitic stainless steels with titanium or niobium. They combine with carbon to produce fairly resistant carbides which do not dissociate even when steels are being austenized at 1323 to 1373 K. In stabilized steels, the content of free carbon, i.e. not bound into titanium and niobium carbides, is small and does not exceed the solubility of carbon in the austenite at room temperature. Therefore, no chromium carbides are formed and the grain boundaries do not become depleted of chromium.

The amount of titanium and niobium added to steel depends on its carbon content and is determined by the following relationships:

$$\%\,Ti = 5\,(\%\,C\text{-}0.03);$$
$$\%\,Nb = 10\,(\%\,C\text{-}0.03).$$

If steel is nitrogen-alloyed, it should be stabilized with niobium, as titanium is consumed to form nitrides. To manufacture superthin tubes having a wall thickness of 0.5 mm or less use should also be made of niobium-bearing steel. Titanium may produce carbides nearly comparable in size with the tube wall thickness.

The resistance of the austenitic stainless steels to intercrystalline corrosion essentially depends upon thermal treatment. The corrosion resistance of parts made of steel liable to intercrystalline attack may be improved by austenizing, provided the operating temperature of the parts does not exceed 873 K. In austenizing, chromium carbides dissociate, and the steel becomes resistant to intercrystalline corrosion. In certain cases it is advisable to subject an austenitic stainless steel to stabilizing annealing at 1073 to 1143 K for 1-3 h. In this case a maximum amount of carbon binds into carbides. The boundary regions of grains become depleted of chromium. However, at 1073 to 1143 K the rate of chromium diffusion is sufficiently high, and its diffusion from the center of grains towards boundaries increases the chromium concentration at the latter and the steel grains resistance to intercrystalline corrosion.

After prolonged service at 773 to 873 K, the austenitic stainless steels stabilized with titanium and niobium become susceptible to intercrystalline corrosion. To eliminate this, the titanium-to-carbon ratio in the steel should be increased and the steel should be subjected to austenization with subsequent stabilization. To make the austenitic stainless steels resistant to intercrystalline corrosion in prolonged operation at 773 to 923 K the titanium-to-carbon ratio should be 10-17.

Carbides precipitate and grain boundaries become depleted of chromium when steel is heated in welding. Steel is heated to 823-923 K in the near-seam area which is most often disposed to intercrystalline attack.

It should be noted that a steel prone to intercrystalline corrosion is attacked, but not in all media. The intercrystalline corrosion proceeds most intensively in acid media at an elevated temperature. At temperatures above 373 K and high pressure, intercrystalline corrosion occurs in water and steam containing oxygen in an amount above 0.1-0.3 mg/kg. In deaerated water and steam, intercrystalline corrosion does not attack steels prone to it when tested by the standard technique as the case is with an aerated water below 373 K.

Testing steels for their liability to intercrystalline attack is standardized. The susceptibility to intercrystalline corrosion is checked on welded specimens.

When manufacturing the most important components, each forging, tube, etc. is tested for the resistance to intercrystalline corrosion. With less important components it will suffice to test the metal of a given melting lot.

Under joint effect of mechanical stresses and corrosive medium the austenitic stainless steels undergo what is known as corrosion cracking. The stress may be either applied or residual but, as a rule, tensile. Corrosion cracking occurs in the form of cracks. The rate of their propagation depends on the composition and parameters of the corrosive medium. Metals may crack from the surface inward trans- or intergranularly. Corrosion cracking is a dangerous type of failure and can render the equipment inoperative. It depends on many factors: stress, medium composition, structure and composition of the metal, temperature, duration of effect, degree of plastic deformation (strain-hardening), nature of protective films on the metal, etc.

In order to make austenitic steel less susceptible to corrosion cracking one has to eliminate strain-hardening. Tensile stresses from strain-hardening are added to the operating tensile stresses and can drastically accelerate cracking.

Increasing the chromium content of the steel containing a constant amount of nickel and also decreasing the content of the elements facilitating the formation of the austenite (carbon, nitrogen) to 0.01-0.002% make this steel more resistant to corrosion cracking. Increas-
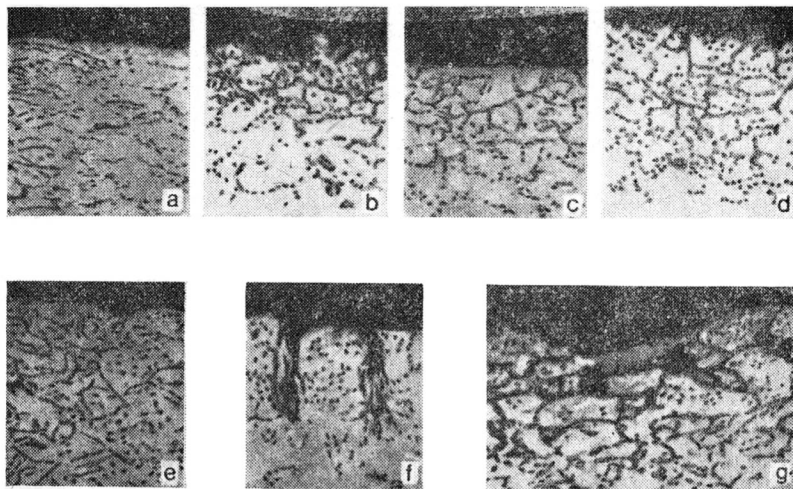
Fig. 8.7 Microstructure of hardened steel, grade 1X18H9T, after testing in neutral medium (water) with different contents of chlorides, mg/kg
a—0.05; b—0.1; c—1.0; d—10; e—100; f—1000; g—10 000 (specimens are etched)

ing the content of the austenite-forming element, nickel, to 10-12% and more makes the austenite more stable and the steel more resistant to corrosion cracking. Alloys, inconel, incalloy, etc. containing substantial percentage of nickel are more resistant to corrosion cracking than steel, grade X18H10T.

The composition of corrosive medium plays an important role in corrosion cracking of the austenitic stainless steels. The austenitic stainless steels crack in solutions containing chlorides and oxygen. As the content of chlorides increases, the area of passivity of the steels decreases (see Fig. 8.6). Figure 8.6 shows that when the solution contains 1000 mg/kg of chlorides the steels completely activate. The greater the amount of chlorides the more pronounced is corrosion cracking of the austenitic stainless steels. Fig. 8.7 gives data on corrosion cracking of one of the steels strain-hardened to 30% in neutral solutions at various contents of chlorides at 583 K without initial deaeration of the solution. With an increase in the content of chlorides corrosion cracking of steel abruptly increases, and specimens fail completely at a chloride concentration of 1000 mg/kg.

Corrosion cracking of the austenitic stainless steels occurs also in the steam phase. However, the most dangerous are the metal areas subjected to alternating wetting and drying, i.e. to local evaporation. Nuclear power reactors employ as the coolant water of high purity. The reactor and feed water is strictly rated as to the content of
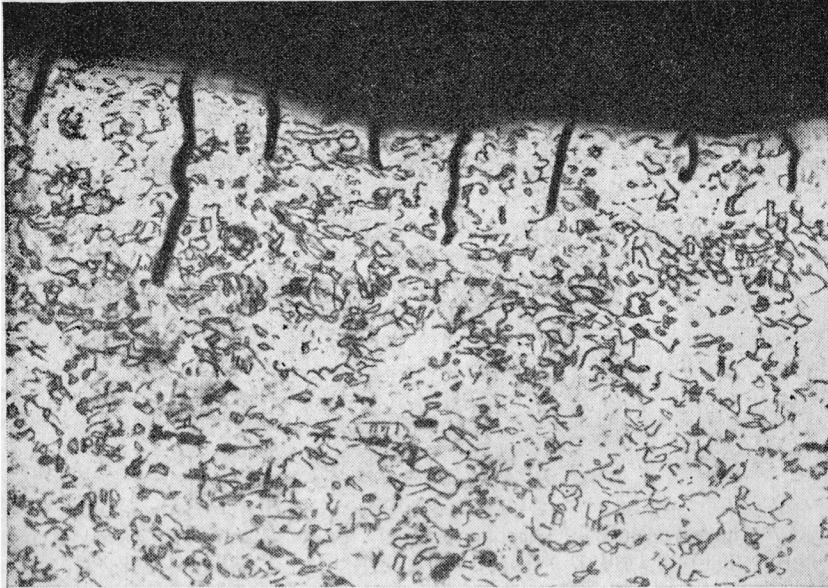
Fig. 8.8 Microstructure of steel, grade 1X18H9T, at the end where tubes are expanded into tube plate of steam generator

chlorides. However, despite the small content of chlorides in reactor water (from 0.1 to 0.5 mg/kg) and in steam generator water (0.5 to 1 mg/kg), evaporation in certain areas (joints of steam generator tubes in the tube plates, stagnant areas and the like) may increase the content of chlorides to concentrations dangerous from the corrosion cracking point of view. Fig. 8.8 displays a microphotograph of a steam generator tube attacked by corrosion resulting from the evaporation of water with a chloride content of 0.5 mg/kg.

In once-through steam generators operating at 3 to 5 MPa the salt solubility in steam is small. As a result, chlorides accumulate in water in the evaporation zone. This excludes the manufacture of steam generators with medium steam parameters of the austenitic stainless steels.

At 18 MPa and above the chloride dissolution in steam accelerates and the chloride concentration in water does not exceed the permissible values. Therefore, once-through steam generators employing heat-exchange tubes of the austenitic steels should be designed only for high pressures. At 3 to 5 MPa, steels should be used to make recirculation steam generators.

Corrosion cracking may occur either at a high or at a relatively low temperature (353-363 K). When water contacts (say, due to leakage)

the outer surface of the tubing heated to 353-373 K, the water evaporates and the concentration of chlorides on the tubing surface increases. Corrosion cracking may be generated by internal strains in the metal arising from cold rolling of tubes and also from chance impacts and scores. As a rule, at 293-313 K the austenitic stainless steels do not develop corrosion cracking. This allows them to be used even in condensers cooled with sea water. Chlorides may find their way into steel from insulation materials, causing stress corrosion. Corrosion cracking of steels proceeds also in the steam phase, when the steam is contaminated with chlorides and oxygen. Cases have been reported of damage to the fuel element claddings caused by nuclear superheated steam on account of the development of corrosion cracking.

The austenitic stainless steels are highly resistant to attack within a wide range of the water pH as regards both general corrosion and corrosion cracking. Oxygen enhances corrosion cracking. Thus, in the presence of chlorides in water corrosion cracking is observed at an oxygen concentration of 1 mg/kg. Increasing the oxygen concentration to 1200 mg/kg does not abruptly accelerate the corrosion cracking, i.e. it is not the oxygen concentration but rather its presence that is of importance. Corrosion cracking of steel may take place also in the absence of oxygen, if water contains other readily reducible elements, say, ferric iron.

In nuclear power plants, the reactor water always contains the radiolytic oxygen produced by radiolysis. Inasmuch as the radiolytic decomposition of water proceeds to a greater extent in boiling reactors, the content of the radiolytic oxygen in steam may reach 40 mg/kg. Therefore, the content of chlorides in the reactor water is strictly rated. So, to prevent corrosion cracking of steel, water, saturated steam, and superheated steam must be maintained at a high level of purity. The liability of the chrome-nickel austenitic steels to corrosion cracking decreases with an increase in the content of nickel.

Lattice imperfections play an essential role in corrosion cracking of metals and alloys. The formation and specific distribution of defects embrittle usually ductile materials.

Nickel has a noticeable effect on the distribution of dislocations in the austenitic stainless steels. An increase in the nickel content increases the energy of stacking faults and facilitates the cross slip.

The distribution of dislocations in deformed austenitic stainless steels depends upon nickel content. Therefore, we should expect a considerable increase in the resistance of stainless steels containing 18% Cr to corrosion cracking with a nickel content above 18 to 20% (Fig. 8.9).

At a high concentration of alkalis and with strains in the metal, the austenitic stainless steels are susceptible to a specific sort of destruction, caustic embrittlement. This may also proceed in the absence of oxygen. The nature of this destruction has not been elucidated
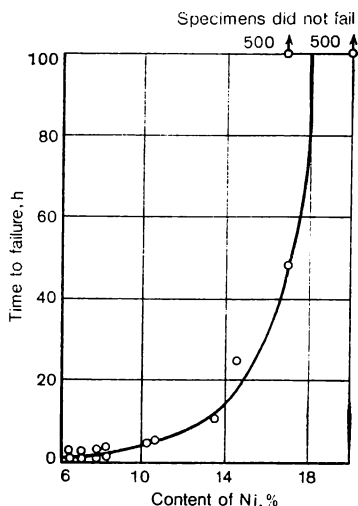
Fig. 8.9 Effect of nickel content in austenitic stainless steel (17-18% Cr) on its liability to corrosion cracking in a boiling $MgCl_2$ solution under 2.8 MPa

yet. Caustic embrittlement takes place, for instance, in the areas where evaporation increases the content of alkalis 10 times and more.

To prevent the austenitic stainless steels from corrosion cracking in nuclear power plants modern facilities of water treatment should be used and conditions under which the metal operates, the quality of metal and welding, and thermal treatment should be improved. The correct choice of the heat flow scheme of the nuclear power plant and design of its components are also of importance.

As has been noted already, the austenitic stainless steels find wide application in the liquid-metal cooled systems (eutectic Pb-Bi, Na, K, eutectic Na-K, Li). The corrosive effect of liquid metal on steel is specific. It differs in nature from chemical and electrochemical corrosion. The effect is most perceptible with the coolant temperature above 773 K.

With the austenitic stainless steels and complex liquid-metal coolants (say, eutectic Na-K) and in the presence of various impurities (C, O, N, H, and others), the interaction becomes far more intricate. The individual components of the liquid metal may selectively interact with components of the solid metal. In the systems of the austenitic stainless steels with liquid-alkali metal coolants, the thermal mass transfer becomes perceptible at 773-873 K at a temperature gradient in the system of the order of a few tens of degrees. Corrosion damage is localized in areas of the highest temperature.

As the flow velocity of a liquid-metal coolant increases, the steel dissolution accelerates. The rate of dissolution is proportional to the liquid metal velocity raised to about 0.8. At higher velocities, corrosion is accompanied by erosion and mechanical damage, particularly in heavy liquid metals. Mass transfer is mainly caused by that the solubility of a given substance considerably varies with temperature (Table 8.14). Hence, nickel or iron contained in steel may dissolve in eutectic Pb-Bi in the core operating at a high temperature and precipitate in the form of the intermetallic compounds or pure metal in the less heated parts of the circuit.

Of great importance in mass transfer is the difference in the con-

TABLE 8.14 Approximate Solubility of Solid Metals
in Liquid Alkali Metals

Liquid metal	Tempera-ture, K	Mass content of solid metal, %				
		Ni	Cr	Fe	Nb	Mo
Li	873	0.1	0.01	0.002	—	—
	1073	1.8	0.02	0.005	—	—
	1273	4.0	—	0.025	< 0.0001	< 0.0001
	1473	—	4.00	0.065	—	0.03-0.10
Na	873	—	0.00001	0.001	—	—
	1073	—	—	0.002	—	—
	1273	0.004	—	0.008	0.0007	—
	1473	—	—	0.060	0.0030	—

centration of a component contained in liquid metal. This may cause for instance, carburization of an austenitic steel at the expense of de-carburization of a perlitic steel, if any, and change the mechanical properties of steel. Hence, in eutectic Pb-Bi, nickel and chromium are leached out of the steel. The result is that the strength and ducti-lity of the steel badly decrease, and the austenite in the interaction zone partially changes to ferrite.

In liquid sodium, the steel components may also dissolve in the hot part of the circuit and precipitate in the cold. The austenitic stain-less steels are fairly resistant in liquid sodium and eutectic Na-K. Thus, at 837 K in a circuit handling a flow of sodium containing 0.002% oxygen the depth of corrosion damage of steel X18H8Б is 2 to 3 μm/year. Therefore, the liquid metal should be primarily clean-ed from oxygen. Besides, carbon is very readily leached out and transferred. Therefore, when designing the reactor circuits made of such steels, utilize steels with the lowest content of carbon and also provide regular cleaning of the liquid metal from carbon.

As compared with other liquid-metal coolants, alkali metals are the least corrosive, and the austenitic stainless steels are most suit-able for continuous operation in them below 873 K. At a higher tempe-rature the surface of stainless steels noticeably carburize. This is es-pecially pronounced in steels alloyed with strong carbide-forming ele-ments, say, titanium. The carburization enhances in the presence of carbon-containing materials in the system and may involve carbon transfer. Mass transfer also increases with a considerable temperature gradient in the system (423-473 K).

Mass transfer is also characteristic of steel components (Ni, Fe, Cr) with concurrent intercrystalline corrosion of the steel. In flowing sodium, the rate of intercrystalline corrosion of the austenitic chro-
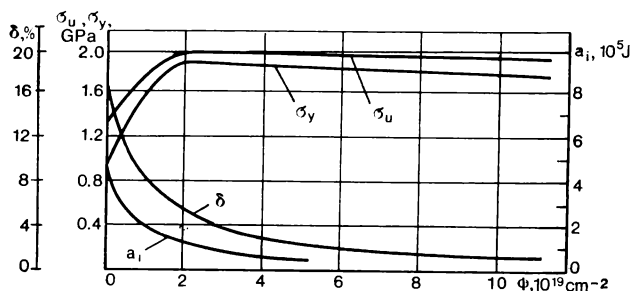
Fig. 8.10 Changes in mechanical properties of Cr-Ni-Mo bearing steel under irradiation

mium-nickel steels is 0.05-0.25 mm/year at 873-973 K. It depends mainly on the oxygen content in sodium, drastically increasing when the oxygen content exceeds 0.005%. The corrosion products arise on the steel surface in the form of complex oxides of iron and sodium which can also dissolve in the flow and then precipitate in the cold portions of the circuit. Above 973 K, high-temperature and heat-resistant metals and their alloys may be used, for example, nickel-based alloy (60-75% Ni, 16-20% Cr, up to 5% Mo, 1-2.5% Ti, up to 10% W). The corrosion resistance of high-temperature steels may be improved by adding up to 30% Al.

At a high sodium temperature (above 1073 K), it is advisable to use refractory metals (Ta, Mo, Nb, W) and their alloys. Oxygen and nitrogen in liquid metal decrease the corrosion resistance of refractory metals.

The corrosion resistance of the austenitic steels in eutectic Na-K is lower than in sodium and decreases still more with an increase in the potassium content of the mixture. In lithium, the rate of corrosion is considerable. Besides, it is not recommended to combine it with steels having a high content of nickel, since nickel is readily leached out. The rate of attack in lithium is essentially enhanced by impurities, first of all, by nitrogen and oxygen. Chromium-nickel steels with lithium coolants may be utilized up to 773 to 873 K. At higher temperatures (973-1073 K), preference should be given to ferritic stainless steels (for example, 0X13, 1X13, 1X12M2БΦ, and others) containing no nickel. Changes in temperature produce thermal stresses in the structural material which depend on the rate of temperature variations. Thermal stresses depend upon the physical and mechanical properties of the material. In the austenitic stainless steels having a relatively low thermal conductivity, thermal stresses may be considerable and may cause destruction of the steel.

Structural materials of the core are subject to irradiation with neutrons, gamma-quanta and electrons.
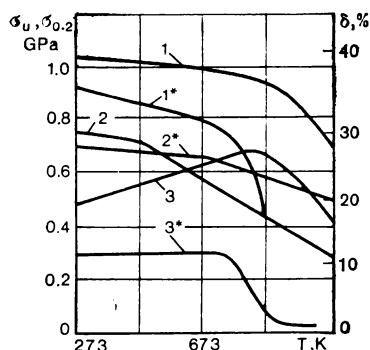
Fig. 8.11 Mechanical properties of nonirradiated (*1-3*) and irradiated with neutron fluence of (*1-3*)·10^{20} cm^{-2} at 423-473 K (*1*-3**) heat resistant nickel alloy, grade XH77TЮP, versus testing temperature
1, 1*$-\sigma_u$; *2, 2**$-\sigma_{0.2}$; *3, 3**$-\delta$

Irradiation affects the mechanical properties of materials: the yield point and ultimate strength (to a lesser degree) increase, whilst the elongation and reduction of area decrease. Therefore, irradiation causes radiation embrittlement of metals and alloys. This combined with thermal and other stresses, vibration, thermal cycles, and corrosive attack of the reactor coolant may lead to failure of the fuel element claddings. Low-temperature irradiation of steel, grade 1X18H10T, with a neutron fluence of up to 4·10^{22} cm^{-2} increases the strength and decreases the ductility of the steel (Fig. 8.10).

Increasing the irradiation temperature above 773 K badly affects the mechanical properties of materials. High-temperature embrittlement is featured both by the austenitic alloy steels and by the nickel-based alloys. Figure 8.11 shows changes in the mechanical properties of superalloy XH77TЮP (20% Cr, 2.5% Ti, 0.8% Al, Ni the rest) irradiated at 423-473 K and tested up to 1073 K. Above 873 K, the elongation and ultimate strength rapidly decrease. The accumulation of helium produced by certain nuclear reactions as well as the formation of the intermetallic phases promote steel embrittlement and drastically decrease the ductility of steel.

9

Materials
of Reactor Vessel
and Other Components
of Nuclear Power Plants

9.1 Perlitic Steels

Composition and Structure. Iron-base steel-alloys are widely used in machine building including nuclear power engineering. Low strength ($\sigma_0 \approx 280\,\text{MPa}$) limits the use of pure iron as a structural material. Iron is an element of group VIII of the periodic table, its atomic number is 26. It is a transition metal. Natural iron consists of isotopes: [54]Fe, 5.84%; [56]Fe, 91.68%; [57]Fe, 2.17%; and [58]Fe, 0.31%. Irradiation with neutrons mainly produces radionuclide ^{59}Fe with

TABLE 9.1 Physical Properties of Iron

Atomic number	26
Atomic weight	55.847
Thermal neutron absorption cross section, m^2	$2.43 \cdot 10^{-28}$
Density, g/cm^3	7.86
Melting point, K	1811
Boiling point, K	3145
Sublimation heat (lattice energy) at 293 K, kJ/mole	405
Coefficient of linear expansion, deg^{-1} :	
363-576 K	$1.07 \cdot 10^{-5}$
576-1460 K	$1.67 \cdot 10^{-5}$
Thermal conductivity, $\text{W m}^{-1}\,\text{K}^{-1}$	74
Crystal structure	α-phase, BCC to 1183 K
	γ-phase, FCC to 1665 K
Lattice parameter, nm	α-phase, $a = 0.286$
	γ-phase, $a = 0.364$
Modulus of elasticity, GPa	217
Shear modulus, GPa	84.7

a 45.1-day half-life, β-radiation energy of 0.475-1.57 MeV and γ-radiation energy of 0.199-1.095 MeV. Table 9.1 gives the physical properties of iron.

At present, steels of perlitic class containing 0.08 to 0.4% of carbon find wide application in reactor engineering. The total content of alloying elements in the steels does not exceed 5-6%. In designing and constructing the first nuclear power reactors, austenitic chrome-nickel stainless steel was utilized as a principal structural material. This was accounted for by its high resistance to corrosion which mi-

nimized the contamination of water in circuit I with corrosion products. As reactor engineering gained experience, it turned out that in a number of cases the austenitic chrome-nickel stainless steel was not the best material for the manufacture of certain components of circuit I. In particular, the strength of the austenitic chrome-nickel stainless steel is not sufficient for the reactor pressure vessel.

The austenitic chrome-nickel stainless steel resistant, generally speaking, to corrosion suffers from corrosion cracking and intercrystalline corrosion. Nickel used to alloy stainless steel always contains impurities of cobalt. Therefore, although in minute amounts, cobalt may be found in the products of corrosion of the stainless austenitic chrome-nickel steels which enter the water of circuit I. Those minute amounts of cobalt are, however, sufficient to impair the radiation situation. A month after a shut-down the main contribution to the radioactivity of the primary circuit equipment is made by the radioisotopes of cobalt.

The cost of the austenitic chrome-nickel stainless steels is high, and this materially affects the cost of electric power generated by atomic power stations. Substituting the perlitic steels for the stainless steels essentially reduces the cost of atomic power stations. The corrosion products of the perlitic steels do not contain cobalt. Most perlitic steels are susceptible to manufacture and are produced on a commercial level. In the case of utilizing the perlitic steels the experience gained by ordinary power engineering widely employing the perlitic steels can be applied to nuclear power engineering. The corrosion resistance of the perlitic steels is lower than that of the stainless steels. If the primary circuit of nuclear power plants utilizes the perlitic steels, measures should be taken to improve their corrosion resistance, in particular, by maintaining the water regime, by using the protective coatings, etc.

Pressure vessels of water-cooled reactors, in order to improve their mechanical characteristics, are made of steels alloyed with Cr, Mo, V, Mn. They are classed with the perlitic steels. They readily lend themselves to rolling. In general the reactor pressure vessel is welded of shells and bottom. Shells, bottom, and cover are made by stamping and forging.

In welding low-alloyed steel hardens near the seams, which generates local stresses. To remove them, the welded vessel should undergo thermal treatment. The same occurs when the reactor, drum-separator, piping flanges, etc. are welded in position inside the vessel. Considerable residual stresses arise in welding sites. The total (operating plus residual) stress causes metal failure because of cracking. This is especially dangerous for items made of high-strength steels, say, grade 16ГНМ, which have a yield point close to the ultimate strength. The stresses exceeding the yield point may cause brittle fracture. A low quality of metal, i.e. nonmetallic impurities in steel
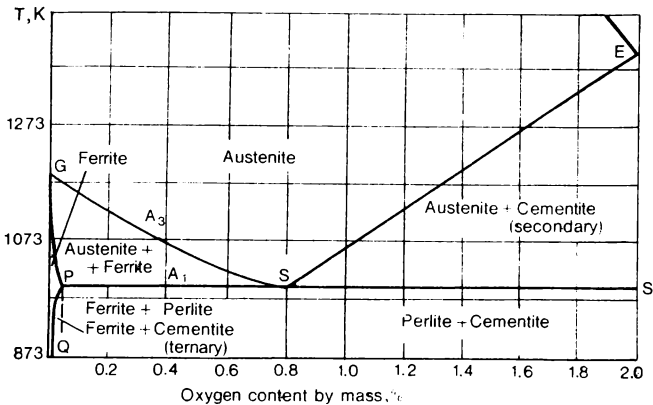
Fig. 9.1 Steel corner of Fe-C phase diagram

and the like, increases the risk of cracking in the area of welding.

In a water-cooled reactor, the vessel and cover made of a perlitic steel are surfaced with a stainless steel in order to reduce the contamination of the primary circuit water with the corrosion products and prevent the vessel from hydrogen absorption. Recently, however, a new trend appeared: maintaining the appropriate water regime allows the perlitic steel vessels to operate without the stainless steel cladding. Table 9.2 gives the composition of some perlitic steels.

The steels listed in Table 9.2 contain less than 0.42% C. According to the constitutional diagram Fe-C (Fig. 9.1) steels containing 0.8% C are hypoeutectoid. When the temperature drops below line GS the austenite starts to transform releasing the ferrite. Austenite is a structural constituent representing a solid solution of carbon in gamma-iron. The gamma-iron crystallizes in the FCC lattice. Ferrite is a structural constituent representing alpha-iron which slightly dissolves carbon. The alpha-iron crystallizes in the BCC lattice. In the GSP region, the hypoeutectoid steel consists of the ferrite and austenite. At $T < 996$ K (horizontal line PS') the eutectoid reaction proceeds: austenite $\rightarrow$ ferrite + cementite.

In steels containing below 0.8% C, the product of transformation is the eutectoid aggregate of ferrite and cementite known as perlite. Following complete transformation the steel consists of ferrite and perlite. Perlitic steels bearing less than 0.8% C have this structure after annealing.

Annealing is the phase recrystallization consisting in heating above temperature Ac_3 (see line A_3 in Fig. 9.1) with subsequent slow cooling. Perlitic steels are usually used in the normalized state. Normalizing is a sort of annealing. In normalizing, cooling is accomplished in the air, and, therefore, it proceeds at a somewhat greater

Table 9.2 Perlitic Steels

Grade	Mass content of alloying elements and impurities, %						
	C	Mn	Si	Ni	Mo	Cr	Other constituents
22K	0.18-0.23	0.7-1.0	0.17-0.57	—	—	—	—
16ГНМ	0.13-0.18	0.8-1.1	0.17-0.37	1.0-1.3	0.40-0.55	—	—
12ХМФ	0.08-0.15	0.4-0.7	0.17-0.37	0.3	0.25-0.35	0.9-1.2	0.25-0.30 V
SA302B	$\leqslant 0.31$	1.1	0.15-0.30	—	0.4-0.6	—	—
Steel 20	0.17-0.24	0.35-0.65	0.17-0.37	< 0.25	—	< 0.25	—
12MX	0.09-0.16	0.4-0.7	0.15-0.30	< 0.30	0.4-0.6	0.4-0.6	—
38X2MЮA	0.35-0.42	0.3-0.6	0.17-0.30	< 0.2	0.15-0.25	1.35-1.65	0.7-1.1 Al
10ХСНД	$\leqslant 0.12$	0.5-0.8	0.8-1.1	0.5-0.8	—	0.6-0.9	0.4-0.65 Cu
25X2HMФ	0.22-0.27	0.3-0.6	0.17-0.37	0.4	0.6-0.8	2.5-3.0	0.25-0.35 V
15X2HMФ	0.11-0.21	0.3-0.6	0.17-0.37	0.4	0.6-0.8	2.0-3.0	0.25-0.35 V

rate than in usual annealing. When cooling at a sufficient rate from a temperature above the critical point Ac_3, hardening takes place. As the cooling rate increases, the temperature of the eutectoid transformation Ar_1 decreases. With a decrease in Ar_1, the ferrite-cementite aggregate grows more and more finely dispersed and hard. If the rate of cooling is so high and overcooling is so considerable that no decomposition of the solid solution occurs, austenite transforms into martensite (a solid solution of carbon in alpha-iron). If metal is rapidly cooled from a temperature above Ac_1 and below Ac_3, it hardens incompletely.

Increasing the content of alloying elements improves the stability of the overcooled austenite. In steels alloyed with several elements, e.g. the Cr-Ni-Mo steels, the perlitic transformation is so delayed, that cooling in the air overcools the austenite to the temperature of the martensite transformation. Welding the pressure vessel may cause hardening of the low-alloyed steel in the seam area, which generates the internal stresses. To remove the stresses, the pressure vessel after welding is subjected to thermal treatment.

Physical and Mechanical Properties. The mechanical properties of steels (Table 9.3) depend not only upon their chemical properties and mode of thermal treatment but also upon the thickness and overall dimensions of the blank. Low-alloyed steels at thicknesses of 161-400 mm have a yield point of 300-550 MPa and belong to strength class 25-70.

At $T > 673\text{-}753$ K, the steel strength is characterized by long-term strength. For steels, grades 12XM and 12XMФ, the long-term strength is 130 and 180 MPa, respectively, at 783 K and test duration of 10^5 h. At 783 K and 120 MPa, the rate of creep is 10^{-5} %/h. Steel, grades 25X2HMФ, 15X2HMФA, SA302B (see Table 9.2) is used to manufacture the vessel shells and covers, steel, grades 16ГHM, 22К, to make drum-separators, steel, grades 12XMФ, 12XM, steel 20, 10ГH2MФA, to produce tubes, steel, grade 10XCHД, to make structural components of the channel-type reactors, and steel, grade 38X2MЮA, to produce fasteners.

Radiation Stability. In service, the reactor pressure vessel is exposed to severe neutron irradiation. This changes the mechanical characteristics of perlitic steels. The steel density and heat conductivity vary but little.

Neutron irradiation changes the critical temperature of brittleness and impact strength, which involves the risk of brittle failure. The low-temperature brittleness consists in a drastic decrease in impact strength and steel embrittlement upon the reduction of temperature below a certain critical value. More than that, irradiation affects the ultimate strength and yield point. Small neutron fluences (up to 10^{17} cm^{-2}) produce only a slight effect on the mechanical properties of carbon and low-alloyed steels. After an incubation period,

Table 9.3 Physical and Mechanical Properties of Perlitic Steels

Grade	σ_u, MPa (293 K)	σ_y, MPa (293 K)	δ, % (293 K)	a_i, J/cm² (293 K)	σ_y, MPa (573 K)	Coefficient of linear expansion, 10^{-6} deg^{-1} (573 K)	Thermal conductivity, W m^{-1} K^{-1} (573 K)
22K	440-560	220-350	20-23	90-150	200-270	12.4-13.4	46
16ГНМ	530-680	280-500	17-28	76-190	260-500	—	—
12ХМФ	510-670	290-530	23-39	150-230	250-400	12.35	36
SA302B	—	350	—	—	300	—	—
Steel 20	510	320	32	50	210	13	44
12МХ	450	280	31	190	270	12.7	50
38Х2МЮА	855	665	16.5	160	580	13.3	—
10ХСНД	540	400	16	—	—	—	—
25Х2НМФ	—	600-630	17-20	—	600-630	—	—
15Х2НМФ	—	480-500	17-20	—	480-500	—	—
15Х2НМФА	620	500	15	248	450	11.3	31
10ГН2МФА	550	350	16	—	300	—	—

18—0816
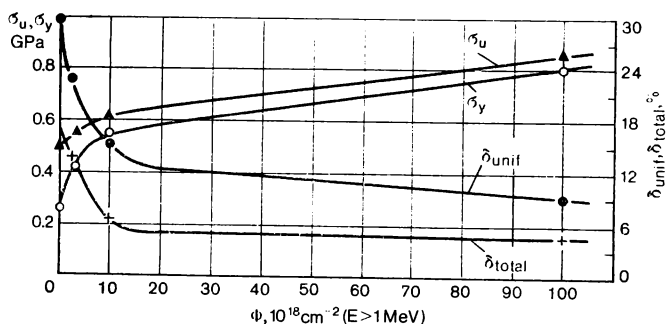
Fig. 9.2 Changes in mechanical characteristics of low-carbon steel (0.2% C, by mass) under irradiation

σ_u—ultimate strength; σ_y—yield point; δ_{unif}—uniform elongation; δ_{total}—total elongation

a further increase in the fluence changes sharply the mechanical characteristics of steel, i.e. the rate of radiation hardening and embrittlement is high. Increasing the fluence further changes the mechanical characteristics but less intensively (Fig. 9.2). At fluences of 10^{18} to 10^{19} cm^{-2}, the yield point of steel changes far more considerably than the ultimate strength. With an increase in fluence, the difference between the ultimate strength and yield point decreases (Table 9.4). This reduces the liability of material to deformation hardening.

TABLE 9.4 Effect of Irradiation at 353 K on Mechanical Properties of Perlitic Steel, Grades 20 and 15X2HMФA

Neutron fluence, 10^{19} cm^{-2} ($E > 1$ MeV)	Steel 20					15X2HMФA	
	–	0.14	3	5	31	–	16
σ_u, MPa	750	810	1060	1160	1130	740	790
σ_y, MPa	460	700	1010	1130	1110	580	640
δ, %	22	15	8	4.5	4.0	—	—

Irradiation with a neutron fluence of 10^{20} cm^{-2} increases the yield point of steel by 100-150% and the ultimate strength only by 30-50%. The ductility decreases to 4%. When irradiated with a fluence of 10^{17}-10^{19} cm^{-2}, the yield point of low-carbon steel increases according to the relationship:

$$\Delta\sigma_y = A\Phi^{1/3},$$

where A is the constant dependent upon the steel type and irradiation conditions; Φ is the thermal neutron fluence in units of 10^{18} cm^{-2}.
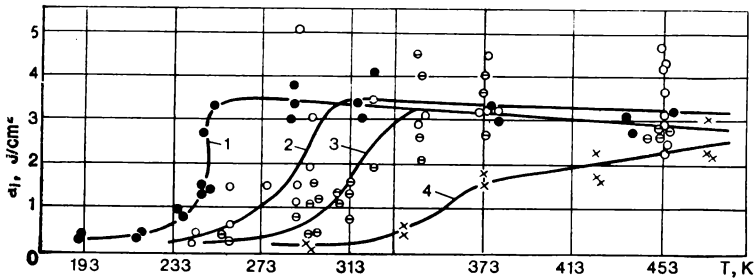
Fig. 9.3 Impact strength a_i of low-carbon steel (0.2% C, by mass) versus temperature after irradiation
1—nonirradiated; *2-4*—irradiation with fluence $2.7 \cdot 10^{18}$, 10^{19}, and 10^{20} cm^{-2}, respectively, (1 kgm/cm^2 = 9.81 J/cm^2)

Hardening of low-alloyed steels under irradiation is accompanied by embrittlement. This is characterized by an increase in temperature at which the material changes from the ductile to brittle condition and by a decrease in the impact strength in the region of ductile failure.

With most low-alloyed fine-grained steels, a perceptible change in the critical temperature of brittleness starts at irradiation of the order of 10^{18} cm^{-2}. At fluences exceeding 10^{18} cm^{-2}, the higher the fluence (Fig. 9.3, Table 9.5), the more considerable is the increase in

TABLE 9.5 Changes in Critical Temperature of Brittleness, T_{crit}, and Impact Strength at $T > T_{crit}$ Depending on Neutron Fluence

Grade	Neutron fluence, 10^{18} cm^{-2} ($E > 1$ MeV)	T_{crit}, K	ΔT, deg	a_i, J/cm^2	Δa_i, %
SA302B	—	298	—	82.7	—
	1	313	15	82.7	0
	4	323	25	77.3	7.0
	7	378	80	69.0	17.0
	17	428	130	59.3	30.0
Steel 20	—	313	—	52.0	—
	5	288	25	45.0	13.5
	12	363	130	33.0	36.5
15X2HMФA	0	353	—	—	—
	70	343	150	—	—

the critical temperature of brittleness of low-alloyed and low-carbon steels. After irradiation with a fluence of the order of 10^{20} cm^{-2}, the critical temperature of steel brittleness rises by 393-403 K, whilst the impact strength at a temperature above the critical decreases by 30-50%. In certain steels more sensitive to radiation and in their welded joints, a gain in the critical temperature of brittleness

18*

reaches 493-523 K following irradiation with a fluence of (1-3) $\times 10^{20}$ cm^{-2}. The dependence between the gain in the critical temperature of brittleness and the thermal neutron fluence is expressed by the following semiempirical relation:

$$\Delta T_{crit} = 17.5\Phi^{1/3},$$

where Φ is the fluence (the ratio of thermal to fast neutrons is 10 : 1) in units of 10^{18} cm^{-2}.

It should be noted that the neutron flux density and, consequently, the time taken to reach a specified fluence have only little effect on the mechanical properties of steel.

The mechanical characteristics of irradiated material depend on temperature of exposure (Table 9.6).

TABLE 9.6 Mechanical Properties of Perlitic Steels at 293 K after Neutron Irradiation

| Grade | Irradiation conditions | | σ_u, MPa | σ_y, MPa | σ, % |
	Neutron fluence, 10^{19} cm^{-2} ($E \geqslant 1$ MeV)	Irradiation temperature, K			
Steel 20	—	—	530	280	25
	2	566	720	535	9
	2	678	590	390	14
12X2MΦ	—	—	860	740	12.9
	4.3	508-538	970	880	11.0

Neutron irradiation of low-alloyed steel at 403-413 K leads to more intensive embrittlement than at 323-333 K. This is probably accounted for either by the movement and coagulation of point defects or by the release of dispersed carbides and nitrides. Starting with 503-533 K, the irradiation effect diminishes. This should be attributed to the mobility and annealing of the formed defects. At a higher temperature, the steel properties change the less, the higher the irradiation temperature. Irradiation of steel at 688 K only slightly changes its properties. Irradiation at 723 to 773 K even with large fluences does not practically affect the properties of low-carbon and low-alloyed steels.

Changes in the properties of low-carbon and low-alloyed steels under neutron irradiation are accounted for by the formation of complex defects. The defects are not stable and become annealed at elevated temperature. With irradiation below 473-493 K, the annealing of defects and, consequently, the recovery of mechanical properties of irradiated steels start at $T \approx 523$ K and complete at 723-753 K. Therefore, irradiation at 723 K even with heavy fluences causes no per-

ceptible change in mechanical characteristics of low-carbon and low-alloyed steels.

The **radiation stability** of steels depends upon their structure. Fine-grained steels are less sensitive to radiation than medium- and coarse-grained steels. With a similar grain size, the radiation-caused changes in the steel properties depend upon the shape of the carbide phase and microstructure before irradiation. With approximately equal amount of carbide phase, a least change in the properties is observed in steels with globular cementite obtained at high-temperature tempering of hardened steel. The properties of irradiated steel are also affected by the shape and distribution of the perlitic phase areas. The size of ferrite grains being equal, the steel with uniformly distributed areas of perlite is less sensitive to irradiation than that with nonuniformly distributed large areas of perlite. Under similar irradiation conditions, changes in the critical temperature of brittleness differ considerably from heat to heat even for the same grade of steel.

Corrosion Resistance. When deciding whether to use the perlitic steels in reactor engineering, especially in boiling reactors, or not, their resistance to corrosion should be primarily taken into account. A lower corrosion resistance of the perlitic steels as compared with the stainless steels causes alarm from the standpoint of contaminating the reactor coolant with the corrosion products, equipment failure due to local corrosion, or embrittlement on absorption of hydrogen.

Kinetics of Electrode Processes. The normal potential of the iron ionization

$$Fe \rightarrow Fe^{2+} + 2e$$
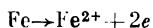
is equal to -0.44 V and is independent of the pH of the medium. Taking into account the actual concentration of the ion of bivalent iron in the medium that is limited by the product of solubility of ferrous iron oxide hydrate, the potential of the reaction in a neutral medium equals -0.52 V. In neutral media, the oxygen ionization and the discharge of the hydrogen ion are the thermodynamically possible cathodic reactions in corrosion of iron, low-carbon, and low-alloy steels. In a neutral medium the normal potentials of the cathodic reactions are equal to $+0.8$ and -0.42 V, respectively. In deaerated media, corrosion of iron and perlitic steels proceeds with hydrogen depolarization. In oxygen-containing media, say, air-saturated water, corrosion of iron proceeds with oxygen and hydrogen depolarization. In neutral air-saturated media, the concentration of the hydrogen ions is small as compared with the concentration of dissolved oxygen. The corrosion potential of iron in water is close to the equilibrium potential of the iron passage into the medium in the form of bivalent
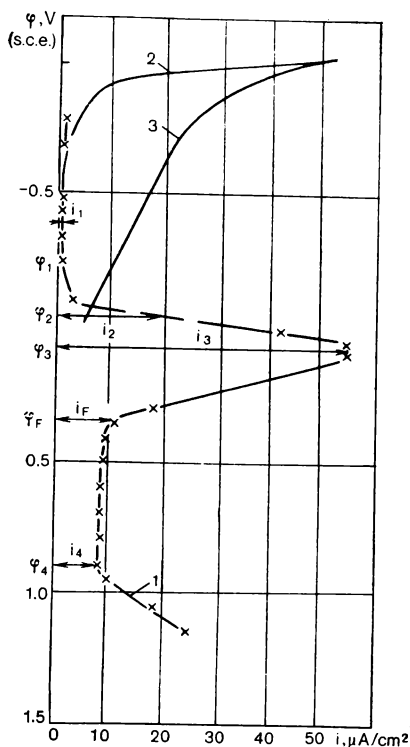
Fig. 9.4 Anodic and cathodic polarization of perlitic steel in neutral medium
(1 N solution of sodium nitrate)
1—anodic curve in deaerated medium; 2—cathodic curve in deaerated medium; 3—cathodic curve in air-saturated medium

ions. Therefore, the cathodic reactions also proceed at this potential.

Generally speaking, the more negative the potential at which the cathodic process takes place as compared with the equilibrium potential, the higher the rate of the process. Taking into account the concentrations of the hydrogen and oxygen ions, and also the potential at which the cathodic processes take place, we may conclude that in a neutral medium corrosion of iron and low-alloyed steels proceeds mainly with oxygen depolarization. When pH of the medium decreases, the concentration of the hydrogen ions increases, and in acid media, corrosion of iron and perlitic steels proceeds predominantly with hydrogen depolarization. In alkaline media, where the concentration of the hydrogen ion is below that in neutral media, corrosion of iron proceeds mainly with oxygen depolarization.

As follows from the data given in Fig. 9.4, in a neutral air-saturated

medium, the corrosion of iron proceeds with oxygen depolarization limited by diffusion.

Let us now consider the anodic processes on iron and perlitic steel in a deaerated medium. At potentials more negative than φ_1 (Fig. 9.4), the rate of the anodic process is independent of potential and is extremely small. We may therefore assume that iron is in the pseudopassive state. Under stationary conditions, the pseudopassive state on steel 20 is preserved within 293-353 K at an oxygen concentration below 0.2 mg/kg.

At potentials more positive than φ_1, the pseudopassive state is disturbed and the steel goes into the region of active dissolution. The rate of the anodic process rises (current i_3 at potential φ_3).

The greatest current of the iron dissolution in the active state is achieved at the potential φ_3. With the further increase in potential iron starts to passivate. The process ends at the Flade potential φ_F. The iron passivity at low temperatures is associated with the formation of the protective adsorption and phase layers. The phase protective passivating layer contains γ-Fe_2O_3.

At a potential more positive than φ_4 the anodic processes of oxygen release and iron dissolution in the repassivation region proceed with the formation of ions of higher valency. At room temperature in a deaerated water of high purity (with an electrical conductivity of 0.1 $\mu S/cm$), the corrosion potential is more negative than φ_1, i.e. it corresponds to the region of pseudopassivity. The corrosion rate under these conditions is low.

Let us consider now the corrosion behavior of the perlitic steels utilized in various parts of the circuit of a boiling channel-type nuclear reactor. In the condensate-feed system, chemically demineralized water with an electrical conductivity of 0.1-1.0 $\mu S/cm$ contains oxygen in an amount of 0.02 mg/kg. In the condensate-feed system at all temperatures of the coolant (293-423 K), steel 20 operates in the pseudopassive state at the corrosion potential, and the rate of the grain-face corrosion is low.

It should be noted that the phase protective film of magnetite forms slowly within the given temperature range. The protective oxide film damages in places where tubes are expanded into tube plates because of friction caused by vibration. This enhances corrosion in areas where the film is damaged.

Influence of Ogyxen. The presence of oxygen in the medium increases the corrosion potential and accordingly the energy of surface atoms and finally enhances the surface diffusion and the rate of restoration of the protective oxide film. More than that, in the presence of oxygen Fe^{2+} oxidizes to Fe^{3+}. The solubility product of $Fe(OH)_3$ is far below that of $Fe(OH)_2$. Therefore, in the presence of oxygen a greater part of the corrosion products deposit in stagnant areas.
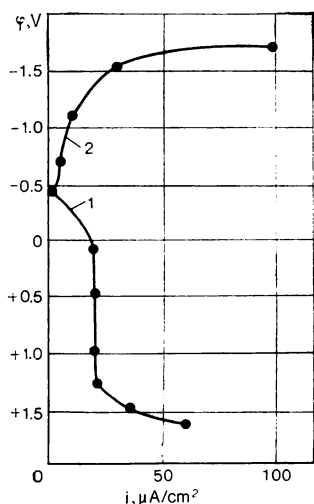
Fig. 9.5 Anodic (1) and cathodic (2) polarization of low-carbon steel in deaerated 10^{-4} N solution of $NaNO_3$ at 573 K

Increasing the oxygen content from 0.02 to 0.3 mg/kg somewhat increases the corrosion rate (kg m^{-2} day^{-1}) of steel 20:

CO_2, mg/kg	293 K	353 K	423 K
0.02	0.02	0.05	0.3
0.20	0.03	0.06	—
0.30	0.07	0.26	0.6

However, enhancing the growth of the protective oxide film in the presence of oxygen and reducing the solubility of the corrosion products prevail. Therefore, in certain cases oxygen in a concentration of 0.2 mg/kg or H_2O_2 in a concentration providing the same oxygen content is injected in the condensate-feed system.

The oxygen content in the heating steam condensate of a boiling reactor does not exceed 0.2 mg/kg. Therefore, the corrosion rate of steel 20 at 420 K is below 0.6 g m^{-2} day^{-1} and decreases with time.

In the recirculation system of boiling channel-type reactors, the oxygen concentration due to radiolysis is close to 0.01-0.05 mg/kg. At an operating temperature of 550 K, the protective oxide film of magnetite (Fig. 9.5) forms within a short period of time. At the corrosion potential, the perlitic steel is in the passive state (Fig. 9.6). The corrosion rate, K, (g m^{-2} day^{-1}) decreases with time (τ_4) due to the formation of the protective oxide film as follows:

$$\log K = 1.2 - 0.6 \log \tau.$$

The rate at which the corrosion products pass into the coolant K_e (g m^{-2} day^{-1}) also decreases with time:

$$\log K_e = 0.6 - 0.5 \log \tau.$$

During prolonged shut-down periods, water is not drained from the recirculation system, as heat must be carried away from the core because of residual heat release. During shut-down periods, the water in the recirculation system saturates with oxygen. Its temperature is close to 350 K. The corrosion rate of steel 20 is close to 2-3 g m^{-2} day^{-1} and practically does not change with time. Eighty per cent of corrosion products pass into the coolant. The oxide film of magnetite that has formed at operating temperatures does not protect the perlitic steel against corrosion during prolonged shut-down periods.

Under the shut-down corrosion conditions, pits up to 0.03 cm deep form on the perlitic steel. The oxygen transport to the bottom of pits is effected by diffusion. When migrating in the medium filling the pits, oxygen is consumed in corrosion occurring on the side surfaces of pits. It is easy to show that the oxygen concentration at the bottom of pits does not exceed 0.2 mg/kg. Therefore, the metal at the pit bottom is in the pseudopassive state. The corrosion rate is small and the pit growth ceases. This proceeds only in a chemically demineralized water. When the chloride ion concentration in water exceeds 0.5 mg/kg, the pseudopassive state is not realized and the pit continu s to grow.

In the light of the above, in the recirculation system the perlitic steels should be used to manufacture thick-walled items, for example bodies of gate valves. If the recirculation system uses pipelines made of perlitic steels, then to prevent the formation of the iron oxide deposits on the fuel elements while the power is raised to a required value, measures should be taken to reduce the rate of corrosion during shut-downs. To this end, an inhibitor. say, $NaNO_2$, may be injected into the system in a concentration of 0.1 g/kg. However, prior to rais-

Fig. 9.6 Magnetite film on perlitic steel after testing in deaerated water at 573 K

ing the power to the required value, the inhibitor-charged medium must be replaced with a chemically demineralized water. This takes several days and, hence, involves an additional out-of-service period, and is not always advisable from the economical point of view.

The places where the recirculation system tubes are welded to a drum-separator or manifold undergo alternating stresses exceeding the yield point. The local deformation may reach 0.3 to 0.5%. This generates the risk of cracking due to small-cycle fatigue. In the presence of corrosive medium the number of cycles to failure essentially decreases. The formation of the oxide film in corrosion is preceded by the oxygen dissolution in metal. The dissolved oxygen forms the Cottrell atmospheres, decelerates the motion of dislocations, and thus facilitates the formation of their flat pile-ups and origination of cracks.

Therefore, to prevent the crack formation due to small-cycle fatigue, the drum-separators and manifolds are surfaced with the austenitic stainless steels. The resistance of the stainless steels in small-cycle fatigue is far higher than that of the perlitic steels.

The surface of steam tubing contacts saturated steam heated to 550 K. A protective oxide film rapidly forms under these conditions. The rate of corrosion is the same as in contact with a chemically demineralized water and is practically independent of the oxygen concentration.

The perlitic steels are used to manufacture the water-shielding tanks. The demineralized water in them has a temperature close to 350 K. The tanks communicate with the atmosphere through breathing tubes about 100 mm in diameter and up to 10-15 m long. Mass transfer of oxygen through the breathing tubes is small. The oxygen dissolved in water in filling the tank is consumed in corrosion. Therefore, the oxygen content of the medium decreases with time. The steel goes to the pseudopassive state and the rate of its corrosion abruptly decreases. This requires no special measures to protect the perlitic steels against corrosion.

In certain cases the design of water-shielding tanks is such that the medium therein is saturated with air. In this situation a volatile corrosion inhibitor, say, ИФХАН-12 is injected, in a 1-% concentration. This reduces the steel corrosion along the water-line and above it.

In the primary circuit of a water-cooled and moderated reactor the accumulation of H_2 suppresses the radiolysis. C_{O_2} is below 0.05 mg/l. For "mild" control boric acid is injected into the circuit. Acidifying a water coolant enhances corrosion of the perlitic steels (Fig. 9.7).

The oxide film of magnetite always contains pores. At 550-570 K, corrosion potential of metal at the bottom of pores at pH $<$ 10 corresponds to the region of active dissolution. At pH $=$ 10-11.7, the
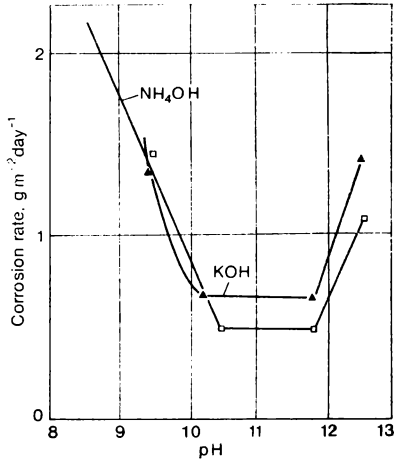
Fig. 9.7 Effect of medium 'pH on corrosion rate of perlitic steel in deaerated water at 573 K

perlitic steel is in the passive state. To reduce the corrosion losses, ammonia and KOH are added to the water of the primary circuit up to pH == 7.3. Alkalifying the medium also decreases the corrosion rate of the perlitic steels in shut-down periods. A circuit employing the perlitic steels must be put into dead storage when it is shut down for a long period of time. In the case of "wet" laying-up the circuit is filled with a deaerated water having pH = 9.5-10.5. The deaeration is performed by adding hydrazine to the medium. The specified value of pH is maintained by introducing ammonia. In "dry" laying-up, the circuit is filled with an inert gas, say, dried nitrogen. This protects perlitic steel against corrosion and reduces the content of corrosion products in the reactor coolant, when the reactor is restarted.

In a deaerated medium of the primary circuit of a water-cooled and moderated reactor, corrosion proceeds with hydrogen depolarization. Part of released hydrogen dissolves in steel. At 550 to 570 K, the rate of hydrogen diffusion in perlitic steel is so high that hydrogen does not form the Cottrell atmospheres. This, therefore, involves no risk of the reversible hydrogen embrittlement. In pores, micropores, and other defects hydrogen atoms join into molecules. With time the pressure of molecular hydrogen in the pore rises and may cause metal failure because of the irreversible hydrogen embrittlement. If pores are located close to the surface, the hydrogen absorption produces blisters on the metal surface.

At 290 K, the H_2 pressure in the pore may reach 10^3 MPa and at 570 K, 2.5 MPa. At $T = 570$ K, a stress of 2.5 MPa cannot affect the

performance of the pressure vessel of a water-cooled and moderated reactor. In rapid cooling, stresses exceeding the ultimate strength may arize in the metal around the pore. When the cooling is slow, the hydrogen has time to leave the pore and no irreversible hydrogen embrittlement takes place. Nevertheless, an abrupt rise in the hydrogen pressure in rapid cooling must be taken into account when evaluating the strength of a reactor pressure vessel and in choosing the rate of cooling.

Irradiation has no essential effect on the corrosion rate of the perlitic steels and accordingly on the rate of hydrogen penetration into the metal and development of the irreversible hydrogen embrittlement.

The service conditions in the secondary circuit of a water-cooled and moderated reactor under which the perlitic steels operate are close to those in boiling reactors. The corrosion products may accumulate in the bottom part of tower-type steam generators. This produces a layer of iron oxide on the heat-transferring surfaces. Because of the "wick" effect alkalis concentrate in the pores of this layer to pH = 11-12.

The hydroxyl ion may interact with magnetite to form soluble compounds called ferrites. This disturbs the passive state and steels may fail because of alkali embrittlement.

Complexone Treatment. To form a protective film use is made of complexones. These are substances capable of forming complex soluble combinations with iron, an example is trilon. When a medium contains complexones, they interact with the iron corrosion products at 360 to 390 K and form soluble compounds. The surface of the perlitic steels clears from corrosion products and protective films form with more ease. At 550 K, the iron complex compounds decompose forming a magnetite coating on the steel surface. Since the magnetite grains form of a material found in water, no mechanical stresses arise in the protective film and its continuity is not affected. When the magnetite crystals form upon the water interaction with steel, the magnetite grains as if interfere with the growth of one another and this generates stresses in the metal.

Carryover and Deposition of Corrosion Products. Corrosion affects the reliable operation of nuclear reactors in two ways. Grain-face and local corrosion reduce the thickness of the perlitic steel products. Moreover, part of corrosion products enter the reactor coolant. The deposition of the corrosion products on the fuel elements may lead to their overheating and make them inoperative. Depositing on the heat-conducting surfaces of heat-exchangers and steam generators, the corrosion products affect the power output of the plant. The deposition of corrosion products in a circuit worsens the radiation situation. Most active are corrosion products formed of materials exposed to neutron irradiation. A smaller contribution to the radio-

activity is made by the corrosion products formed outside the core and activated in the coolant flows through the irradiation field. With perlitic steel it may be assumed that half of the corroded metal enters the water and the other half remains on the steel surface in the form of an oxide protective film. A decrease in pH, or increase in the velocity of medium flow and concentration of oxygen, increase the fraction of products entering the water. Therefore, the deaeration and increase in pH reduce the yield of the corrosion products. In water, the corrosion products may be in a truly dissolved, i.e. ionic, form, in the form of colloidal particles less than 0.1 μm in size, and in the form of suspended particles greater than 0.1 μm in size. Most of corrosion products are in water in the form of particles greater than 1 μm in size. At 520-570 K, the corrosion products are present in a deaerated water in the form of magnetite. When oxygen is present in water, the corrosion products contain hematite. In an oxygen-containing medium, the products of a low-temperature corrosion are oxides and hydroxides.

When nuclear power plants utilize the perlitic steels certain quality requirements should be imposed on the reactor coolant.

Quality Requirements Imposed on the Primary Circuit Water of Water-Cooled and Moderated Reactors when Water Contains Ammonia. To reduce the rate of corrosion and carryover of corrosion products of the perlitic steels the concentration of the chloride-, sulphate- and fluoride-ions in water should not exceed 0.02 mg/kg each. The oxygen concentration should be below 0.02 mg/kg. In a circuit filled with water containing ammonium hydroxide, hydrogen accumulates in an amount of 5 to 50 n.cm^3/kg owing to radiation decomposition. This is enough to suppress the radiolysis and thus prevent oxygen penetration into the circuit.

The radiolysis may be enhanced by the oxygen present in the filling water. Therefore, the primary circuit must be filled with a deaerated water. The oxygen absorbed by the water in transportation or from the air remaining in the circuit should be bound by hydrazine.

In order to reduce the corrosion rate and carryover of corrosion products, the pH in the primary circuit must be maintained at 10-10.5 by adding to the water ammonium hydroxide, which is a donor of hydrogen, suppressing the radiolysis.

In certain cases boric acid is added to the primary circuit of water-cooled and moderated reactor for a "mild" control. The addition of solely ammonium hydroxide to the water is not sufficient to maintain the pH at a value providing a high stability of the perlitic steels. To raise the pH of the medium, lithium or potassium hydroxide is added to the primary circuit water.

The concentration of nonvolatile alkalis depends on the content of boric acid in the water, but it must not exceed 10^{-4} to 10^{-3} N.

Higher concentrations of nonvolatile alkalis involve the risk of damage to items made of the perlitic and stainless steels because of alkali embrittlement.

Nonvolatile alkalis may be added only if the coolant impurities do not concentrate in the primary circuit. If boric acid is added to the water, the components of the primary circuit must be made of low-alloyed rather than carbon steels. The carryover of corrosion products from low-alloyed steels is far lower than from carbon steels.

Quality Requirements Imposed on the Secondary Circuit Water of Water-Cooled and Moderated Reactors. C_{O_2} of circuit II water should not exceed 0.02 mg/kg. When the water condition is not corrected, the electrical conductivity of feed water must not exceed 0.1 μS/cm. When ammonia is added to the water and copper alloys are present in the circuit, the pH must be 9.3-9.6. The presence of nonvolatile alkalis is untolerable. The permissible content of chlorides, sulfates, fluorides and nitrates in the circulation water depends on the design of steam generator and, in particular, on pressure. The content of the substances in water contacting with components made of the perlitic steels on the surface of which impurities do not concentrate must not exceed 0.1 mg/kg for each ion.

Quality Requirements Imposed on Water of Boiling Reactors. High corrosion resistance of the perlitic steels utilized in the condensate-feed system is ensured by the following properties of water:

Electrical conductivity, μS/cm	< 0.1
Concentration of chlorides, fluorides, sulfates each, mg/kg	$\leqslant 0.02$
Concentration of oxygen, mg/kg	$\leqslant 0.02$

Forced Recirculation Loop. Steam generation increases the content of impurities in the water utilized in a forced recirculation loop. Therefore, the content of the chloride-, fluoride- and sulfate-ions is higher than in the condensate-feed system. Reducing their concentration to 0.02 mg/kg by enhancing blowing off and intensifying the internal cleaning of the circuit is not advisable from the economical standpoint. In view of this, one has to agree to a certain increase in the content of impurities in the water, and, therefore, to a certain increase in the corrosion rate of the perlitic steels. The concentration of the chloride-, fluoride- and sulfate-ions should not exceed 0.1 mg/kg each.

The oxygen content in the circulating water must be rated for starting periods, shut-down and naturally for layover periods. It should be noted once more that a high corrosion resistance of the perlitic steels in a forced recirculation loop can be ensured only when one strictly adheres to the specified water operating conditions in reaching the required power and cooling down, and also by taking meas-

ures to protect the equipment against corrosion in the layover periods.

The corrosion resistance of the perlitic steels in a forced recirculation loop may be raised through the use of various methods of passivation (treatment with complexones and the like) with the resultant formation of a protective oxide film on the steel surfaces.

In storage, the components of the perlitic steels must be also treated with rust preventives to protect them against atmospheric corrosion. The preservation technique must be most simple, economical and allow rapid and reliable depreservation of the components before installation. It is most advisable to use in preservation volatile inhibitors (bicyclohexylamine and others) and paper impregnated with volatile inhibitors. Items treated with volatile inhibitors or inhibitor paper are wrapped in polyethylene to prevent the evaporation of inhibitor and put in wooden crates. Prior to preservation, the surfaces of the perlitic steel items should be thoroughly cleared from the products of corrosion and contamination.

The perlitic steels in storage may be protected by readily removable coatings. They protect metal from atmospheric corrosion and are readily removed before installation. The strippable surface coatings consist of vinyl chloride enamel with a 10% additive of acor.

In certain cases the perlitic steels are protected against corrosion with metallic and nonmetallic coatings. Metallic coatings are applied by metallizing, chemical and electrochemical methods. The thickness of metallic coatings is 0.1 to 0.2 mm. The maximum permissible water temperature for various metallic coatings varies as follows:

Zn, 313 K

Cd, 353 K   Al, 373 K

Cu-Ni-Cr (combined), 603 K   Ni (chemically applied), 473 K

To protect the perlitic steels against gas corrosion in the channel-type reactors, use is made of aluminum coatings applied by a hot method or by metallizing. When using paint coatings, one should keep in mind that they must be renewed each 3-5 years. To protect the perlitic steels in water use is made of epoxy enamels. In a steam-air medium at the atmospheric pressure up to 573 K, oleoglyptal-based enamels are utilized and up to 623 K, an organosilicate coating is used. All the above-mentioned coatings are stable under irradiation with a neutron fluence not exceeding 10^{20} cm^{-2}. The efficiency of paint coatings improves when they are applied on the aluminum metallized coating rather than on the steel surfaces. It should be noted that the best coatings are obtained when the surfaces to be protected are thoroughly cleaned and the paint coatings are properly dryed.

One of the causes of introducing the perlitic steels in reactor engineering is their lower cost as compared with the stainless steels and availability.

It should be noted, however, that the perlitic steels must be gastight, i.e. have no micropores and be impermeable to gases. In conventional power engineering such requirements are not imposed on steel, since steam leaks in minute amounts do not affect the performance of power equipment. In nuclear power engineering, even microscopic leaks of active gases and steam may badly impair the radiation situation and interfere with servicing the equipment. The production of a gas-tight perlitic steel and, in particular, testing for gastightness essentially increase the cost of the steel. Therefore, the use of the perlitic steels in nuclear engineering, when it is not dictated by special circumstances, should be weighted against economy. At present, the perlitic steels are 3-7 times cheaper than the austenitic chrome-nickel stainless steels.

9.2 Chromium Stainless Steels

Certain components of nuclear power plants place not only high corrosion resistance demands on the materials but also stringent strength requirements. Thus, pump shafts made together with enclosed electric motors are made from steel, grade 14X17H2. Bearing journals of a shaft are usually protected with driven over bushings of high hardness (R_c45 to R_c60). The bushings are made of hardened chromium steels 95X18 and 14X17H2. Such parts as gears, shafts, guide rods, etc. of the control mechanisms operating in water are made of stainless steels, grades 12X13 and 14X17H2. Chromium steels are also used for making fasteners and spring elements.

Composition and Structure. High corrosion resistance of steels is achieved by their alloying with chromium. Fig. 9.8 gives the constitutional diagram of the Fe-Cr system. Iron forms with chromium a continuous series of solid solutions. In the region of a closed loop the austenite is stable. In the intermediate region, the austenite and ferrite coexist. Outside the loop, only the ferrite is stable. The loop shape and boundaries considerably depend on the presence of other elements in steel, say, carbon and nickel. If the chromium content does not exceed the values corresponding to the boundary of the austenitic loop, the steel is martensitic and can be hardened. When rapidly cooled down from the temperature corresponding to the austenitic region, the phase transformation takes place and martensite is fixed at room temperature. If the chromium content exceeds the value corresponding to the austenitic loop boundary, the steel undergoes no γ-α-transformation and belongs to a ferritic class. With a chromium content corresponding to the intermediate region (austenite + ferrite), the steel is martensitic-ferritic.
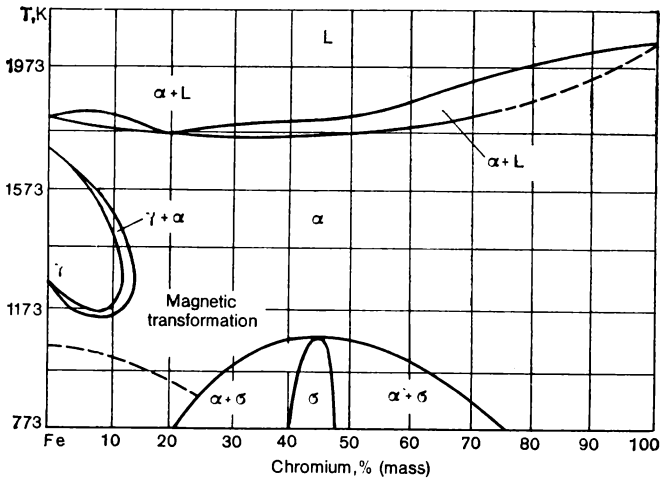
Fig. 9.8 Fe-Cr phase diagram

Use is made of three types of the chromium stainless steels: those containing 12, 17 and 27% Cr. Depending on the required mechanical properties steels containing 12% Cr differ in the content of carbon (from 0.1 to 0.4%). Steels containing 17-18 and 25-28% Cr sometimes include small additions of titanium and nickel which are added to obtain finer grains, and nickel still to improve the mechanical properties. Table 9.7 gives the composition of the chromium stainless steels finding industrial application.

TABLE 9.7 Composition of Chromium Stainless Steels

Class	Type	Grade	Mass content of alloying elements, %					
			C	Cr	Ni	Ti	Mn	Si
F	13% Cr	08X13	≤ 0.08	11-13	—	—	≤ 0.6	≤ 0.6
M-F		12X13	0.09-0.15	12-14	—	—	≤ 0.6	≤ 0.6
M		20X13	0.16-0.24	12-14	—	—	≤ 0.6	≤ 0.6
M		30X13	0.25-0.34	12-14	—	—	≤ 0.6	≤ 0.6
M		40X13	0.35-0.44	12-14	—	—	≤ 0.6	≤ 0.6
F-M		12X14	≤ 0.15	13-15	—	—	≤ 0.6	≤ 0.6
F	17% Cr	12X17	≤ 0.10	16-18	—	—	≤ 0.7	≤ 0.8
F		08X17T	≤ 0.08	16-18	—	5%C-0.8	≤ 0.7	≤ 0.8
M		14X17H2	0.11-0.17	16-18	1.5-2.5	—	≤ 0.8	≤ 0.8
F	25 to 28% Cr	15X25T	≤ 0.15	24-27	—	5%C-0.8	≤ 0.8	≤ 1.0
F		15X28	≤ 0.15	27-30	—	—	≤ 0.8	≤ 1.0

Note. F—ferrite, M—martensite.

Depending upon the carbon content, 12-14% chromium-bearing steels belong to different classes (see Table 9.7). Steel, grade 08X13, is purely ferritic (when the carbon content is below 0.08% and the chromium content is at its upper limit) and ferritic-martensitic (with a medium content of chromium and carbon). Carbon is an austenite-forming element expanding the gamma-region and chromium is a ferrite-forming element reducing the gamma-region. With the lowest content of carbon and the highest content of chromium, the gamma-region decreases and steel, grade 08X13, corresponds to a composition lying outside the austenitic region, i.e. is purely ferritic and undergoes no phase transformation. With the medium contents of carbon and chromium, the steel belongs to the γ-α-region of the diagram shown in Fig. 9.8. The grains of austenite undergo phase transformation and those of ferrite do not, i.e. the transformation is incomplete.

Steel, grade 12X13, containing a minimum of chromium (12%) and a maximum of carbon (0.15%) lies within the gamma-region and experiences complete $\gamma \rightarrow \alpha$-transformation, and when cooled down in the air from the γ-region hardens into martensite. This makes steel, grade 12X13, fairly unstable in properties. Small variations within the grade composition change the steel structure from martensitic to ferritic. Steel, grade 12X14, is ferritic. At a maximum content of carbon, however, it changes into ferritic-martensitic. Steel, grades 20X13, 30X13, and 40X13, is martensitic, while steel, grades 12X17 and 15X (25-28), belongs to the ferritic class.

In compliance with the above considerations, steels after hardening or cooling in the air from 1173-1373 K have the following structure: 08X13 and 12X13, ferrite and martensite in different proportions; 20X13, 30X13, and 40X13, martensite; 12X17, 15X25T, and 15X28, ferrite.

Physical and Mechanical Properties. Hardness and strength of steels after hardening depend upon their content of carbon. With 13% Cr, steel bearing 0.01% C does not harden since phase transformation is impossible in it. Steels with intermediate content of carbon harden to a lesser extent than steels containing 0.35% C.

After hardening steels become less ductile. To improve strength and ductility, steels are subjected to annealing. The lower the annealing temperature, the harder and stronger the steel. Table 9.8 illustrates the thermal treatment conditions for the chromium stainless steels and the resultant mechanical properties.

Steel, grade X13, is the most widespread and cheapest stainless steel. Steels having a low carbon content, grades 08X13, 12X13, and 20X13, are ductile and susceptible for stamping items. Steel, grades 30X13 and 40X13, possesses high hardness and improved strength. Strong parts resistant to wear are made of these steels.

Steels containing 17% Cr are more corrosion resistant. They also

TABLE 9.8 Thermal Treatment Conditions and Mechanical Properties of Chromium Stainless Steels

Grade	Temperature, K		Mechanical properties					
	hard-ening	anneal-ing	HR_c	σ_u, MPa	$\sigma_{0.2}$, MPa	δ, %	ψ, %	a_i, J/cm²
12X13	1273	973	—	600	400	20	60	90
20X13	1323	973	—	850	650	10	50	60
30X13	1323	523	40	1600	1300	—	—	—
40X13	1323	473	50	—	—	—	—	—
12X17, 08X17T	1323	1023	—	450	300	15-25	40-50	20-80
14X17H2	1323	573	—	1100	900	10	35	50
15X25T, 15X28	1323	1023	—	450	300	20	45	—
25X17H2	1323	—	45	1540	1300	10	—	—
25X17H2	1323	573	28	740	630	20	—	—

may be used as heat resistant (resistant to scaling) steels as well as steels bearing 25-28% Cr. A great drawback to these ferritic steels is that their coarse-grain structure arising in overheating, say, in welding, cannot be eliminated by thermal treatment, since they do not undergo phase transformations. The coarse-grain structure accounts for an increased brittleness of steels. The grain growth somewhat decelerates when titanium and nitrogen are added to these materials. Titanium carbides and nitrides located along the grain boundaries impede the grain growth.

Embrittlement occurs in steels containing 17% Cr also in case of fine-grain structure after prolonged holding at 723-973 K (i.e. below the temperature threshold of grain growth), as a result of a considerable release of carbides along grain boundaries at 773 K, or formation of a brittle δ-phase at 973 K. The addition of nickel to steels containing 17% Cr and increase in their carbon content enlarge the γ-region and lead to a $\gamma \rightarrow \alpha$-phase transformation. The transformation, however, is not complete; nevertheless, it results in a marked hardening. Of steels containing 17% Cr steel, grade 14X17H2, is highly strong (see Table 9.8) and finds its applications where increased strength is required along with corrosion resistance. Still more strong is steel, grade 25X17H2.

The physical properties of chromium stainless steels containing 13 to 28% Cr are as follows:

Density, g/cm³	7.7-7.8
Coefficient of thermal expansion at 293-673 K, deg⁻¹	$(11-11.8) \cdot 10^{-6}$
Thermal conductivity at 373-573 K, W m⁻¹K⁻¹	26-30
Thermal neutron absorption cross-section, m²	$2.7 \cdot 10^{-28}$

19*

Martensitic and ferritic-martensitic chromium steels in which austenite transforms into ferrite are susceptible to air hardening in heating during service operations and in welding. This drastically reduces their ductility. Chromium steels are more difficult to weld than low-alloyed or chrome-nickel steels. Chromium steels containing less carbon and chromium, i.e. steels of the type X13 and, in particular, steel, grade 12X13, are more readily welded. Steel, grade 12X17, containing less carbon than steel, grade 95X18, is more weldable. It is not recommended to weld chromium steels bearing carbon in excess of 0.12%. The electrode wire is of the same material or of the austenitic chrome-nickel stainless steel. The welded seams and neighboring regions embrittle when steels of the martensite or ferrite-martensite class are cooled in the air. Therefore, it is good practice to anneal a welded item at 1023-1073 K for 1 h and then slowly cool it down.

In high-chromium steels of a ferritic class, grains grow in welding and high-temperature brittleness arises because of the formation of σ-phase.

With steels of the type X13, which are somewhat more tough, metal sticks to cutting tools. Additives of sulfur and molybdenum improve the machinability of these steels.

Annealed chromium steels reasonably well lend themselves to working: rolling and forging. The fine-grain steels containing 17-27% chromium are readily workable under pressure. Excellent workability under pressure is featured by chromium steels heated to 423-473 K.

Radiation Stability. Irradiation increases the strength and decreases the ductility of the chromium stainless steels. Thus, after irradiation with a neutron fluence of 10^{21} cm^{-2} at 723-773 K, the mechanical properties of annealed steel, grade 12X12MC (12% Cr, 1% Mo, and 1% Si), have changed as follows: the ultimate strength from 665 to 800 MPa, the yield point from 435 to 620 MPa, and the elongation from 28 to 16%. The properties of steel, grades 20X13 and 14X17H2, change in a similar way when irradiated within 773-873 K. At the same time, the properties of niobium-bearing steel, grade 1X17, which does not undergo structural transformations, remain practically unchanged after irradiation.

Corrosion Resistance. The corrosion resistance of chromium steels is directly associated with their ability to passivate. Chromium in a solid solution facilitates the iron passivation. Thus, at pH equal to zero, the Flade potential of iron is 0.58 V. Alloying iron with chromium in an amount of 17% shifts the Flade potential in the negative direction to 0.06 V, i.e. the passivation becomes easier since it occurs at more negative potentials. Chromium stainless steels passivate at the corrosion potential in oxidizing media.

In steels containing 11.8% chromium, 1/8 of all lattice atoms are chromium. Tammann has formulated the 1/8 law which determines

the first boundary of stability. Indeed, corrosion of Fe-Cr alloys sharply decelerates in certain media at a chromium concentration of 12%. With the chromium content of 24%, which corresponds to 2/8 atomic fractions of chromium in the alloy, the second boundary of stability appears. When the content of chromium reaches 36%, i.e. about 3/8 atomic fractions, the boundary of stability even in such active media as a mixture of sulphuric and hydrochloric acids appears.

In the presence of carbon in steel, chromium is partially bound into carbides and its content in the solid solution decreases. This also decreases the corrosion resistance of steel. In the hardened state, when chromium is completely in the solid solution, high-chromium steels with increased carbon content are more stable than in the annealed state, when chromium is partially bound into carbides.

In a deaerated water containing less than 0.1 mg/l of chlorides the chromium stainless steels at the corrosion potential are passive and are close in corrosion resistance to the austenitic chrome-nickel stainless steels. In the presence of oxygen and chlorides, the resistance of the chromium stainless steels appreciably decreases. Corrosion becomes pitting. Chlorides materially reduce the passive region of the chromium stainless steels. This is associated with that in the presence of oxygen the corrosion potential of the chromium steels is more positive than the break-down potential in a chloride-containing medium.

With an increase in the chromium content of steel, the break-down potential shifts to the region of positive values. Therefore, steels containing 25-28% Cr are less susceptible to pitting. A high content of carbon, say 1%, in steel, grade 95X18, enhances pitting. In river water saturated with air, the chromium steels are susceptible to crevice corrosion. High-standard surface finish adds to the corrosion resistance of the chromium steels. The contact with steel, grade 08X18H10T, and the presence of crevices enhance corrosion of the chromium steels. In this case, the corrosion products may block the motion of mating parts.

The ferritic chromium steels are susceptible to intergranular corrosion. At 1373-1473 K, carbides dissolve in ferrite. In cooling, carbides precipitate at grain boundaries. The grain boundaries become chromium-depleted and less resistant to corrosion. Slow cooling or prolonged heating at 823 to 973 K facilitates the coagulation of carbides and equalizes the chromium concentration at the grain boundaries because of the chromium diffusion from the bulk of the grain outward. To prevent intergranular corrosion, the stainless chromium steels are either subjected to stabilizing annealing or are stabilized with titanium. The titanium-to-carbon ratio should be 8 : 1.

In the steam-air medium, the chromium steels, especially of the martensite class, are susceptible to stress corrosion. In contrast to

TABLE 9.9 Chemical Composition of Materials for Condenser Tubes

Material	Mass content, %											
	Cu	Pb	Fe	Sb	Bi	P	Zn	Sn	Mn	C	Si	Ni+Co
Brass JI68	67-70	≤0.030	≤0.1	≤0.005	≤0.002	≤0.01	Remainder	—	—	—	—	—
Brass JI070-1	69-71	≤0.070	≤0.1	≤0.005	≤0.002	≤0.01	Same	1-1.5	—	—	—	—
Cupronickel MH70-30	Remainder	≤0.005	0.6-1	—	—	—	—	—	0.8-1.3	≤0.05	≤0.15	29-33
MH?K5-1	Same	≤0.005	1-1.4	—	—	—	0.5	—	0.3-0.8	≤0.03	—	5-6.5

the austenitic stainless steels, cathodic polarization enhances corrosion cracking of the chromium steels. This is associated with the hydrogen absorption of steels.

Let us consider how this circumstance may affect stress corrosion. In chromium BCC-lattice steels, cross slip is easier as compared with the materials having the FCC lattice. In this connection, the formation of dislocation pile-ups and origination of cracks are less probable in the chromium steels. Hydrogen facilitates the formation of the Cottrell atmospheres near dislocations. They decelerate the movement of dislocations and lead to their pile-ups and generation of cracks. More than that, hydrogen introducing into the lattice deforms it and causes local stresses. Together with residual stresses in hardened steel they cause the crack propagation. The removal of internal stresses in annealing increases the resistance of the chromium steels to corrosion cracking. High-temperature tempering is the best way to remove stresses, whereas low-temperature tempering eliminates them to a smaller degree.

9.3 Copper Alloys

Composition and Structure. The copper alloy piping is used in heat-exchangers, turbine condensers, and low-pressure heaters. Their high thermal conductivity is of essential importance. When condensers are cooled with sea water, copper alloys are not encrusted with marine growth, since copper compounds are poisonous to it. Brasses and cupronickel alloys are most widely used as materials for condensers. The objectionable aftereffects of utilizing copper alloys are the risk of forming copper-containing scales on surfaces transferring much heat, e.g. surfaces of fuel elements, and the contamination of the reactor coolant with radionuclides of zinc that are the products of the brass corrosion. Tables 9.9 and 9.10 give the composition of a number of copper alloys. Copper is also used as the material for spacers.

TABLE 9.10 Chemical Composition and Mechanical Properties
of Tubes Made of Brass with Additive of Arsenic

Material	Mass content, %					Mechanical properties	
	Cu	Sn	Al	As	Pb	$\sigma_{u\,min}$, MPa	δ_{min}, %
Л68+A	67-70	—	—	0.04-0.08	0.03	3.0	38
Л070-1+A	69-71	1-1.5	—	0.04-0.08	0.07	3.0	38
ЛА77-2+A	76-79	—	1.75-2.50	0.04-0.08	0.07	3.8	23

Notes. 1. All grades of brass contain 0.1% Fe; 0.02% Bi; 0.005% Sb; the total of 0.3%.
2. Thermal treatment is annealing.

Zinc forms with copper a number of solid solutions. The alpha-phase rich in copper (with a zinc content less than 30%) is a solid solution with a FCC lattice. The lattice parameters depend on the zinc concentration. Brasses listed in Table 9.8 have the structure of an alpha-solid solution. Within the range of the α-solid solution, the ductility of the alloys rises with increasing the content of zinc.

The structure of α-solid solution is also characteristic of cupro-nickel-zinc alloys containing 5-35% Ni and 13-45% Zn and known as German silver (argentan and argenton). The latter is often an alloy containing no zinc, namely, an alloy of 80% Cu and 20% Ni. The thermal conductivity of brass is high and equals 1.09 J cm^{-2} s^{-1} deg^{-1}; the coefficient of thermal expansion is $18 \cdot 10^{-6}$ deg $^{-1}$; and the density is 8.4 g/cm^3.

Corrosion Resistance. The grain-face corrosion of copper alloys contaminates the reactor coolant with the copper corrosion products, and local corrosion affects the tightness of heat-exchangers. In the former case there is a risk of forming cuprous scale on the fuel elements (in single-circuit atomic power stations). In the latter case the ingress of the condenser-cooling water into the condensate-feed system contaminates the system.

Corrosion of copper alloys proceeds by the electrochemical mechanism. The normal potential of the anodic reaction with the formation of univalent and bivalent ions is equal to 0.526 and 0.356 V, respectively. The corrosion potential of copper is positive. Therefore, the cathodic release of hydrogen on copper is thermodynamically impossible. In view of this, the copper corrosion proceeds with oxygen depolarization. Increasing the content of oxygen and oxidizing agents enhances the attack on copper and copper alloys. In a deaerated water the rate of grain-face corrosion of brass below 393 K is low. At higher temperatures copper may be used in the form of gaskets only in seals of the "lock" type in order to reduce the access of coolant to copper and the carryover of corrosion products to the circuit.

In boiling reactors, steam contains a considerable amount of oxygen. Contacting oxygen-containing steam causes grain-face corrosion of the condenser piping made of copper alloys. Steam jets may cause erosion of condenser tubes. In view of this, the first steam up-stream bundles of condenser tubes are made of the austenitic stainless steels.

The injection of ammonia into the circuit to protect the perlitic steels against attack and suppress the radiolysis in a boiling reactor, promotes failure of copper alloys. Ammonia forms with copper soluble complexes and hinders the formation of protective coatings. If the piping of a condenser and a low-pressure heater are made of copper alloys, the greatest value of pH should not exceed 9.6 when ammonia is injected. At a higher pH, the heat-exchanging piping should be made of the austenitic stainless steels.

When a condenser is cooled with sweet water, the piping is made of brasses, type ЈІ68. When cooling is done by sea water, the corrosion resistant alloys of the type МНЖ are more preferable.

When the steam flow velocity in the condenser is above 2 m/s, the condenser piping undergoes jet corrosion associated with erosion under the action of a steam jet. Jet corrosion is controlled by creating optimum hydrodynamic conditions and alloying brasses with as great an amount of iron and nickel as practicable. More resistant to jet corrosion are admiralty brasses containing 29% Zn and 1% Sn.

When condensers are cooled with sea water, brasses dezinc. In the anodic process, copper and zinc leave the solid solution for the corrosive medium. However, the copper ions precipitate on the brass surface in the form of porous formations, while the zinc ions remain in the solution. In the dezincification, copper forms a continuous layer on the surface of brass tubes. In other cases, form pits filled with a porous copper. This type of attack produces through holes and is of utmost danger. Adding 0.001-0.08% As to brass reduces the dezincification. It is supposed that arsenic increases the overvoltage of the cathodic process by reducing copper. Brasses which contain 15% or less of zinc (tombac) are usually immune. More resistant in sea water are German silver and cupronickel (60% Cu and 40% Ni).

9.4 Titanium and Its Alloys

Many favorable properties of titanium make it a promising material for the manufacture of the heat-exchange surfaces of steam generators and other components of nuclear power plants. It is known for low density, high strength and corrosion resistance. Table 9.11 gives the physical properties of titanium. Heat conductivity of steel is 1.5 to 2 times that of titanium. As the temperature rises, thermal

TABLE 9.11 Physical Properties of Titanium

Atomic number	22
Atomic weight	47.9
Thermal neutron absorption cross section, m^2	$5.6 \cdot 10^{-28}$
Density, g/cm^3	4.5
Melting point, K	1963
Boiling point, K	3908
Specific heat, $J\ g^{-1}\ deg^{-1}$	0.5799
Coefficient of linear expansion, deg^{-1}	$8.5 \cdot 10^{-6}$
Thermal conductivity, $J\ s^{-1}\ cm^{-2}\ deg^{-1}$	1.7154
Crystal structure	α-phase, FCC up to 1155 K
	β-phase, BCC at $T > 1155$ K
Parameters of lattice, nm	α-phase, $a = 0.29504$,
	$c = 0.46833$
	β-phase, $a = 0.33065$

conductivity of titanium somewhat increases, rather than decreases as in steels. The coefficient of linear expansion of titanium is less than that of steel. Titanium poorly conducts electricity. Its electrical resistivity is 5.5 times that of steel and 30 times that of copper.

Oxygen, nitrogen and carbon improve the strength of titanium and decrease its ductility. Hydrogen essentially reduces the impact strength of titanium. Titanium is not recommended for threaded connections because of a high coefficient of friction.

At room temperature, commercial titanium exhibits a perceptible creep. To reduce the creep, Al, V, Zr, and Mo are added to titanium alloys in an amount of a few per cent. As to the ratio of ultimate strength to density, the titanium alloys are superior to all known commercial alloys. Therefore, the titanium alloys are used for manufacturing the items operating under considerable loads and at high temperatures.

The titanium alloys are susceptible to manufacture. They are readily forged, stamped, and rolled (only in the hot state). Most of titanium alloys are readily welded by the argon-arc techniques. Welded seams are ductile. With the metal thickness in excess of 3 mm, welded seams are annealed to remove the internal stresses. Titanium alloys are readily cut. When heated in the air at 923 K for a long period of time, a thin brittle layer affecting the ductility forms on the surface of the alloys. The oxidation is accompanied by the oxygen and nitrogen diffusion inwards the metal. A brittle layer forms under the scaling. It is removed by machining or by pickling, where no machining is specified.

With regard to the corrosion resistance in highly pure water at high temperatures the titanium alloys surpass the austenitic stainless steels. The carryover of the titanium corrosion products to the reactor coolant is negligibly small.

The titanium alloys are not susceptible to contact corrosion, pitting, and, what is more important, stress corrosion.

The titanium alloys do not absorb hydrogen and embrittle when utilized in nuclear power plants for a long period of time. These properties make the titanium alloys find ever growing application in the manufacture of heat-exchanging equipment of nuclear power plants.

Appendix I Physical Characteristics of Certain Elements. Physical Constants of Various Elements

Element	T_{melt}, °C	T_{boil}, °C	ρ, g/cm³	c_p, J kg⁻¹deg⁻¹	λ, J cm⁻¹s⁻¹deg⁻¹	α, 10^{-6} deg⁻¹	a, cm²s⁻¹
H	—259.4	—252.7	$9 \cdot 10^{-5}$	14.435	$18.200 \cdot 10^{-4}$	—	1.40
O	—218.8	—183.0	$1.43 \cdot 10^{-3}$	0.921	$25.94 \cdot 10^{-5}$	—	0.197
N	—210.0	—195.8	$1.25 \cdot 10^{-3}$	1.046	$25.52 \cdot 10^{-5}$	—	0.195
Hg	—38.7	357	13.55	0.138	0.105	261	0.056
K	64	760	0.86	0.745	1.339	83	2.09
Na	98	882	0.97	1.230	1.381	71	1.16
Li	180.5	1327	0.53	3.284	0.711	56	0.408
Sn	232	2270	7.3	0.230	0.669	23	0.398
Bi	271	1430	9.8	1.272	0.100	13.4	0.081
Cd	321	765	8.65	0.234	0.920	31.8	0.454
Pb	327.5	1750	11.34	0.126	0.347	29.3	0.244
Pu	639	3230	19.8	0.134	0.050	46.8	0.019
Mg	650	1120	1.73	1.046	1.715	27.0	0.948
Al	660	2320	2.7	0.849	2.301	22.5	0.912
Cu	1083	2590	8.93	0.381	3.933	16.7	1.156
U	1133	3862	19.0	0.117	0.268	14.6	0.120
Mn	1245	2150	7.4	0.481	—	22.0	—
Be	1315	2450	1.8	1.883	1.883	11.4	0.555
Si	1410	2480	2.4	0.690	0.837	2.8-7.3	0.505
Ni	1452	2800	8.9	0.456	0.669	13.3	0.165
Co	1490	3330	8.9	0.435	0.711	12.2	0.184
Fe	1537	3030	7.86	0.446	0.962	12.3	0.276
Ti	1727	3530	4.5	0.565	0.155	8.4	0.061
Th	1730	4200	11.6	0.113	0.356	11.0	0.272
Zr	1850	4330	6.5	0.289	0.213	6.4	0.114
Cr	1880	2580	7.19	0.448	0.369	6.2	0.208
V	1900	2800	6.1	0.502	0.330	8.7	0.108
B	2030	2550	2.3	0.996	$15.06 \cdot 10^{-3}$	8.3	0.007
Hf	2230	5200	13.1	0.145	0.226	5.9	0.118
Mo	2590	5230	10.2	0.251	1.632	5.1	0.637
Nb	2480	4770	8.57	0.264	0.527	7.1	0.233
Ta	2987	5530	16.6	0.138	0.628	6.3	0.274
W	3397	5930	19.3	0.134	1.674	4.4	0.649
C (graphite)	3500	3900	2.3	0.690	0.251	0.6-4.3	0.158

Note. T_{melt} — melting point, T_{boil} — boiling point, ρ — density, c_p — specific heat capacity, λ — thermal conductivity, α — coefficient of linear expansion, a — thermal diffusivity.

Thermal ($E \approx 0.025$ eV) and Fast ($E = 65 \pm 20$ keV) Neutron Absorption Cross Sections

Element	σ, 10^{-28} m^2	
	thermal neutrons	fast neutrons
O	$2 \cdot 10^{-5}$	—
C (graphite)	$4 \cdot 10^{-3}$	0.0 ± 0.3
Be	0.01	—
Bi	0.032	4.0 ± 3.0
Mg	0.063	2.1 ± 0.7
Si	0.13	2.0 ± 0.7
Pb	0.17	1.0 ± 2.0
Zr	0.18	10.3 ± 2.0
Al	0.23	2.8 ± 0.7
H	0.332	—
Na	0.53	0.7 ± 0.3
Sn	0.65	51 ± 10
Nb	1.1	135
N	1.88	—
K	1.97	4.0 ± 1.0
Mo	2.5	69
Fe	2.53	6.3 ± 2.0
Cr	2.9	3.5 ± 1.0
U	3.51	302
Cu	3.62	25
Ni	4.6	6.5 ± 2.0
V	4.98	3.0 ± 1.0
Ti	5.6	5.0 ± 1.0
Th	7.45	—
Mn	13.4	9.0 ± 1.0
W	19.2	190
Ta	21.3	440
Co	37	18
Li	71	—
Pu (^{239}Pu)	287	—
Hf	105	330
Hg	380	103
B	755	—
Cd	2550	183

Appendix II Physical Properties of Steels. Thermal Conductivity, λ, W m^{-1} deg^{-1}

T, °C	Grade							
	10	20	22K	12ХМФ	15ХМФ	12Х1МФ	20Х2МФА	Х18Н10Т
100	57.0	50.7	49.5	50.2	44.5	41.3	42.0	16.3
200	52.9	48.6	47.7	50.2	41.3	40.8	41.5	17.5
300	—	46.1	45.5	50.2	40.2	40.3	41.1	18.8
400	44.8	42.4	43.5	48.6	39.0	39.7	38.5	21.4
500	—	39.0	41.5	47.0	36.1	39.0	—	23.0
600	37.6	35.6	39.3	46.0	33.7	38.2	—	24.6
700	—	—	—	44.0	—	37.4	—	26.8

Young's Modulus, E, 10^5 MPa

T, °C	Grade				
	10; 20; 25	22K	12XM	15XM	X18H10T
20	2.01	2.07	2.07	2.04	1.98
100	1.92	2.04	2.06	—	1.94
200	1.84	2.01	2.0	—	1.89
300	1.72	1.96	1.95	—	1.82
400	1.63	1.87	1.89	1.89	1.74
500	—	1.76	1.78	1.78	1.66
550	—	1.71	—	—	1.61
600	—	1.62	1.7	1.69	1.57
650	—	—	—	—	1.52
700	—	—	—	—	1.47

Coefficient of Linear Expansion, a, 10^{-6} deg^{-1}

T, °C	Grade							
	10	20	22K	12XM	15XM	12X1MФ	25X2MФА	X18H10T
100	11.6	11.6	—	11.2	11.9	10.8	11.3	16.6
200	12.6	12.6	12.2	12.5	12.6	11.8	12.7	17.0
300	—	—	12.9	12.7	13.2	12.3	—	17.2
400	13.0	13.0	13.3	12.9	13.7	12.8	13.9	17.5
500	—	—	14.0	13.2	14.0	13.2	—	17.9
600	14.6	14.6	13.8	13.5	14.3	13.6	14.4	18.2
700	—	—	—	13.8	—	13.8	—	18.6

Normal Permissible Stress, σ_p, for Steels Used in Manufacturing of Coils, Pressure Vessels, Tube Plates and Other Parts, MPa

T, °C	Grade					
	10	20K	25	22K	15ГС	16НГМ
20	127.5	144.2	161.8	166.7	181.4	196.1
250	109.8	129.4	144.1	147.1	161.8	181.4
275	103.9	123.5	137.3	143.2	157.9	180.4
300	98.1	116.7	129.4	137.3	150.0	178.5
320	93.2	111.8	122.6	133.4	142.2	177.5
340	88.3	106.9	116.7	127.5	134.3	176.5
380	79.4	95.1	103.9	—	118.7	—
400	75.5	90.2	98.1	—	110.8	—
410	75.0	87.3	94.1	—	104.9	—
420	70.6	84.3	91.2	—	100.0	—
430	66.7	81.4	84.3	—	95.1	—
440	58.8	71.6	75.5	—	88.3	—
450	52.0	62.8	66.7	—	81.4	—
470	41.2	48.0	51.0	—	—	—
490	31.4	37.3	38.2	—	—	—
500	29.4	33.3	33.3	—	—	—

T, °C	Grade				
	12XM	15XM	12X1MФ	12X2MФБ	X17H10T
20	144.2	150.0	169.7	137.3	143.2
250	142.2	149.0	162.8	126.5	122.6
300	138.3	144.2	155.9	124.5	117.7
350	134.3	139.2	149.0	120.6	113.8
400	129.4	134.3	142.2	117.7	108.8
420	126.5	132.4	138.3	116.7	107.9
440	123.6	129.4	136.3	114.7	105.9
460	120.6	127.5	133.4	113.8	103.9
480	118.7	123.6	130.4	93.2	103.0
500	94.1	101.0	123.6	78.5	102.0
510	81.4	87.3	115.7	71.6	101.0
520	67.7	77.7	104.9	65.7	101.0
530	55.9	67.7	91.2	59.8	100.0
540	46.1	58.8	81.4	55.9	100.0
550	(33.3)	49.0	72.6	50.0	99.0
560	—	41.2	65.7	46.1	99.0
570	—	(33.3)	58.8	42.2	95.1
580	—	—	52.0	38.1	88.3
590	—	—	(45.1)	35.3	79.4
600	—	—	(39.2)	(32.3)	72.6
610	—	—	—	(29.4)	66.7
620	—	—	—	(26.5)	60.8
630	—	—	—	(24.5)	55.9
640	—	—	—	(20.6)	51.0
650	—	—	—	(15.7)	47.1
660	—	—	—	—	44.1
670	—	—	—	—	40.2
680	—	—	—	—	33.3
700	—	—	—	—	29.4

References

To Chapter One

1. *Two Decades of Nuclear Power Engineering.* Moscow, Atomizdat, 1974 (in Russian).

To Chapter Three

1. *Physical Metallurgy.* Ed. by R. Cahn. V. 1-3. Amsterdam, 1965.
2. Konobeevskiy, S. T.: *Irradiation Effect on Materials.* Moscow, Atomizdat, 1967 (in Russian).
3. Honeycomb, R. W. K. *The Plastic Deformation of Metals.* London, 1968.

To Chapter Four

1. Ulybin, S. A.: *Coolants of Nuclear Power Plants.* Moscow-Leningrad, Energiya, 1966 (in Russian).
2. Kanaev, A. L. and Kopp, I. Z.: *Marine and Stationary Liquid-Metal Power Units.* Leningrad, Sudostroenie, 1968 (in Russian).
3. Nikitin, V. I.: *Interaction of Liquid and Solid Metals: Physicochemical Effects.* Moscow, Atomizdat, 1967 (in Russian).
4. Gerasimov, V. V., Kasperovich, A. I., and Martynova, O. I.: *Water Regime of Atomic Power Stations.* Moscow, Atomizdat, 1976 (in Russian).

To Chapter Five

1. Zhuk, I. A.: *Metal Corrosion and Its Control.* Moscow, Metallurgiya, 1976 (in Russian).
2. Byalobzhesskiy, A. V.: *Radiation Corrosion.* Moscow, Nauka, 1967 (in Russian).
3. Damaskin, B. B. and Petriy, O. A.: *An Introduction to Electrochemical Kinetics.* Moscow, Vysshaya Shkola Publishers, 1975 (in Russian).
4. Gerasimov, V. V.: *Corrosion of Reactor Materials.* Moscow, Atomizdat, 1980 (in Russian).

To Chapter Six

1. Swallow, A. J.: *Radiation Chemistry.* An introduction. Longman, 1973.

To Chapter Seven

1. Zaimovsky, A. S., Kalashnikov, V. V., and Golovnin, I. S.: *Fuel Elements of Nuclear Reactors.* 2nd ed. Moscow, Atomizdat, 1967 (in Russian).
2. Kotelnikov, R. B., Bashlykov, S. N., Kashtanov A. I., et al.: *High-Temperature Nuclear Fuel.* Edited by Yu. N. Sokursky, et al. 2nd ed. Moscow, Atomizdat, 1978 (in Russian).
3. Tsykanov, V. A. and Davydov, E. F.: *Radiation Stability of Nuclear Reactor Fuel Elements.* Moscow, Atomizdat, 1972 (in Russian).

4. Sokursky, Yu. N., Sterlin, Ya. M., and Fedorchenko, V. A.: *Uranium and Its Alloys.* Moscow, Atomizdat, 1971 (in Russian).
5. Samoylov, A. G., Kashtanov, A. I., and Volkov, V. S.: *Dispersion Fuel Elements of Nuclear Reactors.* 2nd ed. Moscow, Atomizdat, 1969 (in Russian).

To Chapters Eight and Nine

1. *Structural Materials of Nuclear Reactors.* V. 1. Moscow, Atomizdat, 1972 (in Russian).
2. Goncharov, V. V., Burdakov N. S., Virgilev, Yu. S., et al.: *Effect of Radiation on Graphite of Nuclear Reactors.* Moscow, Atomizdat, 1978 (in Russian).
3. Skorov, D. M., Bychkov. Yu. F., and Dashkovsky, A. I.: *Reactor Material Engineering.* 2nd ed. Moscow, Atomizdat, 1979 (in Russian).

Index